



TECHNISCHE UNIVERSITÄT MÜNCHEN
FAKULTÄT CHEMIE
LEHRSTUHL FÜR ORGANISCHE CHEMIE II

Investigation of Fimbricide and Beta-Lactone
Targets Related to the Inhibition of Quorum
Sensing-Regulated Bioluminescence in *Vibrios*

Weining Zhao

Vollständiger Abdruck der von der Fakultät für Chemie der Technischen Universität München
zur Erlangung des akademischen Grades eines

DOKTORS DER NATURWISSENSCHAFTEN

genehmigten Dissertation.

Vorsitzende: Univ.-Prof. Dr. Kathrin Lang
Prüfer der Dissertation: 1. Univ.-Prof. Dr. Stephan Sieber
2. Univ.-Prof. Dr. Tobias Gulder

Die Dissertation wurde am 04. 08. 2016 bei der Technischen Universität München
eingereicht und durch die Fakultät für Chemie am 10. 10. 2016 angenommen.

TECHNISCHE UNIVERSITÄT MÜNCHEN

FAKULTÄT CHEMIE

LEHRSTUHL ORGANISCHE CHEMIE II



Investigation of Fimbricide and Beta-Lactone
Targets Related to the Inhibition of Quorum
Sensing-Regulated Bioluminescence in *Vibrios*

DISSERTATION ZUR ERLANGUNG DES AKADEMISCHEN GRADES
EINES DOKTORS DER NATURWISSENSCHAFTEN VON

Weining Zhao

MÜNCHEN

2016

TABLE OF CONTENTS

ACKNOWLEDGEMENTS.....	I
INTRODUCTORY REMARKS.....	II
RESEARCH ABSTRACT.....	III
ABBREVIATIONS.....	VII
I – INTRODUCTION	1
1. BACTERIAL QUORUM SENSING SYSTEM	2
1.1 Quorum Sensing-Regulated Biofilm in Bacteria.....	7
1.2 Quorum Sensing-Regulated Virulence in Bacteria.....	9
1.3 Quorum Sensing in Inter-kingdom Communication	11
2 <i>IN VIVO</i> TARGET IDENTIFICATION OF SMALL MOLECULES.....	13
2.1 Affinity/Activity-Based Proteome Profiling.....	14
II – FIMBROLIDE NATURAL PRODUCTS DISRUPT BIOLUMINESCENCE BY TARGETING AUTOINDUCER BIOSYNTHESIS AND LUCIFERASE ACTIVITY	19
1. INTRODUCTION.....	20
1.1 Halogenated Furanones and Their Bioactivity.....	20
1.2 Possible Mechanisms	22
1.3 The Aim of the Project.....	24
2. RESULTS AND DISCUSSION.....	25
2.1 Synthesis of Fimbroliide Based Probes.....	25
2.2 Biological Activity of Fimbroliides and Their Probes in <i>Vibrios</i>	30
2.3 <i>In Vivo</i> Target Identification via ABPP.....	33
2.3.1 <i>In Situ</i> Analytical Labeling.....	34
2.3.2 Gel-Free Target Identification	35
2.2 Target Validation	42
2.2.1 Validation of LuxS.....	42
2.2.2 Validation of LuxE.....	46
2.2.3 Validation of PhaB.....	49
2.2.4 Validation of IMPD	51

3	CONCLUSION AND OUTLOOK.....	53
III – TARGET INVESTIGATION OF BETA-LACTONES AND THEIR EFFECTS ON QS REGULATED BIOLUMINESCENCE IN <i>VIBRIOS</i>		
1.	INTRODUCTION.....	56
1.1	Bacterial Bioluminescence.....	57
1.2	Regulation of Bioluminescence	60
1.3	The Aim of the Project.....	61
2	RESULTS AND DISCUSSION.....	63
2.1	Analysis of Diverse Beta-Lactone Bioluminescence Inhibitors in <i>Vibrios</i>	63
2.2	Synthesis of Monosubstituted Beta-Lactones	64
2.3	Target Identification	65
2.3.1	Confirmation of Bioactivity	65
2.3.2	<i>In Situ</i> Analytical Labeling.....	66
2.3.3	Gel-Free Target Identification	69
2.3.4	Gel-Based Target Identification.....	71
2.4	Target Validation	72
2.4.1	Target Validation of ACAT	72
2.4.2	Target Validation of DGC.....	73
2.4.3	Target Validation of OmpA.....	75
2.5	Beta Lactones Act Independent of QS.....	77
2.6	Whole Proteome Analysis	79
3	CONCLUSION AND OUTLOOK.....	82
IV – EXPERIMENTAL SECTION		
1	CHEMISTRY.....	85
1.1	Material and Methods.....	85
1.2	Synthetic Procedures.....	87
2.	MICROBIOLOGY.....	103
2.1	Bacterial Strains and Media.....	103
2.2	Cultivation Methods.....	103
2.2.1	Overnight Cultures	103
2.2.2	Cryostocks	104

2.3	Microbial Experiments and Assays	104
2.3.1	Minimal Inhibitory Concentration (MIC) Assay	104
2.3.2	Bioluminescence Assay	104
2.3.3	Growth and Luminescence Production Comparison between <i>V. campbellii</i> ATCC BAA-1116 and Its Δ <i>phaB</i> Mutant	105
2.3.4	Growth and Luminescence Production Comparison between <i>V. campbellii</i> ATCC BAA-1116 and Its Δ <i>ompA</i> Mutant	105
2.3.5	Swimming Assay.....	105
2.3.6	Exoprotease Assay	105
2.3.7	Phosphorylation assay.....	106
3.	PROTEOMICS.....	107
3.1	Activity-Based Protein Profiling Experiments	107
3.1.1	Analytical Gel-Based ABPP	107
3.1.2	Gel-Based ABPP and In Gel Digestion.....	108
3.1.3	Gel Free ABPP and Dimethyl Labeling.....	110
3.2	Whole Proteome Analysis	114
3.2.1	Whole Proteome Comparison between <i>V. harveyi</i> NBRC 15634 and <i>V.</i> <i>campbellii</i> ATCC BAA-1116.....	114
3.2.2	Whole Proteome Analysis of <i>V. campbellii</i> ATCC BAA-1116, Its Chemical Knockdown by Beta-Lactones, and Δ <i>ompA</i> Mutant	115
3.2	Recombinant Proteins	115
3.2.3	Recombinant Expression of LuxS in <i>E. coli</i>	115
3.2.4	Recombinant Expression of PhaB in <i>E. coli</i>	117
3.2.5	Recombinant Expression of LuxE in <i>E. coli</i>	117
3.2.6	Recombinant Expression of <i>Photorhabdus luminescens</i> LuxE in <i>E. coli</i>	118
3.2.7	Recombinant Expression of IMPD in <i>E. coli</i>	118
3.2.8	Recombinant Expression of Pfs in <i>E. coli</i>	118
3.2.9	Recombinant Expression of ACAT in <i>E. coli</i>	119
3.2.10	Recombinant Expression of DGC in <i>E. coli</i>	119
3.2.11	Recombinant Expression of OmpA in <i>E. coli</i>	120
3.3	Binding Site Identification	120
3.3.1	Full Length MS of Intact Proteins	120
3.3.2	Binding Site Identification by MS-MS of LuxS and LuxE.....	121
3.3.3	Binding Site Identification by MS-MS of OmpA.....	121

4	ENZYMATIC ASSAYS.....	123
4.1	LuxS Inhibition Assay	123
4.2	PhaB Inhibition Assay	123
4.3	Inhibition of Bioluminescence in Luminescent <i>E. coli</i> DH5 α by Fimbroside	124
V	BIBLIOGRAPHY.....	125
VI	APPENDICES	134
VII	CURRICULUM VITAE	162

ACKNOWLEDGEMENTS

It is my great pleasure to complete this dissertation and many thanks should be given to the people who help and support me during my PhD study and research.

The first person came into my mind is absolutely my supervisor Prof. Stephan Sieber who has accepted me as a PhD student in his group and instructed me during my research with a lot of efforts. I feel really lucky as I can have such a patient and kind supervisor as well as he is very knowledgeable and keen into research. His strong persistence and high motivation in pursuing high-level and rigorous research inspired me quite a lot, which will benefit me much in my future research and life. The research group has such an excellent working atmosphere which I have never expected before owing to his efforts in organizing the group and taking care of all the members. I would like to give many thanks to this great atmosphere which is very precious for a foreign student.

There are always a lot of fun and useful discussions when I work in Lab B@Sieber group which keeps me in a good mood during my work. Thank Dr. Franziska Mandal, Mathias Hachl, Dr. Johannes Kreuzer, Dr. Tanja Wirth, Barbara Hofbauer, Thomas Gronauer for great companion in Lab B and this experience will be a treasure for me. I would like to thank Franziska Mandal and Mathias Hachl for their help during my daily life. I sincerely acknowledge all the members in Sieber's group during my stay and all of us have created a nice working environment. I get much help from Dr. Matthew Nodwell at the beginning of my study and I would like to give my special thanks to him.

For proofreading I want to thank Prof. Stephan Sieber, Dr. Megan Wright, Dr. Pavel Kielkowski and Annabelle Hoegl.

I would like to thank our Chinese Lunch and Tee club members in department of chemistry, with whom I had a lot of pleasure. Academic discussions, barbecues, tours and Chinese Festival celebration have tied us tightly together in Munich and will keep us in close contact in future in China. Here I want to specially thank Prof. Lei Jiao, Dr. Qi Zhang, Prof. Fangrui Zhong, Prof. Dr. Guoyin Guo, Dr. Youquan Zou and Prof. Dr. Peng Hu who have not only spent much pleasant time with me but also taught me much in research.

As a Chinese proverb goes "while his parents are alive, the son should not go on a long journey", nevertheless, I have been abroad for nearly four years. Here I want to thank my dear parents, brother and sister for their support during this period.

Also, I owe a big debt of gratitude to my wife Fangyuan Zhao and I am so fortunate to have you in my life.

INTRODUCTORY REMARKS

This dissertation was accomplished from October 2012 to July 2016 under the supervision of Prof. Dr. Stephan A. Sieber at the Chair of Organic Chemistry II in Department of Chemistry, Technische Universität München.

PARTS OF THIS THESIS HAVE BEEN PUBLISHED IN:

Zhao, W., Lorenz, N., Jung, K., Sieber, S. A.*, "Fimbricide natural products disrupt bioluminescence of *Vibrio* by targeting autoinducer biosynthesis and luciferase activity", *Angew. Chem. Int. Ed.*, **2016**, *55*, 1187-1191.

Zhao, W., Lorenz, N., Jung, K., Sieber, S. A.*, "Mechanistic analysis of aliphatic β -lactones in *Vibrio harveyi* reveals a QS independent mode of action", *Chem. Commun.*, **2016**, *52*, 11971-11974.

RESEARCH ABSTRACT

Quorum sensing (QS) is a bacterial signaling system which many bacterial strains employ to coordinate their gene expression in accordance with their population density. QS has recently become a potential therapeutic target and a hot research topic. The efforts to unravel the molecular targets of QS inhibitors (QSIs) as well as to find new QSIs will contribute to better manipulation of QS. In this dissertation, I first dissect the protein targets of well known QSIs, fimbrolides via activity-based protein profiling (ABPP). Furthermore, monosubstituted long chain β -lactones are found to be potential new QSIs based on bioluminescence screening in *Vibrios*. Thus, their mode of action in inhibiting QS regulated bacterial bioluminescence is investigated on a proteomic perspective.

Natural products fimbrolides are well-known QS inhibitors and quite often used in QS research. However, their molecular targets remain elusive. The first part of my work describes the synthesis of activity-based fimbrolide probes and natural fimbrolides as well as their application in the identification of protein targets of fimbrolides in bacteria. The fimbrolide and probe exhibiting the best bioactivity in both *Vibrio harveyi* NBRC 15634 and *Vibrio campbellii* BAA-1116 bioluminescence assays were selected for the proteomic study. ABPP with high resolution proteomics was applied to identify the irreversible protein targets of fimbrolide in a quantitative way. Acetoacetyl-CoA reductase (PhaB), autoinducer-2 synthase (LuxS), and long-chain-fatty-acid ligase (LuxE) were identified as the most promising targets for the phenotype in both *Vibrio harveyi* NBRC 15634 and *Vibrio campbellii* BAA-1116 strains. Thus, PhaB, LuxS and LuxE were further validated as the protein targets of fimbrolide. The bioactivity of LuxS could be inhibited by fimbrolide in a dose-dependent manner as shown for PhaB in *in vitro* enzymatic assays. The binding site on LuxS by fimbrolide was identified as Cys83, which is different from the previous report but is more consistent with the catalytic mechanism of this enzyme. A $\Delta phaB$ mutant of *Vibrio campbellii* exhibited no difference in growth and production of bioluminescence compared to the wild type, which excluded PhaB as a protein target for the phenotypic change. LuxE was shown to be inhibited by fimbrolides in an *E. coli* strain which harbored a luminescent system from *Photobacterium luminescens*. The binding site of LuxE by fimbrolide was identified as Cys362 by means of MS-MS sequencing. Cys362 is reported to be important for catalytic activity. Fimbrolide inhibition of LuxE provides a new explanation for bioluminescence inhibition in *Vibrios*.

In the second part of this dissertation, a panel of acyl-homoserine lactone (AHL) structurally related β -lactones were screened in the *Vibrio* bioluminescence assay with natural fimbrolide

as a reference. Surprisingly, one β -lactone with a long aliphatic chain in α position and a methyl group in the β position exhibited excellent bioluminescence inhibition. Furthermore, newly synthesized monosubstituted long chain β -lactones with these features confirmed this observation. Among them, the β -lactone and its corresponding probe which showed the strongest inhibition in bioluminescence assay with IC_{50} values of 1.8 and 0.5 μ M were employed for further study.

After quantitative ABPP experiments, acetyl-CoA transferase (ACAT), GGDEF family protein (DGC) and outer membrane protein precursor (OmpA) were identified as the most promising targets. Each of these three proteins was recombinantly expressed in *E. coli* cells and verified as labeled by β -lactone probe. ACAT has been well studied but without any reports suggesting a link between it and bioluminescence or QS. DGC is a predicted diguanylate cyclase which is responsible for the biosynthesis of cyclic di-3',5'-guanylate (c-di-GMP). A slightly but consistent larger swimming distance in the presence of β -lactones compared to the DMSO treated samples suggested c-di-GMP mediated motility was impaired. A $\Delta ompA$ mutant was generated to investigate the function of OmpA. The $\Delta ompA$ mutant did not differ in growth, bioluminescence and motility compared to the wild type, suggesting that OmpA is not directly responsible for the bioluminescence inhibition by β -lactones. The β -lactones also have similar IC_{50} values in the $\Delta ompA$ mutant as in wild type strain. A whole proteome comparison of *V. campbellii* wild type, its $\Delta ompA$ mutant, and its chemical knock-down by β -lactone was carried out. Malonyl CoA-acyl carrier protein transacylase (FabD), reported to function in the biosynthesis of fatty acid was found to be strongly upregulated in both the $\Delta ompA$ mutant and the chemical knock-down cells. More interestingly, both electron transfer flavoprotein (ETF) α and β subunits were dramatically downregulated in chemical knock-down cells. The role of ETF in β -oxidation of fatty acids linked to acyl- and acetyl-CoA production. Thus, its down-regulation under the treatment of β -lactones may thus stall myristic acid biosynthesis required for luciferase activity, establishing a putative link to bioluminescence inhibition with β -lactones. The next steps should be the investigation of the links between β -lactone treatment, OmpA function and FabD as well as the role of electron transfer flavoprotein α and β subunits in bioluminescence.

In conclusion, the molecular protein targets of fimbrolide such as LuxS and LuxE were discovered via ABPP providing deeper understanding of these QS tool compounds. LuxS, a key QS protein, confirmed the fimbrolide inhibition of QS. LuxE is an essential protein for bioluminescence production. Its inhibition renews the understanding of fimbrolide bioluminescence inhibition. The efforts to new QSIs with bioluminescence assay revealed the

RESEARCH ABSTRACT

monosubstituted long chain β -lactones to be excellent bioluminescence inhibitors. Nevertheless, further proteomic studies show they function in a QS-independent action.

ABBREVIATIONS

AB	autoinducer bioassay
ABC	ammoniumbicarbonate
ABPP	affinity/activity based proteome profiling
ABPs	activity based probes
ACAT/PhaA	acetyl-CoA transferase
ACP	acyl carrier protein
ADP	adenosine diphosphate
<i>agr</i>	accessory gene regulator
AHL	acyl-homoserine lactone
AIPs	auto-inducing peptides
AIs	autoinducers
AMP	adenosine monophosphate
ApoB	apolipoprotein B
ATP	adenosine triphosphate
BCA assay	bicinchoninic acid assay
BHL	<i>N</i> -butyrylhomoserine lactone
brine	saturated NaCl solution
C18	octadecyl carbon chain bonded silica
CAI-1	cholerae autoinducer-1
calcd	calculated
CC	click chemistry
c-di-GMP	cyclic di-3',5'-guanylate, cyclic di-GMP
CETSA	cellular thermal shift assay
ClpP	caseinolytic protease P
CuAAC	copper-catalyzed azide-alkyne cycloaddition
Cys	cysteine
DCM	dichloromethane
DiMe	dimethyl labeling
DMF	dimethylformamide
DMP	Dess–Martin periodinane
DPD	4,5-Dihydroxy-2,3-pentanedione
DTT	dithiothreitol
EAA	ethyl acetoacetate
EDA	ethylenediamine
EPS	extracellular polymeric substances
ESI	electrospray ionization
ETF	electron transfer flavoprotein
FA	formic acid
FabD	malonyl CoA-acyl carrier protein transacylase
FDR	false Discovery Rate
FMN	flavin mononucleotide
FMNH ₂	reduced flavin mononucleotide
DGC	GGDEF family protein

ABBREVIATIONS

GTP	guanosine triphosphate
HAI-1	harveyi autoinducer-1
HBTU	2-(1 <i>H</i> -benzotriazol-1-yl)-1,1,3,3-tetramethyluronium hexafluorophosphate
HCD	high cell density
HECD	higher-energy collisional dissociation
His	histidine
HPLC	high-performance liquid chromatography
HRMS	high-resolution mass spectrometry
Hz	hertz
IAA	2-iodoacetamide
IC50	half maximal inhibitory concentration
IFN- γ	interferon gamma
IL-4	interleukin 4
IL-8	interleukin 8
IMPD	inosine monophosphate dehydrogenase-like protein
IPTG	isopropyl β -D-1-thiogalactopyranoside
IQS	integrated QS signal
iTRAQ	isobaric tag for relative and absolute quantitation
<i>J</i>	coupling constant in Hz
KASII	3-oxoacyl-[acyl-carrier-protein]
LC	liquid chromatography
LCD	low cell density
LDA	lithium diisopropylamide
LTO-FTICR	linear trap quadrupole - Fourier Transform - ion cyclotron resonance
LuxE	long-chain-fatty-acid ligase
LuxS	autoinducer-2 synthase, S-ribosylhomocysteine lyase
<i>m/z</i>	mass to charge ratio
MIC	minimal inhibitory concentration
MS	mass spectrometry
MS/MS	tandem mass spectrometry
MTAN	5'-methylthioadenosine/S-adenosylhomocysteine nucleosidase
MW	molecular weight
NADPH	reduced nicotinamide adenine dinucleotide phosphate
NF- κ B	nuclear factor kappa-light-chain-enhancer of activated B cells
NMR	nuclear magnetic resonance
Nox2	NADPH oxidase 2
OD	optical density
OdDHL	<i>N</i> -3-oxododecanoyl-homoserine
OHHL	<i>N</i> -3-oxohexanoyl-homoserine lactone
OmpA	outer membrane protein A precursor
PBS	phosphate-buffered saline
PCR	polymerase chain reaction
PhaB	acetoacetyl-CoA reductase
PONs	paraoxonases
ppm	parts per million
PQS	<i>Pseudomonas</i> quinolone signal

ABBREVIATIONS

QS	quorum sensing
QSIs	quorum sensing inhibitors
RhN ₃	rhodamine-azide
RLU	relative luminescence units
RP	reversed phase
rpm	rotations per minute
RR	response regulator
RT	room temperature
SAH	S-adenosylhomocysteine
SAR	structure-activity relationship
SAM	S-adenosyl-L-methionine
SDS-PAGE	sodium dodecyl sulfate polyacrylamide gel electrophoresis
SILAC	stable isotope labeling by amino acids in culture
SRH	S-ribosylhomocysteine
TCA	tricarboxylic acid
TCEP	tris-(2-carboxyethyl)-phosphine
TEAB	tetraethylammoniumbromide
TFA	trifluoroacetic acid
TFL	trifunctional linker with rhodamine, biotin and azide groups
THF	tetrahydrofuran
TLC	thin layer chromatography
TMS	trimethylsilyl
TMSCl	trimethylsilyl chloride
TMT	tandem mass tag
TRIS	tris(hydroxymethyl)aminomethane
δ -values	chemical shifts

I – INTRODUCTION

1. Bacterial Quorum Sensing System

Quorum sensing (QS) is a population-dependent signaling which many microbes use to coordinate their group behaviors and gene expression. QS was first discovered by Nealson and Hastings in the late 1960s in *Aliivibrio fischeri* (formerly named as *Photobacterium fischeri* or *Vibrio fischeri*).¹ They found the burst of bioluminescence during the exponential phase of growth was due to increased biosynthesis of an unidentified component but not due to the presence of inhibitors in culture media consumed during growth.² The molecule which was stimulated for its synthesis observed by Nealson and Hastings in *Aliivibrio fischeri* was later identified to be *N*-(3-oxohexanoyl)-homoserine lactone (OHHL) (**1**) by Eberhard in 1981.³ However, it was believed that this kind of AHL based signaling system only existed in marine bacterium at that time. Nevertheless, Williams *et al.* found that this signaling system was utilized in *Erwinia carotovora* in 1992, while a similar discovery in *Pseudomonas aeruginosa* implied a possible role of this signaling system in the regulation of elastase expression.⁴ From this point on, increasing evidence demonstrated that this signaling system not only exists in many other bacterial species but also is very complex and differs from species to species.

The term QS was first proposed by Greenberg *et al.* in 1994 in order to describe the feature that certain group behaviors can only be performed effectively by a sufficiently large population of bacteria.⁵ QS systems have a common mechanism: the production, detection and response of signaling molecules (autoinducers) are the basis of this bacterial cell–cell communication. As the bacterial community grows, the cells produce autoinducers and they diffuse away. However, at the onset of this process, the concentration of autoinducers in the environment is below the threshold of detection due to the low cell density (LCD). As the bacterial population becomes increasingly dense, the accumulation of autoinducers (AIs) leads to a high-local concentration which is sufficient for detection and response.⁶ At this high cell density (HCD), the receptors in the cytoplasm or membrane detect the high concentration of autoinducers leading to the activation of specific gene expression. Moreover, the production of more autoinducers is favored in a positive autoinduction loop mode to promote the synchrony in the community.

Many microbes have been found to communicate via QS signaling system and it can regulate diverse phenotypes, such as virulence and biofilm formation. Moreover, bacteria and their host have crosstalks between bacterial signaling molecules and host-derived hormones. The discovery of this inter-kingdom communication makes QS more intriguing as a therapeutic target. In general, the group behaviors coordinated by QS in bacteria change our view of bacteria from a singular cell to a multi-cellular like organism. Here the interesting role QS

plays in clinically related phenotypes such as biofilm formation, virulence and inter-kingdom communication is summarized in section 1.1-1.3.

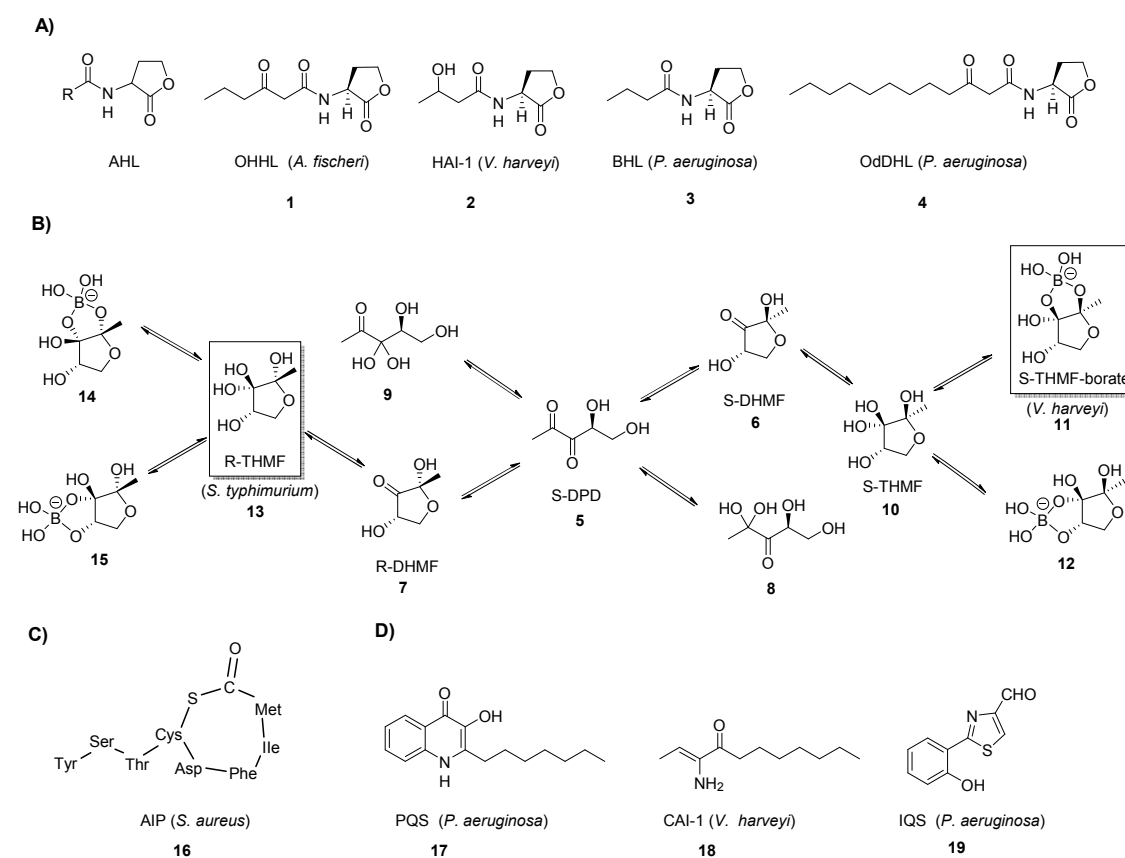


Figure 1: Structures of autoinducers. A) N-acyl homoserine lactones (AHL) based structures. OHHL (**1**): N-3-oxohexanoylhomoserine lactone; HAI-1 (*harveyi* autoinducer-1) (**2**): N-3-hydroxybutyryl homoserine lactone; BHL (**3**): N-butyryl homoserine lactone; OdDHL (**4**): (N-(3-oxododecanoyl)-homoserine. B) Complex equilibria involving DPD (S)-4,5-Dihydroxy-2,3-pentandione (**5**) and its possible derivatives in water and in the presence of borate. **11** and **13** were identified as AI-2 signaling molecules in *V. harveyi* and *S. typhimurium* respectively. C) Autoinducing peptide (AIP) (**16**) in *S. aureus*. D) Some other QS molecules. PQS (*Pseudomonas* quinolone signal) (**17**): 2-heptyl-3-hydroxy-4(1H)-quinolone; CAI-1 (cholerae autoinducer-1) (**18**): (Z)-3-aminoundec-2-en-4-one; IQS (integrated QS signal) (**19**): 2-(2-hydroxyphenyl)-thiazole-4-carbaldehyde.

To date there are three main categories of AIs: (1) N-acyl homoserine lactones (AHLs), which are primarily produced and utilized in Gram-negative bacteria. Their structures typically contain a homoserine lactone ring with an acyl chain. However, the chain differs in its length and composition depending on the species. AHLs can freely diffuse into and out of the bacterial cells and bind to their receptors of the bacteria. (2) Oligopeptides or auto-inducing peptides (AIPs) used by Gram-positive bacteria. These oligopeptides are usually composed of

8 - 10 amino acids and need specific exporters to transport them in and out of the bacterial cells, while their receptors are on the surface of the bacterium. (3) Autoinducer 2 (AI-2), which is considered as a universal signaling molecule for the interspecies communication among Gram-negative bacteria and Gram-positive bacteria. It is produced by the enzyme S-ribosylhomocysteine lyase (LuxS) and has a core structure of (S)-4,5-dihydroxy-2,3-pentanedione (DPD). DPD exists in equilibrium and spontaneously rearranges to form a variety of DPD structures which are known as AI-2 pool. It is noteworthy that LuxS is thought to play a metabolic role in addition to its role in AI-2 biosynthesis. Although the role LuxS plays in QS was controversial in the past, there is increasing evidence that AI-2 can be considered as the universal language in terms of interspecies communication. There are also several other autoinducers which do not fit into the above three categories and they are present in specific species, e.g. PQS (*Pseudomonas* quinolone signal) (17),⁷ CAI-1 (*cholerae* autoinducer-1) (18)^{8,9} and others. (Figure 1)

Every bacterial species can produce multiple autoinducers e.g. *Pseudomonas aeruginosa* produces OdDHL (4), BHL (3), PQS (17) and IQS (19) while different autoinducers have their specific receptors.¹⁰ Although the QS circuits differ from species to species, several simplified models for a single kind of autoinducer can be generalized. Here the three most popular QS model circuits are summarized below.

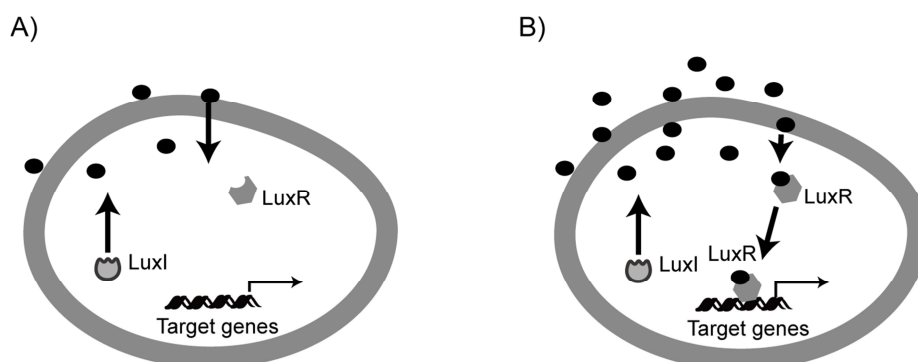


Figure 2: AHL based LuxI/LuxR QS model circuit from *Aliivibrio fischeri*. AHL signals (black dots) are synthesized by the enzyme LuxI or its homologues. These AHL molecules can diffuse freely and bind to LuxR or its homologues. A) At low cell densities (LCD), the concentration of AHL is low and AHL cannot bind to LuxR sufficiently to initiate QS. B) At high cell densities (HCD), AHL, which is at high concentration, binds to LuxR, which results in the expression of targets genes including *luxI* or its homologues. Therefore, this QS circuit is enforced in a positive feedback loop.

In the *Aliivibrio fischeri* LuxI/LuxR QS circuit, LuxI catalyzes the formation of autoinducer *N*-(3-oxohexanoyl)-homoserinelactone (OHHL) using *S*-adenosyl-L-methionine (SAM) as a substrate.

As the AHL molecules are amphipathic owing to the co-presence of the hydrophobic side chain and the hydrophilic homoserine lactone ring, OHHL can diffuse freely in and out of the cell, as can the other AHLs. Although OHHL is produced at a low basal level, high cell density (HCD) ensures sufficient ligand concentration for LuxR binding. When the autoinducer OHHL binds to the protein LuxR, the LuxR protein is activated. This activated LuxR then binds to the promoter region and upregulates the production of many proteins, including luciferase proteins, resulting in a burst of light production. It is noteworthy that *luxI* is also upregulated by the activated LuxR protein. This positive feedback leads to accelerated production of *luxI*, following by accelerated production of autoinducer OHHL. Many Gram-negative bacteria possess a QS circuit similar to the *Aliivibrio fischeri* LuxI/LuxR system. Thus, the homologous *Aliivibrio fischeri* LuxI/LuxR QS circuit proteins found in many other Gram-negative bacteria are known as the LuxI-type synthases and LuxR-type receptors. These include Rh1I/R and LasI/R in *Pseudomonas aeruginosa*, and CepI/R in *Burkholderia cenocepacia*.¹¹ Nevertheless, it must be noted that in some bacterial species the QS system is more complex. For example, in *Vibrio harveyi*, although LuxN is the receptor of its AHL signaling molecule HAI-1 (*harveyi* autoinducer-1, **2**), it is not a homolog of *Aliivibrio fischeri* LuxR. It functions in the QS phosphotransfer system with its histidine and aspartate but not as an activator for the target genes (see Figure 13).¹² (Figure 2)

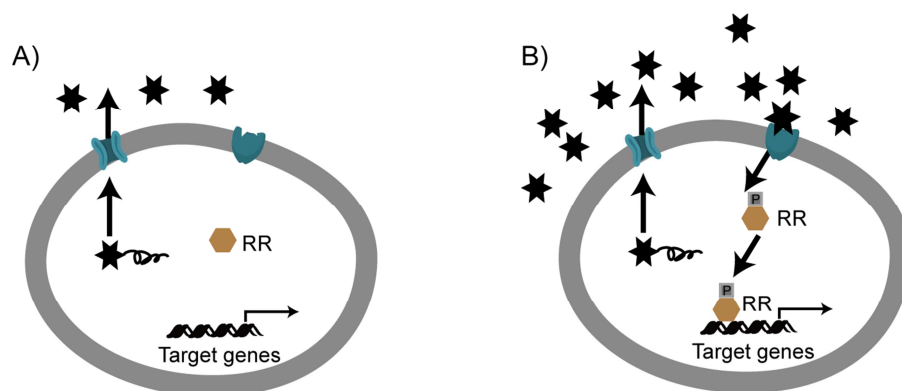


Figure 3: Autoinducer peptides (AIPs)-based QS model circuit. AIPs (black hexagons) are synthesized in cells as precursor peptides which are exported out of the cell. A) At low cell densities (LCD), the concentration of AIP is low outside of the cell and inadequate AIP bind to the receptor to initiate QS. B) At high cell densities (HCD), AIP which is at high concentrations bind to the receptor. The receptor acts as a kinase and phosphorylates the response regulator. The phosphorylated response regulator then activates the expression of target genes. The response regulator (RR) is represented by a brown hexagonal.

The autoinducer peptide (AIP)-based QS systems in Gram-positive bacteria differ substantially from the AHL-based QS system in Gram-negative bacteria with regard to autoinducer synthesis and transport as well as signal recognition and sensing. The *Streptococcus pneumoniae* AIP QS circuit is a classic model for the AIP QS, and is similar to that in *Bacillus* and *Staphylococcus* Gram-positive bacteria species.¹³ The AIPs are synthesized as precursor peptides, modified and exported from cells with specific exporters as they cannot diffuse freely in and out of the cells. In Gram-positive bacteria, the AIPs do not directly bind to their cognate receptors for activation like AHL binding to luxR. The signal transduction is relayed by a two-component system by means of phosphotransfer. This system is composed of a membrane-bound histidine kinase sensor and a response regulator protein. First, the AIP binds to the membrane-bound histidine kinase sensor. This kinase then relays the binding information to its response regulator protein through phosphorylation. Finally, the promoter of target genes is bound by this activated regulator protein and regulation of the gene expression follows. (Figure 3)

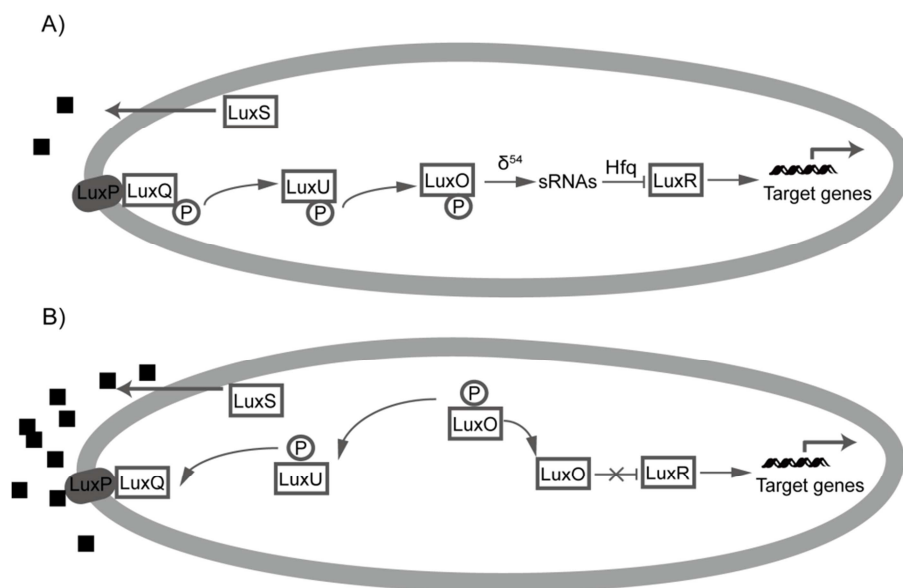


Figure 4: Autoinducer 2 (AI-2, black squares)-based QS circuit in *Vibrio harveyi*. AI-2 is produced by LuxS and sensed by LuxP/LuxQ receptors. A) At low concentrations of AI-2, the receptors autophosphorylate and transfer their phosphoryl groups to LuxU, which in turn phosphorylates LuxO. LuxO~P activates the expression of Qrr1-5 sRNA that, together with the chaperone Hfq, destabilizes *luxR* mRNA. LuxR expression is reduced and it can no longer induce the expression of target genes. B) At high concentrations of AI-2, the autophosphorylation of the receptors is inhibited and the phosphate is drained from the cascade resulting in the expression of transcriptional regulator LuxR. LuxR thus is used to regulate the expression of target genes. P in a grey circle denotes phosphotransfer.

Although AI-2 is considered as the universal language in bacteria, more efforts are needed to identify its binding receptors. The best studied AI-2 based QS system is from *Vibrios*. Interestingly, the AI-2 QS system in *Vibrio harveyi* relays AI-2 binding information in a similar manner to the Gram-positive two component signal transduction system. As mentioned before, AI-2 is synthesized by LuxS and then it diffuses outside of the cells. LuxP in the periplasm associates with LuxQ to form the two component signal transduction cascade. When the concentration of AI-2 is low at low cell density, LuxP/Q acts as a kinase and phosphorylates LuxU, followed by transfer of the phosphate group from LuxU-phosphate to LuxO. The LuxO-phosphate can activate the expression of regulatory small RNAs Qrr1-5 in the presence of sigma factor σ^{54} . The small RNAs Qrr1-5 will suppress the expression of LuxR with the chaperone Hfq by destabilizing the *luxR* mRNA. At high concentration of autoinducers, LuxP/Q is bound by AI-2 and switches to a phosphatase from a kinase. The phosphate is drained from the cascade, resulting in the expression of transcriptional regulator LuxR and thereby activating the expression of the target genes.¹⁴ (Figure 4)

In nature, bacteria always grow in a complex microbial community. Each species has developed multiple signals to communicate within its own species or genus as well as with the other species. The high specificity of the autoinducers to their cognate receptors is an example of the precise signaling in bacteria.¹² Moreover, bacteria have developed the ability to prioritize signal information from multiple autoinducers to keep the fidelity of induced response high. This intriguing signaling system is used by bacteria to accurately control various bacterial phenotypes. However, bacterial phenotypes regulated by QS are quite different from species to species. For example, QS is used to develop bacterial competence in *Bacillus subtilis* and *Streptococcus pneumoniae*, while it is employed to regulate virulence in *Staphylococcus aureus* and bioluminescence in *Vibrio campbellii*.^{13,15-22} As QS is considered as a therapeutic target, studies about its involvement in the regulation of biofilm formation and virulence have become hot topics as well as its role in inter-kingdom communication.

1.1 Quorum Sensing-Regulated Biofilm in Bacteria

Although most studies use the free-floating or planktonic state for bacterial research, in nature bacteria usually live in a quite different living state termed biofilm.^{16,23} Furthermore, their community is usually multiple-species instead of single-species. To date, a lot of research has been carried out into biofilms, but there is no strict definition for biofilm because of its complexity. Nevertheless, a biofilm is often described as any group of microorganisms in which cells stick to each other and these cells often adhere to a surface.

The bacteria in a biofilm are always held together by extracellular polymeric substances (EPS) which are generally composed of extracellular DNA, proteins, and polysaccharides.

Biofilm poses an acute threat to human health, since an estimated 65% of all hospital infections are of biofilm origin.²⁴ Moreover, diseases related to pathogens in the form of biofilm are much more difficult to treat compared with the planktonic state. Research has shown that biofilm bacteria are about 100 to 1000 times more tolerant to antimicrobials than planktonic bacteria from the same species.²⁵ The biofilm provides optimal protection for the embedded cells against noxious agents and the immune system. Therefore, chronic diseases that involve biofilms, such as implant infections, cystic fibrosis, urinary tract infections, always prolong the suffering of the patients and result in high health costs worldwide. QS and biofilm are two bacterial group behaviors and their research has dramatically updated our view about microbes from unicellular organisms to multicellular-like organisms. In fact, QS is believed to coordinate gene expression of individual cells inside the biofilm.

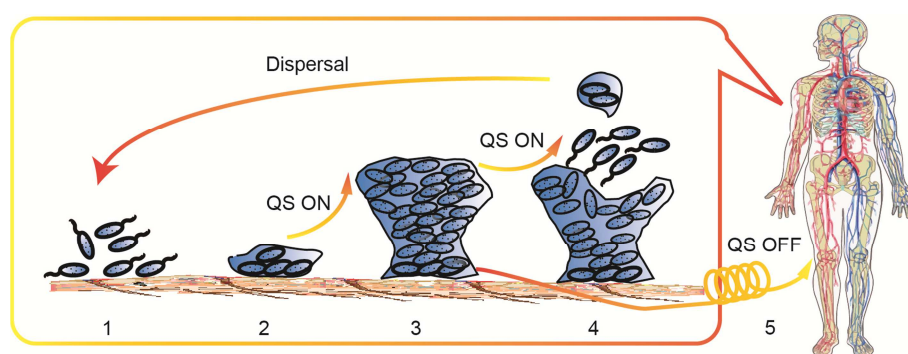


Figure 5: QS and biofilm formation. 1) Free-floating or planktonic bacteria encounter a submerged surface and within minutes adhere to it. The initial adhesion is weak, acting through reversible van der Waals' forces. However, the adhesion becomes more permanent later by means of cell adhesion structure like pili. 2) Slimy extracellular polymeric substances (EPS) are produced by the cells and utilized to colonize the surface. 3) The production of EPS allows the emerging biofilm community to develop a complex three dimensional structure while QS is important for the architecture. 4) The detachment of small or large clumps of biofilm cells and "seeding dispersal" to release individual cells are two ways for the biofilm to propagate. Both types allow bacteria to colonize another surface area or attach to a biofilm downstream of the original community. QS plays an important role in the disruption of the slime to allow both biofilm propagation types to take place. 5) During a prolonged infection, QS is turned off or mutation in QS occurs.

In 1998, the first evidence for the link between biofilm and QS was reported by Greenberg and his coworkers.²⁶ They found that QS was required in the development of biofilm in *Pseudomonas aeruginosa*. The wild type strain developed a complex, three dimensional

biofilm, but the QS *lasI* mutant just formed flat, undifferentiated biofilms which could be easily eradicated by sodium dodecyl sulfate (a detergent). Moreover, when this mutant was cultivated with synthetic external autoinducers, the biofilm architecture became similar to that formed by the wild type. Nevertheless, the following investigations of the relationship between QS and biofilm in *Pseudomonas aeruginosa* show their relationship is not as simple as originally suggested.²⁷ In addition, QS *agr* mutants of *Staphylococci* were found to produce a thicker biofilm than the wild type, although QS plays a role in biofilm structuring. What puzzles researchers is that clinical isolates from biofilm-associated chronic infections are found to be QS mutants in both *Staphylococci*^{28,29} and *Pseudomonas aeruginosa*.³⁰

A new rational model which tried to unify the controversial results was proposed.³¹ QS is important in the formation of complex differentiated biofilm and for acute virulence. It is also beneficial for bacterial dispersal from the biofilm community followed by the formation of a new biofilm. However, during long-term infection, the cells will develop mutations in the QS system or simply turn off QS. (Figure 5) In total, the relationship between QS and biofilm is very dynamic and dependent on the environment. Therefore further research efforts are still required to fully understand this system.²⁷

1.2 Quorum Sensing-Regulated Virulence in Bacteria

Many clinically relevant bacterial strains regulate their virulence factors, as well as associated phenotypes such as swarming and biofilm, with QS.^{6,20,32,33} Owing to the importance of virulence in pathogenicity and human health, significant efforts have been put into investigating the role of QS in bacterial virulence, especially in *Staphylococcus aureus* and *Pseudomonas aeruginosa*.

Staphylococcus aureus can cause both acute and chronic diseases such as bacteremia, sepsis and endocarditis. Moreover, it has developed resistance to multiple antibiotics. It utilizes an AIP-based QS circuit, which is encoded by the accessory gene regulator (*agr*) locus, to regulate its virulence as in many other Gram-positive bacterial strains. Therefore, the *agr* QS system has become an interesting anti-virulence target for the treatment of *Staphylococcus aureus* infection. To date, the *agr* system is thought to regulate 23 known virulence factors, including hemolysins, leukocidins, cell surface adhesins and exoenzymes.³⁴

At the molecular level, AIP first binds its membrane-bound histidine kinase AgrC at high concentration. The autophosphorylated AgrC then will transfer its phosphate group to the response regulator AgrA. The phosphorylated AgrA then binds upstream of the P2 promoter which will drive the expression of transcript RNAII encoding AgrB, AgrD, AgrC and AgrA. In

addition, it activates expression of two virulence factors.³⁵ More importantly, phosphorylated AgrA activates the P3 promoter which activates the expression of RNAIII. RNAIII is a key player in the regulation of virulence factors in *Staphylococcus aureus*. It not only activates the production of α -toxin but also its *hld* gene encodes δ -hemolysin. Moreover, it act as a regulatory RNA to repress expression of *rot*, the repressor of toxins.¹⁵ (Figure 6)

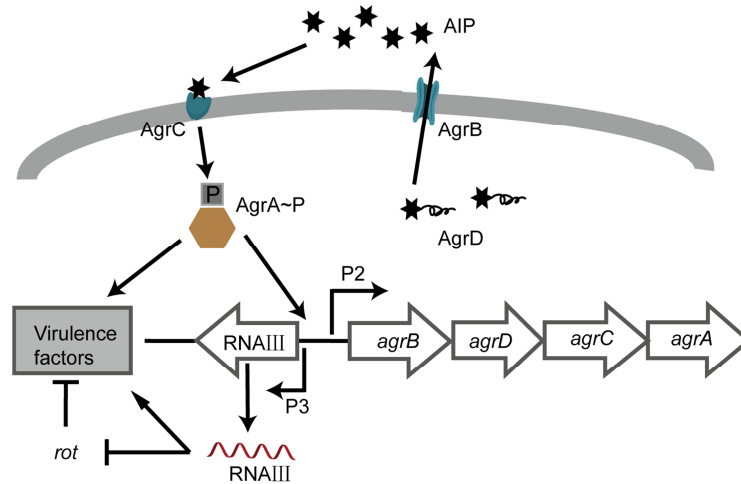


Figure 6: *S. aureus* Agr QS circuit regulates virulence. In cells, the autoinducing peptide (AIP, black hexagams) is synthesized as a precursor from *agrD*. Later it is processed by the transporter *AgrB* and the mature AIP is then transported out of the cells. *AgrC* is a membrane-bound histidine kinase which is the receptor of AIP. The binding information of AIP to *AgrC* is relayed to the response regulator *AgrA* by its phosphorylation. *AgrA~P* then is able to activate the P2 and P3 promoters which respectively encode RNAII (*agr* operon) and the RNAIII regulatory RNA. RNAIII posttranscriptionally activates virulence factor production and represses expression of *rot*. As *rot* is the repressor of toxins, its repression results in a further activation of virulence factors.

Pseudomonas aeruginosa harbors a very complex hierarchical QS network composed of four interconnected QS circuits.¹⁸ The two LuxI/LuxR type QS circuits are the key players in virulence regulation. However, the other two circuits are also involved in this regulation in an indirect way as they are interconnected. The binding of OdDHL with LasR initiates this regulation at high OdDHL concentration. This LasR-OdDHL complex activates transcription of targets genes. It also initiates the positive autoinduction for its own QS circuit as well as activates the production of RhII, the synthase of BHL. As OdDHL, BHL also binds its receptor RhIR at high concentration, followed by the activation of targets genes. The BHL-RhIR and LasR-OdDHL complexes activate genes including virulence related ones. In total, LasA protease, LasB elastase and Apr alkaline protease are regulated by the OdDHL based QS system. The BHL based circuit regulates the production of elastase, rhamnolipids, pyocyanin,

hydrogen cyanide. Meanwhile, pyocyanin, hydrogen cyanide and LecA lectin are influenced by the PQS-based QS. (Figure 7)

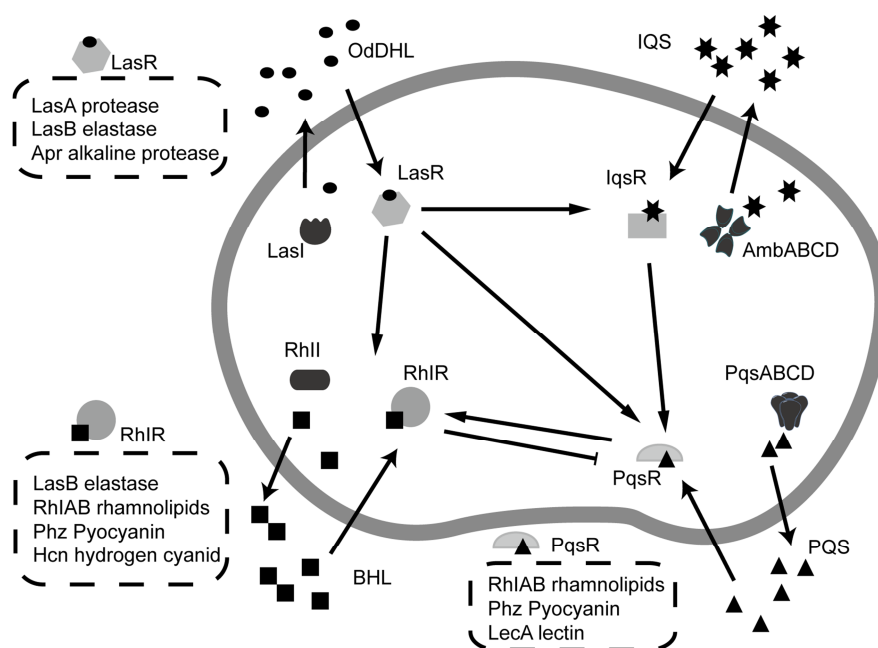


Figure 7: *P. aeruginosa* QS circuits and its virulence factors. OdDHL (4), BHL (3), PQS (17) and IQS (19) are synthesized by LasI, RhII, PqsABCD and AmbABCD and sensed by their cytoplasmic receptors LasR, RhIR, PqsR and IqsR respectively. The arrows between the proteins indicate a stimulated effect while perpendicular lines indicate an inhibitory effect. The arrows across the membrane show the diffusion direction of autoinducers. OdDHL (4), BHL (3), PQS (17) and IQS (19) are symbolized with black dots, squares, triangles and hexagrams.

In addition to its role in *Pseudomonas aeruginosa* and *Staphylococcus aureus*, QS is widely used by other bacterial strains, including *Escherichia coli*, *Vibrio cholerae*, *Bacillus cereus* and *Burkholderia cepacia*, to regulate virulence.²⁴ However, how QS regulates the virulence factors in these strains is less explored. More efforts are still needed in this field.

1.3 Quorum Sensing in Inter-kingdom Communication

For millions of years host cells have been surrounded closely by bacteria leading to the notion that communication should exist between them. Today, more and more pieces of evidence demonstrate that QS not only plays a role within the bacteria for signaling but also in inter-kingdom communication with their host such as plant and animals.³⁶⁻³⁹ Research into QS in inter-kingdom communication gives us a better understanding of the relationship between bacteria and their host.

OdDHL (4) produced in *Pseudomonas aeruginosa* can inhibit the production of interleukin 4 (IL-4) and interferon gamma (IFN- γ), which normally activate the proliferation of Th1 and Th2 T helper cells.⁴⁰ Furthermore, it can influence gene expression by means of disruption of nuclear factor kappa-light-chain-enhancer of activated B cells (NF- κ B).⁴¹ In addition to this anti-inflammatory effect, OdDHL also can induce a proinflammatory response. It can induce the production of interleukin 8 (IL-8) and cyclooxygenase (Cox-2) which will lead to better inflammation.⁴² More roles for OdDHL in bacteria-host communication can be found in its induction of apoptosis in different cell lines.³⁹

In fact, QS works in a complex signaling network in a bidirectional way. Although the autoinducers can affect the biological process within host cells, the QS system is under the influence of the host cells, too. In 2005, Draganov reported paraoxonases (PONs) act as lactonases that degrade AHLs in host cells.⁴³ The opioid dynorphin produced during the intestinal damage can be internalized by *Pseudomonas aeruginosa* to activate PQS-based QS circuit.⁴⁴ Three human sexual hormones, estrogen steroid hormones, estrone, estriol, and estradiol, were discovered to inhibit the expression of QS dependent genes by decreasing the concentration of the autoinducers.⁴⁵

Though the majority of host-pathogen relation research has been done in *Pseudomonas aeruginosa*, it is also reported that NADPH oxidase 2 (Nox2) and apolipoprotein B (ApoB) can inhibit the AIP signaling in *Staphylococcus aureus*.^{46,47} Meanwhile, along with the reports about the interactions between bacteria and human, there are findings in the interaction between bacteria and plants, too. In fact, many QS inhibitors of plant origin or plant extracts such as malabaricone C, halogenated furanones have been discovered.⁴⁸

Although QS has been intensely studied in bacteria, inter-kingdom communication has begun to draw more attention, as it plays an important role in regulating virulence, host defense and so on. Finally, efforts to discover and manipulate the relationship between bacteria and their host could benefit humans.

2 *In Vivo* Target Identification of Small Molecules

Today's cutting edge and versatile organic methodologies enable the modification and optimization of bioactive small molecules as well as their use in elucidation of biological phenotypes and drug discovery. Bioactive small molecules are discovered by phenotypic, cellular and target-based screening after either synthesis or purification from natural resources. Nevertheless, although the treatment of diseases with small molecules has a long history, the identification of their targets is still one of the most challenging and crucial steps in both academia and the pharmaceutical industry. To date, most drug targets fall into only a few select protein classes, such as kinases, G-protein coupled receptors and proteases. There is increasing demand for the discovery of novel protein targets, as well the off-targets of known drugs, which has led to an explosion of research in target engagement in chemical biology. Substantial efforts have been devoted to develop methods for target engagement with either proteomics, genetics, or bioinformatics approaches. Proteomics approaches usually directly interrogate the proteins which normally are the targets of small molecules.

Polypharmacology is the design or use of a single drug molecule able to interact with multiple targets. This concept is supported by observations from both genetic and proteomic research. In fact, because of the phenotypic robustness and network structure in living organisms, many clinically effective drugs address multiple targets instead of single one.⁴⁹ Polypharmacology has important implications for efficacy and toxicity in drug development. Moreover, the detection of protein-ligand interaction with purified proteins may differ to that in living systems, as the complex biological cellular context is lacking. Thus, it is very helpful to investigate the target engagement of bioactive small molecules in living systems to attribute pharmacological effects to perturbation of the protein (or proteins) of interest versus other mechanisms.

In conclusion, although there are versatile methods to study target engagement, widely applicable proteomic methodologies which allow the identification of multiple targets *in vivo* are most encouraging. The well-established method affinity/activity-based protein profiling (ABPP) is described here as a technique that generates an incomplete but very intriguing picture of *in vivo* target engagement. Together with some other emerging methods such as ligand-directed protein labeling, cellular thermal shift assay (CETSA), ABPP can deliver precise and quantitative information about the protein targets of small molecules.

2.1 Affinity/Activity-Based Proteome Profiling

Affinity/activity-based proteome profiling, sometimes known as affinity/activity-based chemical proteomics, is usually abbreviated as ABPP in publications. It was established by Cravatt⁵⁰⁻⁵³ and Bogoy⁵⁴⁻⁵⁶ based on previous work by Powers and Walkers.^{50,51} This functional proteomic technology utilizes chemical probes to react with their targets to gain more insights into the compound and/or proteins.

The cornerstone of ABPP is the design and synthesis of suitable probes analogous to the native bioactive small molecules. The probes should maintain the necessary structural elements to retain bioactivity, in which case structure-activity relationships should be first established. Probes also need to be equipped with a pre-tag at a tolerated position. The pre-tag is usually a terminal alkyne or azide facilitating the appending of reporter groups via click chemistry e.g. copper-catalyzed azide-alkyne cycloaddition (CuAAC). Nevertheless, the investigation of the reversible protein targets requires additional equipment of photoreactive group such as diazirine, benzophenone. This kind of photoreactive group is utilized to form covalent bonds between probes and their targets after UV irradiation. Since reversible force is labile in the experimental procedures, this covalent bond is used to ensure the probe sticking to its targets. (Figure 8)

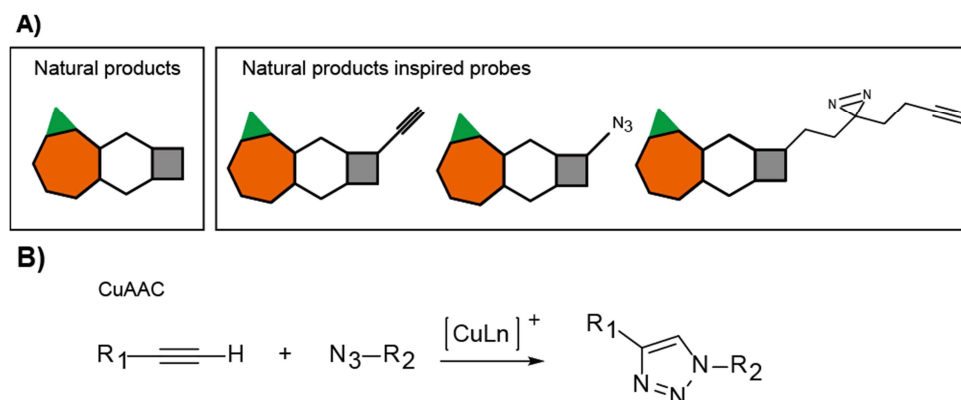


Figure 8. A) Typical activity-based probes based on natural products; B) Classic click chemistry: copper-catalyzed azide-alkyne cycloaddition (CuAAC). R_2 can be functional groups such as fluorophore or biotin.

After the organic synthesis of the affinity/activity-based probes (ABPs), their bioactivity needs to be compared with their native small molecules to ensure they share the same protein targets presumably related to the phenotypic change. A typical ABPP workflow is as follows. The probes or their controls are incubated with the living cells for a certain time at desired temperature (usually room temperature or that used to grow the cells). On one hand, during the incubation, the ligand will direct the probe to bind to its targets in either an irreversible

way or reversible way. For the latter case, the sample is treated with UV irradiation to induce covalent bond formation between the photoreactive group and the probe targets. The covalent bond either formed by spontaneous reaction or by photo-reaction between the ABP and its targets provides a robust complex for subsequent manipulation. With biological ligation, in most cases “click chemistry”, the reporter azide or alkyne tag enables attachment of a functional tag such as biotin or fluorophore. The fluorophore tag can be used for the visualization of protein targets by means of sodium dodecyl sulfate polyacrylamide gel electrophoresis (SDS-PAGE). The biotin tag allows the purification of the covalently bound targets with avidin beads followed by tryptic digestion and liquid chromatography-tandem mass spectrometry analysis (LC-MS/MS). On the other hand, the control samples are processed in parallel with the same procedure to assess for non-specific binding.

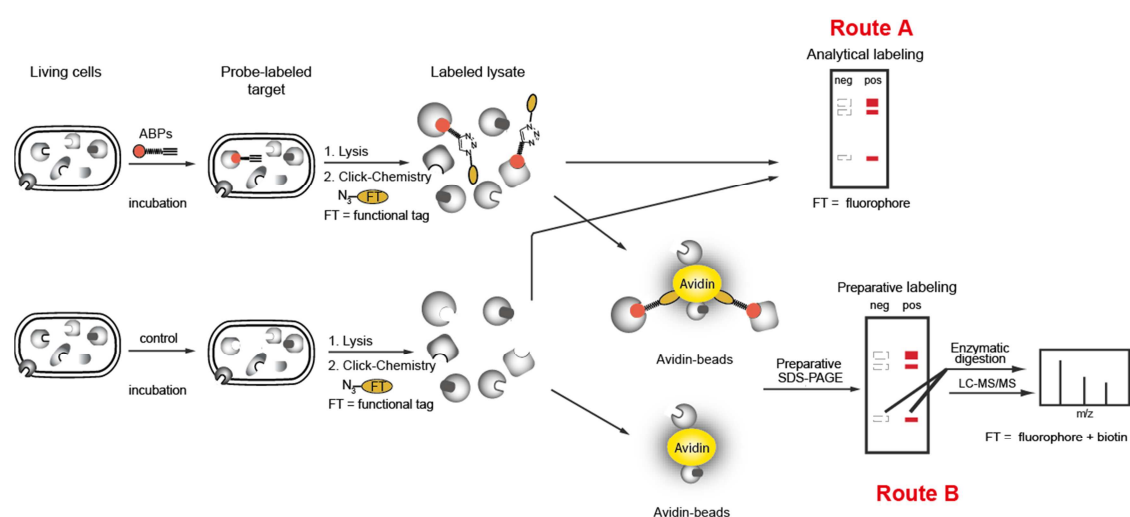


Figure 9: Basic concept of activity based protein profiling (ABPP). Route A: Analytical ABPP on SDS-PAGE for visualization of labeled protein targets; Route B: Preparative ABPP by using avidin-biotin affinity purification to isolate sufficient protein for subsequent LC-MS/MS analysis.

An analytical ABPP labeling by means of SDS-PAGE usually provides information after fluorescent scanning. These fluorescent bands signify the ligand labeled targets. A comparison between probe-treated samples and control samples reports the non-specific protein targets. ABPP via preparative SDS-gel was historically widely used to identify the protein targets of the probes. In this method, a trifunctional reagent containing the azide, biotin and fluorophore should be used in the click chemistry. The biotin enables the enrichment of protein targets on avidin beads. After cutting the promising bands on preparative SDS-gel based on their fluorescence intensity in probe-treated samples as well as their counterparts in the control samples, these cutted bands are then digested and analyzed

by liquid chromatography-tandem mass spectrometry (LC-MS/MS). The mass spectrometry intensities of individual protein targets are then compared between probe-treated samples and control samples. A promising target should exhibit much higher intensity in probe-treated sample than in control samples. Although this gel-based ABPP method is still useful for identification of highly specific or abundant targets, it can miss low-abundant protein targets and is imprecise in the case of cutting SDS-gel bands. Some proteins even cannot be well separated on SDS-gel. (Figure 9)

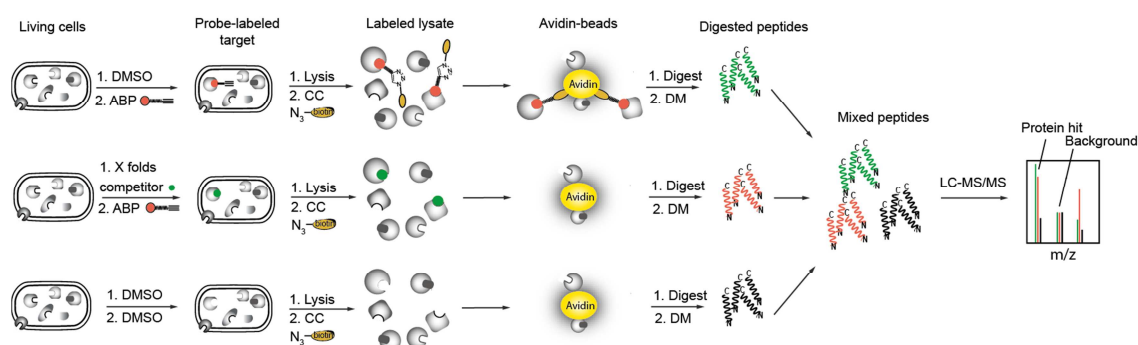


Figure 10: Basic concept of gel-free activity-based protein profiling (ABPP) employing dimethyl labeling. The activity-based probe (ABP) or its competitor or DMSO were incubated with living cells for certain time to allow the competition/binding of compounds to their protein targets. Afterwards, the cells were lysed followed by appending biotin azide to labeled proteins. These labeled proteins were then enriched on avidin beads. After tryptic digestion and isotope labeling, the treated samples were mixed and analyzed on LC-MS/MS to determine isotope ratios. Here CC denotes click chemistry and DM denotes stable isotope dimethyl labeling. The red dots denote ABP while the green dots denote its competitor. The competitor is usually used in excess ($X > 1$).

To date, ABPP is more often used in a gel-free way instead of a gel-based way. The use of quantification in gel-free ABPP aids in the identification of protein targets on a whole proteomic perspective.^{57,58} This quantification is often based on the comparison among vehicle control and probe incubated sample, competition with native bioactive small molecules, different but related probes, biological conditions.⁵⁹ The recent quantification approaches in ABPP can be divided into two sets of methods. The first set of methods is labeling approaches. iTRAQ (isobaric tag for relative and absolute quantitation),⁶⁰ TMT (tandem mass tag), and DiMe (dimethyl labeling)⁶¹ in this set enable chemical labeling of peptides from different samples at the end of protocol with isotopes. (Figure 10) These peptides are then combined and measured in the same LC-MS/MS run. Nevertheless, SILAC (stable isotope labeling by amino acids in culture) incorporates the isotopes into cells during incubation stage, which allows the combination of peptides from different samples directly

after lysis.⁶¹ The second set of quantification approaches is label-free methods including spectral counting and MS¹ intensity-based methods. Here the samples are needed to measure in different LC-MS/MS runs. The recent advances in sensitivity and resolution of LC-MS/MS techniques, and computational algorithms have greatly improved the quantification results with label-free methods.⁶²

A gel-free ABPP approach employing DiMe quantification is utilized in this dissertation. Its workflow is briefly shown above. Three samples are treated in different ways: probe vs. probe + competitor vs. vehicle control. After incubation, the living cells are lysed. After click chemistry and enrichment on avidin beads, the protein targets are digested and labeled with isotopes. The peptides then can be combined and analyzed on LC-MS/MS. Thus, a quantitative result can be obtained after analysis using Maxquant because of isotopes. (Figure 10)

In total, recent developments in high resolution mass spectrometry have had a significant impact on ABPP and the other target identification methodologies. There have also been advances in the software for processing and statistical analysis of LC-MS/MS data. The most promising hits can then be validated by means of techniques in genetics, proteomics and metabolomics. ABPP provides quite a direct determination of protein targets of bioactive small molecules and is becoming increasingly popular in the field of chemical biology. It has been successfully utilized to elucidate the protein targets of many bioactive small molecules such as showdomycin,⁶³ vancomycin,⁶⁴ orlistat,⁶⁵ hypothemicin,⁶⁶ duocarmycin,⁶⁷ and fimbrolides (this work),⁶⁸ and has been reviewed recently.^{59,69-71} However, it is worth noting that there are several limitations for this technique too. First of all, the ABPs always label some non-specific protein targets at high concentrations,⁷² thus a compromise between sufficient enrichment of the protein targets for detection and loss of specificity is required. ABPs sometimes address additional targets compared to the native small molecules on which they are based. Although this problem can be well solved by competitive experiments between probe and parent compound in activity-based protein profiling because of the robust covalent bond, competition may be less effective in affinity-based experiments using photoreactive probes. Second, quantitative proteomics is now popularly used to evaluate the significance of protein targets. However, as the quantitation is always based on the comparison of probe-treated and non-treated samples, it can sometimes give misleading results for protein targets of either very high abundance or low abundance because of the processing capacity and sensitivity of mass spectrum. A possible solution to this is the use of a cleavable linker which allows direct identification of probe modification.^{73,74} Meanwhile, how

to choose the threshold or cut-off criteria in the quantitative proteomics data is a continuing challenge. A final limitation is regarding affinity-based protein profiling. UV irradiation is essential to initiate the photo reaction to form a covalent bond between the probe and its targets. However, the efficiency of this reaction is sometimes low, especially in bacterial organisms which possess thick cell walls. There is also a risk that a probe in the deep pocket of its targets is to some extent shielded from UV resulting in no formation of covalent bond.

II – FIMBROLIDE NATURAL PRODUCTS DISRUPT
BIOLUMINESCENCE BY TARGETING AUTOINDUCER
BIOSYNTHESIS AND LUCIFERASE ACTIVITY

1. Introduction

1.1 Halogenated Furanones and Their Bioactivity

Natural products halogenated furanones (such as compounds **20** - **26** and **F1**) were isolated from the red alga *Delisea pulchra* and first reported in 1977.^{75,76} The red alga *Delisea pulchra* was investigated because it possesses quite special bioactivity. It can effectively stave off colonization by common epiphytes such as mosses, when compared with other algal species. The halogenated furanone natural products produced by this species are commonly described with a general formula $C_9H_9O_2BrRXY$ (X, Y can be either halogen or H; R can be H, OH, or OAc). Wells *et al.* named the compounds in the least polar fraction where R = H fimbrolides (such as compounds **F1** and **20**). (Figure 11)

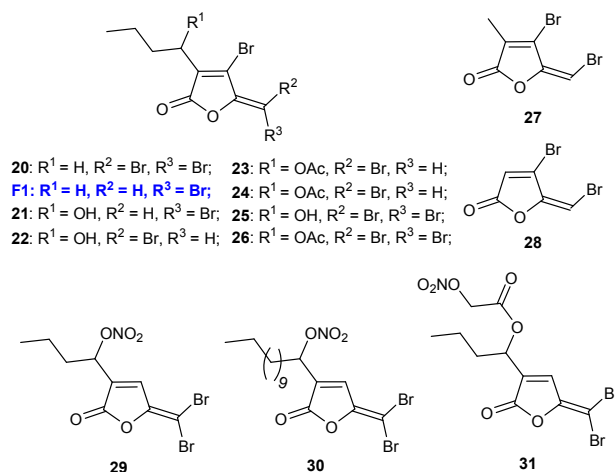


Figure 11: Halogenated furanones. **20** – **26** and **F1** are naturally occurring halogenated furanones. **20** and **F1** (highlighted in blue) belong to the class of compounds known as the fimbrolides. **27:** (*Z*)-4-Bromo-5-(bromomethylene)-3-methylfuran-2(5*H*)-one; **28:** (*Z*)-4-Bromo-5-(bromomethylene)-2(5*H*)-one; **29** – **31:** bioactive synthetic fimbrolide analogues used by Kumar *et al.*⁷⁷

Fimbrolides were first reported in 1996 to inhibit swarming motility of *Proteus Mirabilis*.⁷⁸ Further work has thrown more light on their bioactivities. It has been suggested that the combined use of **28** with Gallium could be an effective way to treat *P. aeruginosa* infections instead of monotherapy with Gallium.⁷⁹ Ren *et al.* employed **27** to reduce the persistence of *E. coli* and *P. aeruginosa* regardless of whether the cells were in a planktonic or biofilm state.⁸⁰⁻⁸³ Although no striking performance has been reported, **28** has been proven to be generally effective on clinical isolates of *P. aeruginosa* in terms of reducing the production of pyocyanin, elastase and alkaline protease.⁸⁴ The synthetic fimbrolide-nitric oxide hybrids **29**, **30**, and **31**

from Kumar *et al.* show better bioactivity as antimicrobials than the natural fimbrolides in both *P. aeruginosa* QS reporter assays and biofilm inhibition assays.⁷⁷ (Figure 11)

Defoird *et al.* reported that brominated furanones can protect brine shrimp larvae against *Vibriosis* by means of inhibition of QS. Furthermore, they synthesized the thiophenone compound **32** to reduce toxicity for use in aquaculture.^{85,86} (Figure 12) In addition to what has been briefly summarized here, brominated furanones have been found to regulate biofilm,⁸⁷⁻⁹³ virulence,⁹⁴⁻⁹⁶ swarming,⁸⁹ bioluminescence^{97,98} and other phenotypes in diverse bacterial strains. Moreover, several studies have demonstrated that brominated furanones have *in vivo* effect against pathogens in mice and brine shrimp experiments.^{85,86,99}

Based on the numerous reports about their bioactivity, halogenated furanones have been employed for device coating. Recently, it was reported that microarc-oxidized titanium implants with **28**-loaded poly(L-lactic acid) nanoparticles successfully prevent peri-implant infections at an early stage.¹⁰⁰⁻¹⁰² Other brominated furanones have been coated on polyvinyl chloride material and investigated for their effects on biofilm formation of *Escherichia coli*^{103,104} and *Staphylococcus aureus*.^{109,110,105} Furthermore, fimbrolide-coated lenses have been demonstrated to be safe as well as antibacterial and anti-acanthamoeba.¹⁰⁶ In addition, brominated furanones have been widely applied as QS inhibition controls, highlighting their importance in QS research.^{97,98,107}

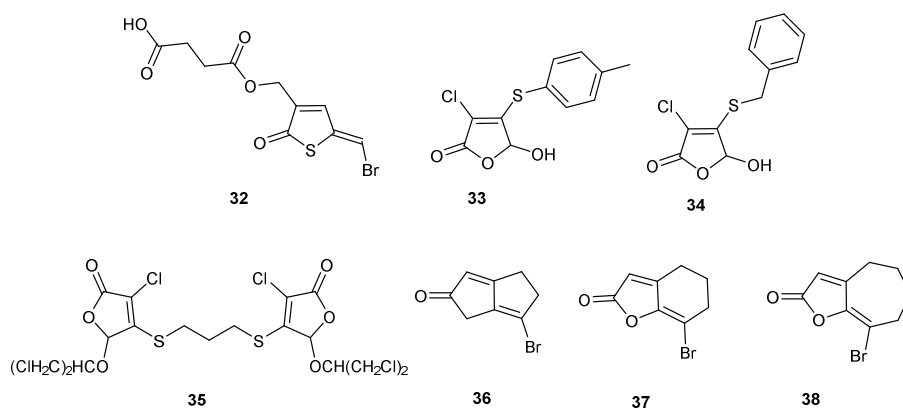


Figure 12: Synthetic 2(5H)-furanone compounds. **32** was reported by Defoirdt *et al.*^{85,86} while **33** – **35** and **36** – **38** were used by Kayumov^{108,109} and Luk¹¹⁰ respectively.

Inspired by the intriguing bioactivity of natural halogenated furanones, various 2(5H)-furanone compounds have been synthesized and tested for their bioactivity. In 2015, Kayumov reported that **33** - **35** can increase the sensitivity of *Bacillus subtilis* to antibiotics and that **34** is capable of disrupting formed *Bacillus subtilis* biofilm.^{108,109} Another new class of brominated furanones, **36** – **38**, which contain a bicyclic structure, exhibited reduced toxicity

to mammalian cells (human neuroblastoma SK-N-SH) while maintaining their ability to inhibit biofilm formation in *P. aeruginosa*. They also showed additional inhibition of virulence factor elastase B production.¹¹⁰ (Figure 12) In fact, some newly discovered brominated aromatic furanones from *Ascidian Synoicum* sp. such as cadiolide and rubrolides also exhibited significant bioactivity in diverse bacterial strains.¹¹¹⁻¹¹³

1.2 Possible Mechanisms

As fimbrolides or brominated furanones are quite often used in QS research, their targets and mode of action have also received much attention. The first efforts to elucidate the mechanism were performed by Givskov *et al.* In 1999, they suggested that brominated furanones bound or disfigured the OHHL binding site of LuxR in *Aliivibrio fischeri*.¹¹⁴ Furthermore, shortly after their first report, the same group reported there was no stable interaction between brominated furanones and the LuxR protein. Instead, the brominated furanones destabilized LuxR to modulate the QS activity: the half-life of LuxR was reduced up to 100 fold in their presence, as revealed by Western blot analysis.¹¹⁵ What made this action mode more puzzling was that the *Aliivibrio fischeri* LuxR mutant proteins were insensitive to inhibition by a known QSI (QS inhibitor) N-(propylsulfanylacetyl)-L-homoserine lactone while the mutagenesis had almost no reduction on inhibition by brominated furanones. The authors suggested that brominated furanones did not compete with OHHL in a “classic” way. However, the mode of action by which the fimbrolides destabilized LuxR remained unknown.¹¹⁶

Defoirdt *et al.* investigated the molecular mechanism by which natural product fimbrolide **F1** disrupted QS in *Vibrio campbellii* BB120 (formerly known as *V. Harveyi* BB120). *V. campbellii* possesses a more complex QS system than *Aliivibrio fischeri*, which consists of three different QS circuits, namely the HAI-1 circuit, AI-2 circuit and CAI-1 circuit. (Figure 13) **F1** was found to inhibit all of these three circuits suggesting its interaction with a downstream target of the LuxO protein. The *luxR_{vh}* mRNA levels in wild-type *V. campbellii* cells were not affected by the presence of **F1** based on the results from reverse transcriptase real-time polymerase chain reaction with specific primers. However, **F1** resulted in a significantly reduced level of LuxR_{vh} regulator protein in cell lysate able to bind to its target promoter sequences in mobility shift assays. The experimental result with purified LuxR_{vh} was in accordance with that in cell lysate. Based on these results, the authors suggested that **F1** manipulated the QS activity by its ability to render the QS master regulator protein LuxR_{vh} unable to bind to the promoter sequences.¹¹⁷

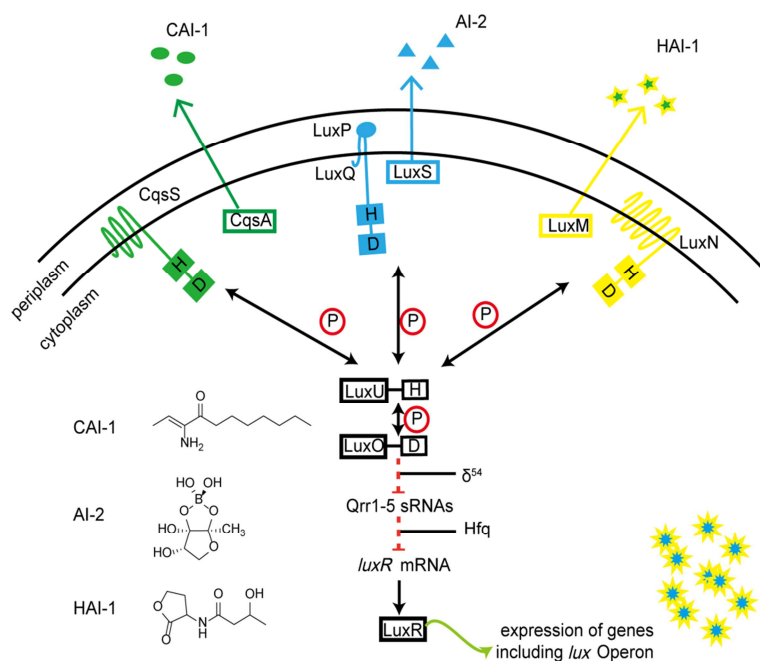
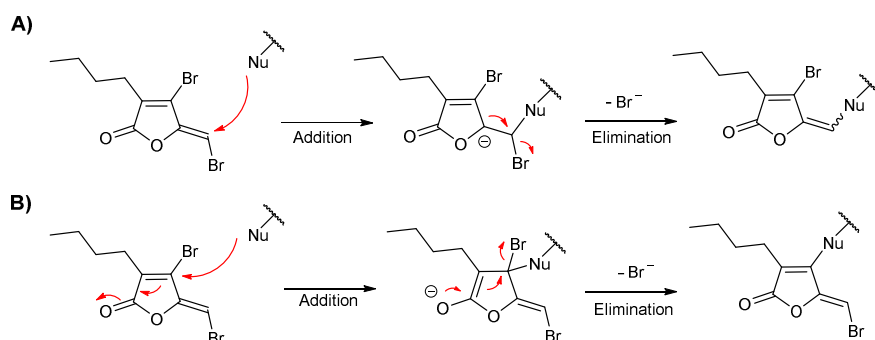


Figure 13. Three QS autoinducers are synthesized by LuxM (HAI-1), LuxS (AI-2) and CqsA (CAI-1) and sensed by LuxN (HAI-1), LuxP/LuxQ (AI-2) and CqsS (CAI-1) receptors. At low concentrations of autoinducers, the receptors autophosphorylate and transfer their phosphoryl groups to LuxU that in turn phosphorylates LuxO. LuxO~P activates the expression of Qrr1-5 sRNA that, together with the chaperone Hfq, destabilizes *luxR* mRNA. At high concentrations of autoinducers, the autophosphorylation of the receptors is inhibited and phosphate is drained from the cascade resulting in the expression of transcriptional regulator LuxR and thereby activating the *lux* operon and bioluminescence. P in red circle denotes phosphotransfer; H (histidine) and D (aspartate) denote the phosphorylation site.

The same natural fimbrolide **F1** was utilized by Zhou *et al.* to investigate the mode of action of fimbrolides.¹¹⁸ Recombinant LuxS from *Bacillus subtilis* was found to be modified by **F1** at Cys126. This alkylation of Cys126 may perturb proper metal binding and/or block substrate binding and then cause a reduction of enzymatic activity. From the suggested mechanism, an addition reaction followed by an elimination step facilitates the modification of LuxS by **F1**. (Scheme 1) An *in vitro* LuxS assay showed that recombinant LuxS was inactivated by **F1**, which further confirmed its role as a target of **F1**. However, Ren *et al.* reported that the reduction of persistence in *E. coli* by synthetic fimbrolide **27** cannot be attributed solely to its inhibition of AI-2 mediated QS. Similar inhibition of **27** can be observed in both wild-type *E. coli* RP437 and its $\Delta luxS$ mutant.⁸¹ Moreover, they proposed that non-QS related targets are involved in the ability of **27** to revert antibiotic tolerance of *P. aeruginosa* PAO1 persister cells.⁸³



Scheme 1: Possible mechanisms for LuxS modification by fimbrolide **F1** via an addition and elimination process. A) A nucleophilic amino acid reacts with the exocyclic vinyl group, followed by the elimination of exocyclic vinyl bromide. B) The nucleophilic amino acid reacts with the cyclic vinyl group followed by the elimination of bromine on the furanone ring. Nu here denotes the nucleophilic amino acid in LuxS.

1.3 The Aim of the Project

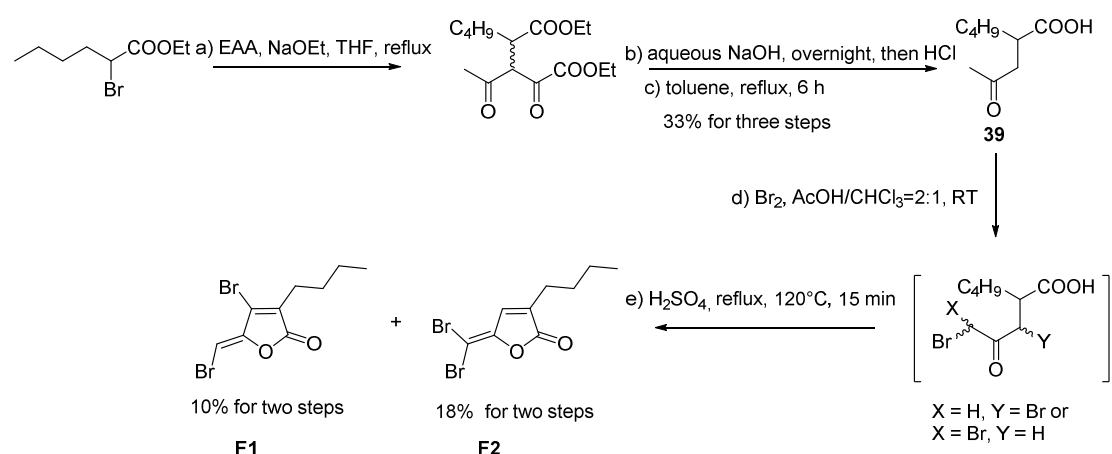
To date, the proposed protein targets of **F1** are controversial and no *in vivo* targets have been identified directly. Since fimbrolides have been applied as gold standards in the elucidation of the QS pathways, a full understanding of their mode of action and cellular targets is required and will have implications for related systems. The aim of the work described in this chapter is to unravel the cellular binding partners of fimbrolides in *Vibrios* by means of activity-based protein profiling with quantitative mass spectrometry, in order to contribute to a better understanding of these QS tool compounds.

2. Results and Discussion

2.1 Synthesis of Fimbroliide Based Probes

The fimbroliide commonly used in the mechanistic research is **F1** (*Z*)-4-Bromo-5-(bromomethylene)-3-butyl-2(*5H*)-furanone. It is often used in fimbroliide bioactivity research or as a control in QS research. Thus, **F1** based structures become the main concern in this project.

In fact, the first synthesis of **F1** by oxidation/dehydration of dibrominated 2-butyllevulinic acid was published shortly after the report of fimbroliides.¹¹⁹ Afterwards, this synthetic method was reinvestigated in details by Steinberg *et al.* in 1997.¹²⁰ It becomes a mature route to synthesize fimbroliides and thus was employed in this dissertation. First, ethyl 2-bromoalkanoates undergoes a nucleophilic reaction with EAA (ethyl acetoacetate) to give diethyl 3-acetyl-2-butyl-4-oxopentane dioate. Second, this diester was hydrolysed to yield diacid product with aqueous NaOH followed by neutralization with HCl. The diacid product can be easily converted to 2-(2-oxopropyl)hexanoic acid via decarboxylation during refluxing in toluene. The bromination of the keto-acid **39** was completed in a mixed solvent of CHCl₃ and AcOH with Br₂, resulting in a mixture of different brominated products. Finally, the multiple brominated 2-butyllevulinic acid was cyclized and dehydrated to give **F1** in concentrated sulfuric acid with **F2** as a byproduct. (Scheme 2)



Scheme 2: Synthesis of **F1** and **F2**. a) EAA, NaOEt, THF, reflux; b) aqueous NaOH, overnight, then HCl; c) toluene, reflux, 6 h, 33% over 3 steps; d) Br₂, AcOH/CHCl₃ = 2:1, RT; e) H₂SO₄, reflux, 120 °C, 15 min, 10% for **F1** and 18% for **F2** over 2 steps. THF = tetrahydrofuran, EAA = ethyl acetoacetate.

For the synthesis of suitable activity-based probes, it is most important to maintain their bioactivity as their parent compounds. To minimize the adverse effects caused by modification, the knowledge of structure-activity relationship is crucial. The previous reports have revealed the influence of individual structural elements of 3-alkyl-5-methylene-2(5*H*)-furanones on their bioactivity.^{92,121} Two major factors have big effects, namely the bromination pattern of the ring structure and the length of the 3-alkyl chain. (Figure 14)

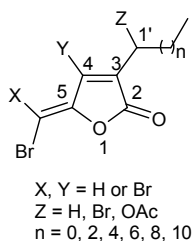


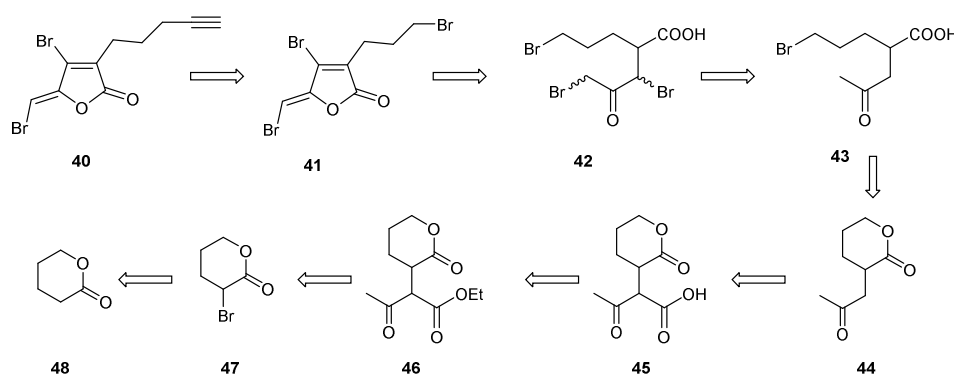
Figure 14: 3-Alkyl-5-methylene-2(5*H*)-furanones. The influence of different structural elements on bioactivity was investigated by Keersmaecker *et al.*¹²¹ and Luk *et al.*⁹²

First, the importance of bromination pattern of furanone ring structure reported by Keersmaecker *et al.*¹²¹ is in accordance with the report from Luk *et al.*⁹² A conjugated exocyclic vinyl bromide but not the vinyl bromide on the furanone ring is believed to be crucial for the bioactive properties. This structural element is essential to keep compounds non-toxic as well as important for fimbrolide inhibition of biofilm formation in *Salmonella* and *Escherichia* and bioluminescence in *Vibrios*. The dibrominated compounds with one bromine atom on the 4-position of furanone ring and the other on the methylene group (X = H, Y = Br) were found to be much more active than those with a dibrominated methylene group (X = Br, Y = H). Thus, the **F1** ring structure should be kept intact during the probe design.

Second, a suitable length of 3-alkyl chain is required for the bioactivity of 1'-unsubstituted 3-alkyl-5-methylene-2(5*H*)-furanones. The absence of the alkyl chain results in growth inhibition in both *Salmonella* and *Vibrio* strains.^{92,121} On the other hand, a long 3-alkyl chain will render 3-alkyl-5-methylene-2(5*H*)-furanones incapable of reducing the biofilm formation (such as octyl chain and longer ones) or bioluminescence (dodecyl chain). 1'-unsubstituted 3-alkyl-5-methylene-2(5*H*)-furanones with ethyl, butyl or hexyl side chains can inhibit the biofilm formation of *Salmonella* at relatively low concentrations while these compounds do not affect the planktonic growth at these concentrations. A butyl to decyl side chain version of 1'-unsubstituted 3-alkyl-5-methylene-2(5*H*)-furanones inhibit the bioluminescence at a concentration-dependent manner without showing any growth inhibition. Therefore, a chain

length of two to six carbon atoms on (*Z*)-4-bromo-5-bromomethylene-3-alkyl-2(*5H*)-furanones should be preferred in our designed probe.

In fact, besides these two major influential factors for the bioactivity, the introduction of functional groups into the 1'-position of 3-alkyl chain has a complex influence. On one hand, the introduction of bromine into 1'-position enhances the bioactivity of (*Z*)-4-bromo-5-bromomethylene-3-alkyl-2(*5H*)-furanones in both biofilm and bioluminescence inhibition compared with their non-substituted counterparts (*Z* = H). On the other hand, this introduction inhibits the bacterial growth and makes it difficult to differentiate quorum quenching and growth inhibition in *Vibrios*, the QS research model systems. When an acetoxy group is introduced to the 1'-position of **F1** 3-alkyl chain, dramatic decrease in bioluminescence inhibition can be observed as the IC_{50} increases from 1.4 μ M to 50 μ M. Since the 1'-position of 3-alkyl chain is very close to the furanone ring, the target binding moiety, a remoter modification on the aliphatic chain rather than 1'-position should be given priority to.

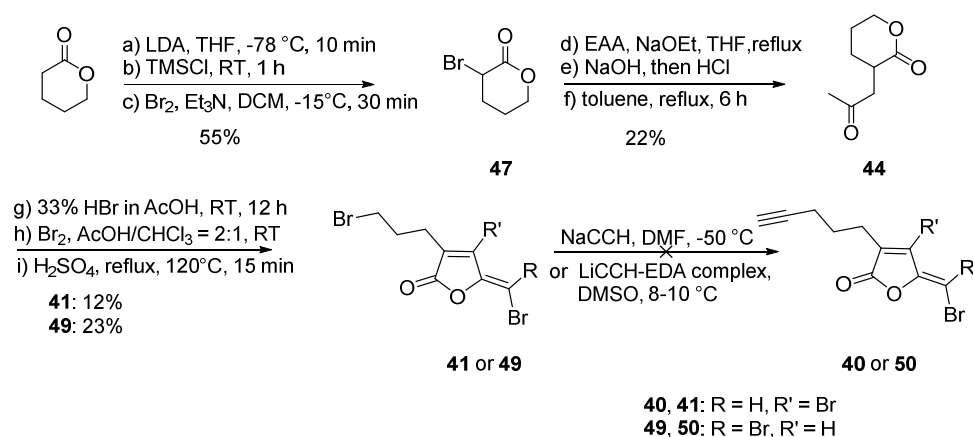


Scheme 3: Retrosynthetic analysis to activity-based probe following a similar route described by Steinberg *et al.*¹²⁰ A bromine atom on the 3'-position of 3-alkyl chain in **43**, **42**, **41** is derived from the ring-opening reaction of **44**.

According to the reported structure activity relationship, the modification required for ABPs should be carried out on 2', 3' or 4'-position of the aliphatic chain of **F1** in order to keep the bioactivity as well as cause no further toxicity in bacterial strains. Nevertheless, although an early insertion of the terminal alkyne is beneficial for a versatile library of probes, the harsh conditions in the synthetic route (scheme 2) significantly impede its realization. On the other hand, the remarkable difference between halogenated furanones and their precursors in structure sheds doubts on an early insertion of the terminal alkyne. As no functional groups such as hydroxyl group, carboxyl group or amino group are on **F1** to allow a straightforward installment of the terminal alkyne, a functional group which can tolerate harsh reaction conditions and facilitate the terminal alkyne incorporation after the fimbrolide core structure

formation needs to be created. Herein, a synthetic route to achieve this goal was designed as shown in scheme 3.

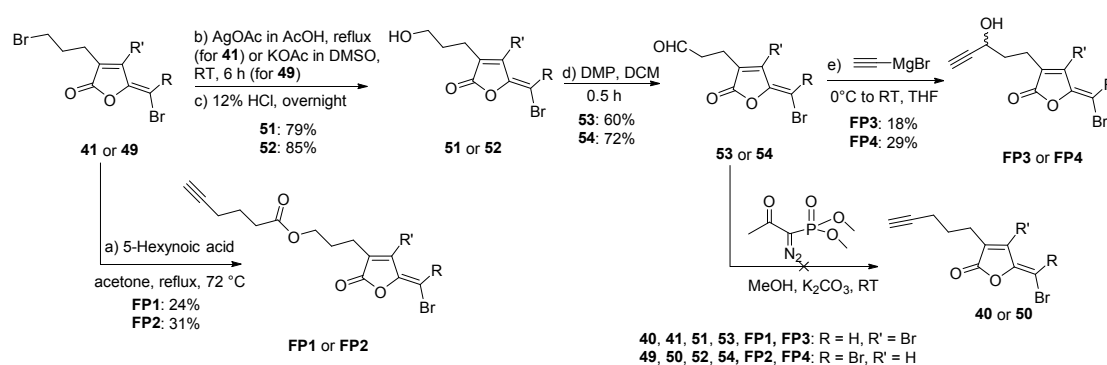
In our retrosynthetic analysis, target probe **40** is derived from **F1** with a minor modification on its aliphatic chain. A bromine atom on the aliphatic chain of **41** is designed to facilitate the installment of the terminal alkyne with well reported lithium or sodium acetylide reagent.^{122,123} The precursor **41** is supposed to be synthesized via cyclization of **42** following bromination of **43**.¹²⁰ Ring-opening of 3-(2-oxopropyl)tetrahydro-2*H*-pyran-2-one **44** with HBr is designed to prepare **43**.^{124,125} The synthesis of **44** starts with α -bromo- δ -valerolactone **48** instead of an ethyl 2-bromoalkanoate but follows a similar synthetic route as **39** in scheme 2. (Scheme 4)



Scheme 4. Synthesis of ABPs **40** and **50**. a) LDA, THF, -78 °C, 10 min; b) TMSCl, RT, 1h; c) Br₂, Et₃N, DCM, -15 °C, 30 min, 55% over 3 steps; d) EAA, NaOEt, THF, reflux; e) aqueous NaOH, overnight, then HCl; f) toluene, reflux, 6 h, 22% over 3 steps; g) 33% HBr in AcOH, RT, 12 h; h) Br₂, AcOH/CHCl₃ = 2:1, RT; i) H₂SO₄, reflux, 120 °C, 15 min, 12% for **41** and 23% for **49** over 3 steps; LDA = lithium diisopropylamide, THF = tetrahydrofuran, TMSCl = trimethylsilyl chloride, EAA = ethyl acetoacetate, DMF = dimethylformamide, EDA = ethylenediamine.

As planned, the starting material α -bromo- δ -valerolactone **47** was synthesized from commercially available δ -lactone in a yield of 55% over three steps.^{126,127} First, the deprotonation of δ -lactone by LDA (lithium diisopropylamide) in a solvent mixture of tetrahydrofuran and heptanes resulted in the lithium enol which was then protected by trimethylsilane. The (3,4-dihydro-2*H*-pyran-6-yloxy) trimethylsilane was brominated by bromine in DCM. In this step, Et₃N acts as a catalyst to polarize the bromine as well as it drives the reaction by its formation of salt with HBr as a byproduct. The synthesis of 3-(2-oxopropyl)tetrahydro-2*H*-pyran-2-one **44** from α -bromo- δ -valerolactone **47** employed a similar synthetic route as **39** in scheme 2. However, the yield dropped to 22% for **47** from 33%

for **39** because of the ready polymerization property of δ -valerolactone and its ring opening side reaction in strong basic condition. The desired ring-opening of 3-(2-oxopropyl)tetrahydro-2*H*-pyran-2-one **44** using 33% HBr in AcOH allowed the incorporation of bromine atom into the alkyl chain and gave 5-bromo-2-(2-oxopropyl)pentanoic acid.^{124,125} This pentanoic acid was brominated with bromine and then cyclized into bromide-substituted precursors **41** and **49** in a yield of 12% and 23%, respectively. However, the initial designed methods with versatile acetylide reagents to install terminal alkyne failed. In fact, it turned out that the fimbrolide main structure is very vulnerable to nucleophilic reagents and basic conditions during our further efforts to incorporate the terminal alkyne.



Scheme 5. Synthesis of fimbrolide based probes from **41** and **49**. a) 5-hexynoic acid, acetone, reflux, 72 °C, 24% for **FP1** and 31% for **FP2**; b) AgOAc in AcOH, reflux, 6 h (for **41**) or KOAc in DMSO, RT, 6 h (for **49**); c) 12% HCl, overnight, 79% for **51** and 85% for **52** over 2 steps; d) DMP, DCM, 0.5 hour, 60% for **53** and 72% for **54**; e) ethynylmagnesium bromide in THF, 0 °C to RT, 18% for **FP3** and 29% for **FP4**. THF = tetrahydrofuran, DMSO = dimethyl sulfoxide, DMP = Dess-Martin periodinane, DCM = dichloromethane.

Prior to employing Seyferth-Gilbert homologation reaction to the desired probes **40** and **50**, two probes **FP1** and **FP2** were synthesized via nucleophilic substitution of **41** and **49** with 5-hexynoic acid. This reaction was performed in acetone with 3 equivalents of carboxylic acid without the presence of any bases. Nevertheless, the yield is only 24% for **FP1** and 31% for **FP2** respectively even in this slightly acidic condition. The terminal alkyne was attached by an ester bond in **FP1** and **FP2** which possibly hydrolyses in the presence of esterase. Nevertheless, a more robust bond to connect the alkyne moiety with the fimbrolide core structure is preferred in ABPP experiments. (Scheme 5)

The preference for acidic condition of fimbrolide **F1** core structure became more obvious in the subsequent synthetic steps. The substitution of bromine with acetoxy group in **49** can be smoothly achieved in DMSO with weak base KOAc in a good yield.¹²⁸ However, the same

condition was not tolerated by **41** containing one exocyclic vinyl bromide but not two as **49**. Thus, AgOAc in pure acetic acid was employed to furnish this substitution.¹²⁹ The fimbrolide structure turned out to be remarkably stable in this acidic condition with heating and refluxing. The acetoxy group substituted products of **41** and **49** were then hydrolysed with 12% aqueous HCl to give the alcohol counterparts **51** and **52** in good yields.¹³⁰ The alcohols were oxidized to aldehydes **53** and **54** via Dess-Martin reagent.^{131,132} The aldehydes were subsequently used in Seyferth-Gilbert homologation reaction with Bestmann-Ohira reagent in order to synthesize **40** and **50**. Nevertheless, the basic condition with K₂CO₃ prevented the success. After screening different methods, the terminal alkyne was finally attached to fimbrolide core structure by the reaction between the ethynylmagnesium bromide and aldehydes **53** and **54**.¹³³ These two ABPs **FP3** and **FP4** possess a robust C-C bond to conjugate the alkyne to their fimbrolide core structure, which is beneficial for their application in ABPP approach. (Scheme 5)

2.2 Biological Activity of Fimbrolides and Their Probes in *Vibrios*

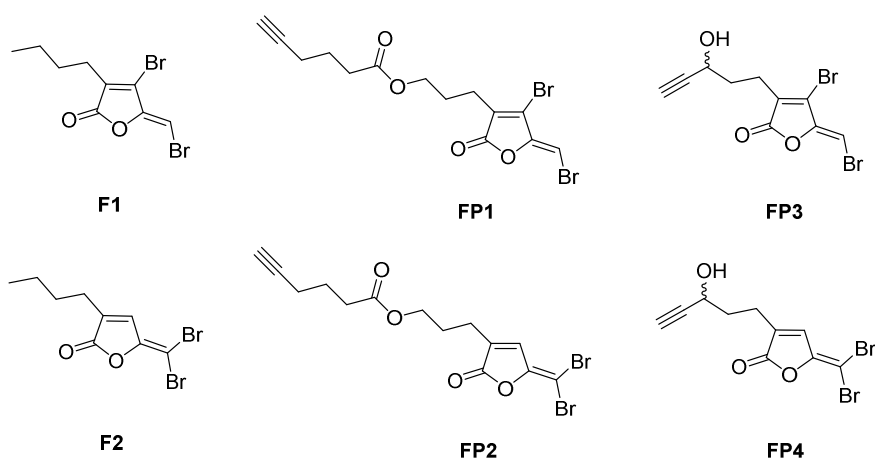


Figure 15: Structures of fimbrolides and their activity-based probes used in biological test.

After the synthesis of fimbrolides (**F1** and **F2**) and their corresponding activity-based probes (**FP1** - **FP4**), their bioactivity needs to be tested. As the aim of this project is to discover the QS related targets of fimbrolide in bacterial strains, a QS regulated phenotype should be employed. Bioluminescence came into my consideration as it is a typical QS research phenotype in *Vibrios*. Meanwhile, bioluminescence assay can be performed in a short time with accessible equipments. In fact, it can be considered as a QS inhibitor screening assay. Moreover, the *Vibrios* are not only the strains where QS was discovered in but also their QS

circuits are most intensely studied and best known.^{12,134} They are the model systems in QS study. All of these traits will benefit this project a lot in the future target profiling, which motivates me to start the research in *Vibrios* and utilize bioluminescence as the fimbrolide bioactivity test phenotype.

QS regulation in bacteria is based on the concentrations of the autoinducers which correlate to the density of the bacterial cells. Thus, the inhibition of bacterial growth should not affect the QS related research. To investigate whether our fimbrolide compounds had any effects on bacterial growth, their minimal inhibitory concentrations (MICs) were tested in *V. harveyi* NBRC 15634 and *V. campbellii* ATCC BAA-1116. In accordance with the previous reports,¹²¹ **F1** and **F2** did not show bacterial growth inhibition below 200 µM in both strains. Three probes, **FP1**, **FP2** and **FP3** exhibited the same bioactivity in this case as **F1** and **F2**. However, probe **FP4** proved to be adverse for the bacterial growth and showed a MIC value of 100 µM in *V. harveyi* NBRC 15634 and 125 µM in *V. campbellii* ATCC BAA-1116. To avoid the confusion of bioluminescence inhibition caused by growth inhibition and QS interruption, **FP4** was thus excluded from the further analysis. On the other hand, the other five fimbrolide compounds were applied in the bioluminescence assay in both *Vibrio* strains.

Table 1. MIC values of fimbrolides in *V. harveyi* NBRC 15634 and *V. campbellii* ATCC BAA-1116.

	<i>Vibrio harveyi</i> NBRC 15634	<i>Vibrio campbellii</i> ATCC BAA-1116
F1	>200µM	>200µM
F2	>200µM	>200µM
FP1	>200µM	>200µM
FP2	>200µM	>200µM
FP3	>200µM	>200µM
FP4	100µM	125µM

In *V. harveyi* NBRC 15634, **F1** and **FP3** which share a mono-bromine substituted exocyclic methylene group exhibited the best inhibition activity in bioluminescence assay. Their IC₅₀ values are 13 µM and 11 µM respectively which are in accordance with the previous report.⁹⁸ Nevertheless, **FP1** possessing the same moiety showed much weaker bioactivity with a IC₅₀ value at 62 µM. This can be explained by the previously mentioned structure activity relationship. A suitable length of 3-alkyl chain is needed for 3-alkyl-5-methylene-2(5*H*)-furanones inhibition of both bioluminescence and biofilm formation. A rather long 3-alkyl

chain such as a dodecyl chain will result in the loss of bioactivity.

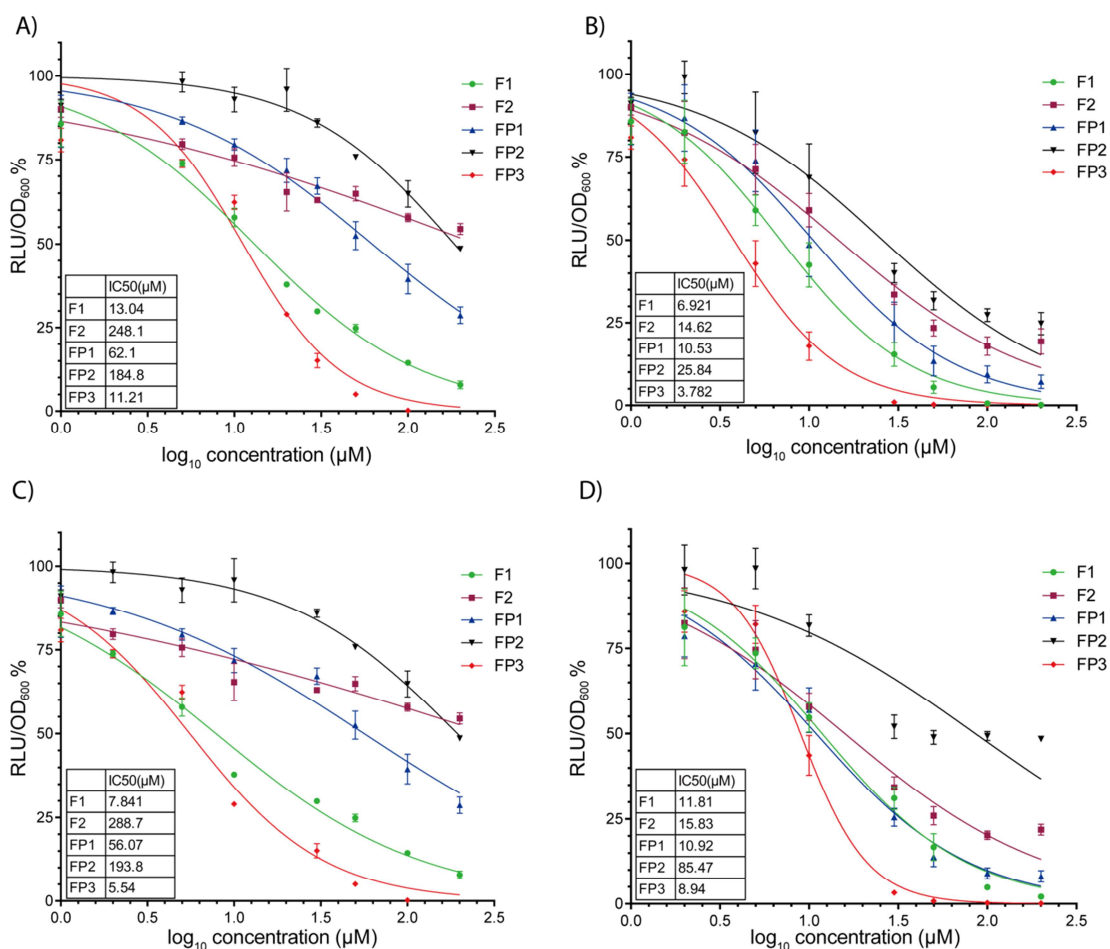


Figure 16: Inhibition of bioluminescence production by fimbrolides after 30 min incubation with *V. harveyi* NBRC 15634 (A), *V. campbellii* ATCC BAA-1116 (B), *V. campbellii* ATCC BAA-1116 $\Delta luxS$ (C), *V. campbellii* ATCC BAA-1116 $\Delta luxO$ (D). Relative luminescence units (RLU) were normalized to cell density (OD₆₀₀) and to the DMSO control. The data was based on three biological experiments with technical triplicates.

The performance of our fimbrolides in bioluminescence assay of *V. campbellii* ATCC BAA-1116 provided much information regarding their targets as well as confirmed the reports from other publications.¹³⁵ As in *V. harveyi* NBRC 15634, **F1** and **FP3** are the best inhibitors among these five fimbrolides in *V. campbellii* ATCC BAA-1116 wild type, its $\Delta luxS$ and $\Delta luxO$ mutant. Nevertheless, the IC₅₀ values are different and provide us a clue to possible fimbrolide targets. **F1** and **FP3** showed the best IC₅₀ values at 6.9 µM and 3.8 µM respectively in the wild type strain. However, the values increased to 7.8 µM and 5.5 µM in $\Delta luxS$ mutant strain and 11.8 µM and 8.9 µM in $\Delta luxO$ mutant strain. The increase of IC₅₀ values indicated some protein

targets upstream of LuxO were possibly involved. Moreover, although LuxS was proposed to be the protein target of fimbrolide **F1**, it cannot be the sole target as **F1** inhibited the bioluminescence in $\Delta luxS$ mutant. The inhibition of bioluminescence production in $\Delta luxO$ mutant by fimbrolides strongly suggested some other protein targets involved in the downstream of LuxO.

What was also intriguing was the different performance of **F2**, **FP1**, **FP2** in bioluminescence assay in three *V. campbellii* ATCC BAA-1116 strains. In the wild type, these compounds were still not as active as **F1** and **FP3**. However, they showed much better bioactivity compared with that in *V. harveyi* NBRC 15634. Their IC_{50} values were 10.6 μ M, 14.5 μ M, 25.8 μ M which were close to those of **F1** and **FP3**. Their similar bioactivity can be observed in *V. campbellii* ATCC BAA-1116 $\Delta luxO$ mutant except that of **FP2**. Nonetheless, **F2**, **FP1**, **FP2** were much worse inhibitors in *V. campbellii* ATCC BAA-1116 $\Delta luxS$ mutant compared with **F1** and **FP3**, which was quite in line with that in *V. harveyi* NBRC 15634.

Given to the excellent performance of natural product **F1** and its corresponding probe **FP3** in bioluminescence assays in *Vibrios*, they were thus employed in the subsequent proteomic experiments.

2.3 *In Vivo* Target Identification via ABPP

Although some QS related proteins such as LuxR, LuxS have been proposed to be the targets of fimbrolide **F1**, most of the data is based on isolated proteins. By now, no comprehensive proteomic analysis of the full complement of bacterial targets is available for fimbrolides. As fimbrolides can be considered as gold standards⁹⁸ in the elucidation of QS pathways, a complete understanding of their mode of action and cellular targets is beneficial for their future use in QS research.

ABPP is a powerful tool to give a rather direct determination of protein targets of small molecules. Its *in vivo* approach allows the target fishing in a physiological environment and thus can be considered as a relatively precise technique of target profiling for bioactive small molecules. A suitable activity-based probe is a prerequisite for the use of ABPP technique and crucial for its success. As **FP3** possesses a terminal alkyne handle and does show a slightly better bioactivity than **F1**, it sufficiently fulfills the requirements for ABPP approaches.

2.3.1 *In Situ* Analytical Labeling

Quantitative ABPP approach is usually time-consuming. As well, it requires an optimal labeling condition. Thus, *in situ* analytical labeling by means of SDS-PAGE is still useful even in the present era of quantitative ABPP. It can be completed in a short time and provides general information how well protein targets can be bound by activity-based probes and competed by the natural products. The information allows optimization of the concentration of compounds in quantitative ABPP, as well as other binding conditions such as buffers, incubation time of living cells with compounds. (Figure 9)

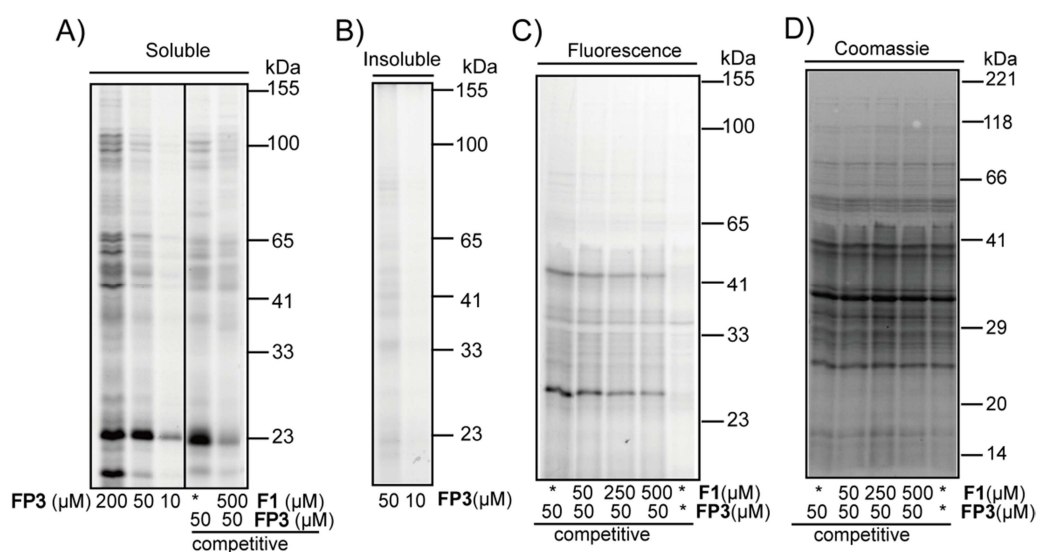


Figure 17. A) Fluorescent SDS-gel of *in situ* labeled *V. Harveyi* with **FP3** (various concentrations) and competitive *in situ* labeling of 50 μM **FP3** versus a 10-fold excess of **F1** (soluble fraction). B) Fluorescent SDS-gel of 50 μM and 10 μM **FP3** *in situ* labeling of *V. harveyi* in insoluble fraction shows much less pronounced labeling compared to the soluble fraction. C) Fluorescent SDS-gel of competitive *in situ* labeling with 50 μM **FP3** versus various concentrations of **F1** in *V. campbellii* ATCC BAA-1116. D) Coomassie stained SDS-gel for C). *denotes where DMSO was added as a control instead of the compounds.

Two kinds of *in situ* analytical labeling in *V. harveyi* NBRC 15634 with **FP3** and **F1** were carried out: the concentration-dependent one and the competitive one. In the concentration-dependent *in situ* analytical labeling, the bacterial cells were incubated with various concentrations of the alkyne-tagged probe **FP3** (here 200 μM , 50 μM , 10 μM were used) for one hour at room temperature. During this stage, the probe was supposed to bind to their protein targets in cells. Afterwards, the excess of **FP3** was washed out. After lysis of the cells, click chemistry facilitated the attachment of a fluorescent dye (rhodamine) with terminal

alkyne moiety of **FP3**. The whole proteome was separated by centrifugation to soluble and insoluble fraction. Both fractions were then separated via SDS-PAGE. The fluorophore enabled the visualization of **FP3** labeled targets by fluorescent scanning. **FP3** binds to its targets in a concentration-dependent manner as revealed by the decreased intensity of the fluorescence with a decreased probe concentration (Figure 17). What was noteworthy was the labeling in soluble fraction was much more pronounced than that in insoluble fraction. Therefore, we focused on the soluble fraction in the future experiments. Nevertheless, it is still hard to tell whether the protein targets labeled by **FP3** are shared by **F1** only with concentration-dependent *in situ* labeling results. Thus, the competitive *in situ* analytical labeling was performed with **FP3** and **F1** in order to investigate how well these protein targets were shared by them. The similar procedure was carried out as in the concentration-dependent experiments. Nevertheless, a 10-fold of **F1** was added to incubate with the bacterial cells for one hour prior to the addition of **FP3**. In this case, most of their shared protein targets should be bound by **F1**. As **F1** does not have a terminal alkyne handle, it is not able to undergo the click chemistry and be attached by the fluorophore. Only the remaining shared protein targets can be labeled by **FP3** and visualized to show decreased fluorescent intensity after the click chemistry and fluorescent scanning. Moreover, the protein targets which can only be labeled by **FP3** will remain their fluorescence intensity as in concentration-dependent *in situ* analytical labeling experiments. It turned out that most of protein targets labeled by **FP3** are shared by **F1**, which enhanced my confidence in successful target identification of natural fimbrolide **F1** with **FP3**. This competitive *in situ* analytical labeling method was also done in *V. campbellii* ATCC BAA-1116. Although a different labeling pattern was present in this strain, most of the protein targets labeled by **FP3** were also shared by **F1**. (Figure 17)

With these *in situ* analytical labeling results, the feasibility of activity-based probe **FP3** to elucidate protein targets of natural fimbrolide was further confirmed besides its bioactivity. Meanwhile, an optimal concentration of **FP3**, 50 μ M was selected for the quantitative ABPP approach as it was sufficient for distinct labeling.

2.3.2 Gel-Free Target Identification

ABPP approach becomes more and more efficient after its implementation with the liquid chromatography-tandem mass spectrometry (LC-MS/MS) analysis. Here I used triplex stable isotope dimethyl labeling in gel-free ABPP target identification method to get a quantitative comparison of labeled protein targets (Figure 10).

Three different types of samples were prepared for gel-free MS analysis to obtain a comprehensive overview of all irreversible **FP3** targets shared with natural product **F1**. Their main difference was how they were incubated with probe **FP3**, natural product **F1** or DMSO. For type 1 samples or the enriched samples, bacterial cells were first incubated with DMSO for two hours and then incubated with **FP3** for one and a half hours at room temperature. The type 2 samples were competitive samples as the bacterial cells were first incubated with 20-fold excess of **F1** for two hours prior their one and a half hours' incubation with **FP3**. Type 3 samples were always treated with DMSO during the incubation time and they were blank control samples. Following the ABPP approach, the enriched proteins of these samples were labeled with light, medium or heavy isotopes via dimethyl labeling after tryptic digest. The samples were then mixed and measured on LC-MS/MS. After quantitative analysis of the mass spectrum data based on the mass difference of the isotopes, two useful sets of ratios can be generated. The first set was the ratios between type 1 samples and type 3 samples, which can be named as **FP3/DMSO**. It was based on enriched folds of the protein targets labeled by **FP3** versus DMSO. It signifies how specific it is for **FP3** to bind its protein targets. In general, the higher value it is, the more specifically **FP3** binds to this protein. Meanwhile, the ratios between type 1 samples and type 2 samples comprise the second set of data. It can be named as **FP3/FP3+F1**. This set provided the information how well the protein targets were shared by **FP3** and **F1**. It diminishes the drawback that the employment of activity-based probe but not the natural products in ABPP approach. In total, these two sets of data are complementary to each other. A more accurate overview of protein targets of natural product fimbrolide **F1** can be generated based on both of them rather than only one of them. In *V. harveyi* NBRC 15634, seven protein targets were well enriched and showed excellent significance above the cut-off criteria in **FP3/DMSO** set data (\log_2 -fold enrichment ≥ 3 and $-\log_{10}(\text{p-value}) \geq 2.5$). And three of them, namely S-ribosylhomocysteine lyase (LuxS), inosine monophosphate dehydrogenase-related protein (IMPD) and acetoacetyl-CoA reductase (PhaB), were well competed (\log_2 -fold enrichment ≥ 3.5 and $-\log_{10}(\text{p-value}) \geq 4$) by natural fimbrolide **F1** as shown in **FP3/FP3+F1** set data. They were supposed to be the most specific protein targets for both **FP3** and **F1**. As **FP3** and **F1** exhibited good inhibition in bioluminescence assay, these shared targets or at least some of them were probably involved in the phenotypic alteration (Figure 18A and 18B).

In *V. campbellii* ATCC BAA-1116, six and four protein targets emerged from the complex proteomic background according to our criteria in **FP3/DMSO** (\log_2 -fold enrichment ≥ 3 and $-\log_{10}(\text{p-value}) \geq 3$) and **FP3/FP3+F1** (\log_2 -fold enrichment ≥ 2 and $-\log_{10}(\text{p-value}) \geq 5$) set data

respectively. Three protein targets are shared by both sets of data in *V. campbellii* ATCC BAA-1116. Two of them, LuxS and IMPD, are also select protein targets from the data of *V. harveyi* NBRC 15634. Although PhaB also emerged as a good target, it was not promising in *V. campbellii* ATCC BAA-1116 as in *V. harveyi* NBRC 15634 regarding both its enrichment by **FP3** and competition by **F1**. (Figure 18)

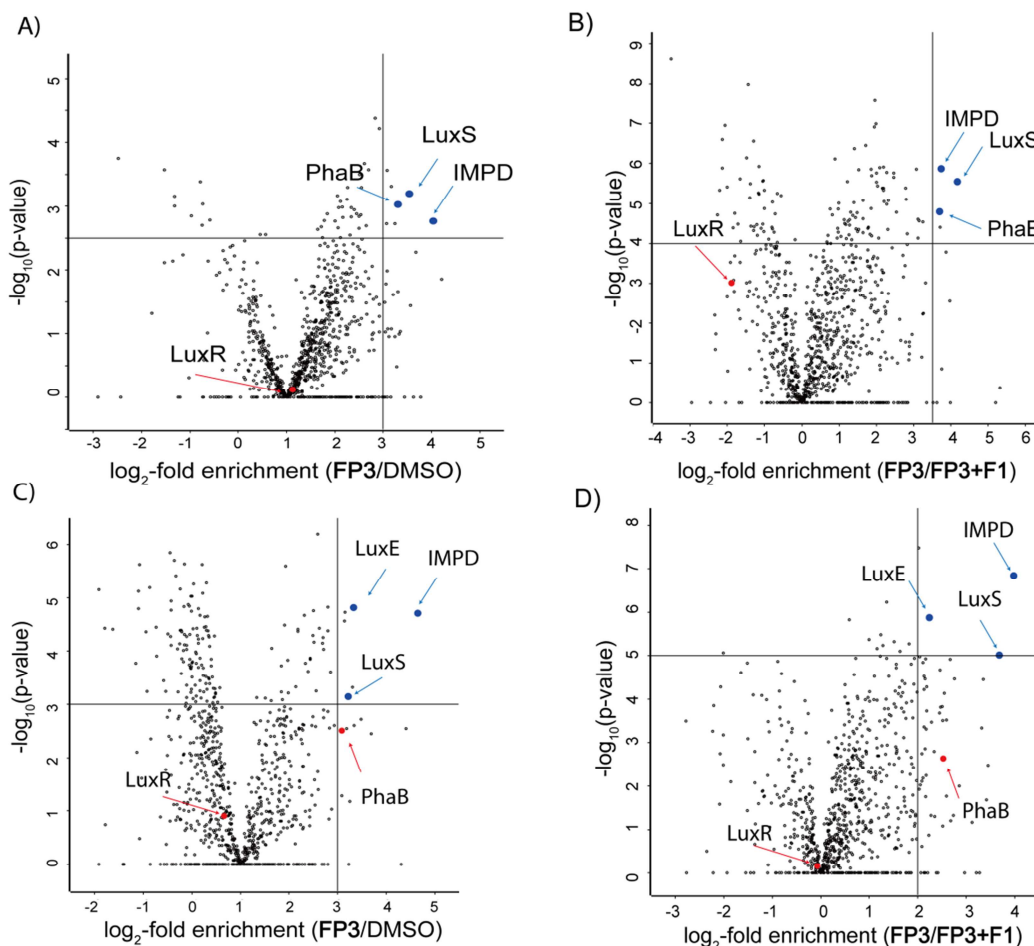


Figure 18: Volcano plots of gel-free ABPP experiments for target identification. A) Volcano plot of gel-free ABPP experiments with 50 μM **FP3** vs. DMSO in *V. harveyi*. Blue dots depict enriched targets (criteria: $\log_2\text{-fold enrichment} \geq 3$ and $-\log_{10}(\text{p-value}) \geq 2.5$) which were competed by **F1**. B) Volcano plot of gel-free competitive ABPP experiment in *V. harveyi* treated with 50 μM **FP3** vs. a 20-fold excess of **F1** (**FP3+F1**). Blue dots depict selected targets that are competed by **F1** (criteria: $\log_2\text{-fold enrichment} \geq 3.5$ and $-\log_{10}(\text{p-value}) \geq 4$) and enriched by **FP3** vs. DMSO. C) Volcano plot of gel-free quantitative ABPP experiments with 50 μM **FP3** vs. DMSO in *V. campbellii*. Blue dots depict enriched targets (criteria: $\log_2\text{-fold enrichment} \geq 3$ and $-\log_{10}(\text{p-value}) \geq 3$) which were competed by **F1**. D) Volcano plot of gel-free competitive ABPP experiment in *V. campbellii* treated with 50 μM **FP3** vs. a 20-fold excess of **F1** (**FP3 + F1**). Blue dots depict selected targets competed by **F1** (criteria: $\log_2\text{-fold enrichment} \geq 2$ and $-\log_{10}(\text{p-value}) \geq 5$) and enriched by **FP3** vs. DMSO. Results are derived from three biological replicates with technical duplicates and $-\log_{10}(\text{p-value})$ were calculated using two sided one sample Student's t-test.

Proteins discussed in the text are shown in red. A full list of targets above the cut-off criteria can be found in Table 2.

One interesting protein in *V. campbellii*, LuxE, replaced PhaB as one of the best targets. LuxE is directly involved in the production of bioluminescence in both *Vibrio* strains. It activates myristic acid as fatty acyl-AMP intermediate that is subsequently transferred to LuxC for further processing. (Figure 31A) Its important role in bioluminescence fits the expectation of a downstream target of LuxO. As the sequence identity of LuxE in these two *Vibrio* strains was 98%, it was very unlikely that its unsuccessful labeling in *V. harveyi* NBRC 15634 by FP3 was because of the difference in protein sequence or structure. What alerted us was that LuxE was not detected in *V. harveyi* NBRC 15634 at all in our ABPP approach. As *V. campbellii* ATCC BAA-1116 exhibits an intrinsically stronger bioluminescence than *V. harveyi* NBRC 15634, we hypothesized that LuxE in *V. Harveyi* was not as abundant as that in *V. campbellii* BAA-1116. This relatively low expression level resulted in our failure in its detection in *V. harveyi* NBRC 15634. Therefore, a full proteome analysis of both strains was carried out. (Figure 18)

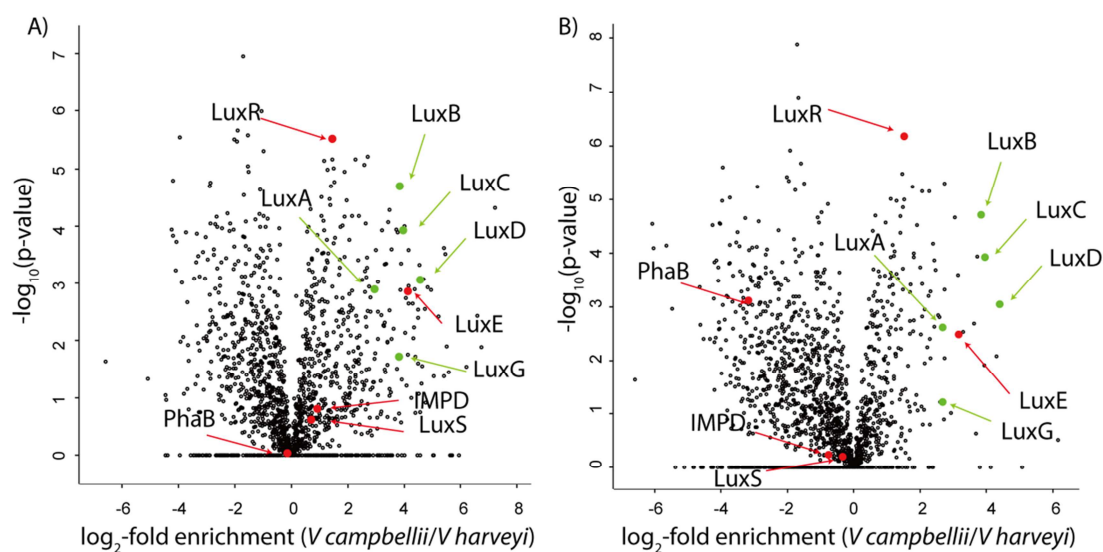


Figure 19: Volcano plots of whole proteome comparison between *V. campbellii* ATCC BAA-1116 and *V. harveyi* NBRC 15634. A) Volcano plot of *V. campbellii* ATCC BAA-1116 versus *V. harveyi* NBRC 15634 based on the *V. campbellii* ATCC BAA-1116 sequence and B) based on the *V. harveyi* NBRC 15634 sequence. $-\log_{10}(p\text{-value})$ were calculated using two sided one sample Student's t-test. LuxE was significantly more abundant in *V. campbellii* ATCC BAA-1116 than in *V. harveyi* NBRC 15634 while PhaB, IMPD, LuxS and LuxR showed almost no difference (highlighted in red). The green dots (LuxC, LuxD, LuxA, LuxB, LuxG) represent proteins from the same operon as LuxE (shown in red). Data was derived from three independent biological experiments. A list of selected proteins and ratios can be obtained in Table 3.

It turned out there was about 10-fold higher LuxCDABE expression in *V. campbellii* ATCC BAA-1116 compared to that in *V. harveyi* NBRC 16534. This explained the observed differences in their bioluminescence production as well as the unsuccessful detection of LuxE in *V. harveyi*. In contrast, the expression levels of IMPD, LuxS remained almost constant. Overall, no significant enrichment or competition for the previously proposed **F1** target LuxR was observed, although it was expressed to the same extent in both strains, indicating that it was at least not an irreversible binder of fimbrolides. (Figure 19)

In total, the four identified targets were grouped in three categories based on available functional data. Category 1 comprises proteins with unknown function such as the 15.6 KDa CBS domain protein IMPD. Proteins with putative roles in QS such as PhaB, an enzyme involved in polyhydroxybutyrate (PHB) biosynthesis, were classified as category 2, while category 3 proteins such as LuxS and LuxE exhibit a confirmed role in QS/bioluminescence pathways. To further confirm that these protein targets are labeled by fimbrolides and investigate whether their functions related to QS or bioluminescence can be altered after the treatment of fimbrolide, their validation was conducted.

Table 2. Targets above the cut-off criteria in gel-free quantitative ABPP figures.

Figure	Accession number	Protein name	log ₂ ratio of exp 1-6 (NaN means no ratio available)							-log ₁₀ (p-value)	Mean ratio
18A	VBIvibHar257948_3913	Inosine monophosphate dehydrogenase-related protein (IMPD)	3.82	3.23	2.63	4.65	3.78	6.12	2.76	16.43	
	VBIvibHar257948_1228	S-ribosylhomocysteine lyase/ Autoinducer-2 production protein LuxS	3.08	3.23	2.43	3.94	4.82	3.72	3.19	11.61	
	VBIvibHar257948_3643	Acetoacetyl-CoA reductase (PhaB)	2.71	2.64	2.95	4.66	3.96	2.96	3.03	9.93	
	VBIvibHar257948_3614	Thioredoxin 2	3.09	3.22	3.43	NaN	NaN	NaN	2.73	9.49	
	VBIvibHar257948_4804	Putative metal chaperone, involved in Zn homeostasis, GTPase of COG0523 family	2.47	3.34	2.91	3.57	NaN	3.53	3.31	8.98	
	VBIvibHar257948_1149	Glycyl-tRNA synthetase alpha chain	3.36	3.32	2.09	2.96	3.75	3.01	3.56	8.47	
	VBIvibHar257948_0229	Glutathione S-transferase	2.73	3.17	2.00	2.74	4.55	3.21	2.72	8.37	
	VBIvibHar257948_1228	S-ribosylhomocysteine lyase/ Autoinducer-2 production protein LuxS	4.28	4.17	3.47	4.37	4.79	3.96	5.55	18.05	
18B	VBIvibHar257948_3913	Inosine monophosphate dehydrogenase-related protein (IMPD)	3.85	3.53	3.31	4.33	3.74	3.69	5.87	13.36	
	VBIvibHar257948_3875	Arsenate reductase	3.73	3.74	3.67	NaN	NaN	NaN	4.40	13.13	
	VBIvibHar257948_3643	Acetoacetyl-CoA reductase (PhaB)	4.38	4.15	3.17	3.74	3.81	2.93	4.79	12.95	
	VBIvibCam343825_1148	Inosine monophosphate dehydrogenase-related protein (IMPD)	4.94	4.47	4.86	4.77	3.61	5.27	4.71	16.43	
	VBIvibCam343825_4098	LuxE, long-chain-fatty-acid ligase	3.32	3.40	3.29	3.31	2.77	3.87	4.81	11.61	
	VBIvibCam343825_4985	FIGO1200492: hypothetical protein	3.31	NaN	2.61	3.48	3.18	3.98	3.32	9.93	
18C	VBIvibCam343825_2716	S-ribosylhomocysteine lyase/ Autoinducer-2 production protein LuxS	2.94	3.74	3.45	3.39	3.93	1.89	3.15	9.49	
	VBIvibCam343825_2558	Phosphate starvation-inducible protein PhoH, predicted ATPase	2.96	3.08	2.77	3.08	3.29	3.75	4.72	8.98	
	VBIvibCam343825_1589	Alkyl hydroperoxide reductase subunit C-like protein	3.12	2.98	3.01	3.02	2.88	3.87	4.56	8.47	
	VBIvibCam343825_1148	Inosine monophosphate dehydrogenase-related protein (IMPD)	3.75	3.96	4.04	4.04	4.38	3.75	6.84	15.86	
	VBIvibCam343825_2716	S-ribosylhomocysteine lyase/ Autoinducer-2 production protein LuxS	3.34	4.61	3.49	3.30	3.47	3.92	5.02	12.90	
	VBIvibCam343825_4098	LuxE, long-chain-fatty-acid ligase	2.30	2.27	1.89	2.28	2.51	2.16	5.87	4.72	
VBIvibCam343825_1830	Inorganic pyrophosphatase	1.86	2.03	2.11	2.02	2.01	2.08	7.49	4.05		

Table 3. Abundance comparison of selected proteins in whole proteome analysis.

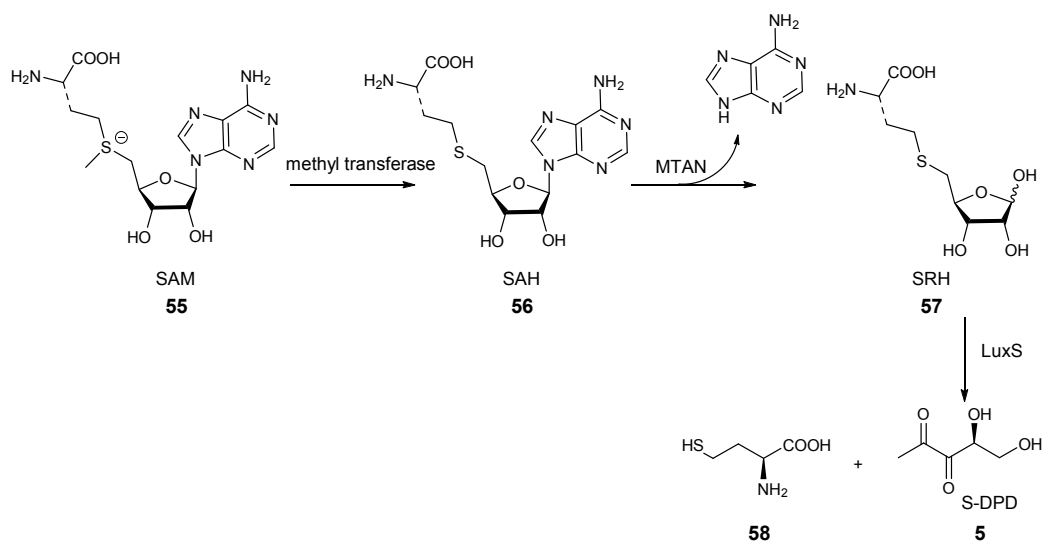
Figure	Accession number	Protein name	log ₂ ratio of exp 1-6 (NaN means no ratio available)						-log ₁₀ (p-value)	Mean ratio
			3.69	2.76	4.17	5.32	7.30	4.11		
19A	VBIVibCam343825_4095	LuxD, acyl transferase	4.67	2.91	2.13	4.29	4.06	6.70	2.86	23.59
	VBIVibCam343825_4098	LuxE, long-chain-fatty-acid ligase	4.81	2.92	4.12	4.88	2.82	4.19	3.92	17.48
	VBIVibCam343825_4094	LuxC, acyl-CoA reductase	4.38	3.13	4.07	4.28	4.21	3.04	4.70	15.53
	VBIVibCam343825_4097	LuxB, luciferase beta chain	NaN	0.33	4.59	3.64	6.54	4.04	1.72	14.44
	VBIVibCam343825_4099	LuxG, NAD(P)H-dependent FMN reductase	4.27	1.14	3.26	3.78	2.47	2.72	2.90	14.22
	VBIVibCam343825_4096	LuxA, luciferase alpha chain	2.64	1.01	1.68	0.08	-1.24	1.30	0.80	7.67
	VBIVibCam343825_1148	Inosine monophosphate dehydrogenase-related protein (IMPD)	1.23	1.54	1.28	1.48	1.55	1.61	5.51	1.88
	VBIVibCam343825_2741	LuxR, Quorum-sensing regulator of virulence HapR	0.24	NaN	-1.06	1.08	1.63	1.59	0.62	2.73
	VBIVibCam343825_2716	S-ribosylhomocysteine lyase/ Autoinducer-2 production protein LuxS	NaN	-3.49	-3.29	3.17	1.38	1.56	0.03	1.62
	VBIVibCam343825_4869	Acetoacetyl-CoA reductase (PhaB)	2.83	2.68	4.17	4.98	6.79	4.97	3.04	0.91
19B	VBIVibHar257948_0150	LuxD, acyl transferase	4.81	2.92	4.12	4.88	2.82	4.19	3.92	21.19
	VBIVibHar257948_0151	LuxC, acyl-CoA reductase	4.38	3.13	4.02	4.27	4.21	3.04	4.71	15.53
	VBIVibHar257948_0148	LuxB, luciferase beta chain	1.52	2.32	2.13	3.70	3.80	5.55	2.49	14.33
	VBIVibHar257948_0147	LuxE, long-chain-fatty-acid ligase	4.27	1.14	3.32	3.09	1.54	2.72	2.61	9.00
	VBIVibHar257948_0149	LuxA, luciferase alpha chain	NaN	0.26	NaN	2.69	4.65	3.12	1.22	6.41
	VBIVibHar257948_0146	LuxG, NAD(P)H-dependent FMN reductase	1.66	1.54	1.30	1.48	1.55	1.56	6.18	6.40
	VBIVibHar257948_1249	LuxR, Quorum-sensing regulator of virulence HapR	NaN	NaN	0.32	-0.79	-1.82	0.96	0.20	2.86
	VBIVibHar257948_3913	Inosine monophosphate dehydrogenase-related protein (IMPD)	NaN	NaN	NaN	1.30	-2.55	-1.00	0.24	0.79
	VBIVibHar257948_1228	S-ribosylhomocysteine lyase/ Autoinducer-2 production protein LuxS	NaN	NaN	NaN	NaN	NaN	NaN	0.24	0.59
	VBIVibHar257948_3643	Acetoacetyl-CoA reductase (PhaB)	NaN	-3.55	-3.29	-4.08	-2.03	-2.93	3.12	0.11

2.2 Target Validation

Target validation is aimed to validate the binding of their targets by small molecules which results in an activity alteration followed by a potential phenotypic change. It is considered as another key step in drug development as its identification. The four identified proteins, namely LuxS, LuxE, PhaB and IMPD were validated one by one according to their available function.

2.2.1 Validation of LuxS

AI-2 based QS is one universal circuit used in many bacterial strains for the interspecies communication. Despite of its significant importance, it is still far from explored compared with AHL based QS. Moreover, the majority of its research related to its inhibitors has so far been performed *in vitro* while it is well known that *in vitro* behavior is not always in line with *in vivo* behavior.¹¹



Scheme 6: Enzymatic Synthesis of DPD (5). SAM (55): S-adenosylmethionine; SAH (56): S-adenosylhomocysteine; MTAN: 5'-methylthioadenosine/S-adenosylhomocysteine nucleosidase; DPD (5): 4,5-dihydroxy-2,3-pentanedione; SRH (57): S-ribosylhomocysteine; LuxS: S-ribosylhomocysteine lyase; 58: homocysteine.

In principle, LuxS is the synthase of AI-2 and its homologues exist in about 50% of all sequenced bacteria.¹³⁶ Nevertheless, it is noteworthy mentioning that LuxS also participates in the activated methyl cycle besides its role in QS. Its substrate, S-ribosyl-L-homocysteine (SRH) (57) is derived from the common methyl group transferring material, S-adenosylmethionine (SAM) (55). The methyltransferase converts SAM (55) to S-

adenosylhomocysteine (SAH) (**56**) which is then hydrolyzed to *S*-ribosylhomocysteine (SRH) (**57**) under the catalysis of 5'-methylthioadenosine/*S*-adenosylhomocysteine nucleosidase (MTAN) enzyme (also known as *Pfs* nucleosidase). The LuxS finally cleaves SRH to L-homocysteine and 4,5-Dihydroxy-2,3-pentanedione (DPD) (**5**). DPD then forms the so called AI-2 pool with or without borate (Scheme 6). Although all compounds of the AI-2 pool are derived from DPD, it must be highlighted that different members can be used to trigger AI-2 QS in different strains e.g. *R*-THMF in *S. Typhimurium*, *S*-THMF-borate in *V. Harveyi*. (Figure 1)

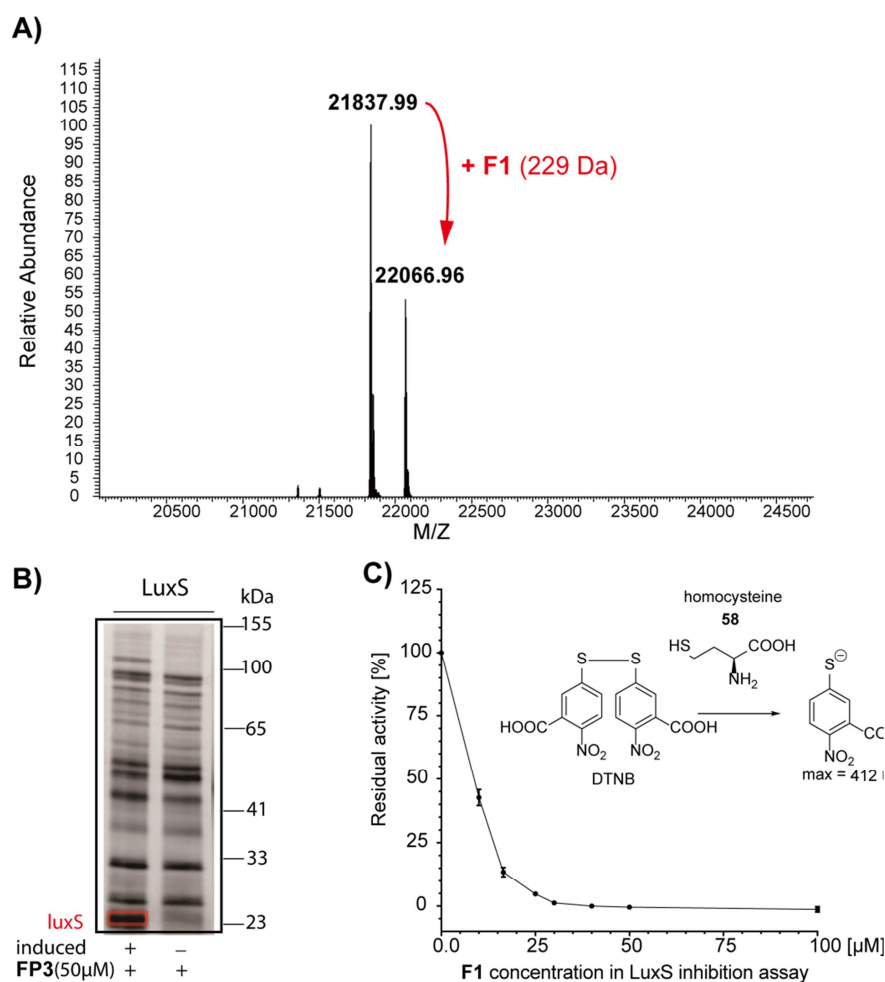


Figure 20. A) Full-length MS measurements of intact recombinant LuxS after incubation with **F1**. B) Analytical *in situ* labeling of recombinant LuxS expressed in *E. coli* with 50 μM **FP3**. Here induced denotes induction of protein overexpression. C) LuxS activity was inhibited *in vitro* by **F1** in a concentration-dependent manner employing Ellman's reagent. The residual activity was normalized to DMSO control. Data was derived from three independent replicates with technical duplicates and error bars represent the standard deviation of the means.

Recombinant *V. harveyi* NBRC 15634 LuxS was expressed in *E. coli* BL21DE(3) with a His tag and purified with immobilized metal affinity chromatography (IMAC). Recombinant LuxS was

observed to be modified with **F1** in full-length MS-analysis, which was in accordance with the report from Zhou (Figure 20A).¹¹⁸ Since a 229 Da (average molecular weight of $C_9H_{10}BrO_2$) is the molecular weight minus one bromine atom, it logically indicates that probably this modification follows an addition-elimination mechanism. First, a nucleophile in LuxS undergoes an addition reaction with the fimbrolide and then one bromine atom is eliminated in the form of HBr. However, whether the bromine on the furanone ring or the exocyclic vinyl one acts as the active bromine cannot be differentiated from the mass data. Nevertheless, as it was reported consistently that the exocyclic vinyl bromine is crucial to keep the bioactivity of fimbrolides in bioluminescence inhibition, the nucleophilic reaction on the exocyclic vinyl group should be favored (Scheme 1).

Recombinant LuxS was also used to test whether it can be labeled by probe **FP3** *in situ*. As visualized after fluorescent scanning, there was one labeled band missing around 23 KDa in the non-induced *E. coli* cells compared with that in induced cells (Figure 20B).

Although the covalent modification of LuxS protein by either fimbrolide **F1** or its probe **FP3** was confirmed, whether this binding will influence its activity or not still needs our quest. As a same amount of the byproduct homocysteine (**58**) is produced as AI-2 during the catalytic reaction, the activity of LuxS was measured by quantifying homocysteine with 5'-dithiobis-2-nitrobenzoic acid (DTNB, Ellman's reagent). The free thiol reacts with DTNB to form nitrobenzoic acid (TNB). TNB has an extinction coefficient of $13,700\text{ M}^{-1}\text{ cm}^{-1}$ at its maximal absorption wavelength 412 nm. Following the assay in the previous report,¹³⁷ recombinant LuxS treated with various concentrations of fimbrolide was tested for their activity. As shown below, the LuxS activity decreases in a fimbrolide concentration-dependent manner (Figure 20C).

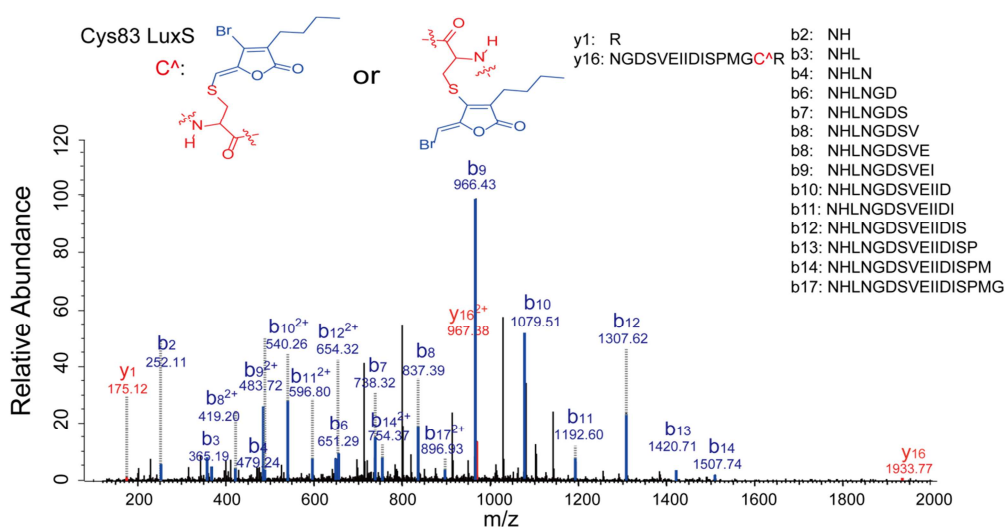


Figure 21. MS/MS sequencing shows the binding of **F1** to Cys83 of LuxS.

II – FIMBROLIDES • RESULTS AND DISCUSSION

The fimbrolide binding site was identified by MS-MS sequencing. In general, recombinant LuxS was first incubated with fimbrolide at room temperature for 40 min in pH = 7.4 PBS and then digested with trypsin after removal of excess of fimbrolide by filtration. The resulting peptides were measured on mass-spectrometry and the subsequent data was analyzed on Maxquant software with C₉H₁₀BrO₂ (average mass 229 Da) as the modification mode. Cys83 was identified as the binding site. (Figure 21)

Since the binding site of fimbrolide in *B. subtilis* LuxS was previously reported, LuxS sequence comparison between *V. harveyi* NBRC 15634 and *B. subtilis* 168 was performed. Cys83, Cys128 in *V. harveyi* NBRC 15634 correspond to Cys84, Cys126 in *B. subtilis*168 based on the alignments. Nevertheless, the fimbrolide binding site was proposed to be Cys126 in *B. subtilis*, which was not in line with our result in *V. harveyi*. (Figure 22)

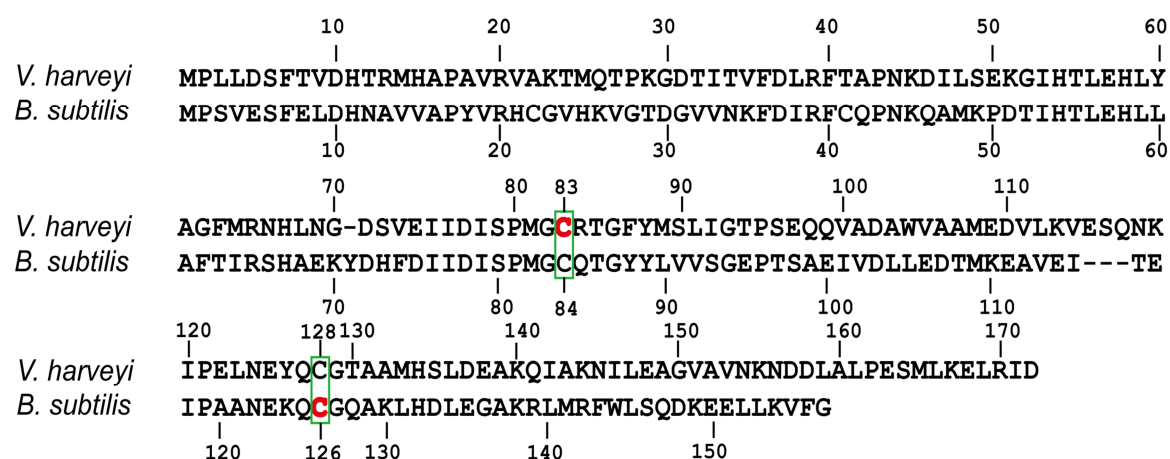


Figure 22. Sequence alignments of LuxS proteins from *V. harveyi* NBRC 15634 and *B. subtilis* 168. Cys83, Cys128 in *V. harveyi* NBRC 15634 correspond to Cys84, Cys126 in *B. subtilis*168 from the alignments.

To date, several crystal structures of LuxS from different organisms have been published, such as *B. subtilis*,¹³⁸⁻¹⁴⁰ *H. pylori*, *D. radiodurans*, *H. influenzae*.¹⁴¹ Among them, the *B. subtilis* LuxS structure-function assignment is best investigated. In fact, the Cys84 and Cys126 in *B. subtilis* are intensely discussed during the investigation of LuxS structure.

LuxS is a metalloenzyme containing a divalent metal in the active site. The metal cation can change its type during the reaction. It is believed to play a key role in stabilizing varying intermediates in the catalytic pathway. This metal ion was coordinated by the conserved residues His54, His58 and Cys126 by donation of a single monomer chain. Thus, Cys126 was considered as one important cysteine in *B. subtilis* LuxS. More attention was drawn by Cys126 during the onset of the research in two reports in 2001.^{139,140} However, Cys84 was oxidized in both cases while the importance of Cys126 was highlighted. Meanwhile, it was pointed out

there that the unusual feature of Cys84 was potentially important for substrate binding or catalysis. Moreover, Pei *et al.* have reported a series of achievement during their investigation on catalytic mechanism of *B. subtilis* LuxS since 2003.^{138,142-144} In their proposed mechanism, Cys84 is a general base used to abstract proton. Thus it is crucial for the catalytic activity. More direct evidence for the importance of Cys84 in LuxS is that a C84A LuxS mutant does not show catalytic activity and a C84D or C84S results in a 220-fold reduced activity.¹⁴⁴ As a reduced Cys84 thiolate is an excellent nucleophile, it is logically ready to react with the electrophilic fimbrolide. Because of its importance in the catalysis, Cys84 modification will thus cause a decreased activity. This kind of chemical property and biological functionality are in line with our finding that Cys83 rather Cys128 in *Vibrio harveyi* is the binding site of fimbrolide in LuxS. Nevertheless, it cannot be excluded that this difference in binding site of LuxS by fimbrolide is owing to different biological systems.

2.2.2 Validation of LuxE

Although bioluminescence assay has been quite often employed in QS research, the proteins in the catalytic machinery for continuous light production have never been considered as possible targets of fimbrolide. To our surprise, the long chain fatty-acid-luciferin-component ligase protein, LuxE emerged as one promising target of fimbrolide in our target identification step. In luminous *Vibrios*, the catalytic machinery for bioluminescence consists of luciferase and fatty acid reductase. The luciferase is encoded by *luxA* and *luxB* while the reductase is comprised of 12 polypeptides (four copies of polypeptides encoded by the *luxC*, *luxD*, and *luxE* genes). LuxE activates myristic acid generated by LuxD as fatty acyl-AMP intermediate that is subsequently transferred to LuxC for reduction to fatty aldehyde. Besides reduced flavin mononucleotide (FMNH₂) and molecular oxygen, the long chain fatty aldehyde is another essential substrate for luciferase to produce bioluminescence. Thus, LuxE plays a crucial role in bioluminescence production.

V. Campbellii LuxE was cloned into pDest 007 plasmid and tested for its overexpression with a Strep tag. After screening overexpression conditions such as temperature, concentration of inducers, induction time, *E. coli* overexpression strains, the optimal condition (432 nM anhydrotetracycline, grow at 15 °C for 5 h after induction, *E. coli* Arctic Express strain) was chosen. To investigate whether LuxE can be modified by **F1** *in vitro*, the purified LuxE after immobilized metal affinity chromatography (IMAC) was incubated with **F1** at 4 °C for 2 hours in pH = 7.4 PBS. The treated LuxE was measured for full-length MS analysis and revealed a covalent modification of LuxE with **F1**. As that in LuxS, the modification caused an increase of

molecular weight equals to that of $C_9H_{10}BrO_2$. **FP3** exhibited different *in situ* labeling performance in induced and non-induced *E. coli* Arctic Express cells, which confirmed the modification of recombinant LuxE by fimbrolide. Recombinant LuxE was labeled by **FP3** and it was the only promising band after fluorescent scanning. In contrast, this band disappeared in the non-induced *E. coli* Arctic Express samples. (Figure 23)

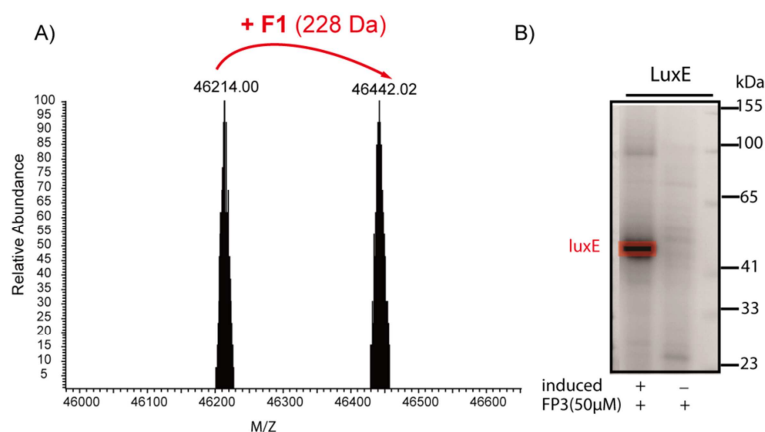


Figure 23. A) Full-length MS measurements of intact recombinant LuxE after incubation with **F1**. B) Analytical *in situ* labeling of recombinant LuxE expressed in *E. coli* with 50 μ M **FP3**. Here induced denotes induction of protein overexpression.

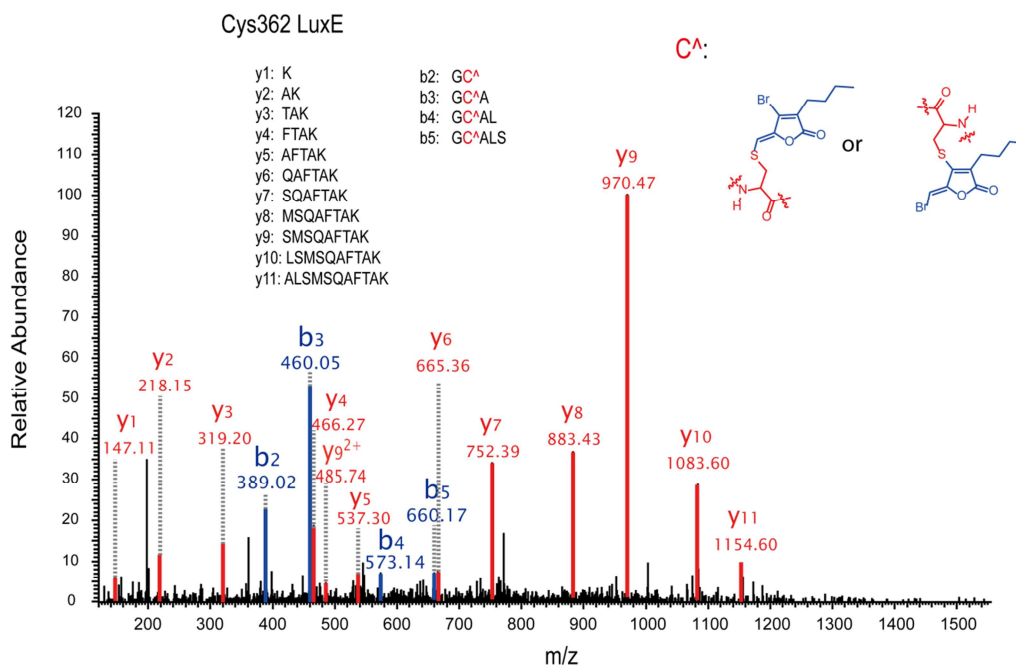


Figure 24. Cys362 was identified as **F1** binding site by MS/MS sequencing in LuxE.

MS-MS sequencing was carried out to identify the binding site identification of **F1** on LuxE. After removal of the excess of **F1**, the treated recombinant LuxE was digested with trypsin.

After measuring the digested peptides on mass spectrometry, the analysis of the mass data on Maxquant software revealed Cys362 as the binding site of **F1**. (Figure 24)

In fact, Cys362 was reported to be a crucial amino acid for the activity of LuxE.¹⁴⁵ LuxE acts as a synthase in the reductase complex and catalyzes autoacylation and acyl transfer to reductase LuxC. First of all, it produces an enzyme bound fatty acyl-AMP intermediate by activating the free fatty acid with ATP. Secondly, one amino acid in LuxE which acts as a nucleophile attacks fatty acyl-AMP intermediate. LuxE then turns into an acyl LuxE. In the last step, the fatty acyl group is transferred to LuxC and be reduced to aldehyde with NADPH (Figure 25). Cys362 is the nucleophilic amino acid in LuxE in the second step of this catalytic procedure. Therefore, the chemical modification of Cys362 has a great influence on the activity of LuxE.

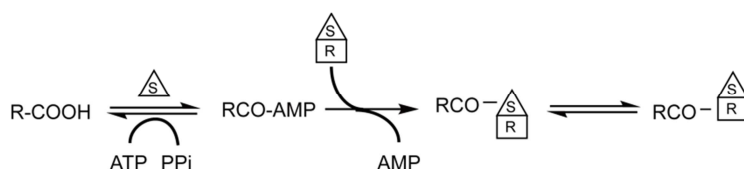


Figure 25: Acyl transfer from LuxE to LuxC. RCOOH denotes the fatty acid. S in triangle and R in rectangle mean synthase LuxE and reductase LuxC respectively.

The fatty acid reduction cycle requires four copies of LuxC, LuxD, LuxE to form a reductase complex to complete. The *in vitro* assay only with LuxE is supposed to have no activity and turnovers in reduction of fatty acid. To overcome this problem, an alternative *in vivo* way to validate the biological effects of fimbrolide on LuxE was performed by means of one luminescent *E. coli* strain. This *Escherichia coli* DH5α with a pBluelux plasmid, containing *luxCDABE* operon from *Photobacterium luminescens* (LuxE sequence identity 62%) under the control of a *lac* promoter produces bioluminescence independent of QS circuit. In this case, the influence effect from the inhibition of LuxS by fimbrolides can be excluded. **F1** and **FP3** dose-dependently reduced bioluminescence with a respective IC_{50} of 24 μM and 9 μM, supporting that LuxE was an additional target of fimbrolides. In line with our previous results, **FP3** showed slightly better inhibition activity than **F1**. At the same time, *P. luminescens* LuxE was expressed in *E. coli*. This recombinant LuxE was proved to be labeled by probe **FP3** as a decreased fluorescence intensity of labeled LuxE was observed in a **FP3** concentration-dependent way. Meanwhile, a missing fluorescent band in non-induced *E. coli* cells verified the labeling of *P. luminescens* LuxE by **FP3**. As LuxE is an essential protein for bioluminescence production, the validated LuxE which is downstream of LuxO as a protein target of fimbrolides

provides another alternative explanation instead of LuxR for the inhibition of bioluminescence in *Vibrios*.

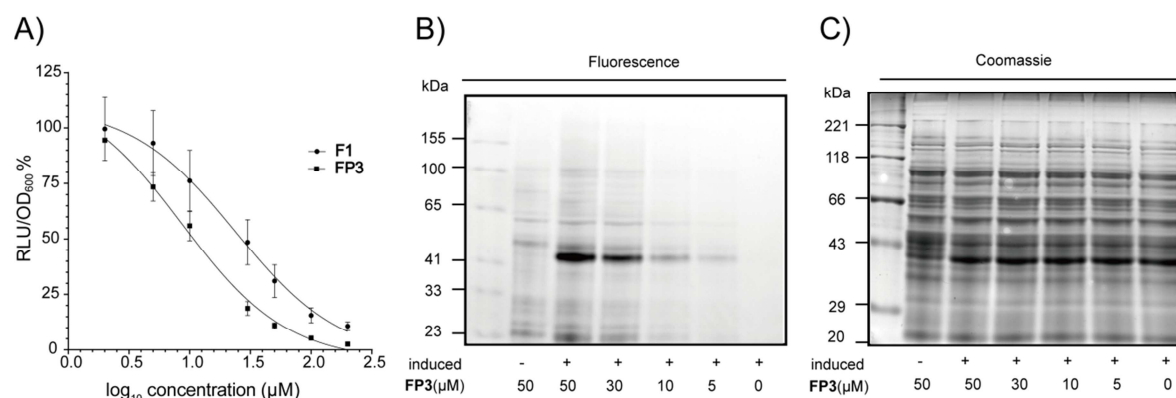
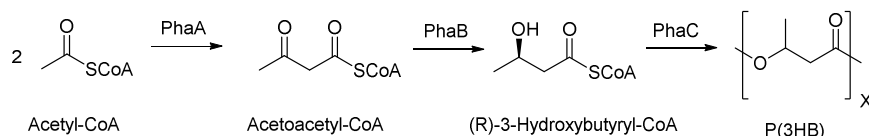


Figure 26. A) Bioluminescence production of luminescent *E. coli* DH5α pBluelux containing luxCDABE operon under the control of *lacZ* promoter was inhibited by **F1** and **FP3**. RLU (relative luminescence units) were normalized to cell density (OD₆₀₀) and then to DMSO control. The data is derived from three biological experiments with technical triplicates and error bars indicate standard deviation from the means. B and C) Concentration-dependent *in situ* labeling of recombinant *Photorhabdus luminescens* LuxE expressed in *E. coli* with **FP3**. Induced denotes induction of protein overproduction. 0 means DMSO was added instead of **FP3**.

2.2.3 Validation of PhaB

PhaB is the acetoacetyl-CoA reductase in *Vibrios* to reduce acetoacetyl-CoA to (R)-3-hydroxybutyryl-CoA. It is involved in the production of poly-3-hydroxy-butyrate (P(3HB)). Usually, the cells produce P(3HB) in three steps. Acetyl-CoA acetyltransferase (PhaA or ACAT) catalyzes two acetyl-CoA molecules to form acetoacetyl-CoA. This intermediate is then reduced by PhaB to (R)-3-hydroxybutyryl-CoA with NADPH. Finally the polymerase (PhaC) catalyzes the polymerization of (R)-3-hydroxybutyryl-CoA to produce polymer P(3HB).



Scheme 7: Enzymatic synthesis of P(3HB) by PhaA, PhaB and PhaC. PhaA: acetyl-CoA acetyltransferase; PhaB: acetyl-CoA reductase; PhaC: polymerase; P(3HB): poly-3-hydroxy-butyrate.

The P(3HB) is one common bio-degradable bio-plastics produced by bacteria and archaea. It is used as the energy-storage molecule. PhaB becomes interesting as a target for fimbrolide

because of its role in this important energy repository for bioluminescence.^{146,147} Recombinant *V. campbellii* PhaB in *E. coli* was overexpressed and purified. After incubation of recombinant PhaB protein with **F1** in 10 mM sodium phosphate buffer at room temperature for 1 hour, a full-length mass analysis showed a molecular weight increase equals to that of C₉H₁₀BrO₂ in **F1** treated PhaB. An *in situ* analytical labeling of **FP3** in induced and non-induced *E. coli* cells with a pET300/NT-Dest plasmid containing *phaB* gene was compared. A distinct fluorescent band around 30 KDa was present in the induced sample while absent in the non-induced one, which confirmed recombinant PhaB labeling by fimbrolide.

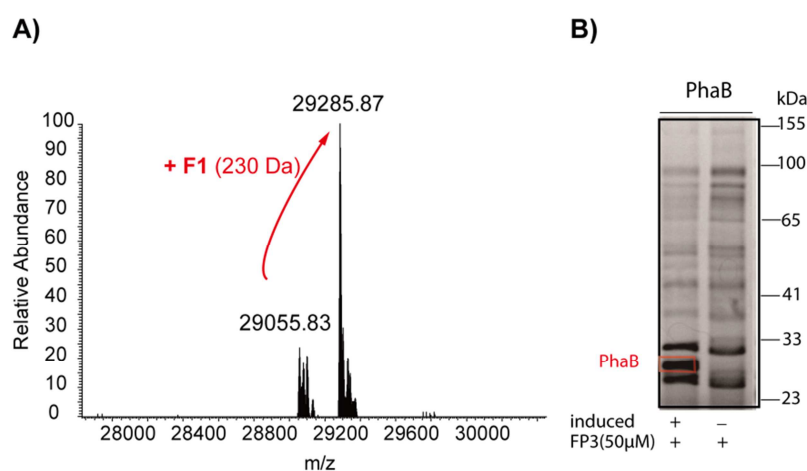


Figure 27. A) Full-length MS measurement of intact recombinant PhaB after incubation with **F1**. B) Analytical *in situ* labeling of recombinant PhaB expressed in *E. coli* with 50 µM **FP3**. Here induced denotes induction of protein overexpression.

Following the previous reports, the inhibition of **F1** was tested in the PhaB assay as described with some slight modifications.^{148,149} Various concentrations of **F1** or DMSO were preincubated with PhaB at 25 °C for 10 min. Then the treated PhaB was added to a mixture of 200 µM acetoacetyl-CoA sodium salt, 800 µM NADPH in 200 µM DTT, 125 mM Tris-HCl buffer, pH 8.0. Enzyme activities were monitored by the change in absorbance at 340 nm due to oxidation of NADPH with time. As shown, PhaB activity was inhibited in a **F1** dose-dependent manner. (Figure 28)

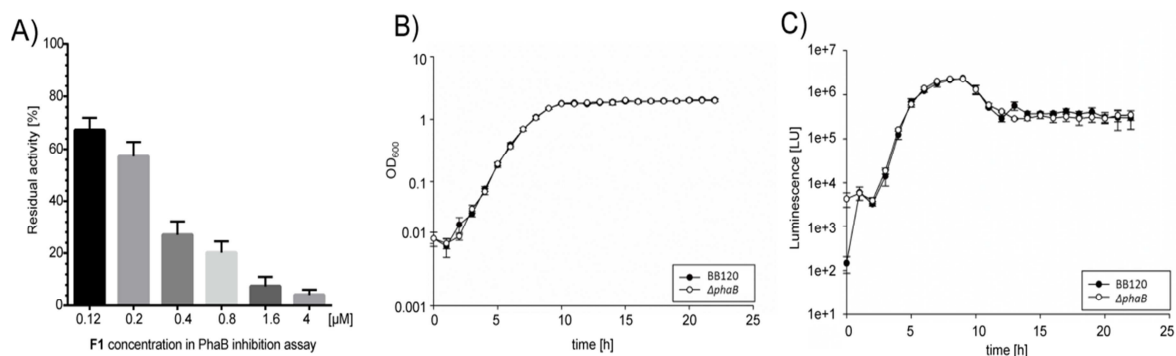


Figure 28. A) PhaB activity was inhibited by **F1**. The residual activity was normalized to DMSO control. Data was derived from three independent experiments with technical duplicates and error bars represent the standard deviation of the means. B) Growth curve of *V. campbellii* ATCC BAA-1116 and *V. campbellii* Δ *phaB* mutant showed no differences. Data was derived from three biological replicates. C) Luminescence production curve of *V. campbellii* ATCC BAA-1116 and *V. campbellii* Δ *phaB* mutant. Data was derived from three biological replicates. Figure 28B and 28C were obtained from Nicola from Kirsten Jung’s group at LMU.

Nevertheless, the inhibition of PhaB activity by **F1** cannot give a direct implication whether PhaB is involved in bioluminescence inhibition by fimbrolide as no clear roles were reported for it in bioluminescence or QS. Therefore, a *phaB* deletion strain of *V. campbellii* was generated by our collaborator (Nicola Lorenz from Prof. Kirsten Jung’s group, Ludwig-Maximilians Universität München, Department Biologie I). Its growth and production of bioluminescence were compared with the wild type. However, this mutant did not show any difference with the wild type. These remaining unchanged properties suggest that PhaB is not a QS/bioluminescence-associated fimbrolide target. (Figure 28)

2.2.4 Validation of IMPD

Inosine monophosphate dehydrogenase-like protein (IMPD) is an uncharacterized protein containing a CBS domain. IMPD is the best identified protein target for fimbrolide in *Vibrios*. Nevertheless, no potential links between it and QS or bioluminescence have been reported. Recombinant IMPD was expressed in *E. coli* and purified with IMAC. The purified IMPD was modified with **F1** once or twice as determined by full-length mass measurement. A distinct fluorescent band revealed recombinant IMPD was labeled by **FP3** in induced *E. coli* BL21DE(3) cells with a pET300/NT-Dest plasmid containing the corresponding gene.

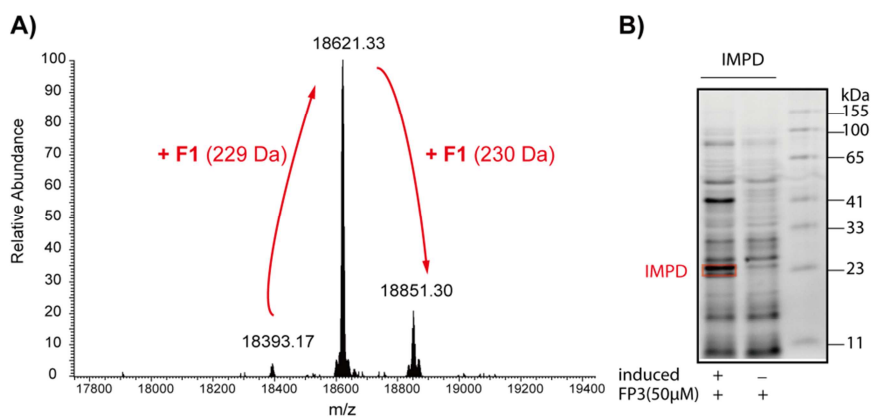


Figure 29. A) Full-length MS measurements of intact recombinant IMPD after incubation with **F1**. B) Analytical *in situ* labeling of recombinant IMPD expressed in *E. coli* with 50 μ M **FP3**. Here induced denotes induction of protein overexpression.

3 Conclusion and Outlook

Natural product fimbrolides represent important tools for quorum sensing (QS) study, and are potent QS disruptors. However, their molecular protein targets still remain elusive. Several structure-activity relationship studies revealed that a vinyl bromide at the methylene position of the extended conjugation of the furanone ring and a suitable length of alkyl chain are crucial for fimbrolide bioactivity. To fulfill the requirements of activity-based protein profiling technique to elucidate fimbrolide protein targets, a terminal alkyne was incorporated into the fimbrolide structure by organic synthesis. Four fimbrolide-based probes **FP1 - FP4** were synthesized as well as two parent fimbrolides **F1** and **F2**. Nevertheless, **FP4** was excluded for further experiments as it showed growth inhibition in *Vibrios* while the others did not.

FP1 - FP3, **F1** and **F2** were then applied in the bioluminescence production assays in *V. harveyi* NBRC 15634 and *V. campbellii* ATCC BAA-1116. As expected, the natural fimbrolide **F1** exhibited good bioluminescence inhibition. Moreover, its corresponding probe **FP3** turned out to be a better inhibitor. As **F1** and **FP3** showed the best bioactivity among our fimbrolides, they were thus used in ABPP approach.

To obtain a comprehensive overview of all irreversible **FP3** targets shared with the natural product **F1**, samples were prepared for gel-free MS analysis in both *V. harveyi* NBRC 15634 and *V. campbellii* ATCC BAA-1116 strains. The MS data was then analyzed based on enrichment by **FP3** and competition by **F1**. IMPD, LuxS are the best protein targets in *V. harveyi* NBRC 15634 as well as in *V. campbellii* ATCC BAA-1116. Although PhaB emerged as one of the best targets in *V. harveyi* NBRC 15634, it was less promising in *V. campbellii* ATCC BAA-1116. To our surprise, LuxE, one of *luxCDABE* operon proteins essential for the bioluminescence production, was identified as the best protein target in *V. campbellii* ATCC BAA-1116. Interestingly, it was not detected in *V. harveyi* NBRC 15634. As the sequence identity of LuxE in the two strains was 98%, a full proteome analysis was carried out to reveal the cause for this difference. A 10-fold higher LuxCDABE expression in *V. campbellii* ATCC BAA-1116 compared to that in *V. harveyi* NBRC 16534 likely explains no detection of LuxE in *V. harveyi* NBRC 16534.

Thus, four proteins namely IMPD, PhaB, LuxS and LuxE were found to be promising irreversible targets of **F1**. They were categorized into three groups based on their available functional information. Category 1 comprises the 15.6 KDa CBS domain protein IMPD with unknown function. PhaB involved in the biosynthesis of energy storage molecule P(3HB) was classified as category 2 as it has a putative role in QS and bioluminescence. The category 3

contains the autoinducer 2 synthase, LuxS and long-chain-fatty-acid-luciferin-component ligase, LuxE.

All of these four targets were recombinantly expressed in *E. coli* cells and purified on IMAC. They were shown to be labeled by **FP3** via *in situ* analytical ABPP labeling. Moreover, the full-length mass measurements indicate the modification of these protein targets by fimbrolide following an addition and elimination cascade, which highlighted the importance of bromine on fimbrolide.

Category 2 and 3 proteins were further validated to unravel the fimbrolide protein targets related to bioluminescence or QS. Although the enzymatic activity of PhaB can be inhibited by **F1**, a *V. campbellii* Δ *phaB* mutant showed no difference in growth and bioluminescence production with its wild type. Thus, PhaB should not be a QS/bioluminescence-associated fimbrolide target. The activity of AI-2 producer, LuxS, was found to be inhibited by **F1**. Moreover, its Cys83, an essential nucleophilic cysteine acting as a base in LuxS catalysis, was identified as the binding site via MS-MS sequencing. The bioluminescent production of a luminescent *E. coli* strain harbouring a bioluminescence system from *Photorhabdus luminescens* was inhibited by fimbrolide, indicating fimbrolide inhibition of LuxE activity. This protein target downstream of LuxO provides another explanation to bioluminescence production inhibition in *Vibrios* by fimbrolide, which is different from the previous proposed LuxR.

Overall, it is intriguing to note that one natural product targets different proteins of a single pathway at divergent steps to achieve one phenotype. This research renews the opinion of the QS tool compound fimbrolide from a full proteomic perspective.

III – TARGET INVESTIGATION OF BETA-LACTONES AND THEIR EFFECTS ON QS REGULATED BIOLUMINESCENCE IN *VIBRIOS*

1. Introduction

Bioluminescence is light emission produced as a consequence of a chemical reaction which originates in a living organism. The most common bioluminescence on land is the firefly, while bioluminescence in the ocean is quite poetic.¹⁵⁰ The ribbons and specks of light around boats and oars, radiant waves, the regions of shining water “milky seas” - all of these are splendid examples of ocean bioluminescence. However, bioluminescence should be differentiated from autofluorescence. Autofluorescence is the natural emission of light by biological structures when they absorb external light of suitable wavelength. This kind of light is not produced because of a chemical reaction but by the excitation of biological structures such as mitochondria, lysosomes and keratin. Therefore, the “glowing” sea turtles, sharks and so on, are not bioluminescent organisms.¹⁵¹

There are diverse bioluminescent creatures on almost every branch of the life tree, from bacteria to vertebrates. Nevertheless, the distribution in different branches differs. For example, no bioluminescent representatives have been discovered in plants, tetrapods, arachnids, or lepidopterans.¹⁵²⁻¹⁵⁴ In contrast, some other branches, such as teleosts and crustaceans, are rich in bioluminescent species. The various habitats from tropical jungles to barren fields, from sunny beaches to dark caves, and from oceanic surface waters to abyssal depths for these creatures provide a wide area for bioluminescence to take place. Although bioluminescence in terrestrial habitats has always received more attention and research efforts owing to its accessibility to researchers, it has to be mentioned here that those various terrestrial luminous organisms usually only belong to a few taxonomic groups, such as arthropods (a few families of luminous insects) and fungi. In fact, bioluminescence is still mainly a marine phenomenon and can be considered as the predominant source of light in the deep ocean. It has evolved many times from bacteria to fish and is distributed in all oceanic dimensions. Moreover, it has a powerful influence on behavioral and ecosystem dynamics.¹⁵⁵ On the other hand, it is rarely observed in freshwater even in the deepest lake, Lake Baikal. The difference between the marine and terrestrial bioluminescence has not been well explored and is not fully understood. However, a long uninterrupted evolutionary history in comparatively stable and clear environmental oceanic conditions which lack abundant light, makes bioluminescence beneficial during interactions between various organisms. 80% of more than 700 genera which contain luminous species are marine.¹⁵⁶ Nevertheless, the function of bioluminescence varies widely from species to species. Given the popularity of bioluminescence in the ocean, it likely serves many distinct functions there. However, only a

few of the numerous proposed functions such as attraction, defense and warning have been validated or verified by experimental evidence while the others remain elusive. Thus, more efforts are needed to unravel the roles of bioluminescence.¹⁵⁷

The most widely distributed light-emitting organisms are luminous bacteria such as *Photobacterium*, *Vibrio* and *Photorhabdus*. Most of them exist in the ocean and are capable of free living, but are usually found to live with host organisms in nature. Bacterial bioluminescence is evolutionarily distinct from the other kinds of bioluminescence in terrestrial and marine eukaryotic organisms. The mechanism and relationship with QS of bacterial bioluminescence is further illustrated below.

1.1 Bacterial Bioluminescence

Although the luminous bacterial species are quite different in many aspects such as growing condition and the reaction kinetics of luciferase, most of them are rod-shaped, Gram-negative microorganisms with flagella. In fact, most of them can be grouped as members of three families: *Vibrionaceae* (*Aliivibrio*, *Photobacterium*, *Vibrio*), *Enterobacteriaceae* (*Photorhabdus*) and *Shewanellaceae* (*Shewanella*).¹⁵³ Luminous bacteria usually employ the same enzymatic reaction and luciferase for light production and contain the necessary *lux* operon for bioluminescence.^{158,159} (Figure 30A)

Reduced flavin mononucleotide (FMNH₂), a long-chain aliphatic (eight carbons or longer) aldehyde (RCHO) and O₂ are three substrates needed in the chemical reaction. Nevertheless, the luminous bacterial strains are facultative anaerobes; in other words, they can still grow even when there is only limited available oxygen. FMNH₂ and long fatty aldehyde are specific in bacterial bioluminescence and the luciferase enzyme is conserved. Bioluminescent eukaryotes employ some other chemical reactions to produce light and their luciferases are not homologous to those in bacteria at the protein or gene sequence levels.¹⁶⁰ In general, bacterial luciferases catalyze the oxidation of FMNH₂ and long chain aliphatic aldehyde RCHO with O₂ to flavin mononucleotide (FMN) and fatty acid with H₂O as the byproduct. The release of the energy from this chemical reaction results in emission of blue/green light ($\lambda_{\text{MAX}} \sim 490$ nm). (Figure 30B)

The fatty acid reductase is essential for continuous production of bioluminescence. The fatty acid reductase is used to synthesize the fatty aldehyde from fatty acid. This recyclization supplies necessary fatty aldehyde for continuous bioluminescence. The approximate 500 KDa fatty acid reductase is a 12 polypeptide complex and composed of four copies of LuxC, LuxD, and LuxE.¹⁶¹⁻¹⁶³ As shown above, both this reductase and the luciferase are encoded by the *lux*

operon. (Figure 30A) LuxD is the transferase which transfers the acyl moiety of activated acyl donors such as fatty acyl-ACP (acyl carrier protein), generated in the universal fatty acid biosynthetic pathway, to its serine. The ester is then converted to a fatty acid after hydrolysis. LuxE acts as a synthase to further process the fatty acid to a fatty acyl-AMP intermediate. This intermediate is then transferred to LuxC and reduced to fatty aldehyde. (Figure 31A)

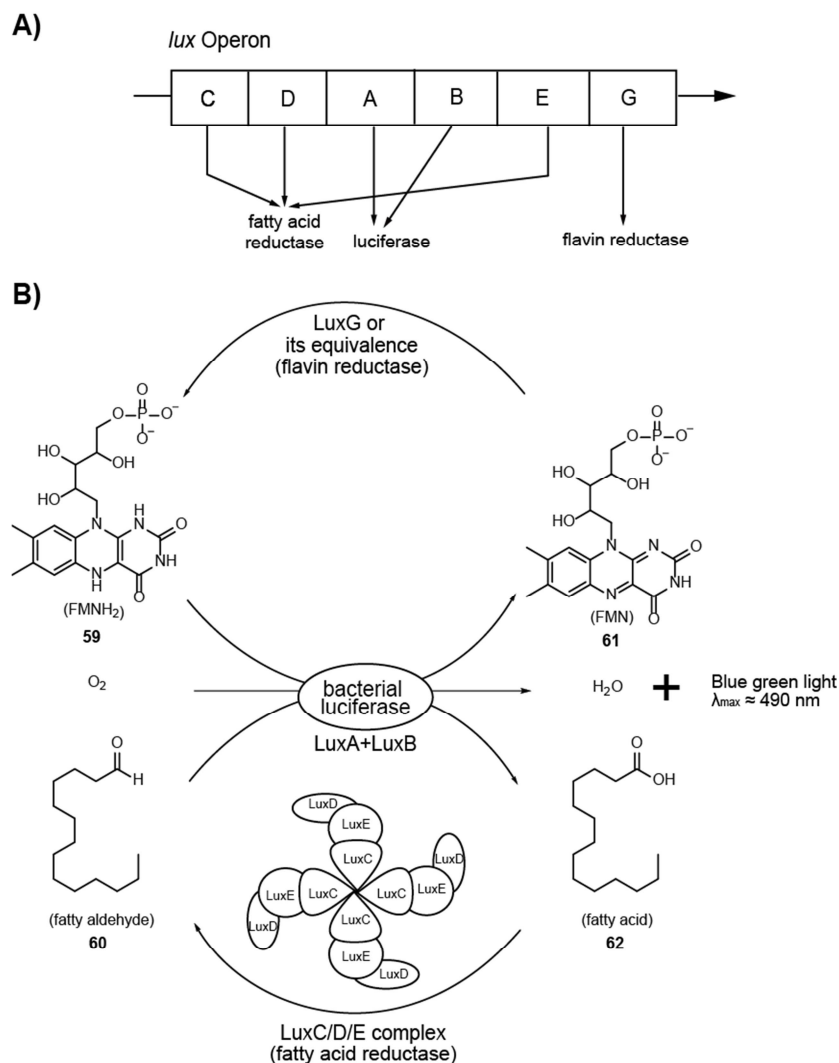


Figure 30. Illustration of *lux* operon and mechanism of bacterial light production. A) The common genes in the *lux* operon encode for various enzymes that function together in bioluminescence production. LuxA and LuxB encoded by *luxA* and *luxB* comprise α , β subunit of luciferase. *luxC*, *luxD*, *luxE* encode LuxC, LuxD and LuxE, four copies of which consist of fatty acid reductase. LuxG encoded by *luxG* is reported to be the flavin reductase. *luxG* is absent in the *lux* operons of *Photorhabdus luminescens* and newly characterized species of *Candidatus Photodesmus*. Nevertheless, the flavin reductase activity is compensated by an *Escherichia coli fre*-like gene. B) Chemical equation of the bacterial luciferase catalyzed reaction. Bacterial luciferase (LuxA/B), fatty acid reductase (LuxC/D/E complex) and flavin

reductase (LuxG or its equivalence) compose the molecular machinery to produce continuous bioluminescence.

The FMN reductase is commonly encoded by *luxG*. Nevertheless, when *luxG* is absent in the *lux* operons such as in *Photobacterium luminescens* and *Candidatus Photodesmus*, the flavin reductase activity can be replaced by an *Escherichia coli fre*-like gene.¹⁶⁴⁻¹⁶⁶ In fact, the insertion of *luxCDABE* genes is sufficient to convert a non-luminous bacterium to one that produces bioluminescence, which indicates that FMNH₂ can be provided from the other electron transport chain in all bacteria. In luminous bacterium, FMNH₂ used in bioluminescence production is usually supplied by the activity of flavin reductase (NADH:FMN oxidoreductase). It extracts reductant from reduced nicotinamide adenine dinucleotide (NADH) from other metabolic pathways such as tricarboxylic acid (TCA) cycle to reduce FMN. The reductant from FMNH₂ can diffuse freely to bacterial luciferase.¹⁶⁷ (Figure 31B)

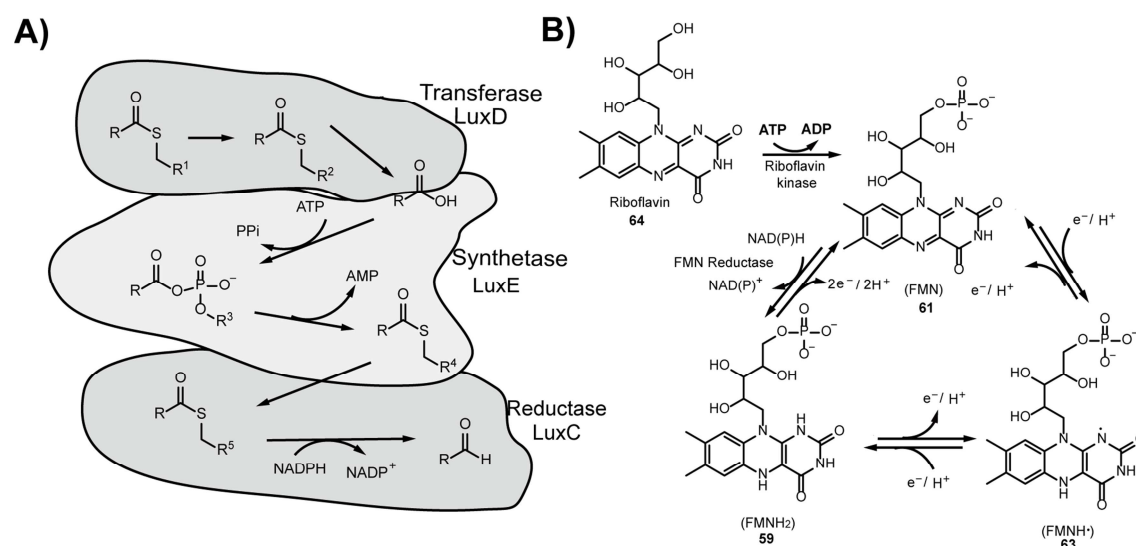
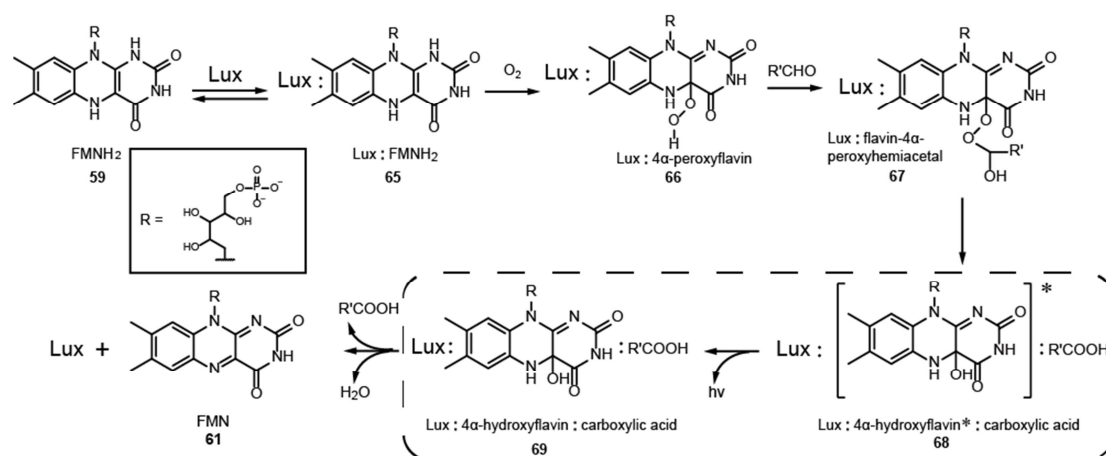


Figure 31. Mechanism of fatty acid reductase and FMN reductase. A) Simplified reactions in the fatty acid reductase enzyme complex. B) Production of FMNH₂ in luminous bacterial cells. FMN (**61**) is produced by phosphorylation of riboflavin. FMN reductase reduce FMN to FMNH₂ with NAD(P)H which is tapped from the other metabolic pathways such as the tricarboxylic acid (TCA) cycle. ATP: adenosine triphosphate; ADP: adenosine diphosphate; AMP: Adenosine monophosphate; NADPH: reduced nicotinamide adenine dinucleotide phosphate.

The bacterial luciferase is the most important enzyme for bioluminescence production. The unique bacterial luciferase is a heterodimeric protein with 80 KDa mass which is composed of α and β subunits. The α subunit is around 40 KDa while the β subunit is around 37 KDa, and they are encoded by *luxA* and *luxB* respectively.¹⁶⁸ A detailed mechanism for the production

of bioluminescence is as follows. First, FMNH₂ (**59**) binds to the luciferase. This complex (**65**) is then reacted with O₂ to form the 4α-peroxyflavin complex (**66**). Second, the 4α-peroxyflavin complex (**66**) associates with fatty aldehyde to produce the stable flavin-4α-peroxyhemiacetal (**67**).¹⁶⁹ This stable intermediate (**67**) gradually decomposes to excited 4α-hydroxyflavin (**68**) and a carboxylic acid. Finally, the excited 4α-hydroxyflavin returns to its ground state resulting in a characteristic light emission. However, how the excited 4α-hydroxyflavin is generated is still not well understood.^{170,171} Oxidized FMN is slowly released after all of these oxygenation and flavin oxidation steps. Meanwhile, it is believed that a slow conformational change of the luciferase to its original active state for FMNH₂ association is one rate-limiting step in luciferase reaction.¹⁶³ (Scheme 8)



Scheme 8: Catalytic mechanism and intermediates during bacterial luciferase reaction. The steps in dashed rectangle are still not well investigated. Here Lux denotes luciferase.

1.2 Regulation of Bioluminescence

QS was first discovered during the study of the bioluminescence pattern and luciferase synthesis in *V. harveyi*. Later it was intensively investigated in two luminous bacteria, namely *Vibrio harveyi* and *Aliivibrio fischeri*, because of the easy measurement and sensitivity of bioluminescence in these strains. These studies greatly deepen our understanding of QS mechanisms as well as how bioluminescence is regulated by QS. It is worth noting that *Aliivibrio fischeri* was formerly classified as *Vibrio fischeri* and that the best studied strain *Vibrio harveyi* BAA-1116 was recognized as a member of *Vibrio campbellii* after whole genome sequencing. It was renamed *V. campbellii* BAA-1116.¹¹⁷ Energetically consuming bioluminescence regulated by QS is now known to be a characteristic of many luminous bacteria. In the following section, the mechanism of QS regulated bioluminescence in *V.*

campbellii BAA-1116 is outlined and discussed, since it is an important model system in QS research as well as the one used in the current research.

V. campbellii utilizes HAI-1, CAI-1 and AI-2-based QS circuits which consist of multicomponent phosphorylation/dephosphorylation cascades to regulate its gene expression, including expression of the *lux* operon. The three autoinducers have different structures. HAI-1 (harveyi autoinducer-1) is 3-hydroxybutanoyl homoserine lactone while AI-2 is (2S,4S)-2-methyl-2,3,3,4-tetrahydroxytetrahydrofuran borate and CAI-1 (cholerae autoinducer) is (Z)-3-aminoundec-2-en-4-one.⁹ They are synthesized by LuxM, LuxS and CqsA in cells and detected by LuxN, LuxP/Q and CqsS, respectively. At low concentrations of the three autoinducers, correlating with low cell density, the receptors which are not bound by their autoinducers become autophosphorylated and then relay their phosphoryl group to LuxU then to LuxO. The phosphorylated LuxO can activate the production of Qrr1-5 sRNA. Qrr1-5 sRNA can destabilize *luxR* mRNA in the presence of the chaperone Hfq. This will lead to an inhibition of *luxR* expression which further causes low expression of the *lux* operon. When the autoinducer concentrations are high, the receptors act as phosphatases and tap the phosphoryl groups from LuxO and LuxU. Thus, LuxO will not be phosphorylated resulting in the expression of LuxR. The transcriptional LuxR then activates gene expression. The *lux* operon is thus expressed in this case and a boost of bioluminescence production takes place. (Figure 13) Luciferase levels are 100 – 1000-fold higher and production of bioluminescence is 10^3 – 10^6 -fold higher in high autoinducer concentration cells than in low autoinducer concentration ones. In fact, because of the sensitivity between bioluminescence production and QS signaling system, bioluminescence is often used in QS research and high-throughput screening.¹⁵³

1.3 The Aim of the Project

Owing to the high detectability and quantum efficiency of bioluminescence as well as advances in sensitive bioluminescence instruments, there are a dramatically increasing number of novel applications of bioluminescence in the fields of environmental, pharmaceutical, forensic and food research.¹⁵²⁻¹⁵⁴ At the same time, QS regulated bioluminescence is an applicable assay for researchers to screen QS inhibitors (QSIs).^{7,172,173}

Many compounds active in QS inhibition contain certain structural motifs derived from N-acyl homoserine lactone (AHL) scaffold.¹¹ Among other features, the length of the acyl chain as well as the homoserine lactone core is identified as essential for QS. Structurally related fimbrolide natural products are potent irreversible inhibitors of QS/bioluminescence which

address LuxS and LuxE - the autoinducer 2 synthase and an essential protein for bioluminescence production, respectively.⁶⁸ These results indicate that the scope of AHL inspired molecules extends beyond the direct interaction with LuxR or transmembrane sensors offering opportunities to unravel additional QS-related targets.

Previously, natural product inspired aliphatic β -lactones were investigated in gram-positive bacteria and target identification studies by chemical proteomics revealed caseinolytic protease P (ClpP) and a few other members of the serine hydrolase family as specific targets.¹⁷⁴⁻¹⁷⁶ The structural composition of these compounds resembles some features of AHL produced by gram-negative bacteria raising the question of whether their interference with QS pathways is possible.

Here, an in-house screening of compounds revealed that β -lactones with a long aliphatic chain are excellent inhibitors of bioluminescence production in *Vibrios*. These compounds show even better bioactivity than the natural product fimbrolide. The inhibition of bioluminescence by β -lactones is intriguing as β -lactones could be potential QSIs and investigation into their mode of action will also provide a better understanding of bioluminescence, beneficial for its development in biotechnology. To achieve this goal, organic synthesis of customized probes and quantitative ABPP approach were employed to elucidate the protein targets of β -lactones *in vivo* in the QS model organism *Vibrio campbellii*.

2 Results and Discussion

2.1 Analysis of Diverse Beta-Lactone Bioluminescence Inhibitors in *Vibrios*

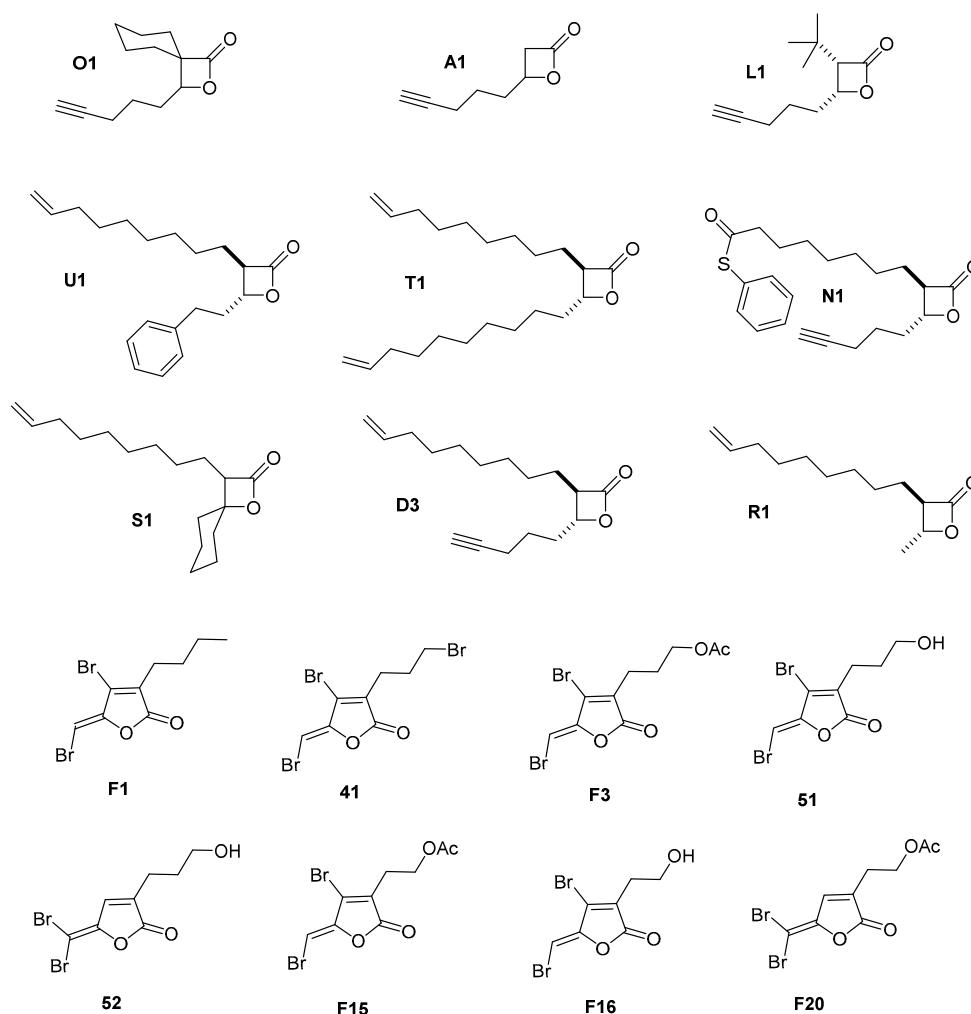


Figure 32: Structures of selected β -lactones and fimbrolide compounds.

To unravel if the electrophilic β -lactone scaffold could replace the larger and unreactive γ -lactone in AHLs, a panel of established β -lactones was tested in bioluminescence assays (Figure 32). In order to benchmark their potencies, fimbrolides were included as gold standard QS and bioluminescence inhibitors. All compounds were added at 50 μ M to *V. harveyi* NBRC 15634 strain cells and corresponding luminescence was detected on a plate reader. Out of the lactones tested, **R1** decorated with a nonenyl-chain in α -position and a methyl group in β -position revealed a strong reduction of luminescence by 90%, comparable to fimbrolides that ranged from 75 - 97% inhibition (Figure 33). A closer analysis of β -lactone structures revealed that although some of them exhibited an identical nonenyl-substituent in

α -position, larger moieties in β -position such as decenyl (**T1**), pentynyl (**D3**) or phenylethyl (**U1**) significantly decreased potency to 20%. Thus a small substituent in β -position seems to be a key structural requirement for bioluminescence inhibition.

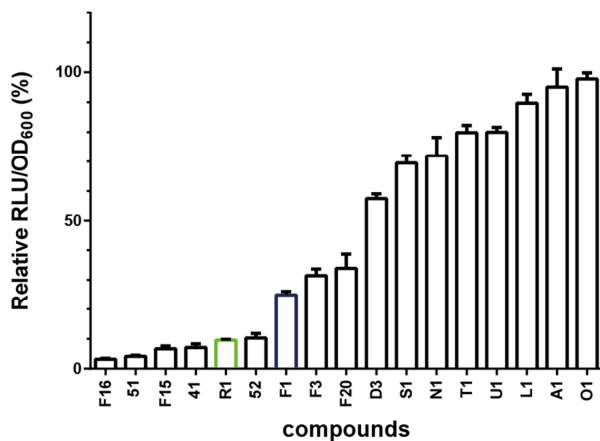
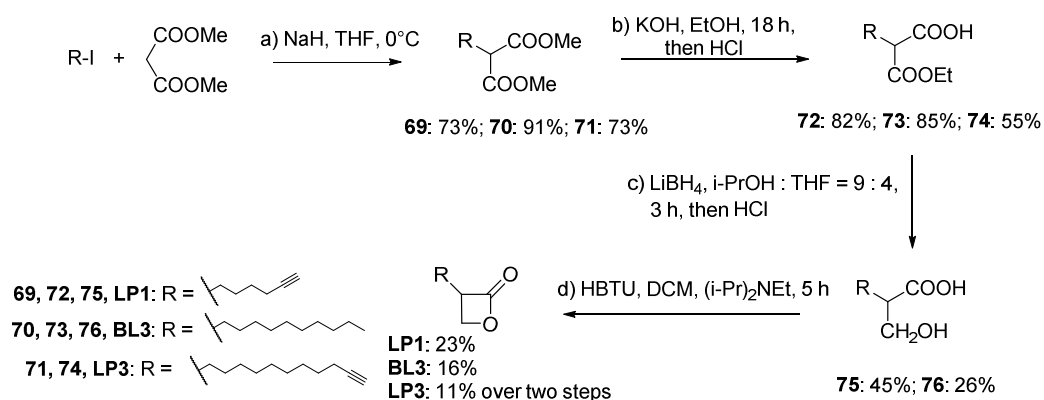


Figure 33: Residual bioluminescence activity of *V. harveyi* NBRC 15634 cells after 30 min incubation of 50 μ M selected β -lactone and fimbrolide compounds. Here the blue column signifies natural fimbrolide **F1** while the green column denotes **R1**. Relative luminescence units (RLU) were normalized to cell density (OD_{600}) and to the DMSO control. The data was based on three biological experiments with technical triplicates.

2.2 Synthesis of Monosubstituted Beta-Lactones



Scheme 9: Synthesis of β -lactones. a) NaH, THF, 0 °C, then add R-I; b) KOH, EtOH, rt, 18 h, then add HCl; c) LiBH₄, i-PrOH : THF = 9 : 4, 3 h, then add HCl; d) HBTU, DCM, (i-Pr)₂NEt, 5 h. THF = tetrahydrofuran, DCM = dichloromethane, HBTU = 2-(1H-benzotriazol-1-yl)-1,1,3,3-tetramethyluronium hexafluorophosphate.

Based on SAR (structure-activity relationship) information from our previous screening data, three monosubstituted β -lactones bearing a long aliphatic chain on their α -position without

any substituents on the β -position were synthesized.

Probe **LP1** was designed to incorporate a hexynyl group at the α -position. The synthetic route starts from dimethylmalonate, which was deprotonated with NaH in dried THF at 0 °C to produce a strong nucleophilic carbanion that was subsequently reacted with 6-iodo-1-hexyne to give dimethyl 2-(hex-5-yn-1-yl)malonate **69** in a 73% yield. This diester was then treated with KOH in ethanol for 18 hours at room temperature followed by neutralization with HCl, which leads to its partial hydrolysis to mono-ester **72** in a yield of 82%. To reduce the remaining ester group in **72** to an alcohol group, LiBH₄ was used. A solvent mixture of i-PrOH and THF was necessary to dissolve **72**, which had low solubility in i-PrOH owing to its long aliphatic chain. After reduction of **72** in 45% yield, 2-(hydroxymethyl)oct-7-ynoic acid **75** was cyclized with HBTU (2-(1H-benzotriazol-1-yl)-1,1,3,3-tetramethyluronium hexafluorophosphate) in 23% yield. The product **LP1** is an activity-based probe containing a terminal alkyne handle. (Scheme 9)

To confirm whether compounds containing longer aliphatic chains show improved bioactivity, another β -lactone **BL3** possessing a longer aliphatic chain than **LP1** was synthesized in a similar synthetic route. However, it showed lower yields in both reduction and cyclization steps compared with those in the synthesis of **LP1** due to poor solubility in the reaction solvent. Moreover, its corresponding probe **LP3** was synthesized as well. Its synthesis started from 10-decyn-1-ol, which was converted to 11-iodo-1-undecyne for the next steps. (Scheme 9)

2.3 Target Identification

2.3.1 Confirmation of Bioactivity

The synthesized compounds were applied in bioluminescence assays in *Vibrio campbellii* BAA-1116 to test their bioactivity in comparison to a previously established β -lactone compounds, **AV17**.¹⁷⁷ The natural fimbrolide **F1** was utilized as a reference.

It was found that β -lactone containing longer aliphatic chains exhibited excellent inhibition. Probe **LP3** was proved to be the best inhibitor with a IC₅₀ value of 0.5 μ M while **BL3** also showed excellent inhibition with a IC₅₀ value 1.8 μ M. Nevertheless, probe **LP1** with a short aliphatic chain was found to have a IC₅₀ 10.5 μ M which was much higher than **BL3** and **LP3**. In contrast, **AV17**, containing a decyl carbon alkyl chain at its β -position, showed a much higher IC₅₀ 25.3 μ M. All of these results confirmed our previous SAR expectation. As the probe **LP3** exhibited the best bioactivity, it was used in target identification via ABPP with **BL3**. (Figure 34)

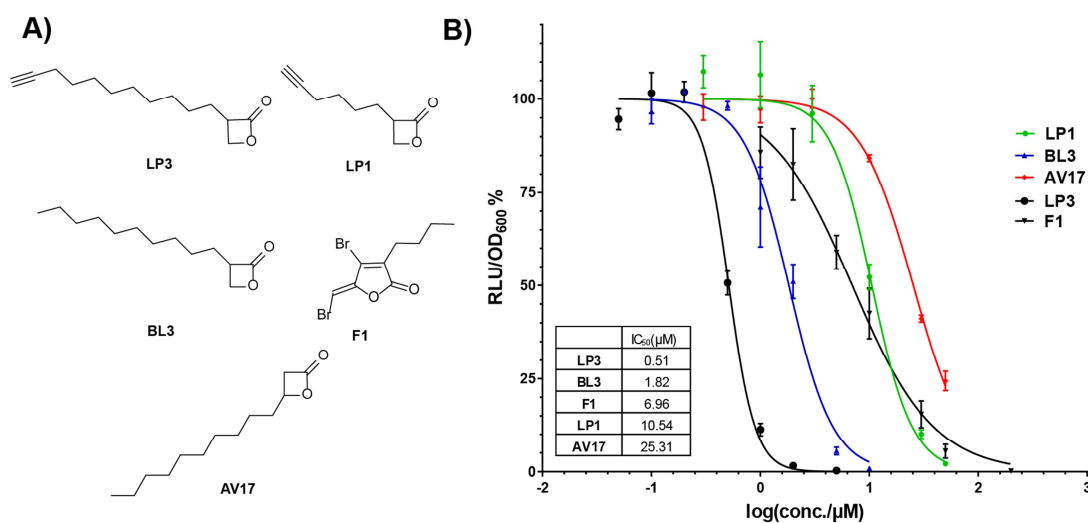


Figure 34. A) Structure of collected compounds used in determination of IC₅₀ values in bioluminescence assay in *V. campbellii*. B) Inhibition of bioluminescence production with collected compounds after 30 min incubation in *V. campbellii*. Relative luminescence units (RLU) were normalized to cell density (OD₆₀₀) and to the DMSO control. The well known QS inhibitor **F1** was used as a reference. The data was based on three biological experiments with technical triplicates.

2.3.2 *In Situ* Analytical Labeling

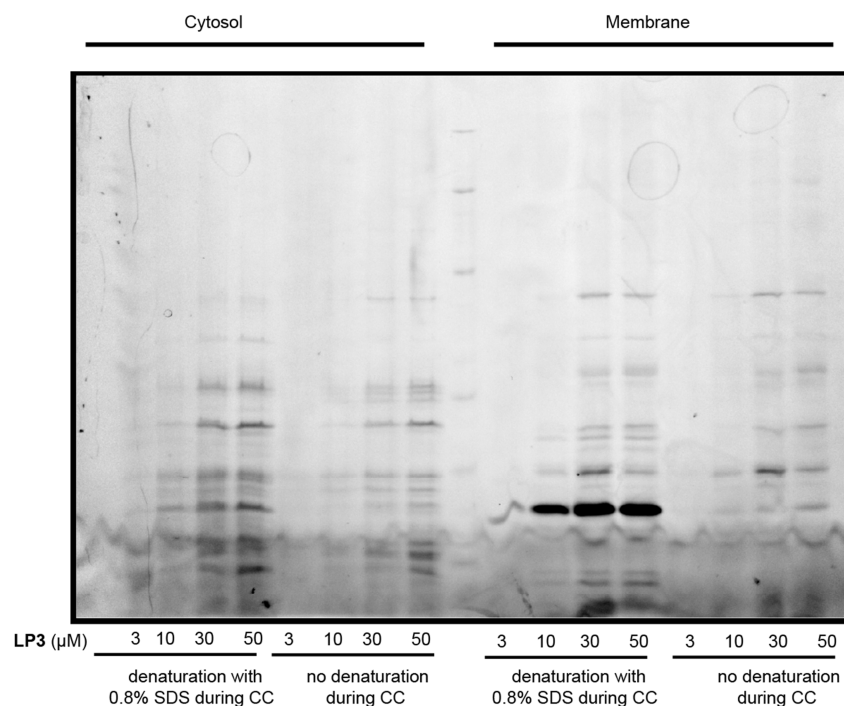


Figure 35: Fluorescent SDS-gel of *in situ* labeled *V. campbellii* with **LP3** (various concentrations) in soluble (cytosol) and insoluble (membrane) fraction. CC here denotes click chemistry. 0.8% SDS during

III – BETA-LACTONES • RESULTS AND DISCUSSION

CC means the addition of SDS to a final concentration of 0.8% during click chemistry to denature the proteins. No denaturation means SDS was not added during click chemistry.

Gel-based analytical *in situ* labeling was carried out to determine whether **LP3** can efficiently label protein targets as well as to optimize labeling conditions. However, the labeling of *Vibrio campbellii* cells using **LP3** resulted in poor fluorescence intensity and did not generate a reproducible labeling pattern. As the long aliphatic chain is crucial for the bioactivity of β -lactones, a possible cause may be inefficient click chemistry due to the poor accessibility to the alkyne. Since the alkyne is on a long aliphatic chain, its deep binding into the target pocket may impede the accessibility of the terminal alkyne towards click chemistry reagents in our ABPP approach. To overcome this obstacle, denaturation of the protein targets after molecular binding but before click chemistry is necessary. Therefore, 0.8% sodium dodecyl sulfate (SDS) PBS buffer was utilized in the click chemistry step after incubation of bacterial cells with probe **LP3** in pure PBS. Interestingly, the labeling of **LP3** exhibited much more intense labeling signals after fluorescent scanning on SDS gel in both soluble and insoluble samples. Nevertheless, the labeling of **LP3** in the insoluble fraction was much stronger than that in the soluble fraction. (Figure 35)

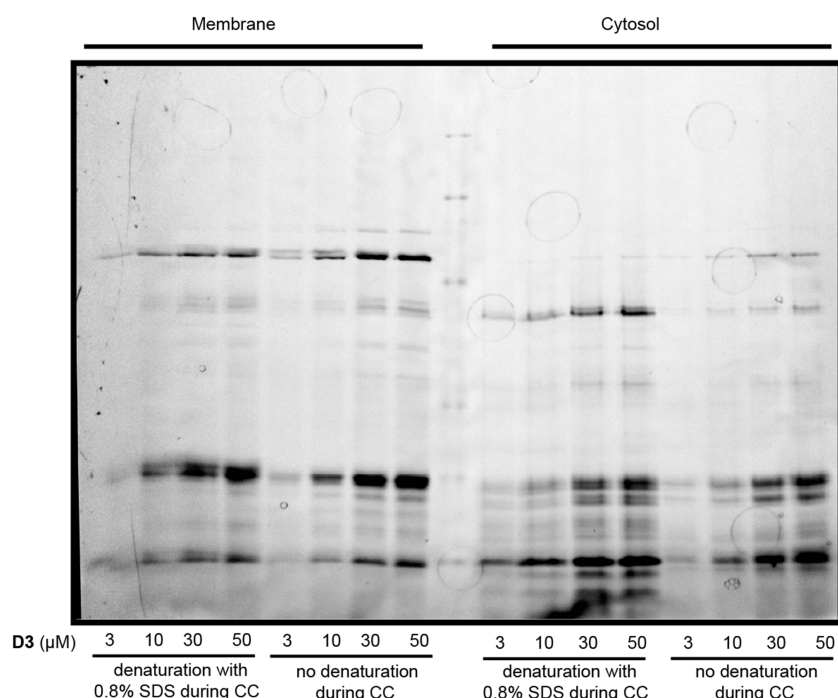


Figure 36: Fluorescent SDS-gel of *in situ* labeled *V. campbellii* with **D3** (various concentrations) in soluble (cytosol) and insoluble (membrane) fraction. CC here denotes click chemistry. 0.8% SDS during CC means the addition of SDS to a final concentration of 0.8% during click chemistry to denature the proteins. No denaturation means SDS was not added during click chemistry.

To confirm probe specificity, a **D3** probe that effectively labels ClpP *in vivo* was employed in analytical labeling for comparison.¹⁷⁶ **D3** exhibited a distinct labeling pattern from **LP3** in *Vibrio campbellii* BAA-1116 cells. As **D3** showed much weaker inhibition of bioluminescence in this strain than **LP3**, the different performance in *in situ* labeling of these two probes was encouraging. Since the fluorescent bands signified their labeled protein targets, this result also indicated that **LP3** and **D3** had different protein targets. Moreover, unlike **LP3**, the labeling of **D3** in 0.8% SDS PBS buffer showed only little difference when compared to that in pure PBS buffer after fluorescent scanning. This labeling difference can be explained by the difference in structure of these two probes. The terminal alkyne in **LP3** is on the long aliphatic chain which is essential for bioactivity, and is possibly hidden inside the binding pocket of the protein targets. By comparison, the terminal alkyne in **D3** is much more flexible than that of **LP3**. This result verified that the use of detergent was necessary in **LP3** labeling and its use did not increase unspecific labeling. (Figure 36)

After optimization of the click chemistry conditions, concentration-dependent labeling experiments were carried out to determine the optimal **LP3** concentration for ABPP experiments. An increase in fluorescence intensity can be observed in a **LP3** concentration-dependent manner in both the soluble and insoluble fraction. It was shown that 10 μ M of the probe was sufficient to observe a distinct labeling after fluorescent scanning. Thus, this concentration was used in subsequent experiments. As our synthetic β -lactone **BL3** exhibited similarly excellent bioactivity as **LP3**, it was used in analytical competitive labeling with **LP3**.

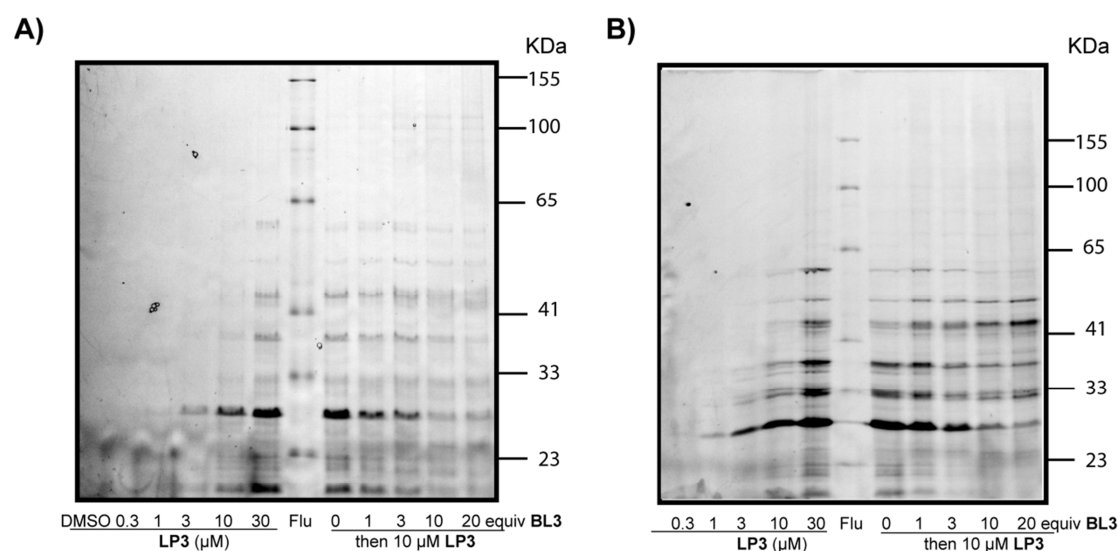


Figure 37: Fluorescent SDS-gel of *in situ* labeled *V. campbellii* with **LP3** (various concentrations) and competitive *in situ* labeling of 10 μ M **LP3** versus a various folds excess of **BL3**. A) Soluble fraction. B)

Insoluble fraction. DMSO denotes addition of DMSO instead of compounds. Flu means where fluorescent marker was applied.

As discussed previously, this experiment provides information as to whether the bands labeled by activity-based probes are the same as non-alkynylated counterparts. DMSO or 1, 3, 10, 20 equivalents of **BL3** were incubated with intact bacterial cells for 1 hour at room temperature prior to their incubation with **LP3** (final concentration = 10 μ M) for another hour. The labeling pattern was then visualized with fluorescent scanning after lysis of the cells, separation of the soluble and insoluble fractions and click chemistry. A concentration-dependent decrease in fluorescence intensity was observed suggesting that many protein targets are shared between **LP3** and **BL3**. (Figure 37)

2.3.3 Gel-Free Target Identification

To get a full understanding of irreversible protein targets of the bioactive β -lactones on a proteomic level, quantitative ABPP was conducted with our synthetic probe **LP3** and its counterpart **BL3**.

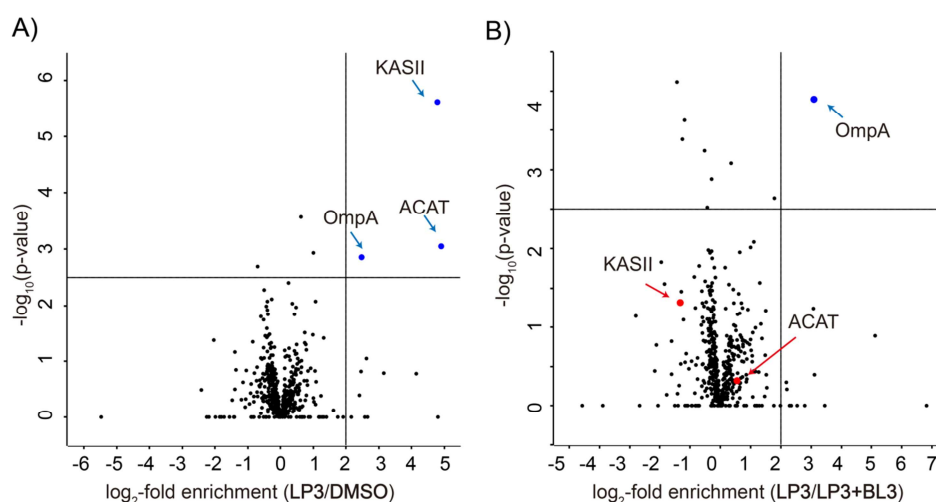


Figure 38: A) Volcano plot of gel-free quantitative ABPP experiments with 10 μ M **LP3** vs. DMSO in *V. campbellii* soluble fraction. Blue dots depict enriched targets (criteria: $\log_2\text{-fold enrichment} \geq 2$ and $-\log_{10}(\text{p-value}) \geq 2.5$). B) Volcano plot of gel-free competitive ABPP experiment in *V. campbellii* soluble fraction treated with 10 μ M **LP3** vs. a 20-fold excess of **BL3** (**LP3** + **BL3**). Blue dots depict selected targets that are competed by **BL3** (criteria: $\log_2\text{-fold enrichment} \geq 2$ and $-\log_{10}(\text{p-value}) \geq 2.5$). The red dots denote those targets enriched by **LP3** but not competed by **BL3**. Both results were derived from three biological replicates with technical triplicates and $-\log_{10}(\text{p-value})$ were calculated using two sided one sample Student's t-test based on Z scores with Perseus.

The bacterial cells were incubated with **LP3**, **BL3** or DMSO in three different ways as described in the previous chapter. The first sample set here named as **LP3** samples, were incubated first with DMSO for 1 hour then with **LP3** for another hour (final concentration = 10 μ M). For the second set, the **LP3 + BL3** samples, the cells were treated with 20 equivalents of **BL3** for 1 hour and then **LP3** for another hour. Finally, the third sample set, the DMSO samples were consistently incubated with DMSO for 2 hours. After ABPP, the samples were measured by mass spectrometry and analyzed using Maxquant software to give a quantitative overview of protein targets. (Figure 10) The results were further processed using Perseus and generated a volcano plot based on one sample Student's t-test analysis.

From the volcano plot of gel-free quantitative ABPP experiments from the soluble fraction, KASII (3-oxoacyl-[acyl-carrier-protein]), OmpA (out membrane protein A precursor) and ACAT (acetyl-CoA transferase) were most enriched by **LP3** (cut-off criteria: \log_2 -fold enrichment ≥ 2 and $-\log_{10}(\text{p-value}) \geq 2.5$). Nevertheless, only OmpA was well competed by **BL3** as can be shown in the competitive graph (cut-off criteria: \log_2 -fold enrichment ≥ 2 and $-\log_{10}(\text{p-value}) \geq 2.5$). (Figure 38)

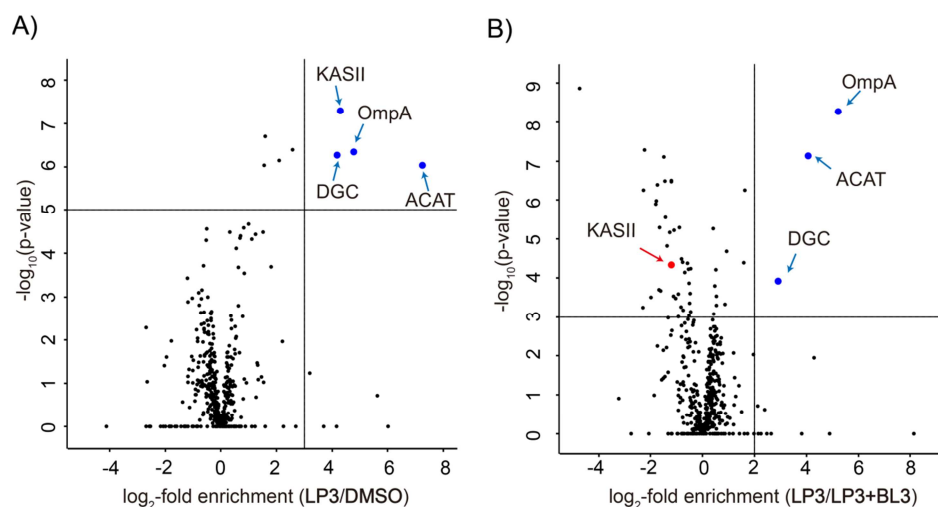


Figure 39: A) Volcano plot of gel-free quantitative ABPP experiments with 10 μ M **LP3** vs. DMSO in *V. campbellii* insoluble fraction. Blue dots depict enriched targets (criteria: \log_2 -fold enrichment ≥ 3 and $-\log_{10}(\text{p-value}) \geq 5$). B) Volcano plot of gel-free competitive ABPP experiment in *V. campbellii* insoluble fraction treated with 10 μ M **LP3** vs. a 20-fold excess of **BL3** (**LP3+BL3**). Blue dots depict selected targets that are competed by **BL3** (criteria: \log_2 -fold enrichment ≥ 2 and $-\log_{10}(\text{p-value}) \geq 3$). The red dots denote those targets enriched by **LP3** but not competed by **BL3**. Both results were derived from three biological replicates with technical triplicates and $-\log_{10}(\text{p-value})$ were calculated using two sided one sample Student's t-test based on Z scores with Perseus.

Nevertheless, the protein targets of **LP3** were generally much better enriched in the insoluble

fraction than in soluble fraction, which was consistent with the results from analytical labeling on SDS-gel by **LP3**. In fact, KASII was found to be well enriched by **LP3** but not competed by **BL3** in the insoluble fraction, which was in line with that in the soluble fraction. This excludes it from being a target that accounts for the bioactivity of β -lactones containing long aliphatic chains in bioluminescence assays. Although ACAT was not well competed by **BL3** in the soluble fraction, it was not the same in the insoluble fraction, as it exhibited promising enrichment by **LP3** and competition by **BL3**. Thus, it was believed to be a possible protein target responsible for the bioactivity of β -lactones. Another protein target DGC (GGDEF family protein) was found to be both well enriched and competed in our insoluble fraction data in spite of the fact that it was not detected in the soluble fraction at all. The most promising target was OmpA which showed excellent enrichment and best competition performance in both soluble and insoluble fractions. (Figure 39)

In total, ACAT, DGC and OmpA were chosen to be possible phenotype-related protein targets of β -lactones based on their performance in our quantitative ABPP experiments.

2.3.4 Gel-Based Target Identification

A gel-based ABPP technique was also employed to discover the protein targets of **LP3** in *Vibrio campbellii*. This technique is similar to analytical *in situ* labeling, but with several differences. First, more bacterial cells were necessary to assure sufficient amount of protein targets bound by probe. Second, after lysis of the bacterial cells, a trifunctional reagent containing not only fluorophore and azide groups but also a biotin group was utilized in the click chemistry step. Third, the biotin group was used to enrich the protein targets on avidin beads and remove most of the background proteins. After releasing the enriched protein targets from the avidin beads, the samples were visualized by SDS-gel electrophoresis and fluorescent scanning. The promising fluorescent bands as well as their corresponding areas in the blank control on gels were carefully cut out and digested. After measuring the peptides by mass spectrometry, a comparison of the MS-intensity of the detected proteins between enriched samples and the blank control were performed. A putative protein target should have a high intensity in the probe treated samples while a low or non-existent intensity in the control samples. (Figure 9)

With this technique, we indentified the protein target band which showed the strongest fluorescent intensity on SDS gel. This labeling band turned out to be OmpA, which was also the most promising target from our gel-free ABPP approach. The consistency of these two approaches confirmed and enhanced our confidence in our selected protein targets, ACAT,

DGC and OmpA. Furthermore, their validation was carried out in the next steps.

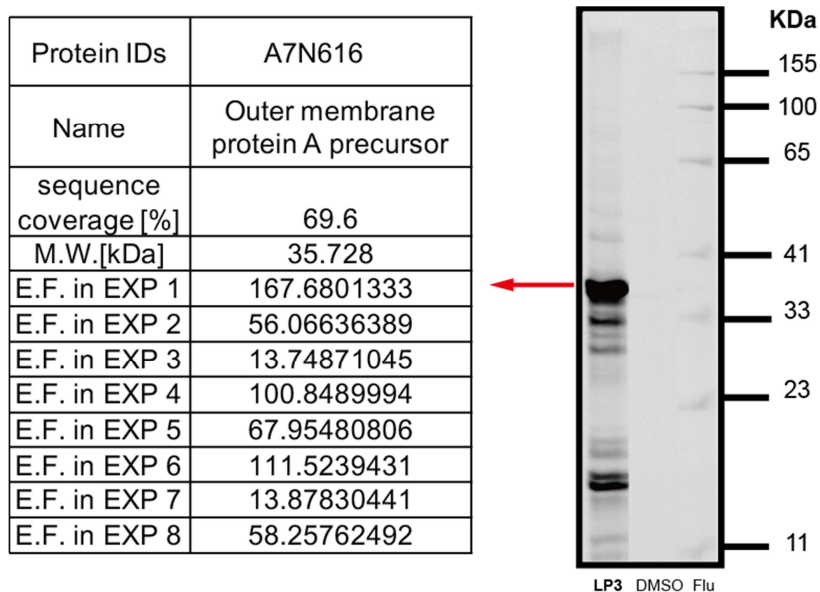


Figure 40: The most significant band on preparative SDS gel after ABPP approach with 10 μ M **LP3** or DMSO in *V. campbellii* insoluble fraction was revealed to be OmpA (uniprot ID: A7N616). E. F. denotes the enrichment factor which is calculated by mass intensity of the **LP3**-treated versus the DMSO-treated sample. The data show above is from eight experiments (two biological experiments with technical triplicates and one biological experiment with technical duplicates). Flu = fluorescent marker.

2.4 Target Validation

2.4.1 Target Validation of ACAT

ACAT or acetyl-CoA acetyltransferase (also abbreviated as PhaA), catalyzes two acetyl-CoA molecules to form acetoacetyl-CoA.¹⁷⁸ It is involved in many metabolic pathways such as fatty acid biosynthesis, tryptophan metabolism, terpenoid backbone biosynthesis and so on. It is quite surprising to identify ACAT as one of the best targets for β -lactones while PhaB emerged as a promising target for fimbrolides. Both ACAT and PhaB are involved in the energy storage molecule P(3HB) biosynthesis.^{146,147,149} (Scheme 7)

ACAT was recombinantly overexpressed in *E. coli* cells. These *E. coli* cells with or without induction were employed in *in situ* analytical labeling by **LP3**. After fluorescent scanning, a distinct band which was present in induced cells but absent in non-induced cells revealed recombinant ACAT can be labeled by **LP3**. Meanwhile, purified ACAT was found to be covalently modified by probe **LP3** in intact protein full-length mass spectrum. (Figure 41)

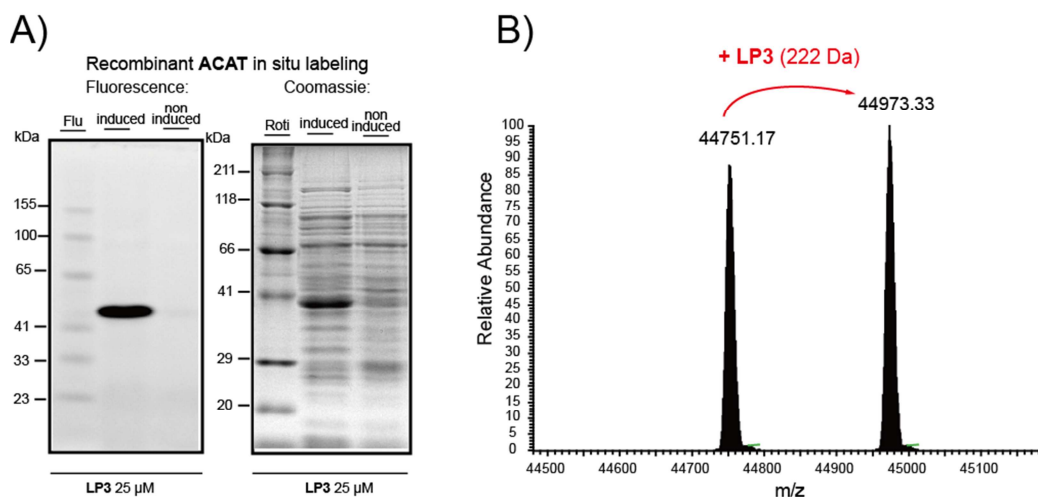
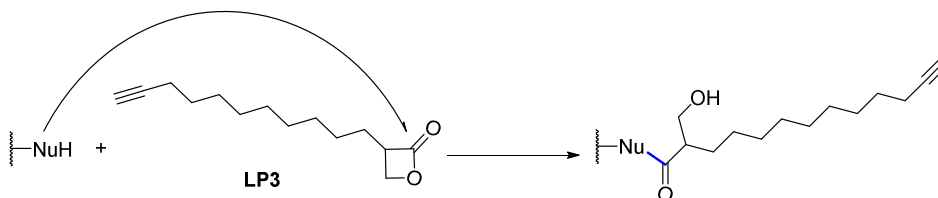


Figure 41: A) Analytical *in situ* labeling of recombinant ACAT expressed in *E. coli* with 25 μM LP3. Here, induced denotes induction of protein overexpression. B) Full-length MS measurements of intact recombinant protein ACAT after incubation with 2.5 equivalents of LP3 for 10 min in PBS buffer at room temperature.

An increase of 222 Da is equal to the molecular weight of LP3, which suggests this modification probably undergoes a nucleophilic reaction between ACAT and LP3. (Scheme 10)



Scheme 10: Possible mechanism of LP3 modification on protein targets.

In the validation of fimbrolide targets, no difference of bioluminescence production was observed between a $\Delta phaB$ mutant and the wild type. Therefore, a direct link between bioluminescence and the P(3HB) biosynthetic pathway possibly cannot be established here.⁶⁸ However, the involvement of ACAT in fatty acid biosynthesis suggests a putative role for it in bioluminescence production in *Vibrios*, which needs more investigation.

2.4.2 Target Validation of DGC

DGC (GGDEF family protein) is a 68.6 KDa protein and a predicted diguanylate cyclase. The diguanylate cyclases require two molecules of guanosine triphosphate (GTP) as their substrates and produce two molecules of diphosphate and one molecule of c-di-GMP (cyclic di-3',5'-guanylate, cyclic di-GMP). C-di-GMP is an important and universal second messenger

which has been shown to regulate biofilm formation, motility, virulence, the cell cycle, differentiation, and other processes.¹⁷⁹⁻¹⁸⁶ Moreover, the links between QS and c-di-GMP have been reported in *Vibrios*¹⁸⁷⁻¹⁸⁹ as well as in other bacterial strains.¹⁹⁰⁻¹⁹²

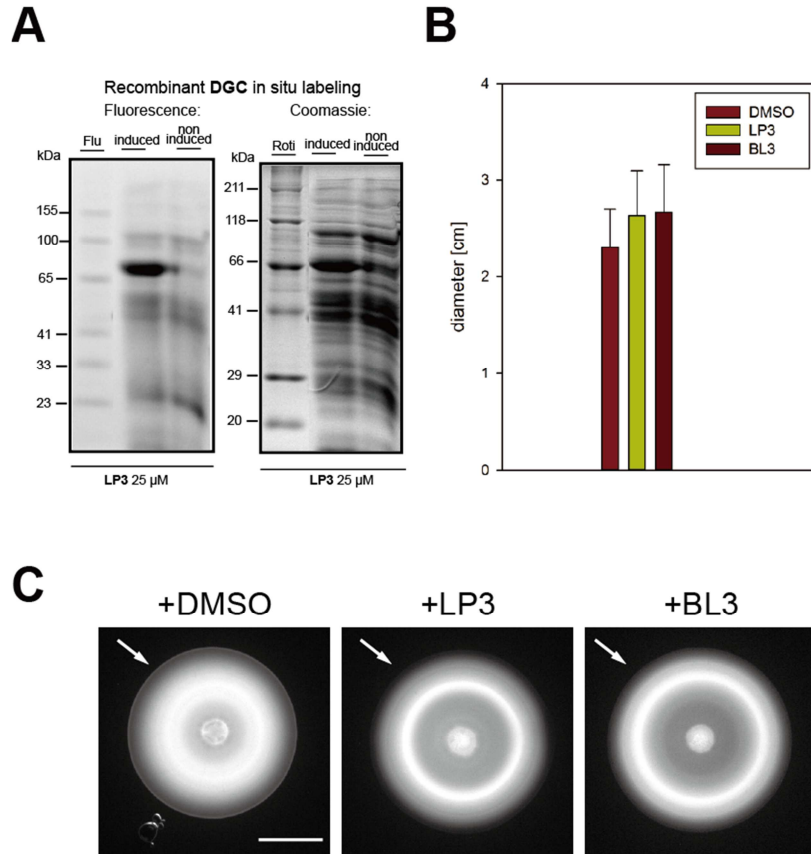


Figure 42: Recombinant DGC labeling with **LP3** and effects of **LP3** and **BL3** supplementation to the plates on the motility and colony size of *V. campbellii* ATCC BAA-1116. A) Analytical *in situ* labeling of recombinant DGC expressed in *E. coli* with 25 µM **LP3**. Here induced denotes induction of protein overexpression. B) Swimming motility on AB plates [0.3% (w/v) agar] supplemented with DMSO (left), 50 µM **LP3** (middle) or 50 µM **BL3** (right). Arrows indicate the differences in the outer ring formation (sharp vs. diffuse). The scale bar represents 1 cm. C) Diameter (cm) of the colony after growth of cells on AB plates [0.3% (w/v) agar] with DMSO/ 50 µM **LP3**/ 50 µM **BL3** and incubation at 30 °C. The experiment was performed in triplicate, and error bars indicate standard deviation of the mean. Figure 42B and 42C are from Nicola Lorenz in Prof. Kirsten Jung’s group at the LMU.

Recombinant DGC was overexpressed in *E. coli* cells. As expected, analytical *in situ* labeling indicated that recombinant DGC was labeled by **LP3**. (Figure 42A) C-di-GMP is believed to promote biofilm formation as it stimulates the biosynthesis of adhesions and exopolysaccharide matrix substances in biofilms. On the other hand, it inhibits bacterial motility. In general, it is crucial for bacteria to switch between motile planktonic and biofilm

living states.¹⁹³ Thus, a *V. campbellii* swimming assay was conducted with or without treatment of **BL3** and **LP3** to reveal the function of the protein target DGC. As shown below, in the presence of **BL3** or **LP3**, bacterial cells consistently swim a slightly larger distance compared to the DMSO treated samples. Moreover, bacterial cells treated with β -lactones exhibited a diffuse outer ring on the swimming plates which was much sharper than DMSO treated ones. This suggested that cells were not fully chemotactic in the presence of **BL3** or **LP3**. (Figure 42B and 42C)

31 proteins with largely unknown function are predicted as GGDEF family proteins in *V. campbellii*, which implies that the production of c-di-GMP is an important trait. Although the exact role of our protein target DGC in *V. campbellii* remains elusive and it is still not clear whether the other homologs could compensate for its inactivity, the effects observed in the swimming plate assays indicate the impairment of c-di-GMP mediated motility by β -lactones. As motility is an energy-consuming phenotype, this alteration possibly contributes to the reduction of bioluminescence production in *V. campbellii* in the presence of β -lactones.

2.4.3 Target Validation of OmpA

The protein target OmpA, which we identified by **LP3**, is known as outer membrane protein A precursor according to the annotation in PATRIC database (uniprot ID: A7N6I6). Its name is inferred from homology and OmpA is a putative membrane-bound channel protein with unknown function. However, it should be noted that there are four other proteins named outer membrane protein A precursor and they are poorly analogous to each other.

The validation of this target started with its recombinant expression in *E. coli* cells. As shown in the *in situ* analytical labeling SDS-gel, a distinct fluorescent band signified that OmpA was labeled by **LP3** in induced *E. coli* cells, while it was absent in non-induced *E. coli* cells. (Figure 43A) β -lactones preferentially react with serine or cysteine residues of elevated nucleophilicity e.g. in enzyme active sites. Prior to the investigation of OmpA function, its modification site by **LP3** was revealed to be serine167 after LC-MS/MS sequencing with recombinant OmpA employing an *in situ* labeling method. (Figure 43C)

As OmpA was an uncharacterized protein lacking known enzymatic activity, a $\Delta ompA$ mutant strain of *Vibrio campbellii* BAA-1116 was generated to gain more insights into its protein functions by our collaborator (Nicola Lorenz from group of Prof. Kirsten Jung, Ludwig-Maximilians Universität München, Department Biologie I). A comparison of *in situ* labeling ABPP experiment with **LP3** in the *V. campbellii* wild type and its $\Delta ompA$ mutant strain was carried out to verify the absence of OmpA. To our expectation, a distinct band at a height of

III – BETA-LACTONES • RESULTS AND DISCUSSION

36 KDa was present in the wild type samples but absent in the $\Delta ompA$ mutant samples. Meanwhile, the strongest fluorescent band at the height of 28 KDa was observed to be missing in the $\Delta ompA$ mutant strain, suggesting a maturation process of OmpA took place in the bacterial cells. (Figure 43B)

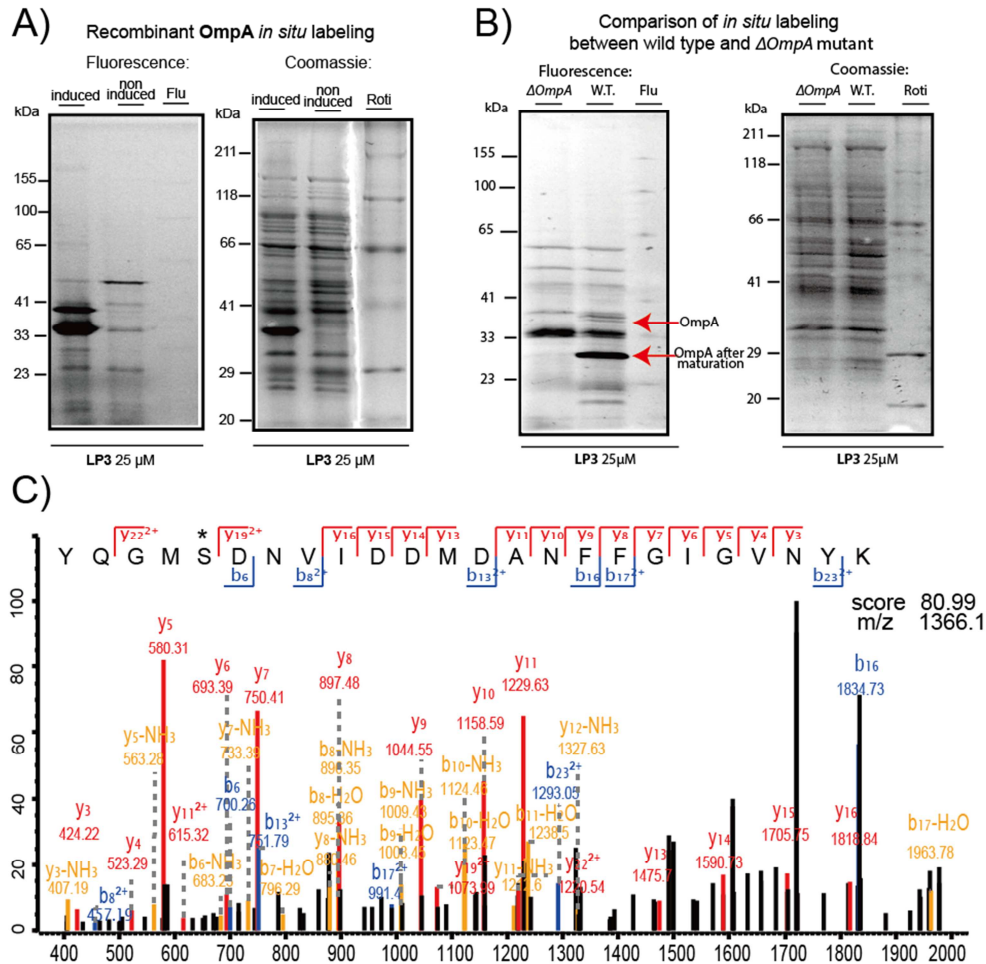


Figure 43: A) Analytical *in situ* labeling of recombinant OmpA expressed in *E. coli* with 25 μ M LP3. B) Comparison of analytical *in situ* labeling between *V. campbellii* wild type and its $\Delta ompA$ mutant. C) MS/MS sequencing shows the binding of LP3 to Ser167 of OmpA. * denotes the modified amino acid.

What we were most interested in is whether OmpA is involved in the production of bioluminescence/QS in *Vibrios* or not. Thus, the growth, bioluminescence production and motility were compared between the wild type and its $\Delta ompA$ mutant. Unfortunately, almost no difference can be observed in these phenotypes. Furthermore, LP3 and BL3 were employed in the bioluminescence assay in *V. campbellii* $\Delta ompA$ strain. An IC_{50} of 0.5 μ M for LP3 and 2.5 μ M for BL3 were very close to their IC_{50} values in the wild type. All of these results lead to the conclusion that either OmpA is not directly involved in the bioluminescence

production or its role can be substituted by some other proteins. (Figure 44)

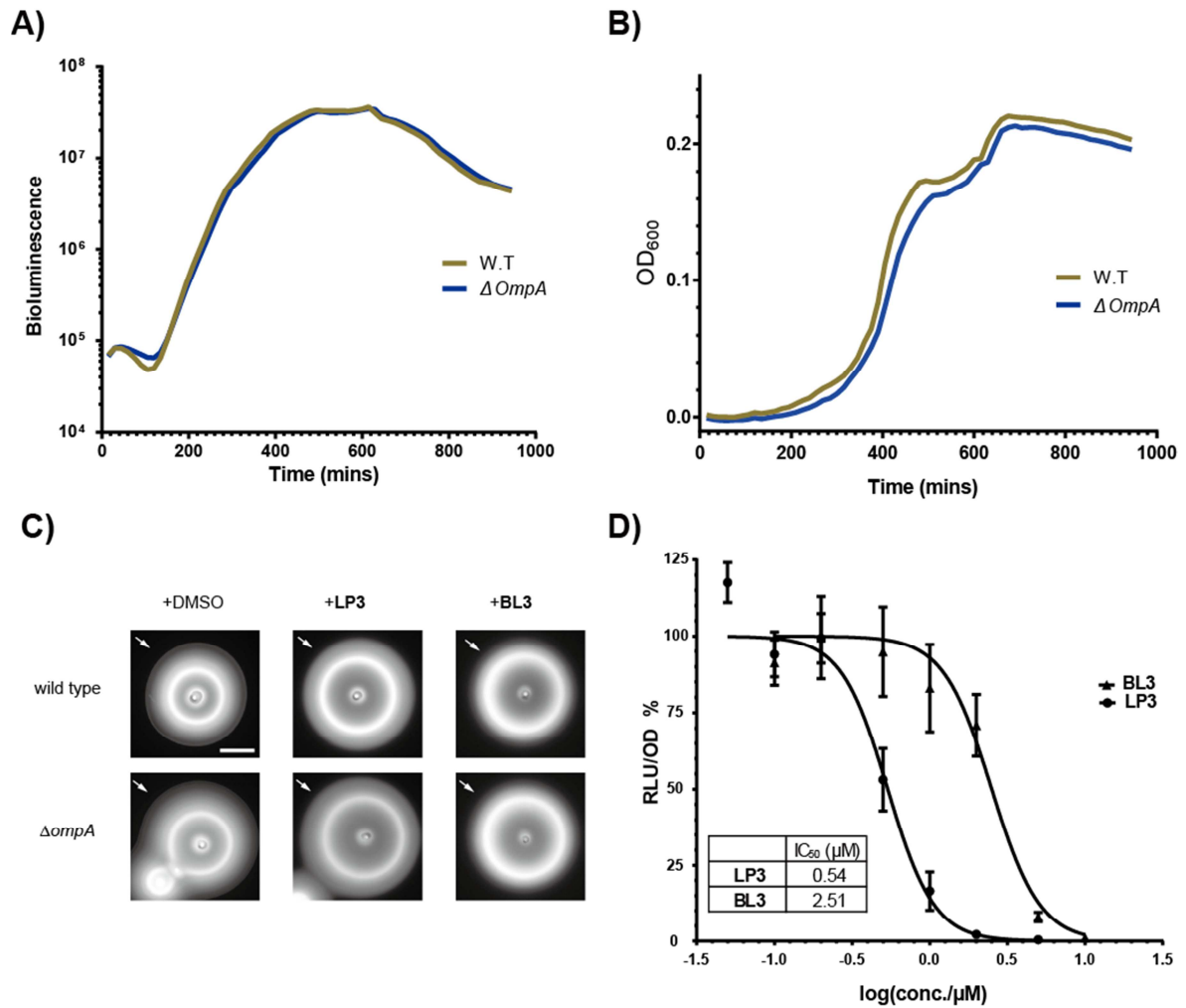


Figure 44: Assays for functional analysis of OmpA. A) Bioluminescence production comparison of *V. campbellii* ATCC BAA-1116 $\Delta ompA$ and its wild type. B) Growth comparison of *V. campbellii* ATCC BAA-1116 $\Delta ompA$ and its wild type. C) Effects of LP3 and BL3 on swimming motility of wild type *V. campbellii* ATCC BAA-1116 and the $\Delta ompA$ mutant. Swimming motility was analyzed after incubation of cells on AB plates [0.3% (w/v) agar] supplemented with DMSO, 50 μM LP3 or 50 μM BL3 at 30 °C for 20 h. Arrows indicate the differences in the outer ring formation (sharp vs. diffuse). Scale bar represents 1 cm. All experiments were performed at least three times, the standard deviation was less than 15%. D) Inhibition of bioluminescence production with BL3 and LP3 after 30 min incubation in *V. campbellii* $\Delta ompA$. Relative luminescence units (RLU) were normalized to cell density (OD_{600}) and to the DMSO control. The data was based on three biological experiments with technical triplicates. Figure 44C is from Nicola Lorenz in Prof. Kirsten Jung's group at the LMU.

2.5 Beta Lactones Act Independent of QS

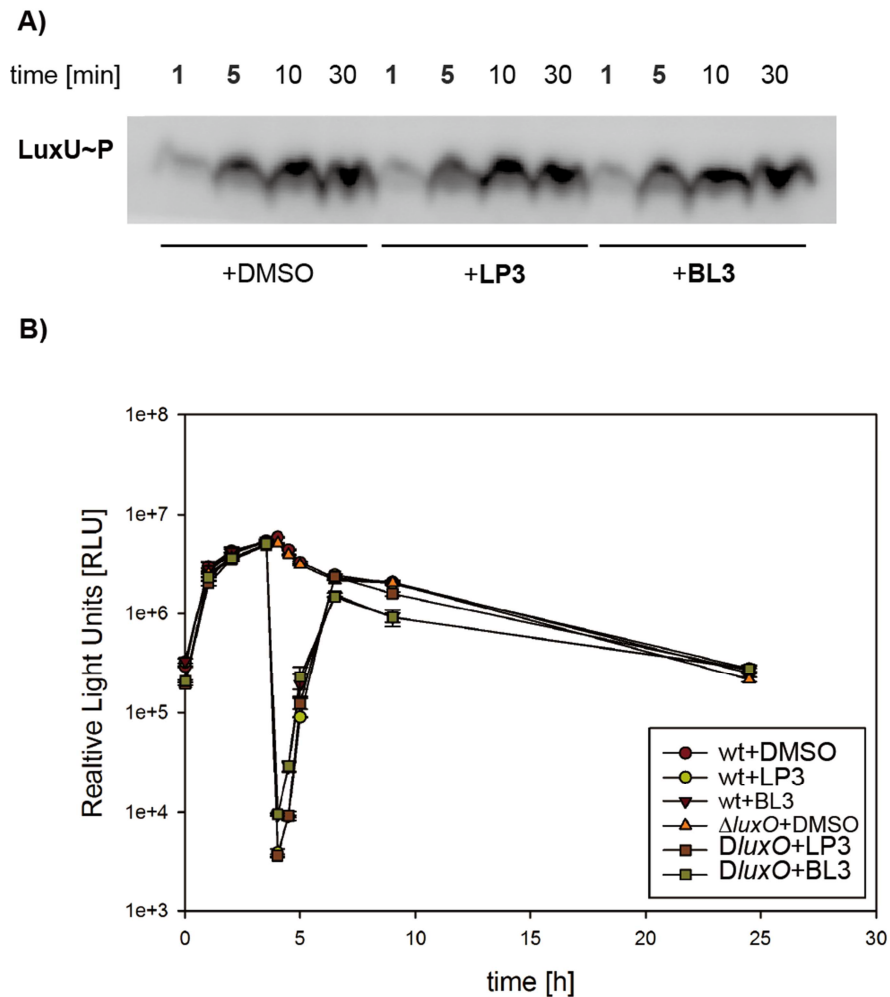


Figure 45: Effect of β -lactones on individual QS related proteins/strains. A) Effect of **LP3** and **BL3** on LuxN mediated phosphotransfer to the Hpt protein LuxU *in vitro*. Inverted membrane vesicles containing the hybrid histidine kinase LuxN were mixed with LuxU, and the reaction was started with [γ - 32 P] Mg $^{2+}$ ATP. When indicated **LP3** or **BL3** (10 μ M final concentration) or the corresponding volume of DMSO was added. At the indicated times (1, 5, 10 and 30 min) the phosphorylation reaction was stopped, proteins were separated by SDS-PAGE followed by exposure to a phosphoscreen. Shown are autoradiographs of LuxU parts of the gels, which are representative for three independent experiments. B) Effect of **LP3** and **BL3** on bioluminescence production of wild type (wt) *V. campbellii* ATCC BAA-1116 and the $\Delta luxO$ mutant (constitutively QS-ON). Cells from an overnight culture were inoculated in fresh AB-medium and grown aerobically at 30 °C in microtiter plates using a Tecan infinite F500 system. Bioluminescence and growth (OD $_{600}$) were recorded every hour. **LP3** and **BL3** were added in the exponential growth phase to a final concentration of 10 μ M. As control, the corresponding volume of DMSO was added to the cells. RLU, relative light units in counts per second per milliliter per OD $_{600}$. The experiment was performed in triplicate, and error bars indicate standard deviation of the mean. Figure 45 is from Nicola Lorenz in Prof. Kirsten Jung's group at the LMU.

To tell whether β -lactones act in a QS-related manner or not to inhibit the bioluminescence

production in *V. campbellii*, several assays were carried out. First, QS is regulated in a phosphorylation cascade in *V. campbellii* and the phosphorylation flow can be measured between different QS proteins.¹² As β -lactones are structurally related to AHLs, the phosphorylation between AHL receptor LuxN and its following functional protein LuxU in QS cascade was measured with or without the treatment of β -lactones. Neither **LP3** nor **BL3** altered the phosphorylation, which indicated no direct interaction between β -lactone and LuxN. (Figure 45A) Meanwhile, the production of bioluminescence in an intrinsically luminous $\Delta luxO$ mutant strain was still inhibited by **LP3** and **BL3**. This suggested a target downstream of LuxO is involved in the phenotypic change. (Figure 45B)

Moreover, the exoproteolytic activity, which should be enhanced by QS induction, was measured in the presence or absence of **LP3** and **BL3**.¹³⁴ Both lactones did not result in any change in the exoproteolytic activity. (Figure 46) This clarified that QS system was not addressed by β -lactones.

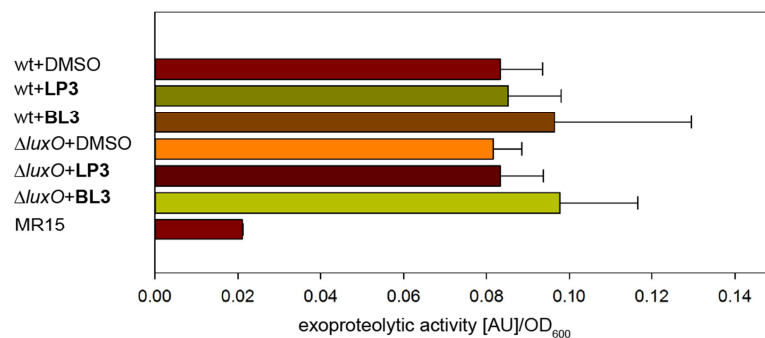


Figure 46: Influence of **LP3** and **BL3** on the exoproteolytic activity of wild type (wt) *V. campbellii* ATCC BAA-1116, the $\Delta luxO$ mutant (constitutively QS-ON) and the MR15 mutant ($\Delta cqsA$, $\Delta luxS$, $\Delta luxM$, constitutively QS-OFF). Exoproteolytic activity was determined in cell-free culture fluids in all strains. When indicated, 50 μ M **LP3**, 50 μ M **BL3** or the appropriate volume of DMSO was added prior cultivation. Culture fluids were obtained from cells grown for 16h. The experiment was performed in triplicate, and error bars indicate standard deviation of the mean. Figure 46 is from Nicola Lorenz in Prof. Kirsten Jung group in LMU.

2.6 Whole Proteome Analysis

Until now, no direct links between our three identified protein targets and bioluminescence can be established. Moreover, QS is not involved in the inhibition of bioluminescence production in *V. campbellii* by β -lactones. Therefore, a global proteome analysis was conducted to dissect their mode of action. More specifically, the protein expression level of

the $\Delta ompA$ mutant and chemical knock-down by **BL3** was compared with the wild type respectively.

The experiments were performed as follows. First, two sets of *V. campbellii* BAA-1116 and one set of its $\Delta ompA$ mutant strain cells were grown to $OD_{600} = 0.8$ in AB media. Then DMSO was added to one set of *V. campbellii* BAA-1116 cultures and its $\Delta ompA$ mutant strain culture while **BL3** was added to the other set of wild type culture to a final concentration of 25 μ M. After cultivating the cultures for another two hours, the bacterial cells were harvested, lyzed and digested to peptides, followed by stable isotope dimethyl labeling. The samples were measured on mass spectrometry and a quantitative result was obtained after analysis of the mass data on Maxquant.

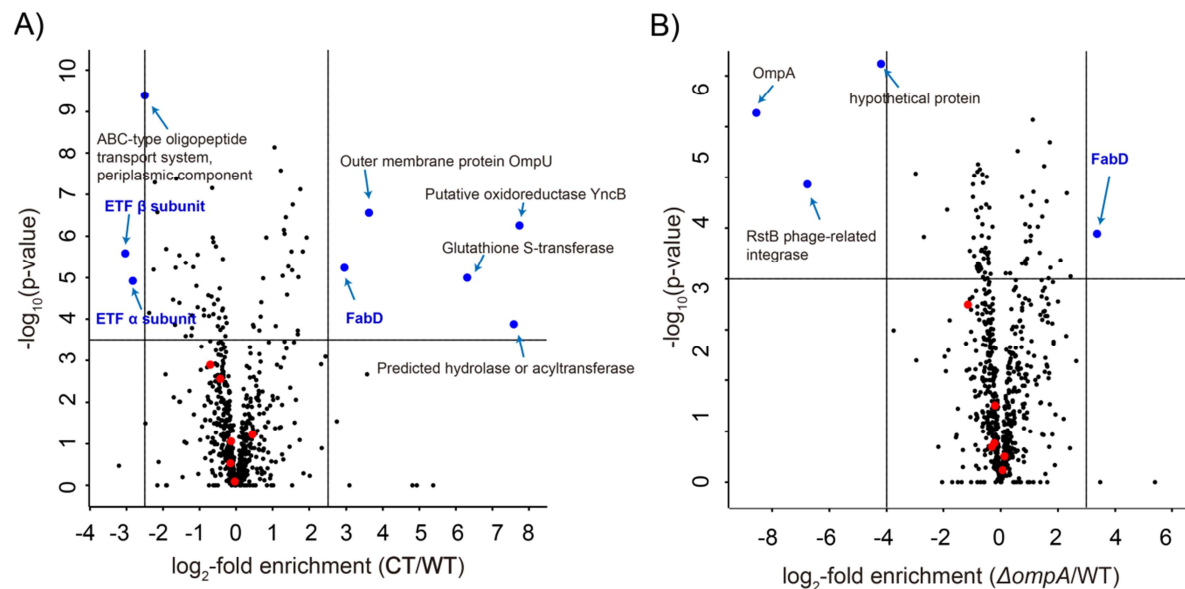


Figure 47: A) Volcano plot of whole proteome comparison between 25 μ M **BL3** treated *V. campbellii* ATCC BAA-1116 and its wild type. Blue dots depict selected targets that are significantly upregulated or downregulated (criteria: \log_2 -fold enrichment ≥ 2.5 or ≤ -2.5 and $-\log_{10}(p\text{-value}) \geq 3.5$). B) Volcano plot of whole proteome comparison between *V. campbellii* ATCC BAA-1116 $\Delta ompA$ and its wild type. Blue dots depict selected targets that are significantly upregulated or downregulated (criteria: \log_2 -fold enrichment ≥ 3 or ≤ -4 and $-\log_{10}(p\text{-value}) \geq 3$). Red dots denote proteins expressed from *luxCDABEG* operon which are essential for bioluminescence production in *V. campbellii* ATCC BAA-1116. WT denotes *V. campbellii* ATCC wild type while CT denotes the chemical knock-down. The targets discussed in the text are highlighted in blue in graphs. Data was derived from three biological replicates with technical triplicates and $-\log_{10}(p\text{-value})$ were calculated using two sided one sample Student's t-test based on Z scores with Perseus.

Interestingly, electron transfer flavoprotein (ETF) α subunit and β subunit were dramatically

downregulated in β -lactone-treated samples compared with the wild type. They are involved in the β -oxidation of fatty acids and thus linked to acyl- and acetyl CoA production.^{194,195} Therefore, the down-regulation of ETF under β -lactone may stall myristic acid biosynthesis required for luciferase activity establishing a putative link to bioluminescence inhibition with β -lactone.¹⁶² (Figure 46A)

Malonyl CoA-acyl carrier protein transacylase (FabD), one of the most upregulated proteins in both the *V. campbellii* BB120 $\Delta ompA$ mutant and chemical knock-down samples, was intriguing as it is involved in fatty acid biosynthesis. In other words, both the absence of OmpA and treatment of β -lactones will result in an increased expression level of malonyl CoA-acyl carrier protein transacylase in *V. campbellii* cells. Although the reason behind this observation remains elusive, a compensation effect can be a possible explanation. The expression levels of *luxCDABEG* operon did not show significant changes in both gene and chemical knockout strains, which is in line with our conclusion that QS is not addressed by β -lactones. (Figure 46)

3 Conclusion and Outlook

A panel of β -lactones was screened with bioluminescence assay in *V. campbellii* providing interesting SAR information. A long aliphatic chain at the α -position of the β -lactone as well as a small substituent at the β -position is crucial for inhibition of bioluminescence production. Several β -lactones (**LP1**, **BL3** and **LP3**) were synthesized according to this SAR information. These monosubstituted β -lactones possessed a long aliphatic chain at their α -position. Meanwhile, **LP1** and **LP3**, containing terminal alkyne handles, were designed to act as activity-based probes.

The newly synthesized β -lactones (**LP1**, **BL3** and **LP3**), containing various substitutions at the β -lactones as well as other available β -lactones (**AV17**) were tested in the bioluminescence assay, confirming that monosubstituted long chain β -lactones are excellent bioluminescence inhibitors. Compounds **LP3** and **BL3** were selected for our proteomic study because they were the best inhibitors with IC_{50} values of 0.5 and 1.8 μ M, respectively.

The *in situ* analytical labeling with **LP3** initially did not provide a reproducible labeling pattern after fluorescent scanning. However, slight modification of the ABPP protocol by the addition of detergent to denature proteins after the incubation of bacterial cells with **LP3** but before their lysis and ligation reaction greatly improved the fluorescence intensity of the labeled protein targets and generated reproducible results. A control probe **D3**, which had its flexible terminal alkyne at the β -position, confirmed that the labeling difference was probe-specific. Afterwards, a gel free ABPP approach served to identify ACAT, DGC and OmpA as the most promising protein targets of these bioactive β -lactones.

Each of these three proteins was recombinantly expressed in *E. coli* cells and successfully labeled by **LP3**. ACAT was well explored, but showed no direct links to QS/bioluminescence. DGC is a predicted diguanylate cyclase which produces the universal second messenger c-di-GMP. The c-di-GMP can switch biofilm formation and motility phenotypes in *Vibrios*. Bacterial cells consistently swam a slightly larger distance compared to the DMSO treated samples in the presence of **BL3** or **LP3**. This is suggestive of the impairment of c-di-GMP-mediated motility by β -lactones. A $\Delta ompA$ mutant was generated to investigate the function of OmpA. However, it was concluded to not be a target directly responsible for bioluminescence inhibition by β -lactones as the $\Delta ompA$ mutant did not show significant difference in growth, bioluminescence and motility with the wild type. Meanwhile, the similar IC_{50} values of **LP3** and **BL3** in the $\Delta ompA$ mutant and wild type strains consolidated this conclusion.

QS is not addressed by β -lactones as their application did not result in differences in several QS features such as phosphorylation and exoproteolytic activity. At the same time, the production of

bioluminescence in an intrinsically luminous $\Delta luxO$ mutant strain was still inhibited by LP3 and BL3.

A whole proteome comparison was performed with the *V. campbellii* wild type, its $\Delta ompA$ mutant, and its chemical knock-down cells. Malonyl CoA-acyl carrier protein transacylase (FabD) was found to be upregulated in the $\Delta ompA$ mutant as well as the chemical knock-down cells, compared to the wild type cells. Its function in the biosynthesis of fatty acids establishes a possible link to bioluminescence. Although no direct link between β -lactone treatment, OmpA function and FabD up-regulation can be established at this time, a compensation effect can be a possible explanation. Interestingly, the electron transfer flavoprotein (ETF) α and β subunits were dramatically downregulated in the chemical knock-down cells compared to the wild type cells. Their function in FMNH₂ reduction and cycle finally establish a link to bioluminescence inhibition by β -lactones. Nevertheless, a deeper understanding of their roles still requires more investigation.

IV – EXPERIMENTAL SECTION

1 Chemistry

1.1 Material and Methods

All chemical reagents and solvents were purchased in reagent grade or higher purity from the commercial sources Fluka/Sigma-Aldrich, Alfa-Aesar, AppliChem, Acros Organics, TCI Europe or Merck and used without further purification. All reactions sensitive to air and moisture were carried out in flame-dried glassware under an inert atmosphere of nitrogen or argon. Solvents removed under reduced pressure were evaporated at 40 °C. The yields of the substances refer to purified, dried compounds unless otherwise reported.

Flash column chromatography was performed on silica gel by Merck (Geduran Si 60, 40-63 μm), elution solvents were distilled prior to use and in case of solvent mixtures, ratios are given at the synthetic procedures for each product. Analytical thin-layer chromatography was carried out on aluminium-baked TLC Silica gel 60 F254 plates (Merck) and components were visualized by UV detection at 254 nm or stained via aqueous $\text{KMnO}_4/\text{K}_2\text{CO}_3$.

Reversed-phase HPLC analysis was performed on a Waters 2695 separation module equipped with a Waters XBridge C18 column (3.5 μm , 4.6 x 100 mm, flow rate = 1.2 mL/min) and a Waters 2996 PDA detector. Preparative RP-HPLC was accomplished with a Waters 2545 quaternary gradient module, equipped with a Waters XBridge C18 column (5.0 μm , 30 x 150 mm, flow rate = 50 mL/min) and an YMC Triart C18 column (3.5 μm , 10 x 250 mm, flow rate = 10 mL/min). Detection and fractionation was done on a Waters 2998 PDA detector and a Waters Fraction Collector III. Solvents used as mobile phase for elution were a gradient mixture of 0.1% (v/v) TFA in water (buffer A, HPLC-grade) and 0.1% (v/v) TFA in acetonitrile (buffer B, HPLC-grade).

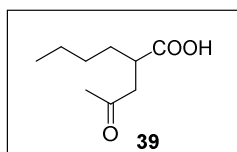
^1H NMR and ^{13}C NMR spectra were recorded on a Bruker Avance 360, Avance 500 or Avance III 500 spectrometer with CDCl_3 , d^6 -DMSO and d^6 -acetone as solvents. Chemical shifts (δ -values) were referenced to the residual proton or carbon signal of the deuterated solvent and are reported in parts per million (ppm). Coupling constants (J) are reported in Hertz (Hz) and the following abbreviations are used for the description of the multiplicity of the signals: s = singlet, d = doublet, t = triplet, q = quartet, m = multiplet.

Reversed-phase HPLC-ESI-HR-MS or HPLC-APCI-HR-MS analysis was performed on a Thermo Finnigan LTQ FT-ICR equipped with a Dionex Ultimate 3000 separation module eluting on a Waters XBridge C18 column (3.5 μm , 4.6 x 100 mm, flow rate = 1.1 ml/min). The column

temperature was maintained at 30 °C. The mobile phase for elution consisted of a gradient mixture of 0.1% (v/v) formic acid in water (buffer A, HPLC-MS grade) and 0.1% (v/v) formic acid in acetonitrile : water 90:10 (buffer B, HPLC-MS grade).

1.2 Synthetic Procedures

2-(2-oxopropyl)hexanoic acid (39)



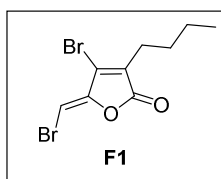
To a stirred solution of sodium ethoxide (545 mg, 8 mmol) in dried THF (30 mL) was added ethyl acetoacetate (945 mg, 7.3 mmol) at RT. The solution was stirred at RT for 30 min and then heated up to 80°C. After 1.5 h, ethyl 2-bromohexanoate (1.63 g, 7.3 mmol) was added to the stirred solution over 2 h via dropping funnel. The mixture was refluxed overnight and then cooled to RT. The precipitate was filtered off through celite, washed with EtOAc and the solvent was removed under reduced pressure to afford diethyl 3-acetyl-2-butyl-4-oxopentanedioate. The resulting product was used for the next step without purification.

Diethyl 3-acetyl-2-butyl-4-oxopentanedioate from the previous step was stirred with aqueous NaOH (5%, 30 mL) at RT overnight and then the HCl (12 M, 10 mL) was poured into the mixture in ice-bath. The aqueous phase was extracted with EtOAc (monitored by TLC until only trace product can be extracted). The combined organic layers were dried over Na₂SO₄, filtered and concentrated under reduced pressure to afford 3-acetyl-2-butyl-4-oxopentanedioic acid. The acid was dissolved in toluene (50 mL) and the solution was refluxed overnight. The mixture was cooled to RT and concentrated under reduced pressure to afford crude product, which was purified by silica gel column chromatography (hexane/EtOAc = 1/2, R_f = 0.35) to provide pure 2-(2-oxopropyl)hexanoic acid (430 mg, 2.5 mmol, 33% yield over 3 steps).

¹H NMR (360 MHz, CDCl₃): δ 11.37 (s, 1H), 2.83 – 2.70 (m, 2H), 2.50 – 2.36 (m, 1H), 2.04 (s, 3H), 1.60 – 1.47 (m, 1H), 1.47 – 1.34 (m, 1H), 1.19 (dq, *J* = 7.3, 3.6 Hz, 4H), 0.77 (t, *J* = 7.0 Hz, 3H).

¹³C NMR (91 MHz, CDCl₃): δ 207.08, 181.05, 44.45, 39.81, 31.20, 29.68, 28.92, 22.33, 13.64.

(*Z*)-4-Bromo-5-(bromomethylene)-3-butyl-2(5*H*)-furanone (F1)



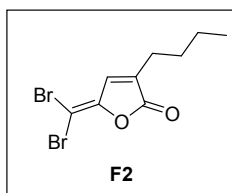
To a solution of 2-(2-oxopropyl)hexanoic acid **39** (344 mg, 2 mmol) in CHCl_3 (5 mL) and AcOH (10 mL), Br_2 (240 μL , 745 mg, 4.68 mmol) was added. The mixture was stirred at RT for 12 h. Then the reaction mixture was diluted with H_2O (20 mL) and extracted with 50 mL CH_2Cl_2 , washed with sat. aq. NaHCO_3 , sat. aq. $\text{Na}_2\text{S}_2\text{O}_3$ and brine, dried over Na_2SO_4 . The reaction mixture was filtered and concentrated under reduced pressure without further purification. The mixture was then refluxed in 3 mL concentrated H_2SO_4 at 120 °C for 15 min and then poured carefully into ice. The mixture was then extracted with CH_2Cl_2 (50 mL \times 3) and dried over Na_2SO_4 . After removal of the solvent, the crude product was purified on silica gel column chromatography (eluent, hexane/ CH_2Cl_2 = 3/2) to give **F1** (R_f = 0.60, 62 mg, 10% yield over 2 steps) a yellow liquid and **F2** (R_f = 0.70, 112 mg, 18% yield for 2 steps) as white solid. (**F1** and **F2** are synthesized according to the method outlined in previous literature and the NMR data is in accordance with previous reports.^{98,120})

^1H NMR (360 MHz, CDCl_3): δ 6.27 (s, 1H), 2.42 (t, J = 9.0 Hz, 2H), 1.67 – 1.53 (m, 2H), 1.39 (m, 2H), 0.95 (t, J = 7.3 Hz, 3H).

^{13}C NMR (91 MHz, CDCl_3): δ 166.09, 150.00, 133.94, 130.11, 90.86, 29.02, 25.05, 22.40, 13.66.

HRMS (pos. ESI) calcd for $\text{C}_9\text{H}_{10}\text{Br}_2\text{O}_2$ ($\text{M}+\text{H}^+$): 308.9126, found 308.9130.

3-Butyl-5-(dibromomethylene)-2(5H)-furanone (F2)

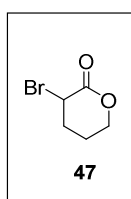


^1H NMR (360 MHz, CDCl_3): δ 7.29 (s, 1H), 2.37 (t, J = 7.3 Hz, 2H), 1.88 – 1.57 (m, 2H), 1.46 – 1.37 (m, 2H), 0.96 (t, J = 7.3 Hz, 3H).

^{13}C NMR (91 MHz, CDCl_3): δ 168.70, 149.75, 138.06, 134.04, 78.77, 29.40, 25.47, 22.27, 13.69.

HRMS (pos. ESI) calcd for $\text{C}_9\text{H}_{10}\text{Br}_2\text{O}_2$ ($\text{M}+\text{H}^+$): 310.9105, found 310.9107.

3-bromotetrahydro-2H-pyran-2-one (47)



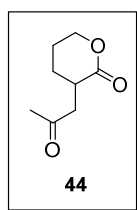
To a 1 M solution of LDA in THF (1.05 equiv., 166 mL, 166 mmol) at -78°C was added dropwise a solution of δ -valerolactone (1.0 equiv., 15.8 g, 158 mmol) in 150 mL THF over 1 h. The mixture was then stirred at -78°C for 10 min. Then the reaction mixture was naturally warmed up to RT for 20 min. Then chlorotrimethylsilane (1.08 equiv., 21.7 mL, 18.6 g, 171 mmol) was added in one portion and the mixture was stirred for 2 h at RT. The precipitate was removed by centrifugation and the solvent was removed under reduced pressure. The crude product was purified by distillation under reduced pressure to give ((3,4-dihydro-2*H*-pyran-6-yl)oxy)trimethylsilane (16.3 g) in a 60% yield as a colorless liquid (30 mbar, 68°C).

To a solution of ((3,4-dihydro-2*H*-pyran-6-yl)oxy)trimethylsilane (15.8 g, 90 mmol, 1.0 eq.) in CH_2Cl_2 (120 mL) was added Et_3N (14.25 mL, 103.5 mmol, 1.15 equiv.) and the mixture was cooled down to -15°C . A solution of Br_2 (4.5 mL, 14 g, 88 mmol, 1 equiv.) in CH_2Cl_2 (25 mL) was then added dropwise over 30 min and the reaction mixture was stirred at the same temperature for 1 h. The reaction was then quenched with sat. NaHCO_3 aqueous solution, extracted and washed sequentially with saturated $\text{Na}_2\text{S}_2\text{O}_3$ aqueous solution, brine and dried over anhydrous Na_2SO_4 . After removal of the solvent, the crude product was quickly filtered through a short silica gel column with DCM to give light yellow oil (14.8 g, 83 mmol, 92%).

^1H NMR (250 MHz, CDCl_3): δ 4.60 – 4.50 (m, 2H), 4.43 – 4.33 (m, 1H), 2.50 – 2.15 (m, 3H), 1.92 – 1.82 (m, 1H).

^{13}C NMR (63 MHz, CDCl_3): δ 166.85, 69.91, 40.93, 30.26, 19.95.

3-(2-oxopropyl)tetrahydro-2*H*-pyran-2-one (44)



To a stirred solution of sodium ethoxide (5.45 g, 80 mmol) in dried THF (80 mL) was added ethyl acetoacetate (9.45 g, 73 mmol) at RT. The solution was stirred at RT for 30 min and then heated up to 80°C . After 1.5 h, 3-bromotetrahydro-2*H*-pyran-2-one **47** (13.0 g, 73 mmol) was added to the stirred solution over 2 h via dropping funnel. The mixture was refluxed overnight and then cooled to RT. The precipitate was filtered off through celite, washed with EtOAc and the solvent was removed under reduced pressure to afford ethyl 3-oxo-2-(2-oxotetrahydro-2*H*-pyran-3-yl)butanoate as a crude yellow oil. The resulting product was used for the next step without purification.

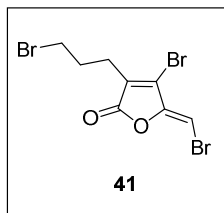
Ethyl 3-oxo-2-(2-oxotetrahydro-2*H*-pyran-3-yl)butanoate from the previous step was stirred with aqueous NaOH (5%, 300 mL) at RT overnight and then the HCl (12 M, 100 mL) was poured into the mixture in ice-bath. The aqueous phase was extracted with EtOAc (monitored by TLC until only trace product can be extracted) and the combined organic layers were dried over Na₂SO₄, filtered and concentrated under reduced pressure to afford 3-oxo-2-(2-oxotetrahydro-2*H*-pyran-3-yl)butanoic acid as a light yellow oil. The acid was dissolved in toluene (150 mL) and the solution was refluxed overnight. The mixture was cooled to RT and concentrated under reduced pressure to afford crude product, which was purified by silica gel column chromatography (hexane/EtOAc = 1/2, R_f = 0.4) to provide pure 3-(2-oxopropyl)tetrahydro-2*H*-pyran-2-one (2.5 g, 16 mmol, 22% yield over 3 steps) as a light yellow oil.

¹H NMR (360 MHz, CDCl₃): δ 4.36 (t, *J* = 5.8 Hz, 2H), 3.09 – 2.83 (m, 2H), 2.75 – 2.58 (m, 1H), 2.19 (s, 3H), 2.07 (dq, *J* = 12.6, 6.2 Hz, 1H), 1.91 (m, 2H), 1.57 (m, 1H).

¹³C NMR (91 MHz, CDCl₃): δ 206.05, 173.97, 68.48, 44.57, 35.46, 30.14, 24.87, 22.30.

HRMS (pos. ESI) calcd for C₈H₁₂O₃ (M+H)⁺: 157.0865, found 157.0860.

(*Z*)-4-Bromo-5-(bromomethylene)-3-(3-bromo-propyl)-2(5*H*)-furanone (41)



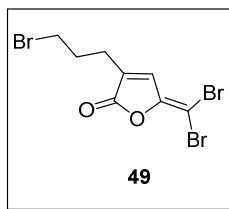
In a 100 mL sealed tube, lactone **44** (1.57 g, 10 mmol) was suspended in 15 mL 33% HBr in AcOH and 25 mL CHCl₃ and stirred overnight. Then, Br₂ (1.2 mL, 3.7 g, 23.4 mmol) in 35 mL AcOH was added and the mixture was stirred at RT for 20 h. The reaction mixture was diluted with H₂O (50 mL) and extracted with CH₂Cl₂ (50 mL × 3), washed with sat. aq. NaHCO₃, sat. aq. Na₂S₂O₃ and brine, dried over Na₂SO₄. After filtration and concentration, the mixture was then refluxed in 15 mL concentrated H₂SO₄ at 120 °C for 15 min. The reaction mixture was carefully poured into ice, extracted with CH₂Cl₂ (50 mL × 3) and dried over Na₂SO₄. After removal of the solvent, the mixture was purified on silica gel column chromatography (eluent, hexane/ CH₂Cl₂ = 3/2, R_f = 0.30) to give **41** as yellow liquid (449 mg, 12% yield over 3 steps) and **49** as white solid (R_f = 0.35, 862 mg, 23% yield over 3 steps).

¹H NMR (360 MHz, CDCl₃): δ 6.33 (s, 1H), 3.43 (t, *J* = 6.4 Hz, 2H), 2.69 – 2.52 (m, 2H), 2.28 – 2.07 (m, 2H).

¹³C NMR (91 MHz, CDCl₃): δ 165.86, 149.92, 132.08, 131.26, 91.93, 32.16, 29.56, 24.12.

HRMS (pos. ESI) calcd for $C_8H_7Br_3O_2$ ($M+Na$)⁺: 396.7873, found 396.7873.

3-(3-bromo-propyl)-butyl-5-(dibromomethylene)-2(5H)-furanone (49)

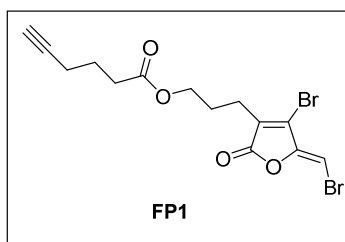


¹H NMR (360 MHz, CDCl₃): δ 7.38 (s, 1H), 3.45 (t, *J* = 6.4 Hz, 2H), 2.60 -2.56 (m, 2H), 2.23 – 2.15 (m, 2H).

¹³C NMR (91 MHz, CDCl₃): δ 168.33, 149.54, 135.85, 135.05, 79.90, 32.25, 29.81, 24.44.

HRMS (pos. ESI) calcd for $C_8H_7Br_3O_2$ ($M+Na$)⁺: 396.7873, found 396.7874.

3-(4-bromo-5-(bromomethylene)-2-oxo-2,5-dihydrofuran-3-yl)propyl hex-5-ynoate (FP1)



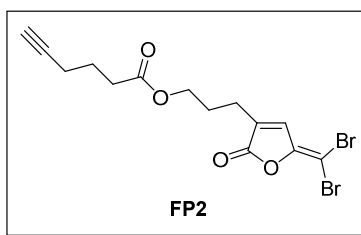
To a solution of compound **41** (375 mg, 1 mmol) in 20 mL acetone, 5-hexynoic acid (330 μL, 336 mg, 3 mmol, 3 eq.) and K₂CO₃ (414 mg, 3 mmol, 3 eq.) was added and the reaction mixture was refluxed at 72 °C for 6 h. The reaction mixture was filtered and concentrated under reduced pressure. The crude product was purified by silica gel column chromatography (CH₂Cl₂, R_f = 0.50) to provide pure **FP1** (97 mg, 0.24 mmol, 24% yield) as light yellow oil.

¹H NMR (360 MHz, CDCl₃): δ 6.32 (s, 1H), 4.12 (t, *J* = 6.2 Hz, 2H), 2.45 – 2.55 (m, 4H), 2.29 (td, *J* = 6.9, 2.6 Hz, 2H), 2.07 – 1.92 (m, 3H), 1.83 – 1.91 (m, 2H).

¹³C NMR (91 MHz, CDCl₃): δ 172.87, 165.85, 149.90, 132.64, 130.80, 91.64, 83.21, 69.20, 63.22, 32.77, 25.80, 23.54, 22.23, 17.85.

HRMS (pos. ESI) calcd for $C_{14}H_{14}Br_2O_4$ ($M+H$)⁺: 406.9317, found 406.9320.

3-(5-(dibromomethylene)-2-oxo-2,5-dihydrofuran-3-yl)propyl hex-5-ynoate (FP2)



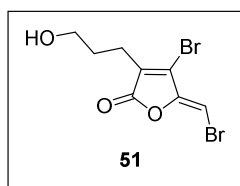
FP2 was obtained with a same procedure as **FP1** from **49** (375 mg, 1 mmol) and purified by silica gel column chromatography (CH_2Cl_2 , $R_f = 0.55$, 31% yield) as a colorless oil.

^1H NMR (360 MHz, CDCl_3): δ 7.35 (s, 1H), 4.14 (t, $J = 6.3$ Hz, 2H), 2.55–2.45 (m, 4H), 2.28 (td, $J = 6.9, 2.7$ Hz, 2H), 2.09–1.92 (m, 3H), 1.89–1.82 (m, 2H).

^{13}C NMR (91 MHz, CDCl_3): δ 172.98, 168.39, 149.57, 136.59, 134.59, 83.13, 79.62, 69.25, 63.18, 32.79, 26.32, 23.54, 22.62, 17.85.

HRMS (pos. ESI) calcd for $\text{C}_{14}\text{H}_{14}\text{Br}_2\text{O}_4$ ($\text{M}+\text{H}$) $^+$: 406.9317, found 406.9321.

(Z)-4-Bromo-5-(bromomethylene)-3-(3-hydroxypropyl)-2(5H)-furanone (51)



To a solution of compound **41** (375 mg, 1 mmol) in AcOH (15 mL), AgOAc (408 mg, 3 mmol) was added and the reaction mixture was refluxed at 120°C for 6 h in the darkness. The reaction mixture was filtered, concentrated under reduced pressure and used for the next step without further purification.

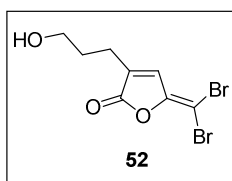
The concentrated mixture was dissolved in 10 mL THF and mixed with 5 mL 12% HCl. The solution was stirred overnight at RT, diluted with 20 mL H_2O and extracted with CH_2Cl_2 (20 mL \times 3). After combination and removal of the solvent, the residue was purified by silica gel column chromatography (eluent, hexane/EtOAc = 1/1) to give **51** ($R_f = 0.45$, 246 mg, 0.79 mmol, 79% yield over 2 steps) as a yellow oil.

^1H NMR (360 MHz, CDCl_3): δ 6.30 (s, 1H), 3.67 (t, $J = 6.1$ Hz, 2H), 2.53 (t, $J = 7.5$ Hz, 2H), 2.47 (s, 1H), 1.95–1.77 (m, 2H).

^{13}C NMR (91 MHz, CDCl_3): δ 166.52, 149.97, 133.34, 130.65, 91.58, 61.52, 29.70, 21.77.

HRMS (pos. ESI) calcd for $\text{C}_8\text{H}_8\text{Br}_2\text{O}_3$ ($\text{M}+\text{H}$) $^+$: 312.8898, found 312.8892.

3-(hydroxypropyl)-butyl-5-(dibromomethylene)-2(5H)-furanone (52)



To a solution of compound **49** (375 mg, 1 mmol) in DMSO (10 mL), KOAc (294 mg, 3 mmol) was added and the reaction mixture was stirred at RT for 6 h. The reaction mixture was filtered, extracted, concentrated under reduced pressure and used for the next step without further purification.

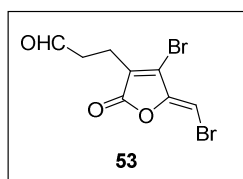
The concentrated mixture was dissolved in 10 mL THF and mixed with 5 mL 12% HCl. The solution was stirred overnight at RT, diluted with 20 mL H₂O and extracted with CH₂Cl₂ (20 mL × 3). After removal of the solvent, the residue was purified by silica gel column chromatography (eluent, hexane/EtOAc = 1/1) to give **52** (R_f = 0.50, 266 mg, 85% yield over 2 steps) as white solid.

¹H NMR (250 MHz, CDCl₃): δ 7.34 (t, J = 1.4 Hz, 1H), 3.69 (t, J = 6.1 Hz, 2H), 2.56 – 2.38 (m, 2H), 1.96 – 1.82 (m, 2H), 1.80 (s, 1H).

¹³C NMR (63 MHz, CDCl₃): δ 168.85, 149.64, 137.25, 134.61, 79.41, 61.46, 30.21, 22.20.

HRMS (pos. ESI) calcd for C₈H₈Br₂O₃ (M+H)⁺: 312.8898, found 312.8890.

(Z)-3-(4-bromo-5-(bromomethylene)-2-oxo-2,5-dihydrofuran-3-yl)propanal (53)

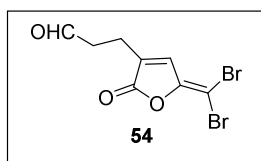


To a solution of compound **51** (156 mg, 0.5 mmol) in CH₂Cl₂ (10 ml), DMP (466 mg, 1.1 mmol) was added and stirred for 30 min at RT. The reaction mixture was then filtered and the filtrate was concentrated under reduced pressure. The crude product was purified by silica gel column chromatography (eluent, CH₂Cl₂, R_f = 0.57) to give **53** (93 mg, 0.30mmol, 60% yield) as a yellow oil.

¹H NMR (360 MHz, CDCl₃): δ 9.81 (s, 1H), 6.33 (s, 1H), 2.90 – 2.84 (t, J = 6.9 Hz, 2H), 2.71 (t, J = 7.0 Hz, 2H).

¹³C NMR (91 MHz, CDCl₃): δ 199.35, 165.76, 149.86, 131.62, 131.20, 92.07, 39.96, 18.27.

HRMS (pos. ESI) calcd for C₈H₆Br₂O₃ (M+Na)⁺: 332.8561, found 332.8556.

3-(5-(dibromomethylene)-2-oxo-2,5-dihydrofuran-3-yl)propanal (**54**)

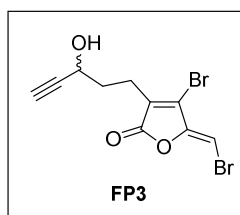
The compound was obtained with a similar procedure as **53** from **52** (156 mg, 0.5 mmol) as colorless liquid (eluent: CH₂Cl₂, R_f = 0.60, 112 mg, 72% yield).

¹H NMR (360 MHz, CDCl₃): δ 9.81 (s, 1H), 7.36 (t, *J* = 1.4 Hz, 1H), 2.88 – 2.84 (t, *J* = 6.9 Hz, 2H), 2.69 (t, *J* = 7.2 Hz, 2H).

¹³C NMR (91 MHz, CDCl₃): δ 199.59, 168.31, 149.45, 135.52, 135.42, 80.17, 40.81, 18.39.

HRMS(pos. ESI) calcd for C₈H₆Br₂O₃ (M+Na)⁺: 332.8561, found 332.8557.

(Z)-4-bromo-5-(bromomethylene)-3-(3-hydroxypent-4-yn-1-yl)furan-2(5H)-one (FP3)



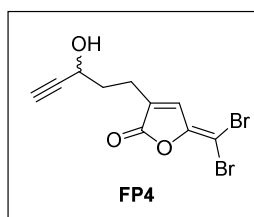
To a solution of compound **53** (310 mg, 1 mmol) in THF (4 mL), ethynylmagnesium bromide (2 mL, 1 mmol, 0.5 M solution in THF) was added at 0°C slowly and then the solution was warmed to RT. The reaction mixture was stirred overnight and then quenched with 10 mL 1M HCl. After extraction with CH₂Cl₂ (20 mL × 3), the solvent was removed and the residue was purified by silica gel column chromatography (CH₂Cl₂, R_f = 0.31) to give **FP3** (60.5 mg, 0.18 mmol, 18% yield) as a light yellow oil (isomers).

¹H NMR (360 MHz, CDCl₃): δ 6.31 (s, 1H), 4.47 – 4.43 (m, 1H), 2.68 – 2.60 (m, 2H), 2.533(s, 0.5H), 2.527(s, 0.5H), 2.10 – 1.91 (m, 3H).

¹³C NMR (91 MHz, CDCl₃): δ 166.19, 149.96, 132.80, 130.83, 91.63, 83.69, 73.86, 61.21, 34.15, 21.03.

HRMS (pos. ESI) calcd for C₁₀H₈Br₂O₃ (M+H)⁺: 336.8898, found 336.8895.

5-(dibromomethylene)-3-(3-hydroxypent-4-yn-1-yl)furan-2(5H)-one (FP4)



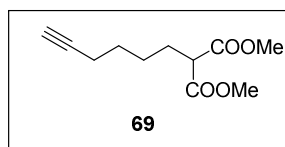
The compound was obtained using a similar procedure as **FP3** from **54** (310 mg, 1 mmol) as colorless liquid (CH₂Cl₂, R_f = 0.35, 97 mg, 29% yield, isomers).

¹H NMR (360 MHz, CDCl₃): δ 7.36 (t, *J* = 1.5 Hz, 1H), 4.49 – 4.45 (m, 1H), 2.62 – 2.57 (m, 2H), 2.539 (s, 0.5H), 2.533 (s, 0.5H), 2.10 – 1.99 (m, 3H).

¹³C NMR (91 MHz, CDCl₃): δ 168.60, 149.60, 136.72, 134.71, 83.73, 79.63, 73.97, 61.15, 34.69, 21.48.

HRMS (pos. ESI) calcd for C₁₀H₈Br₂O₃ (M+H)⁺: 336.8898, found 336.8896.

dimethyl 2-(hex-5-yn-1-yl)malonate (**69**)



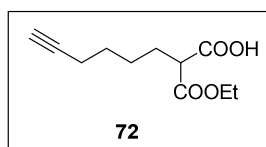
Dimethylmalonate (4.35 mL, 5.01 g, 38 mmol) was added dropwise to an ice cold suspension of NaH (720 mg, 30 mmol, 95% purity) in THF (85 mL) at 0 °C over 15 min under inert (Ar) atmosphere. The resulting slurry was stirred for 10 min at 0 °C and then 20 min at room temperature. After addition of 6-iodohex-1-yne (3.3 mL, 5.3 g, 25.5 mmol), the reaction mixture was refluxed for 3 hours and then cooled to room temperature. Brine (50 mL) was added and the resulting biphasic mixture was partitioned between Et₂O (50 mL) and H₂O (60 mL). The layers were separated and the aqueous layer was extracted three times with Et₂O (50 mL). The organic layer was combined and dried over Na₂SO₄. After removal of the organic solvent, the residue was purified by silica gel column chromatography (elution, hexane/EtOAc = 4/1) to give dimethyl 2-(hex-5-yn-1-yl)malonate **69** (R_f = 0.60, 3.9 g, 73% yield).

¹H NMR (300 MHz, CDCl₃): δ 3.70 (s, 6H), 3.33 (t, *J* = 7.5 Hz, 1H), 2.16 (td, *J* = 6.9, 2.6 Hz, 2H), 1.97 – 1.79 (m, 3H), 1.51 (m, *J* = 7.1 Hz, 2H), 1.46 – 1.32 (m, 2H).

¹³C NMR (75 MHz, CDCl₃): δ 169.70, 83.92, 68.53, 52.43, 51.47, 28.25, 27.93, 26.31, 18.07.

HRMS (pos. ESI) calcd for C₁₁H₁₆O₄ (M+H)⁺: 213.1127, found 213.1124.

2-(ethoxycarbonyl)oct-7-ynoic acid (**72**)



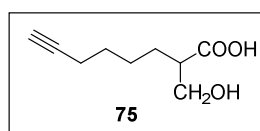
KOH (615 mg, 11 mmol) in EtOH (5.8 mL) was added dropwise via syringe to dimethyl 2-(hex-5-yn-1-yl)malonate **69** (1866 mg, 8.8 mmol) in ice bath under 0 °C over 50 min. The mixture was allowed to warm up to room temperature and stirred overnight for 18 hours. Then H₂O (40 mL) was added and the aqueous layer was acidified with HCl to pH 1.0. The mixture was extracted three times with AcOEt (40 mL) and the organic layer was combined. The combined organic layer was further washed with saturated brine (60 mL) and dried with Na₂SO₄. After removal of the solvent under reduced pressure, the residue was purified by silica gel column chromatography (elution, DCM/MeOH = 20/3) to give 2-(ethoxycarbonyl) oct-7-ynoic acid **72** (*R_f* = 0.67, 1.5 g, 82% yield).

¹H NMR (300 MHz, CDCl₃): δ 11.01 (s, 1H), 4.22 (q, *J* = 7.0 Hz, 2H), 3.39 (s, 1H), 2.22 – 2.18 (m, 2H), 1.96 – 1.92 (m, 3H), 1.59 – 1.46 (m, 4H), 1.28 (t, *J* = 7.1 Hz, 3H).

¹³C NMR (75 MHz, CDCl₃): δ 175.09, 170.37, 84.05, 68.58, 61.71, 52.05, 28.60, 27.98, 26.39, 18.12, 14.03.

HRMS (pos. ESI) calcd for C₁₁H₁₆O₄ (M+H)⁺: 213.1127, found 213.1123.

2-(hydroxymethyl)oct-7-ynoic acid (**75**)



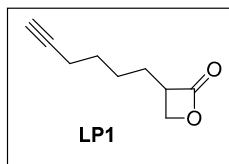
2-(ethoxycarbonyl)oct-7-ynoic acid **72** (1050 mg, 5 mmol) was dissolved in dried i-PrOH (9 mL) and THF (4 mL) under inert (Ar) atmosphere. Then LiBH₄ (220 mg, 10 mmol) dissolved in THF (2 mL) was added dropwise under 0 °C. The reaction mixture was then further stirred 3 hours at room temperature. The reaction was quenched with aqueous 3 M HCl (3 mL) and then diluted with H₂O (50 mL). The aqueous layer was extracted three times with AcOEt (50 mL) and then the organic layer was combined. After dryness of the organic layer with Na₂SO₄, the solvent was removed under reduced pressure. The crude product was purified by silica gel column chromatography (elution, DCM/MeOH = 20/3) to give 2-(hydroxymethyl)oct-7-ynoic acid **75** (*R_f* = 0.35, 383 mg, 45% yield).

¹H NMR (300 MHz, (CD₃)₂CO): δ 3.75 (dd, *J* = 10.5, 7.3 Hz, 1H), 3.66 (dd, *J* = 10.5, 5.5 Hz, 1H), 2.57 – 2.48 (m, 1H), 2.33 (t, *J* = 2.7 Hz, 1H), 2.22 – 2.17 (m, 2H), 1.68 – 1.39 (m, 6H).

^{13}C NMR (75 MHz, CDCl_3): δ 179.93, 84.23, 68.63, 62.93, 47.67, 28.23, 27.74, 26.27, 18.17.

HRMS (pos. ESI) calcd for $\text{C}_9\text{H}_{14}\text{O}_3$ ($\text{M}+\text{H}$) $^+$: 171.1021, found 171.1017.

3-(hex-5-yn-1-yl)oxetan-2-one (LP1)

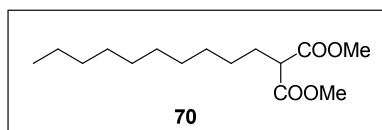


2-(hydroxymethyl)oct-7-ynoic acid **75** (354 mg, 2.1 mmol) dissolved in DCM (5 mL) was added to a solution of HBTU (915 mg, 2.4 mmol) and $\text{EtN}(\text{i-Pr})_2$ (968 mg, 1300 μL , 7.5 mmol) in DCM (25 mL). The mixture was stirred 5 hours at room temperature and then it was quenched by addition of saturated brine (25 mL). The reaction mixture was extracted three times with DCM (50 mL) and organic layer was combined. After dryness of the organic layer over Na_2SO_4 , the organic solvent was removed under reduced pressure. The residue was purified by silica gel column chromatography (elution, hexane/ AcOEt = 5/1) to give 3-(hex-5-yn-1-yl) oxetan-2-one **LP1** (R_f = 0.48, 73 mg, 23% yield).

^1H NMR (300 MHz, CDCl_3): δ 4.31 (dd, J = 6.3, 5.2 Hz, 1H), 3.98 – 3.94 (m, 1H), 3.66 (dtd, J = 8.4, 6.5, 4.5 Hz, 1H), 2.16 (td, J = 6.7, 2.7 Hz, 2H), 1.89 (t, J = 2.7 Hz, 1H), 1.87 – 1.61 (m, 2H), 1.59 – 1.39 (m, 4H).

^{13}C NMR (75 MHz, CDCl_3): δ 171.59, 83.81, 68.77, 64.95, 51.96, 27.91, 27.64, 25.85, 18.15.

dimethyl 2-decylmalonate (70)



Dimethylmalonate (4.35 mL, 5.01 g, 38 mmol) was added dropwise to an ice cold suspension of NaH (720 mg, 30 mmol, 95% purity) in THF (85 mL) at 0 °C over 15 min under inert (Ar) atmosphere. The resulting slurry was stirred for 10 min at 0 °C and then 20 min at room temperature. After addition of 1-iododecane (6.8 g, 25.5 mmol), the reaction mixture was refluxed for 3 hours and then cooled to room temperature. Brine (50 mL) was added and the resulting biphasic mixture was partitioned between Et_2O (50 mL) and H_2O (60 mL). The layers were separated and the aqueous layer was extracted three times with Et_2O (50 mL). The organic layer was combined and dried over Na_2SO_4 . After removal of the organic solvent, the

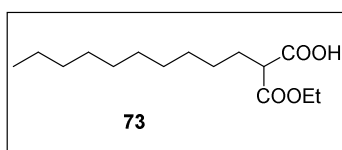
residue was purified by silica gel column chromatography (elution, DCM) to give dimethyl 2-decylmalonate **70** ($R_f = 0.60$, 6.3 g, 91% yield).

^1H NMR (360 MHz, CDCl_3): δ 3.67 (s, 6H), 3.29 (t, $J = 7.6$ Hz, 1H), 1.86 – 1.79 (m, 2H), 1.53 – 1.50 (m, 2H), 1.20 (m, 14H), 0.81 (t, $J = 6.6$ Hz, 3H).

^{13}C NMR (63 MHz, CDCl_3): δ 169.94, 52.36, 51.70, 31.85, 29.49 (2 CH_2), 29.25 (2 CH_2), 29.14, 28.82, 27.30, 22.62, 14.04.

HRMS (pos. ESI) calcd for $\text{C}_{15}\text{H}_{28}\text{O}_4$ ($\text{M}+\text{H}$) $^+$: 273.2066, found 273.2061.

2-(ethoxycarbonyl)dodecanoic acid (**73**)



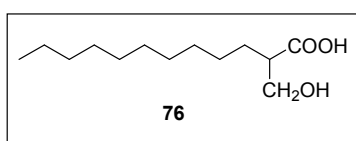
KOH (1.6 g, 28.7 mmol) in EtOH (16 mL) was added dropwise via syringe to dimethyl 2-decylmalonate **70** (6.0 g, 22 mmol) in ice bath under 0 °C over 50 min. The mixture was allowed to warm up to room temperature and stirred overnight for 18 hours. Then H_2O (50 mL) was added and the aqueous layer was acidified with HCl to pH 1.0. The mixture was extracted three times with AcOEt (50 mL) and the organic layer was combined. The combined organic layer was further washed with saturated brine (50 mL) and dried with Na_2SO_4 . After removal of the solvent under reduced pressure, the residue was purified by silica gel column chromatography (elution, DCM/MeOH = 20/3) to give 2-(ethoxycarbonyl)dodecanoic acid **73** ($R_f = 0.52$, 5.1 g, 85% yield).

^1H NMR (360 MHz, CDCl_3) δ 9.03 (s, 1H), 4.26 – 4.11 (m, 2H), 3.38 (t, $J = 7.4$ Hz, 1H), 2.03 – 1.82 (m, 2H), 1.37 – 1.20 (m, 19H), 0.89 (t, $J = 7.2$ Hz, 3H).

^{13}C NMR (91 MHz, CDCl_3): δ 175.33, 169.43, 61.63, 51.74, 31.86, 29.52, 29.48, 29.27, 29.25, 29.15, 28.85, 27.23, 22.64, 14.05, 14.00.

HRMS (pos. ESI) calcd for $\text{C}_{15}\text{H}_{28}\text{O}_4$ ($\text{M}+\text{H}$) $^+$: 273.2066, found 273.2061.

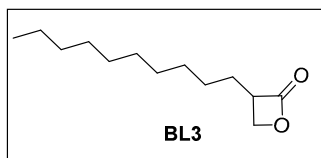
2-(hydroxymethyl)dodecanoic acid (**76**)



2-(ethoxycarbonyl)dodecanoic acid **73** (1360 mg, 5 mmol) was dissolved in dried i-PrOH (9 mL) and THF (4 mL) under inert (Ar) atmosphere. Then LiBH₄ (220 mg, 10 mmol) dissolved in THF (2 mL) was added dropwise under 0 °C. The reaction mixture was then further stirred 3 hours at room temperature. Then it was quenched with aqueous 3 M HCl (3 mL) and diluted with H₂O (50 mL). The reaction mixture was extracted three times with AcOEt (50 ml) and then the organic layer was combined. After dryness of the organic layer with Na₂SO₄, the residue was purified by silica gel column chromatography (elution, DCM/MeOH = 25/1) to give 2-(hydroxymethyl)dodecanoic acid **76** (R_f = 0.55, 298 mg, 26% yield).

HRMS (pos. ESI) calcd for C₁₃H₂₆O₃ (M+H)⁺: 231.1960, found 231.1957.

3-decyloxetan-2-one (BL3)



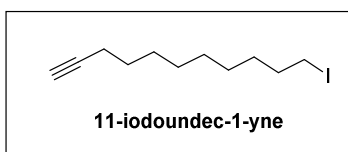
2-(hydroxymethyl)dodecanoic acid **76** (230 mg, 1 mmol) dissolved in DCM (2.5 mL) was added to a solution of HBTU (458 mg, 1.2 mmol) and EtN(i-Pr)₂ (484 mg, 650 μL, 3.75 mmol) in DCM (12 mL). The mixture was stirred 5 hours at room temperature and then it was quenched by addition of saturated brine (12 mL). The aqueous fraction was extracted three times with DCM (25 mL) and organic layer was combined. After dryness of the organic layer over Na₂SO₄, the organic solvent was removed under reduced pressure. The residue was purified by silica gel column chromatography (elution, hexane/AcOEt = 5/1) to give 3-(hex-5-yn-1-yl) oxetan-2-one **BL3** (R_f = 0.35, 34 mg, 16% yield).

¹H NMR (360 MHz, CDCl₃): δ 4.37 (dd, *J* = 6.3, 5.1 Hz, 1H), 4.08 – 3.98 (m, 1H), 3.72 (dtd, *J* = 8.5, 6.5, 4.5 Hz, 1H), 1.95 – 1.70 (m, 2H), 1.29 (d, *J* = 7.9 Hz, 16H), 0.93 – 0.88 (t, *J* = 7.2 Hz, 3H).

¹³C NMR (91 MHz, CDCl₃): δ 171.73, 64.97, 52.15, 31.86, 29.53, 29.48, 29.30, 29.26, 29.21, 28.12, 26.80, 22.64, 14.06.

HRMS (pos. ESI) calcd for C₁₃H₂₄O₂ (M+Na)⁺: 235.1674, found 235.1687.

11-iodoundec-1-yne

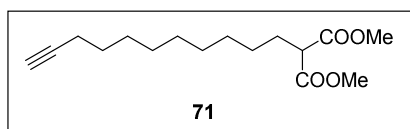


To a solution of imidazole (5.2g, 76 mmol) and triphenylphosphane (12 g, 46 mmol) in dried DCM (120 mL) was added I₂ (11.7 g, 46 mmol) in portions at 0 °C over the course of one hour. The reaction mixture was then stirred at room temperature for 1 hour after addition of undec-10-yn-1-ol (5.1 g, 30.5 mmol). The reaction was quenched by addition of saturated Na₂S₂O₃ aqueous solution (120 mL). The reaction mixture was diluted with DCM (200 mL), washed three times with saturated brine (100 mL). Then the organic layer was dried with Na₂SO₄. After removal of solvents, the product was purified by silica gel column chromatography (elution, hexane) to give 11-iodoundec-1-yne (R_f = 0.25, 4.6 g, 54% yield).

¹H NMR (300 MHz, CDCl₃): δ 3.21 (t, *J* = 7.0 Hz, 2H), 2.20 (td, *J* = 7.0, 2.7 Hz, 2H), 1.96 (t, *J* = 2.6 Hz, 1H), 1.84 (m, 2H), 1.65 – 1.47 (m, 2H), 1.46 – 1.25 (m, 10H).

¹³C NMR (75 MHz, CDCl₃): δ 84.74, 68.12, 33.54, 30.48, 29.27, 29.00, 28.69, 28.49, 28.45, 18.40, 7.37.

dimethyl 2-(undec-10-yn-1-yl)malonate (71)



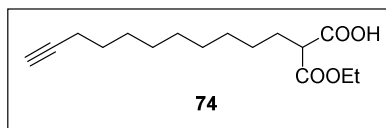
Dimethylmalonate (2.17 mL, 2.5 g, 19 mmol) was added dropwise to an ice cold suspension of NaH (360 mg, 15 mmol, 95% purity) in THF (40 mL) at 0 °C over 15 min under inert (Ar) atmosphere. The resulting slurry was stirred for 10 min at 0° C and then 20 min at room temperature. After addition of 11-iodoundec-1-yne (3.6 g, 13 mmol), the reaction mixture was refluxed for 3 hours and then cooled to room temperature. Brine (60 mL) was added and the resulting biphasic mixture was partitioned between Et₂O (50 mL) and H₂O (50 mL). The layers were separated and the aqueous layer was extracted three times with Et₂O (50 mL). The organic layer was combined and dried over Na₂SO₄. After removal of the organic solvent, the residue was purified by silica gel column chromatography (elution, hexane/AcOEt = 4/1) to give dimethyl 2-(undec-10-yn-1-yl)malonate **71** (R_f = 0.45, 2.3 g, 64% yield).

¹H NMR (300 MHz, CDCl₃): δ 3.75 (s, 6H), 3.37 (t, *J* = 7.6 Hz, 1H), 2.19 (td, *J* = 7.0, 2.7 Hz, 2H), 1.95 (t, *J* = 2.7 Hz, 1H), 1.93 – 1.83 (m, 2H), 1.60 – 1.46 (m, 2H), 1.42 – 1.24 (m, 12H).

¹³C NMR (75 MHz, CDCl₃): δ 169.97, 84.75, 68.08, 52.45, 51.70, 29.32, 29.22, 29.15, 29.02, 28.84, 28.70, 28.45, 27.31, 18.38.

HRMS (pos. ESI) calcd for $C_{16}H_{26}O_4$ (M+H)⁺: 283.1909, found 283.1909.

2-(ethoxycarbonyl)tridec-12-ynoic acid (**74**)



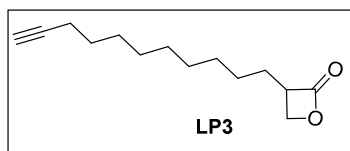
KOH (307 mg, 5.5 mmol) in EtOH (3 mL) was added dropwise via syringe to dimethyl 2-(undec-10-yn-1-yl)malonate **71** (1240 mg, 4.4 mmol) in ice bath under 0 °C over 50 min. The mixture was allowed to warm up to room temperature and stirred overnight for 18 hours. Then H₂O (30 mL) was added and the aqueous layer was acidified with HCl to pH 1.0. The mixture was extracted three times with AcOEt (40 mL) and the organic layer was combined. The combined organic layer was further washed with saturated brine (40 mL) and dried with Na₂SO₄. After removal of the solvent under reduced pressure, the residue was purified by silica gel column chromatography (elution, DCM/MeOH = 10/1) to give 2-(ethoxycarbonyl)tridec-12-ynoic acid **74** (R_f = 0.45, 682 mg, 55% yield).

¹H NMR (300 MHz, CDCl₃): δ 4.23 (q, *J* = 7.0 Hz, 2H), 3.34 (t, *J* = 7.0 Hz, 1H), 2.20 (td, *J* = 7.0, 2.6 Hz, 2H), 1.96 (t, *J* = 2.7 Hz, 1H), 1.91 – 1.89 (m, 2H), 1.60 – 1.47 (m, 2H), 1.46 – 1.22 (m, 15H).

¹³C NMR (75 MHz, CDCl₃): δ 175.58, 170.89, 84.64, 68.11, 61.53, 52.28, 29.40, 29.30 (2CH₂), 29.23, 29.05, 28.71, 28.45, 27.40, 18.36, 14.03.

HRMS (pos. ESI) calcd for $C_{16}H_{26}O_4$ (M+H)⁺: 283.1909, found 283.1905.

3-(undec-10-yn-1-yl)oxetan-2-one (LP3)



2-(ethoxycarbonyl)tridec-12-ynoic acid **74** (564 mg, 2 mmol) was dissolved in dried *i*-PrOH (4.5 mL) and THF (2 mL) under inert (Ar) atmosphere. Then LiBH₄ (88 mg, 4 mmol) dissolved in THF (1 mL) was added dropwise under 0 °C. The reaction mixture was then further stirred 3 hours at room temperature. Afterwards, the reaction was quenched with aqueous 3 M HCl (1.5 mL) and diluted with H₂O (30 mL). The aqueous layer was extracted three times with

AcOEt (40 ml) and then the organic layer was combined. After dryness of the organic layer with Na₂SO₄, the residue was used for the next step without further purification.

The residue suspended in DCM (5 mL) was added to a solution of HBTU (916 mg, 2.4 mmol) and EtN(i-Pr)₂ (968 mg, 1300 μL, 7.5 mmol) in DCM (25 mL). The mixture was stirred 5 hours at room temperature and then it was quenched by addition of saturated brine (30 mL). The reaction mixture was extracted three times with DCM (50 mL) and organic layer was combined. After dryness of the organic layer over Na₂SO₄, the organic solvent was removed under reduced pressure. The residue was purified by silica gel column chromatography (elution, hexane/AcOEt = 6/1) to give 3-(undec-10-yn-1-yl)oxetan-2-one **LP3** (R_f = 0.4, 48.8 mg, 11% yield over two steps).

¹H NMR (300 MHz, CDCl₃): δ 4.44 – 4.32 (m, 1H), 4.05 – 4.01 (m, 1H), 3.83 – 3.63 (m, 1H), 2.23 – 2.17 (m, 2H), 1.96 (t, *J* = 2.5 Hz, 1H), 1.92 – 1.72 (m, 2H), 1.53 – 1.28 (m, 14H).

¹³C NMR (75 MHz, CDCl₃): δ 171.85, 84.75, 68.10, 65.03, 52.11, 29.34, 29.27, 29.21, 29.03, 28.69, 28.45, 28.12, 26.80, 18.39.

HRMS (pos. APCI) calcd for C₁₄H₂₂O₂ (M+H)⁺: 223.1698, found 223.1692.

2. Microbiology

2.1 Bacterial Strains and Media

Different cultivation conditions were employed in our two projects. During the fimbrolide research, the bacterial strains and media used was described as follows. *Vibrio harveyi* NBRC 15634 was purchased from *Deutsche Sammlung von Mikroorganismen und Zellkulturen GmbH* and cultivated in BACTO Marine Broth at 28 °C with agitation (DIFCO 2216, for per liter: Bacto peptone 5.00 g, Bacto yeast extract 1.00 g, Fe(III) citrate 0.10 g, NaCl 19.45 g, MgCl₂ (dried) 5.90 g, Na₂SO₄ 3.24 g, CaCl₂ 1.80 g, KCl 0.55 g, Na₂CO₃ 0.16 g, KBr 0.08 g, SrCl₂ 34.00 mg, H₃BO₃ 22.00 mg, Na-silicate 4.00 mg, NaF 2.40 mg, (NH₄)NO₃ 1.60 mg, Na₂HPO₄ 8.00 mg, Agar if required 15.0-18.0 g. Final pH should be 7.6 ± 0.2 at 25 °C. If using the complete medium from Difco, 37.4 g add to 1 L water.). *Vibrio campbellii* ATCC BAA-1116, *V. campbellii* ATCC BAA-1116 $\Delta luxS$ and *V. campbellii* ATCC BAA-1116 $\Delta luxO$ were generally cultivated in BACTO Marine Broth at 30 °C with agitation when the medium was not specified.

On the other hand, in our research about β -lactones, *Vibrio harveyi* NBRC 15634 was cultivated in BACTO Marine Broth at 28 °C with agitation as above. Nevertheless, *Vibrio campbellii* ATCC BAA-1116 and its $\Delta ompA$, $\Delta luxO$ mutants were cultivated in autoinducer bioassay (AB) medium at 30 °C with agitation.¹⁹⁶ The AB base medium contained 17.5 g NaCl, 12.3 g MgSO₄, 2.0 g casamino acids, 970 mL distilled water. The base medium was adjusted to pH 7.5 with 3 N NaOH. Fresh AB medium was made before its use by addition of 1 mL 1M potassium phosphate (pH 7.0), 1 mL 0.1 M L-arginine and 1 mL glycerol to 100 mL AB base medium.

Recombinant proteins were expressed in different *E. coli* cells but all of them were cultivated in lysogeny broth (LB) (10.0 g peptone ex casein, 5.00 g NaCl, 5.00 g yeast extract in 1 L distilled water, pH 7.5). The super optimal broth with catabolite repression (SOC) was prepared for our transformation experiments as follows: 20.0 g yeast extract, 5.00 g tryptone, 0.50 g NaCl, 0.20 g KCl, 1.00 g MgCl₂, 1.20 g MgSO₄, 3.60 g glucose in 1 L distilled water, pH 7.3.

2.2 Cultivation Methods

2.2.1 Overnight Cultures

5 mL of the particular medium for cultivation were inoculated with 5 μ L of the desired bacterial cryostock (1:1000) with a sterile pipette tip in a plastic culture tube. The culture was

then incubated overnight (16 h, 200 rpm) in an Innova incubator shaker at desired degree. Overnight cultures were always prepared freshly to avoid genetic variations. A sterile control (medium containing no bacteria) was performed each time.

2.2.2 Cryostocks

1 mL of an overnight culture of the desired bacteria were harvested by centrifugation (10 min, 4 °C, 6000 rpm) and the pelletized cells were resuspended in 250 μ L fresh, sterile medium. 250 μ L of sterilized glycerin were added, the stocks were mixed, frozen in liquid nitrogen and stored at -80 °C in 20 μ L aliquots prior to use. After inoculating fresh media with the aliquot, the leftover amount of the cryostock was discarded.

2.3 Microbial Experiments and Assays

2.3.1 Minimal Inhibitory Concentration (MIC) Assay

The overnight culture was diluted to a final $OD_{600} = 0.001$ and 100 μ L aliquots were added to 96 well plates which contain various concentrations of compounds (1 μ L in DMSO) with DMSO as a positive control and blank medium as a negative control. After 18 h incubation at 200 rpm at 30°C (*V. campbellii* ATCC BAA-1116) or 28 °C (*V. harveyi* NBRC 15634), the optical density was measured at 600 nm with a plate reader (infinite M200Pro plate reader).

2.3.2 Bioluminescence Assay

The assay was performed as described before with little modifications.⁹⁸ An overnight culture of *Vibrio* strains, grown in Marine broth or AB medium at 30 °C or 28 °C, was diluted 1:100 and grown to an OD_{600} of ~ 1 . At this point, OD_{600} was measured and the culture was diluted to a final $OD_{600} = 0.5$ with fresh medium. 100 μ L aliquots of the culture were added to a Corning® 96 well plates (clear flat bottom) which contain 1 μ L various concentrations of compounds or DMSO per well. After incubation at 30 °C or 28 °C with agitation for 30 min, luminescence and OD_{600} were measured in an infinite M200Pro plate reader (Tecan). After deduction of the background (fresh medium), luminescence units were normalized to cell density. DMSO treated control samples were normalized to 100% activity and the residual activity of inhibitor treated samples was determined. The average values of technical triplicates were calculated and then the standard deviation of the means was calculated over three independent experiments. Residual activities for the respective compound

concentration were fitted to $Y = 100/(1+10^{((\log IC_{50}-X)*HillSlope)})$ (Y: residual activity in%; X: $\log_{10}(\text{concentration})$) and then IC_{50} was calculated in GraphPad Prism 6.0.

2.3.3 Growth and Luminescence Production Comparison between *V. campbellii* ATCC BAA-1116 and Its $\Delta phaB$ Mutant

For the comparison of growth and luminescence production between *V. campbellii* ATCC BAA-1116 and *V. campbellii* $\Delta phaB$, cells from a culture grown overnight in LM medium (20 g/liter NaCl, 10 g/L tryptone, 5 g/liter) were diluted 1:5000 in AB medium. Luminescence and OD_{600} were determined every hour in microtiter plates with a Tecan Infinite F500 system (Tecan) for 0.1 s and data are reported as light units (LU).

2.3.4 Growth and Luminescence Production Comparison between *V. campbellii* ATCC BAA-1116 and Its $\Delta ompA$ Mutant

For the comparison of growth and luminescence production between *V. campbellii* ATCC BAA-1116 and *V. campbellii* $\Delta ompA$, cells from a culture grown overnight in AB medium were diluted to a final $OD_{600} = 0.0005$ in fresh AB medium. The inoculated medium was then aliquoted 100 μL per well on a Corning® 96 well plates (clear flat bottom). Luminescence and OD_{600} were determined every 15 min in microtiter plates with an infinite M200Pro plate reader (Tecan) for 0.1 s and data are reported as light units (LU).

2.3.5 Swimming Assay

Swimming behavior of the bacteria was analyzed by using autoinducer bioassay (AB) medium plates containing 0.3% (w/v) agar and supplemented with 50 μM LP3 or BL3, respectively. As control the appropriate volume of DMSO was added to the plates. 1 μL of bacterial culture ($OD_{600} = 1$) was dropped in the middle of the plate. After 20 - 24 h of incubation at 30 °C the diameter of the bacterial lawn was measured and a chemoluminescence picture was taken (10 s exposure time).

2.3.6 Exoprotease Assay

Exoproteolytic activity of *V. campbellii* strains was measured by incubating hide powder azure (Sigma-Aldrich, Darmstadt, Germany) in phosphate buffered saline (pH 7.2) with cell-free culture fluids at 37 °C.^{134,197} The reaction was stopped with trichloroacetic acid [6.7% (v/v)] after 2 h, and the absorbance at 600 nm was measured. The activity was calculated by the

difference between initial and final absorption after 2 h (AU), and normalized by the OD₆₀₀ (AU/OD₆₀₀).

2.3.7 Phosphorylation assay

E. coli TKR2000 was transformed with plasmid pNKN encoding wild-type LuxN. Inside-out membrane vesicles were prepared as described before.¹⁹⁸ LuxU was overproduced using *E. coli* JM109 transformed with pQE30LuxU-6His, and purified as described. All proteins were stored at -80 °C.

Phosphorylation reactions were performed in phosphorylation buffer (50 mM Tris/HCl pH 8.0, 10% (v/v) glycerol, 500 mM KCl, 2 mM DTT) at room temperature. The hybrid histidine kinase LuxN was used as full-length membrane integrated protein in inverted membrane vesicles. LuxN containing membrane vesicles were added at final concentrations of 5.5 mg/ml and LuxU 0.36 mg/ml. The β -lactones (**LP3**, **BL3**) were added in a final concentration of 50 μ M. The phosphorylation reaction was started by adding radiolabelled Mg²⁺-ATP, typically 100 μ M [γ -³²P] ATP (0.94 Ci/mmol; Perkin-Elmer, Rodgau-Jügesheim, Germany) and 110 μ M MgCl₂, and stopped at various time points by the addition of SDS loading buffer, followed by fractionation of the reaction on SDS polyacrylamide gels. Gels were dried at 80 °C on filter paper, exposed to a phosphoscreen for at least 24 h and scanned using a Typhoon Trio variable mode imager (GE Healthcare, Munich, Germany).

3. Proteomics

3.1 Activity-Based Protein Profiling Experiments

Bacterial strains were cultivated under defined growth conditions to stationary phase otherwise specified and OD₆₀₀ was measured on Novaspec Plus visible spectrophotometer. Cultures were collected in a 50 mL falcon tube, pelletized at 6000 rpm for 5 min at 4 °C and washed with PBS. The pellet was then resuspended in PBS to a final OD₆₀₀ = 40. Here the PBS buffer was always pH = 7.4 in the following steps.

3.1.1 Analytical Gel-Based ABPP

100 µL aliquots of bacterial suspension were treated with various concentrations of compounds, probes or DMSO at RT for 1 h (for the competitive experiments: the suspension was first treated with the compound used for competition or DMSO for 1 hour at RT and then treated sequentially with the corresponding probe at RT for another hour). After incubation, the samples were pelletized and washed twice with 1 mL PBS to remove the residual compounds or probes. The pellet was suspended in 120 µL PBS and then lysed by sonication with a Bandelin Sonopuls with 3 x 15 sec. pulsed at 70% max. power on ice. After that, the samples were pelletized (13000 rpm, 4 °C, 30 min). 88 µL supernatant was transferred to a new Eppendorf tube while the pellet was washed twice with 500 µL PBS and resuspended in 88 µL PBS. Additional 20% sodium dodecyl sulfate (SDS) in PBS was added in β-lactone research to a final concentration of 0.8% to denature the proteins when necessary but not in the fimbrolide research. The samples were then used to append a reporter tag via click chemistry (CC). For each 88 µL sample, add 2 µL RhN₃ (5 mM rhodamine-azide in DMSO), 2 µL freshly made TCEP (52 mM tris(2-carboxyethyl)phosphine in ddH₂O), 6 µL TBTA ligand (tris[(1-benzyl-1H-1,2,3-triazol-4-yl)methyl]amine, 1.667 mM in t-BuOH/DMSO = 4:1). Samples were gently vortexed and 2 µL CuSO₄ (50 mM CuSO₄ in ddH₂O) was added to initiate the cycloaddition reaction. After the addition of CC reagents, the total reaction volume was 100 µL. The samples were incubated at RT for 1 h and then 100 µL 2× SDS loading buffer were added. The samples were mixed and stored at -20 °C after 1 hour incubation at RT. 50 µL of the samples was applied on the analytical gel and 10 µL fluorescent marker was used as ladder in parallel (BenchMark Fluorescent protein standard was diluted with 4 fold ddH₂O and 5 fold 2× SDS loading buffer). Fluorescence was recorded in a Fujifilm Las-3000 Fluoreszenz Darkbox with a Fujinon VRF 43LMD Lens, 605DF40 filter and 520 nm EPI excitation wavelength.

3.1.2 Gel-Based ABPP and In Gel Digestion

The approach was utilized in β -lactones research. 500 μ L of the bacterial suspension were treated with optimal concentration of probe (**LP3** with a final concentration of 10 μ M) or DMSO at RT for 1 hour in Protein LoBind tube from Eppendorf. After incubation, the samples were pelletized and washed twice with 1 mL PBS to remove the residual probe. The pellet was suspended in 500 μ L PBS and then lysed by sonication with a Bandelin Sonopuls with 3 x 15 sec. pulsed at 70% max. power on ice. The samples were pelletized at 13000 rpm at 4 °C for 30 min and then 500 μ L supernatant was transferred to a new Protein LoBind eppi while the pellet was washed twice with 1 mL PBS and resuspended in 500 μ L PBS. 20% sodium dodecyl sulfate (SDS) in PBS was added into both soluble and insoluble samples to a final concentration of 0.8%.

The samples were then used to append a reporter tag via CC. For each 500 μ L sample, add 3 μ L TFL (trifunctional linker with rhodamine, biotin and azide groups 8: 5(6)-(1-[5-(4-Azido-benzoylamino)-1-carbamoylpentylcarbamoyl]-5-(6-biotinoylamino-hexanoylamino)-pentyl-carbamoyl)-tetramethylrhodamin; 10 mM in DMSO), 10 μ L freshly made TCEP (52 mM tris(2-carboxyethyl)phosphine in ddH₂O), 30 μ L TBTA ligand (tris[(1-benzyl-1H-1,2,3-triazol-4-yl)methyl]amine, 1.667 mM in t-BuOH/DMSO = 4:1). Samples were gently vortexed and 10 μ L CuSO₄ (50 mM CuSO₄ in ddH₂O) was used to initiate the cycloaddition. Samples were incubated at room temperature for 1 h. After CC, proteins were precipitated using two fold volumes of pre-chilled (-80 °C) acetone. The samples were stored at -20 °C overnight to allow sufficient precipitation of the proteins. Then they were pelletized at 13000 rpm for 30 min at 4 °C. The supernatant was discarded and the pellet washed twice with pre-chilled (-80°C) methanol. Subsequently, the pellet was dissolved in 500 μ L PBS with 0.4% SDS by sonication at RT and incubated under gentle mixing with 50 μ L of avidin-agarose beads from Sigma-Aldrich (avidin-agarose beads should be pre-washed with 1 mL PBS with 0.2% SDS three times) overnight at room temperature. The beads were washed three times with 3 mL 0.4% SDS PBS, twice with 1 mL of 6 M urea and three times with 1 mL PBS (1500 rpm, 2 min, RT). 50 μ L of 2 \times SDS loading buffer were added and the proteins were released for preparative SDS-PAGE by 10 min incubation at 95 °C. Then beads were centrifuged (13000 rpm, 2 min, RT) and the supernatant was analyzed via SDS PAGE (10% agarose gel (PEQLAB Biotechnologie GmbH, Erlangen, PerfectBlue Dual Gel System, 4 h, 300 V, 16 μ L fluorescent protein standard) And the fluorescence imaging was done on GE Healthcare, ImageQuant LAS-4000. Fluorescent bands were carefully excised with a new scalpel for every band and the bands

were cut into cubes. The gel pieces were stored in 0.5 mL microcentrifuge tubes at -20 °C if necessary.

All the steps (the excision of the bands, washing, reduction and alkylation) were conducted with lab coat, gloves, bouffant cap and a hygiene mask to prevent keratin contamination of the samples. All solutions containing ABC were prepared freshly and HPLC-MS grade water and acetonitrile were used in the next steps.

The gel pieces were washed with 100 μ L H₂O for 15 min (25 °C, 550 rpm), 200 μ L acetonitrile (ACN)/50 mM ABC in H₂O (1:1) for 15 min (25 °C, 550 rpm), and 100 μ L ACN for 10 min (25 °C, 550 rpm) sequentially. Then 100 μ L of 50 mM ABC in H₂O were added, the microcentrifuge tubes were mixed for 5 min (25 °C, 550 rpm) and then additional 100 μ L of ACN were added. After shaking for 15 min (25 °C, 550 rpm), the supernatant was removed from the gel pieces and a final washing step with 100 μ L ACN was conducted (10 min, 25 °C, 550 rpm). The gel pieces were dried in a centrifugal evaporator at 30 °C, 5 mbar for about 15 min.

Reduction of disulfide bonds was performed with 100 μ L 10 mM dithiothreitol (DTT) in 50 mM ABC for 45 min (56 °C, 550 rpm). After the removal of supernatant, the reduced disulfide bonds were alkylated with 100 μ L 55 mM 2-iodoacetamide (IAA) in 50 mM ABC. The reaction was conducted in dark at RT and 550 rpm for 30 min. After removing the supernatant, gel pieces were washed twice with 100 μ L ACN/50 mM ABC in H₂O (1:1) for 15 min and then once with 100 μ L ACN for 10 min. After the removal of supernatant, the gel pieces were dried in a centrifugal evaporator at 30 °C, 5 mbar for 15 min.

The dried gel pieces were covered with 100 μ L trypsin solution (1 μ L sequencing grade modified trypsin (0.5 μ g/ μ L) in 100 μ L 25 mM ABC) and incubated overnight (37 °C, 300 rpm). Then the trypsin digest solution was transferred to a new 1.5 mL Protein LoBind Eppendorf tube. 100 μ L 25 mM ABC was added to the gel pieces and sonicated for 15 min for further extraction. After combination of the supernatant to trypsin digest solution, 100 μ L 5% formic acid aqueous solution were added and after sonicated for 15 min. Then additional 100 μ L ACN were added. After sonication for 15 min, the supernatant was combined to the trypsin digest solution. This step was repeated one more time. The solvent of the trypsin digest solution was removed in a centrifugal evaporator at 40 °C, 5 mbar for more than 4 h and the dried peptides were stored at -20 °C.

Prior to HPLC-MS measurements, peptides were dissolved in 30 μ L 1% formic acid (FA) by sonication for 10 min and filtered through an equilibrated VWR 0.45 μ m centrifugal filter (2 min, 13000 rpm). Pre-equilibration of the centrifugal filter was done by centrifuging the filter

twice with 500 μ L H₂O, one time with 500 μ L 0.05 M NaOH and twice with 500 μ L 1% formic acid (2 min, 13000 rpm).

The digested peptides were analyzed on a UltiMate 3000 nano HPLC system (Dionex, Sunnyvale, California, USA) coupled to a Orbitrap Fusion™ Tribrid™ mass spectrometer (Thermo Fisher Scientific Inc., Waltham, Massachusetts, USA). Samples were loaded on a Acclaim C18 PepMap100 75 μ m ID x 2 cm trap and transferred to a Acclaim C18 PepMap RSLC, 75 μ m ID x 15 cm separation column (0.1% FA, 5% DMSO, gradient 10 min 3% ACN, 120 min from 3% to 25% ACN, 5 min to 40% ACN, 0.1 min to 90% ACN and 4.9 min hold at 90% ACN, 0.1 min to 3% ACN and 9.9 min 3% ACN). The mass spectrometer was operated in data dependent top speed mode selecting the most intense precursors with a minimal threshold of 5E3. Precursors were measured in the Orbitrap at a resolution of 120,000 and an ion target of 4E5 (max inj. time of 50 ms) in a scan range from 300 to 1700 m/z. Monoisotopic precursor selection was enabled. Charge states from 1 to 7 were triggered. Dynamic exclusion duration was set to 60 s with a mass tolerance of 10 ppm. Precursors were isolated in the quadrupole (isol. window 1.6 m/z) and fragmentation was performed using higher-energy collisional dissociation (HECD). Resulting fragments were measured in the ion trap using a rapid scan rate (AGC target: 1E4 and max inj. time 40 ms).

After the measurement, assignment of the peptides to proteins was done with Proteome Discoverer 1.3.0.339 (Thermo Fisher Scientific, Massachusetts, USA) software. Precursor mass tolerance: 10 ppm; Fragment mass tolerance: 0.8 Da. Default settings were used except the following listed parameters: Mass precision: 2 ppm; Precursor ions area detector for quantification; Spectrum selection: lowest charge state: 2, highest charge state: 4, max. precursor mass: 5000 Da, mass analyzer: ITMS, FTMS, ionization source: nanospray, polarity mode: +; Sequest: Protein database: PATRIC database for *Vibrio campbellii* BB120 and *Vibrio harveyi* NBRC 15634. Enzyme name: trypsin (full), dynamic N-terminal modification: acetyl / +42.011 (any N-terminus), dynamic modification: oxidation / +15.995 Da (M), static modification: carbamidomethyl / +57.021 Da (C); Peptide validation: FDR min 5%.

3.1.3 Gel Free ABPP and Dimethyl Labeling

In fimbrolide research, 500 μ L of the bacterial suspension were incubated first with **F1** (final conc. = 1 mM) for competition or with DMSO for enrichment at RT for 2 h and then incubated sequentially with the corresponding probe **FP3** (final conc. = 50 μ M) at RT for another 1.5 h. Also, one sample was treated only with DMSO as a blank control.

In β -lactone research, 500 μ L of the bacteria suspension were incubated first with **BL3** (final conc. = 200 μ M) for competition or with DMSO for enrichment at RT for 1 h and then incubated sequentially with the corresponding probe **LP3** (final conc. = 10 μ M) at RT for another 1 h. Also, one sample was treated only with DMSO as a blank control.

Technical replicates were performed with the same bacterial suspension in parallel while biological replicates were experiments performed with bacteria harvested on different days. After incubation, the samples were pelletized and washed twice with 1 mL PBS to remove the residual probe. The pellet was resuspended in 500 μ L PBS and then lysed by sonication with a Bandelin Sonopuls with 3 x 15 sec. pulsed at 70% max. power on ice. After centrifugation at 13000 rpm at 4 $^{\circ}$ C for 30 min to separate the soluble and insoluble fractions, the insoluble fractions was resuspended in 500 μ L PBS while the supernatant was transferred to a new Protein LoBind Eppendorf tube. Additional 20% sodium dodecyl sulfate (SDS) in PBS was added into the samples in the β -lactone research to a final concentration of 0.8% but not in fimbrolide research. The samples were then used to append a reporter tag via CC. For each 500 μ L sample, add 3 μ L azide-PEG3-biotin conjugate (Jena Bioscience, bifunctional linker with biotin and azide groups; 10 mM in DMSO), 10 μ L freshly made TCEP (52 mM tris(2-carboxyethyl)phosphine in ddH₂O), 30 μ L TBTA ligand (tris[(1-benzyl-1H-1,2,3-triazol-4-yl)methyl]amine, 1.667 mM in t-BuOH/DMSO = 4:1). The cycloaddition was initiated by addition of 10 μ L CuSO₄ (50 mM CuSO₄ in ddH₂O) and then the sample was incubated at RT for 1 h. After CC, proteins were precipitated with two fold volumes of pre-chilled (-80 $^{\circ}$ C) acetone. The samples were stored at -20 $^{\circ}$ C overnight to get sufficient precipitation of the proteins. Then they were pelletized at 13000 rpm for 30 min at 4 $^{\circ}$ C. The supernatant was discarded and the pellet was washed twice with pre-chilled (-80 $^{\circ}$ C) methanol. Subsequently, the pellet was dissolved in 500 μ L PBS with 0.4% SDS by sonication at RT and the protein concentration was measured with BCA assay. All samples were adjusted to same protein amount accordingly. They were incubated under gentle mixing with 50 μ L of avidin-agarose beads from Sigma-Aldrich (avidin-agarose beads were pre-washed with 1 mL PBS with 0.4% SDS three times) overnight at RT. After that, the beads were washed three times with 1 mL of 0.4% SDS in PBS, twice with 1 mL of 6 M urea and three times with 1 mL PBS (collect at 1500 rpm, 2 min, RT after each washing step). The beads were resuspended with 200 μ L denaturation buffer (7 M urea, 2 M thiourea in 20 mM pH 7.5 HEPES buffer). Dithiothreitol (DTT, 100 mM, 2 μ L) was added and the tubes were mixed by vortexing shortly and incubated in a thermomixer (450 rpm, 45 min, RT). Then 2-Iodoacetamide (IAA, 550 mM, 2 μ L) was added. The tubes were mixed again by vortexing shortly and incubated in the darkness (450

rpm, 30 min, RT). The excess of IAA was quenched by the addition of dithiothreitol (DTT, 100 mM, 8 μ L). The tubes were shortly mixed by vortexing and incubated in a thermomixer (450 rpm, 30 min, RT). 1 μ L LysC (0.5 μ g/ μ L) which was thawed on ice was added to each microcentrifuge tube. The tubes were mixed by shortly vortexing and incubated in a thermomixer (450 rpm, 4 h, RT, in the darkness). 600 μ L TEAB solution (tetraethylammonium bromide, 50 mM in water) and 1.5 μ L trypsin (0.5 μ g/ μ L in 50 mM acetic acid) were added to the tubes. The microcentrifuge tubes were incubated in a thermomixer overnight (450 rpm, 13 - 15 h, 37 °C).

The digestion was stopped by adding 6 μ L formic acid (FA) and the solution was collected by centrifugation (3000 rpm, 2 min, RT). The trypsin digest solution was transferred to a new Protein LoBind Eppendorf tube. Further extraction was done with 50 μ L 0.1% FA (aqueous solution) twice (3000 rpm, 2 min, RT). Finally, the tubes were centrifuged for 3 min at 13000 rpm to collect the residual supernatant. All the supernatant was combined to the trypsin digest solution. The pH values of the samples were checked and more 1% FA was added if the pH was above 3. 50 mg SepPak C18 columns were pre-equilibrated by gravity flow with 1 mL acetonitrile, 0.5 mL elution buffer (80% ACN, 0.5% FA) and 1 mL 0.1% TFA aqueous solution. Subsequently the samples were loaded and washed with 500 μ L 0.1% TFA aqueous solution twice, 500 μ L 0.5% FA aqueous solution once. The peptides were then eluted into new 2.0 mL Protein LoBind Eppendorf tubes twice with 250 μ L elution buffer (80% ACN, 0.5%FA) under reduced pressure until no liquid comes out from the SepPak C18 columns.

The filtrates were dried in a lyophilizer and resuspended in 100 μ L TEAB buffer (tetraethylammonium bromide, 100 mM TEAB, 0.36% FA, pH = 6) by pipetting up and down. The solution was vortexed, sonicated and spun down afterwards. 8 μ L respective fresh isotope labeling solution (light labeling solution: 2% CH₂O, 0.3 M NaBH₃CN in ddH₂O; medium labeling solution: 2% CD₂O, 0.3 M NaBH₃CN in ddH₂O; heavy labeling solution: 2% ¹³CD₂O, 0.3 M NaBD₃CN in ddH₂O) was added and briefly vortexed. The mixture was incubated 1 h (450 rpm, 25 °C). After incubation, the samples were cooled on ice for 3 min and quenched with 16 μ L pre-chilled 1% ammonia solution, 8 μ L pre-chilled 5% FA solution with short vortexing and centrifugation after final addition. Differentially labeled peptide solutions were mixed in a new Protein LoBind Eppendorf tube, lyophilized and the peptides were stored at -20 °C afterwards. Before MS measurement the samples were dissolved in 35 μ L 1% FA in ddH₂O by pipetting up and down, vortexing and sonication for 15 min. Then, the supernatants were collected by centrifugation. The VWR 0.45 μ m centrifugal filter were pre-equilibrated with 500 μ L ddH₂O twice, 500 μ L 0.05 N NaOH once and 500 μ L 1% FA twice (centrifugation of the

filters: 13000 rpm, 1 min, RT). The peptide solutions were filtered through the equilibrated filters (centrifugation: 13000 rpm, 2 min, RT)

The digested peptides were analyzed on a UltiMate 3000 nano HPLC system (Dionex, Sunnyvale, California, USA) coupled to a Orbitrap Fusion™ Tribrid™ mass spectrometer (Thermo Fisher Scientific Inc., Waltham, Massachusetts, USA). Samples were loaded on a Acclaim C18 PepMap100 75 μm ID x 2 cm trap and transferred to a Acclaim C18 PepMap RSLC, 75 μm ID x 15 cm separation column (0.1% FA, 5% DMSO, gradient 10 min 3% ACN, 120 min from 3% to 25% ACN, 5 min to 40% ACN, 0.1 min to 90% ACN and 4.9 min hold at 90% ACN, 0.1 min to 3% ACN and 9.9 min 3% ACN). The mass spectrometer was operated in data dependent top speed mode selecting the most intense precursors with a minimal threshold of 5E3. Precursors were measured in the Orbitrap at a resolution of 120,000 and an ion target of 4E5 (max inj. time of 50 ms) in a scan range from 300 to 1700 m/z. Monoisotopic precursor selection was enabled. Charge states from 1 to 7 were triggered. Dynamic exclusion duration was set to 60 s with a mass tolerance of 10 ppm. Precursors were isolated in the quadrupole (isol. window 1.6 m/z) and fragmentation was performed using higher-energy collisional dissociation (HECD). Resulting fragments were measured in the ion trap using a rapid scan rate (AGC target: 1E4 and max inj. time 40 ms). Peptide and protein identifications were performed using Maxquant 1.4.0.8 software with Andromeda as search engine using following parameters: Carbamidomethylation of cysteines as fixed and oxidation of methionine as well as acetylation of N-termini as dynamic modifications, trypsin/P as the proteolytic enzyme, 4.5 ppm for precursor mass tolerance (main search ppm) and 0.5 Da for fragment mass tolerance (ITMS MS/MS tolerance). Searches were done against the PATRIC database sequence (www.patricbrc.org) for *V. campbellii* ATCC BAA-1116 and *V. harveyi* NBRC 15634 (downloaded on 28.07.2014). Quantification was performed using dimethyl labeling with the following settings: light: DimethLys0, DimethNter0; medium: DimethLys4, DimethNter4 and heavy: DimethLys8, DimethNter8. Variable modifications were included for quantification. I = L and requantify options were used. Identification was done with at least 2 unique peptides and quantification only with unique peptides. Statistical analysis was performed with Perseus 1.5.1.6. Putative contaminants, reverse peptides and peptides only identified by site were omitted from further processing. Dimethyl labeling ratios obtained from Maxquant 1.4.0.8 were transformed with $\log_2(x)$. $-\log_{10}(p\text{-value})$ were obtained by a two sided one sample t-test over six gel-free ABPP experiment results (three biological replicates with technical duplicates) in fimbrolide research while nine gel-free ABPP experiment results (three biological replicates with technical triplicates) in β -lactone research.

3.2 Whole Proteome Analysis

3.2.1 Whole Proteome Comparison between *V. harveyi* NBRC 15634 and *V. campbellii* ATCC BAA-1116

V. harveyi NBRC 15634 and *V. campbellii* ATCC BAA-1116 were cultivated in marine broth respectively at 30 °C and 28 °C to stationary phase. The OD₆₀₀ was monitored on Novaspec Plus visible spectrophotometer. Cultures were collected in a 50 mL falcon tube and pelleted at 6000 rpm for 5 min at 4 °C and washed with PBS. The pellet was then resuspended in cold lysis buffer (8 M urea, 1 mM EDTA, one tablet of protease inhibitor cocktail per 5 mL (complete, EDTA-free, Roche), 75 mM NaCl, 50 mM Tris-HCl, pH 8.2 at 4 °C) to a final OD₆₀₀ = 300. The suspension was lysed by homogenization with 5 x 20 sec. pulsed at 80% max. power on ice. The debris was removed by centrifugation (13000 rpm, 30 min, 4 °C) and the supernatant was filtered through 0.2 µm filter. The filtrate was collected in a new Protein LoBind tube from Eppendorf and the concentration of the proteins was measured by BCA assay. Adjust the samples to the same protein amount accordingly and add urea, thiourea to make a final concentration 7 M and 2 M respectively (add lysis buffer to make the right final concentration). Transfer 500 µg proteins to a new 1.5 mL tube, reduce with 1 mM DTT (500 rpm, 1h, 37 °C) and alkylate with 5.5 mM iodoacetamide (500 rpm, 30 min, RT, in the darkness). The reaction was quenched with 4 mM DTT (500 rpm, 30 min, RT) and the solution was pre-digested with Lys-C (1:200, 25 °C, 4 h). After a 1:4 dilution with 50 mM TEAB in ddH₂O (tetraethylammonium bromide), the solution was digested with trypsin (1:100, 37 °C, 12 h). The digestion was stopped by addition of FA to a final concentration of 1%. The pH value had to be below 3 (if not, more formic acid was added). 50 mg SepPak C18 columns were pre-equilibrated by gravity flow with 1 mL acetonitrile, 0.5 mL elution buffer (80% ACN, 0.5% FA) and three times 1 mL aqueous 0.5% FA solution. Subsequently, the samples were loaded and washed with 1 mL aqueous 0.5% FA solution five times. Flush each of the columns with 1 mL of the respective isotope labeling reagent five times over 20 min (light labeling solution: 0.2% CH₂O, 0.03 M NaBH₃CN in 50 mM sodium phosphate, pH 7.5; medium labeling solution: 0.2% CD₂O, 0.03 M NaBD₃CN in 50mM sodium phosphate, pH 7.5; heavy labeling solution: 0.2% ¹³CD₂O, 0.03 M NaBD₃CN in 50mM sodium phosphate, pH 7.5). The columns were washed twice with 1 mL 0.5% FA aqueous solution. The peptides were then eluted into 2 mL Protein LoBind tubes with 250 µL elution buffer twice (80% ACN, 0.5% FA) under reduced pressure until no liquid came out from the SepPak C18 columns. The differentially

labeled peptide solutions were mixed and lyophilized to get the dried peptides which can be stored at -20 °C.

The peptides were dissolved in 35 µL 1% FA in ddH₂O before MS measurement by pipetting up and down, vortexing and sonication for 15 min. The samples were spin down with centrifugation. The VWR 0.45 µm centrifugal filter were pre-equilibrated with 500 µL ddH₂O twice, 500 µL 0.05 N NaOH and 500 µL 1% FA twice (centrifugation of the filters: 13000 rpm, 1 min, RT). Then the peptide solutions were filtered through the equilibrated filters (centrifugation: 13000 rpm, 2 min, RT) and analyzed on Orbitrap Fusion™ Tribrid™ mass spectrometer with the parameters mentioned before. Statistical analysis was performed with Perseus 1.5.1.6. Putative contaminants, reverse peptides and peptides only identified by site were omitted from further processing. Dimethyl labeling ratios obtained from Maxquant 1.4.0.8 were transformed with $\log_2(x)$. $-\log_{10}(p\text{-value})$ were obtained by a two sided one sample Student's t-test over three biological experiments against *V. campbellii* ATCC BAA-1116 or *V. harveyi* NBRC 15634 sequence from PATRIC database (www.patricbrc.org, downloaded on 28.07.2014).

3.2.2 Whole Proteome Analysis of *V. campbellii* ATCC BAA-1116, Its Chemical Knockdown by Beta-Lactones, and $\Delta ompA$ Mutant

Two sets of *V. campbellii* ATCC BAA-1116 and one set of its $\Delta ompA$ mutant cultures were cultivated in AB medium at 30 °C to OD₆₀₀ = 0.80. The OD₆₀₀ was monitored on Novaspec Plus visible spectrophotometer. Then one set of *V. campbellii* ATCC BAA-1116 cultures were treated with **BL3** with a final concentration 25 µM by addition of concentrated stocks in DMSO while the other set and $\Delta ompA$ mutant were treated with equivalent volume of DMSO. These cultures were then allowed to grow for another two hours before harvest. Then the samples were processed as “Whole proteome analysis between *V. harveyi* NBRC 15634 and *V. campbellii* ATCC BAA-1116” section. Then the peptide solutions were analyzed on LTQ Orbitrap XL mass spectrometer. The *V. campbellii* ATCC BAA-1116 sequence was from PATRIC database (www.patricbrc.org, downloaded on 31.08.2015).

3.2 Recombinant Proteins

3.2.3 Recombinant Expression of LuxS in *E. coli*

V. harveyi NBRC 15634 LuxS was recombinantly expressed in *E. coli* BL21DE(3) using the Invitrogen™ Gateway® Cloning Technology. The *luxS* gene was amplified from the

corresponding genome (*V. harveyi* NBRC 15634) by PCR via a Phusion® High-Fidelity DNA Polymerase kit (New England BioLabs® Inc.). 40 ng *V. harveyi* NBRC 15634 genomic DNA was prepared by standard protocols (Quiagen DNeasy® Blood & Tissue Kit 50). The *attB1* forward primer and *attB2* reverse primer were designed to yield *attB*-PCR Products needed for Gateway® Technology. PCR products were identified on agarose gels and extracted with an Omega Bio-tek Inc. E.Z.N.A.® MicroElute® Gel Extraction Kit. The DNA concentrations were recorded by a Tecan Infinite® M200 PRO plate reader. Then 100 fmol *attB*-PCR product and 50 fmol *attP*-containing donor vector pDONR™ 201 (Invitrogen™) in TE buffer were mixed for BP recombination reaction with BP Clonase™ II enzyme mix (Invitrogen™) to give the *attL*-containing entry clone. The resulting entry clone was then transformed into chemically competent One Shot® *E. coli* TOP10 (Invitrogen™) and then cells were selected on LB agar with 25 µg/mL kanamycin. The selected clones were cultivated in LB media with kanamycin and the cells were harvested to isolate the plasmids with Omega Bio-tek Inc. E.Z.N.A.® MicroElute® Plasmid Mini Kit. 50 fmol isolated plasmids and 50 fmol *attR*-containing destination vector pET300/NT-Dest were subsequently used in LR recombination reaction with LR Clonase™ II enzyme mix (Invitrogen™) in TE buffer. The clone was then transformed into chemically competent *E. coli* BL21(DE3) cells by heat shock and then selected with LB agar plates with 100 µg/mL ampicillin. The selected colonies were grown in LB media with ampicillin and the culture was used to make working stocks for future protein over-expression and isolation of the expression plasmids. The plasmid sequence was confirmed by sanger-sequencing service of GATC Biotech. Recombinant *E. coli* BL21(DE3) was grown at 37 °C in LB media until an OD₆₀₀ ≈ 0.5 and then expression was induced with 1 mM Isopropyl β-D-1-thiogalactopyranoside (IPTG) for 6 h at 37 °C. The bacteria were harvested and washed with PBS. The resulting pellet was suspended in lysis buffer (20 mM Trizma, 10 mM imidazole, 150 mM NaCl, 2 mM 2-mercaptoethanol, 0.2% NP-40) and lysed by sonication. The protein was then purified with HisTrap™ HP columns (GE Healthcare Life Sciences) and stored in His elution buffer (20 mM Trizma, 0.5 M imidazole, 150 mM NaCl, 2 mM 2-mercaptoethanol) at – 80 °C. The protein was concentrated and further purified on size exclusion chromatography (HiLoad 16/60 Superdex 200 prep grade, GE healthcare) with LuxS assay buffer (10 mM sodium phosphate, pH 7.5). Then the protein was stored at - 80°C with 10% glycerol with 2 mM TCEP (for long-time storage) or with 10 µM DTT (for direct use in assay). The protein purity was determined by MS and SDS-gel.

forward primer:

5'-

GGGGACAAGTTTGTACAAAAAAGCAGGCTTTGAGAATCTTTATTTTCAGGGCCCTTTATTAGACAGTT
TTACC-3'

reverse primer:

5'-GGGGACCACTTTGTACAAGAAAGCTGGGTGTTAGTCGATACGTAACCTTT-3'

3.2.4 Recombinant Expression of PhaB in *E. coli*

V. campbellii ATCC BAA-1116 PhaB was recombinantly expressed in pET300/NT-Dest plasmid in *E. coli* BL21DE(3) using the Invitrogen™ Gateway® Cloning Technology described in LuxS section. The protein was purified with HisTrap™ HP columns (GE Healthcare Life Sciences) and stored in the His elution buffer (20 mM Trizma, 0.5 M imidazole, 150 mM NaCl, 2 mM DTT) at -80 °C without further purification. The protein purity was determined by MS and SDS-gel.

forward primer:

5'-

GGGGACAAGTTTGTACAAAAAAGCAGGCTTTGAGAATCTTTATTTTCAGGGCAAGAAAGTCGCTTTGA
TCACCGG-3'

reverse primer:

5'-GGGACCACTTTGTACAAGAAAGCTGGGTGTTAGTGCATGTATAGGCCGCCAT-3'

3.2.5 Recombinant Expression of LuxE in *E. coli*

V. campbellii ATCC BAA-1116 LuxE was recombinantly expressed in pDest 007 plasmid in *E. coli* Arctic Express using the Invitrogen™ Gateway® Cloning Technology similar to what described in LuxS section. Nevertheless, the bacteria were grown at 37 °C until OD₆₀₀ ≈ 0.5 and then induced by 432 nM anhydrotetracycline at 15 °C for 5 h. The bacteria were harvested and washed with PBS. The resulting pellet was resuspended in binding buffer (100 mM Tris-HCl pH 8.0, 150 mM NaCl), lysed by sonication. The protein was then purified with Strep Trap™ HP columns (GE Healthcare Life Sciences) and stored at -80 °C in the elution buffer (100 mM Tris-HCl, 150 mM NaCl, 1 mM EDTA, 2.5 mM desthiobiotin, pH 8.0). The protein purity was determined by MS and SDS-gel.

forward primer:

5'-GGGGACAAGTTTGTACAAAAAAGCAGGCTTTGAGAATCTTTATTTTCAGGGC
GAAGTACTTTCAGCGGTTAAG-3'

reverse primer:

5'-GGGGACCACTTTGTACAAGAAAGCTGGGTGTCAGTTGCCTCCTTCATTCTT-3'

3.2.6 Recombinant Expression of *Photorhabdus luminescens* LuxE in *E. coli*

Photorhabdus luminescens TT01 LuxE was recombinantly expressed in pDest 007 plasmid in *E. coli* BL21DE(3) using the Invitrogen™ Gateway® Cloning Technology similar to the description in the LuxS section. The bacteria were grown at 37 °C until OD₆₀₀ ≈ 0.5 and then induced by 432 nM anhydrotetracycline at 37 °C for 5 h. The bacteria were harvested and washed with PBS. The resulting pellet was resuspended in PBS to OD₆₀₀ = 40 and then used for *in situ* labeling with FP3. The non-induced bacterial cells with this plasmid were used for comparison in *in situ* labeling.

forward primer:

5'- GGGGACAAGTTTGTACAAAAAAGCAGGCTTACTTCATATGTTGATAACAAGA -3'

reverse primer:

5'- GGGGACCACTTTGTACAAGAAAGCTGGGTGTCAACTATTAATGCTTGTTTA -3'

3.2.7 Recombinant Expression of IMPD in *E. coli*

V. campbellii ATCC BAA-1116 IMPD was recombinantly expressed in pET300/NT-Dest plasmid in *E. coli* BL21DE(3) using the Invitrogen™ Gateway® Cloning Technology as described before. The protein was purified with HisTrap™ HP columns (GE Healthcare Life Sciences) and stored in the His elution buffer (20 mM Trizma, 0.5 M imidazole, 150 mM NaCl, 2 mM DTT) at -80 °C without further purification. The protein purity was determined by MS and SDS-gel.

forward primer:

5'-

GGGGACAAGTTTGTACAAAAAAGCAGGCTTTGAGAATCTTTATTTTCAGGGCCACTCACTTAAAGTTA
AAG-3'

reverse primer:

5'- GGGGACCACTTTGTACAAGAAAGCTGGGTGTTAAACGGGATGTTGAAAA-3'

3.2.8 Recombinant Expression of Pfs in *E. coli*

E. coli BL21DE(3) was transformed with plasmid pQE30Pfs-6 His. Recombinant bacterial cells were grown to OD₆₀₀ ≈ 0.5 and then induced with 1mM IPTG for 6 h at 37 °C. The protein was purified with HisTrap™ HP columns (GE Healthcare Life Sciences) and stored in His-elution buffer (20 mM Trizma, 0.5 M imidazole, 150 mM NaCl, 2 mM 2-mercaptoethanol) at -80 °C. The protein was concentrated and further purified on size exclusion chromatography (HiLoad 16/60 Superdex 200 prep grade, GE healthcare) with LuxS assay buffer (10 mM sodium

phosphate, pH 7.5). Then the protein was stored at -80 °C in 10 mM sodium phosphate, 10 µM DTT, pH 7.5. The protein purity was determined by MS and SDS-gel.

3.2.9 Recombinant Expression of ACAT in *E. coli*

V. campbellii ATCC BAA-1116 ACAT was recombinantly expressed in pDest 007 plasmid in *E. coli* Arctic Express using the Invitrogen™ Gateway® Cloning Technology similar to what described in LuxS section. Nevertheless, the bacteria were grown at 37 °C until OD₆₀₀ ≈ 0.5 and then induced by 432 nM anhydrotetracycline at 15 °C for 12 hours. The bacteria were harvested and washed with PBS. The resulting pellet was resuspended in binding buffer (100 mM Tris-HCl pH 8.0, 150 mM NaCl), lysed by sonication. The protein was then purified with StrepTrap™ HP columns (GE Healthcare Life Sciences) and stored at - 80 °C in the elution buffer (100 mM Tris-HCl, 150 mM NaCl, 1 mM EDTA, 2.5 mM desthiobiotin, pH 8.0). The protein purity was determined by MS and SDS-gel.

forward primer:

5'-

GGGACAAGTTTGTACAAAAAAGCAGGCTTTGAGAATCTTTATTTTCAGGGCGAAAAAGTATTTATTGT
TGC-3'

reverse primer:

5'-GGGGACCACTTTGTACAAGAAAGCTGGGTGCTATTTAACTGCTTTTACAA-3'

3.2.10 Recombinant Expression of DGC in *E. coli*

V. campbellii ATCC BAA-1116 GGDEF family protein was recombinantly expressed in pDest 007 plasmid in *E. coli* BL21DE(3) using the Invitrogen™ Gateway® Cloning Technology similar to what described in LuxS section. Nevertheless, the bacteria were grown at 37 °C until OD₆₀₀ ≈ 0.5 and then induced by 432 nM anhydrotetracycline at 37 °C for 4 hours. The bacteria were harvested and washed with PBS. After pelletizing, the pellet of cells was stored in - 80 °C freezer before being used.

forward primer:

5'-GGGGACAAGTTTGTACAAAAAAGCAGGCTTTGCTCATGAACAAAAAAGTATCCAGTTA-3'

reverse primer:

5'-GGGGACCACTTTGTACAAGAAAGCTGGGTGTTATGCGCTCTTCATTTGTTTGTCATT-3'

3.2.11 Recombinant Expression of OmpA in *E. coli*

V. campbellii ATCC BAA-1116 OmpA was recombinantly expressed in pDest 007 plasmid in *E. coli* BL21DE(3) using the Invitrogen™ Gateway® Cloning Technology similar to what described in LuxS section. Nevertheless, the bacteria were grown at 37 °C until OD₆₀₀ ≈ 0.5 and then induced by 432 nM anhydrotetracycline at 37 °C for 4 hours. The bacteria were harvested and washed with PBS. After pelletizing, the pellet of cells was stored in - 80 °C freezer before being used.

forward primer:

5'-GGGGACAAGTTTGTACAAAAAAGCAGGCTTTCATCAATACAAGGAAACACTATG-3'

reverse primer:

5'-GGGGACCACTTTGTACAAGAAAGCTGGGTGTTATTCTGGTTGTACAAGTTCTTC-3'

3.3 Binding Site Identification

3.3.1 Full Length MS of Intact Proteins

The full length mass of intact proteins was measured on a Thermo Finnigan LTQ FT-ICR equipped with a Dionex Ultimate 3000 separation module. The conditions for incubation of the proteins with corresponding compounds were as follows:

3.2 μL 390 μM LuxS was incubated with 2.5 μL 500 μM **F1** in 245 μL (pH 7.4) PBS at room temperature for 40 min.

15 μL 35.4 μM LuxE was incubated with 2.6 μL 200 μM **F1** in 235 μL (pH 7.4) PBS at 4 °C for 2 h.

50 μL 40 μM PhaB in Strep elution buffer was incubated with 5 equiv **F1** (2 μL, 5 mM) in 200 μL 10 mM sodium phosphate buffer pH =8 at room temperature for 1 h.

5 μL 1.3 mM IMPD in His elution buffer was incubated at room temperature with 0.5 μL 20 mM **F1** in 200 μL PBS for 20 min.

10 μL 0.0755 mM ACAT in Strep elution buffer was incubated at room temperature with 2 μL 1mM **LP3** for 10 min.

The mass spectrum data were then analyzed on Xcalibur™ software.

3.3.2 Binding Site Identification by MS-MS of LuxS and LuxE

Recombinant protein was pre-incubated with **F1** under defined conditions (3.2 μL 390 μM LuxS was incubated with 2.5 μL 500 μM **F1** in 245 μL pH 7.4 PBS at RT for 40 min; 15 μL 35.4 μM LuxE was incubated with 2.6 μL 200 μM **F1** in 235 μL pH 7.4 PBS at 4 $^{\circ}\text{C}$ for 2 hour). After incubation, the residual probe was removed by centrifugation with a vivaspin 500 μL centrifugal concentrator (Sartorius, 10000 MWCO PES) and the protein was washed with 200 μL PBS twice.

LuxS was dissolved in 100 μL X buffer (2 M thiourea, 7 M urea, in 20 mM HEPES buffer pH 7.5) and transferred to a new Protein LoBind tube. The protein was reduced with 10 mM DTT (500 rpm, 45 min, RT), alkylated with 30 mM IAA (500 rpm, 30 min, RT, in the darkness). The reaction was quenched with additional 30 mM DTT and then 300 μL 50 mM TEAB solution in ddH₂O was added. After addition of trypsin (final protein/enzyme concentration ration 40:1), the solution was incubated overnight (450 rpm, 37 $^{\circ}\text{C}$). The digestion was stopped by addition of 100% FA to a final concentration about 5% (pH 2-3).

LuxE was dissolved in 100 μL 25 mM ABC buffer and transferred to a new Protein LoBind tube. The protein was reduced with 10 mM DTT (500 rpm, 45 min, RT), alkylated with 30 mM IAA (500 rpm, 30 min, RT, in the darkness). The reaction was quenched with additional 30 mM DTT. After addition of trypsin (final protein/enzyme concentration ration 40:1), the solution was incubated overnight (450 rpm, 37 $^{\circ}\text{C}$). The digestion was stopped by addition of 10% TFA aqueous solution to a final concentration about 1%.

Stage tips were prepared with C18 2X paper and pre-equilibrated with 200 μL acetonitrile twice, 200 μL elution buffer (80% ACN, 0.5% FA), 200 μL 0.5% FA in ddH₂O twice before use (13000 rpm, 1 min). The digested solution was loaded on the stage tips and remained at RT for about 5 min. The solvent was removed by centrifugation (13000 rpm, 1 min) and washed four times with 200 μL 0.5% FA in ddH₂O (13000 rpm, 1 min). The peptides were eluted into a new 1.5 mL LoBind Eppendorf tube with 50 μL elution buffer (80% ACN, 0.5% FA) three times (13000 rpm, 1 min). The elution was lyophilized to get dried peptides and the samples for mass measurement were prepared as described above and measured on Orbitrap Fusion™ Tribrid™ mass spectrometer. The data was analyzed on Maxquant 1.4.0.8 software for binding site identification against the protein sequence.

3.3.3 Binding Site Identification by MS-MS of OmpA

E. coli BL21DE(3) cells with a pDest 007 plasmid containing *V. campbellii* ATCC BAA-1116 *ompA* gene was cultivated in LB medium at 37 $^{\circ}\text{C}$ to OD₆₀₀ \approx 0.5 and then induced by 432 nM

anhydrotetracycline at 37 °C for 4 hours. Afterwards, the bacterial cells were harvested and pelletized. The pellet was re-suspended in PBS to a final OD₆₀₀ ≈ 40. The bacterial cells were then incubated with **LP3** (final concentration: 25 μM) at room temperature for 1 hour. After removal of the excess of **LP3** by centrifugation and washing the pellet with PBS, the pellet was then resuspended in cold lysis buffer (8 M urea, 1 mM EDTA, one tablet of protease inhibitor cocktail per 5 mL (complete, EDTA-free, Roche), 75 mM NaCl, 50 mM Tris-HCl, pH 8.2 at 4 °C) to a final OD₆₀₀ = 300. The suspension was lysed by homogenization with 5 x 20 sec. pulsed at 80% max. power on ice. The debris was removed by centrifugation (13000 rpm, 30 min, 4 °C) and the supernatant was filtered through 0.2 μm filter. The filtrate was collected in a new Protein LoBind tube from Eppendorf and the concentration of the proteins was measured by BCA assay. Adjust the samples to the same protein amount accordingly and add urea, thiourea to make a final concentration 7 M and 2 M respectively (add lysis buffer to make the final equal concentration). Transfer 500 μg proteins to a new 1.5 mL tube, reduce with 1 mM DTT (500 rpm, 1h, 37 °C) and alkylate with 5.5 mM iodoacetamide (500 rpm, 30 min, RT, in the darkness). The reaction was quenched with 4 mM DTT (500 rpm, 30 min, RT) and the solution was pre-digested with Lys-C (1:200, 25 °C, 4 h). After a 1:4 dilution with 50 mM TEAB in ddH₂O, the solution was digested with trypsin (1:100, 37 °C, 12 h). The digestion was stopped by addition of FA to a final concentration of 1%. The pH value had to be below 3 (if not, more formic acid was added). 50 mg SepPak C18 columns were pre-equilibrated by gravity flow with 1 mL acetonitrile, 0.5 mL elution buffer (80% ACN, 0.5% FA) and three times 1 mL aqueous 0.5% FA solution. Subsequently, the samples were loaded and washed with 1 mL aqueous 0.5% FA solution five times. The peptides were then eluted into 2 mL Protein LoBind tubes with 250 μL elution buffer twice (80% ACN, 0.5% FA) under reduced pressure until no liquid came out from the SepPak C18 columns. The differentially labeled peptide solutions were mixed and lyophilized to get the dried peptides which can be stored at -20 °C. The peptides were dissolved in 300 μL 1% FA in ddH₂O before MS measurement by pipetting up and down, vortexing and sonication for 15 min. The samples were spun down with centrifugation. The VWR 0.2 μm centrifugal filters were pre-equilibrated with 500 μL 1% FA twice (centrifugation of the filters: 13000 rpm, 1 min, RT). Then the peptide solutions were filtered through the equilibrated filters (centrifugation: 13000 rpm, 2 min, RT) and analyzed on LTQ Orbitrap XL™ mass spectrometer. Analysis was performed on 1.5.2.8 against *V. campbellii* ATCC BAA-1116 sequence from PATRIC database (www.patricbrc.org, downloaded on 31.08.2015).

4 Enzymatic Assays

4.1 LuxS Inhibition Assay

The assay was performed as described previously with some modifications.¹³⁷ Recombinant LuxS (19.1 μ L, 10.45 mg/mL) was pre-incubated with different equivalents of natural product **F1** (1 μ L concentrated stocks in DMSO was used) and DMSO as control in 80 μ L assay buffer (10 mM sodium phosphate, pH 7.5) at 25 °C with shaking for 30 min. 17.2 μ L recombinant Pfs (11.6 mg/mL) and 20 μ L 10 mM S-adenosyl-L-homocysteine (SAH, dissolved in assay buffer) were premixed in 62.8 μ L assay buffer (10 mM sodium phosphate, pH 7.5) on a 96 well plate. The blank control was performed with 17.2 μ L recombinant Pfs (11.6 mg/mL) in 82.8 μ L assay buffer without addition of SAH. Then the above mentioned pre-incubated LuxS was added to the pre-mixture of Pfs and SAH in assay buffer or the blank control. The reaction was carried out at 37 °C with shaking for 15 min and the solution was centrifuged with a vivaspin 500 μ L centrifugal concentrator (Sartorius, 10000 MWCO PES) at 13000 rpm for 15 min. 90 μ L filtrate was mixed with 180 μ L 800 μ M Ellman's reagent (5'5-dithio-bis-(2-nitrobenzoic acid)) in 100 mM sodium phosphate, 0.1 mM EDTA, pH 7.2 buffer on a well plate for 5 min at RT. The absorption of the mixture was measured at 412 nm. After deduction of the background, DMSO treated control samples were normalized to 100% activity and the residual activity of inhibitor treated samples was determined. The average values of technical replicates were calculated and then the standard deviation of the means was calculated over three independent experiments.

4.2 PhaB Inhibition Assay

The assay was performed as described before with some modifications.^{148,149} Pre-warm 100 μ L 200 μ M acetoacetyl-CoA sodium salt (from Santa Cruz Biotechnology), 800 μ M NADPH (reduced nicotinamide adenine dinucleotide phosphate from Roth) in 200 μ M DTT, 125 mM Tris-HCl, pH 8.0 buffer per well on a well plate at 37 °C on Tecan reader. 50 μ L PhaB solution (10 μ M in 125 mM Tris-HCl, 200 μ M DTT, pH 8.0 buffer) was incubated with different equivalents of natural product **F1** (0.1 μ L concentrated stocks in DMSO was used) and DMSO as control at 25 °C for 10 min. Then 4 μ L pre-incubated PhaB solution was added to the pre-warmed substance solution on the well plate while 4 μ L 125 mM Tris-HCl, 200 μ M DTT, pH 8.0 buffer was added to the blank control. The absorption of the solution was recorded at 340 nm with time. After deduction of the background, activities were calculated from initial

reaction rates. DMSO treated control samples were normalized to 100% activity and the residual activity of inhibitor treated samples was determined. The average values of technical replicates were calculated and then the standard deviation of the means was calculated over three independent experiments.

4.3 Inhibition of Bioluminescence in Luminescent *E. coli* DH5 α by Fimbroside

The luminescent *Escherichia coli* DH5 α with a pBluelux plasmid, containing *luxCDABE* operon under the control of a *lac* promoter¹⁹⁹ was kindly donated by Prof. Tom Coenye and used to test the inhibition of bioluminescence by fimbroside. An overnight culture of *E. coli* DH5 α in LB media was cultivated to OD₆₀₀ \approx 3.3 at 37 °C with agitation, then the culture was diluted in 50 mL fresh LB media to a final OD₆₀₀ = 0.1. The culture was grown at 37 °C to OD₆₀₀ \approx 1.5. At this point, OD₆₀₀ was measured and the culture was diluted to a final OD₆₀₀ = 0.75 with fresh LB media. 100 μ L aliquots of the culture were added to 96 well plates which contained 1 μ L various concentrations of compounds or DMSO per well. After 2 h incubation at 37 °C with agitation, luminescence and OD₆₀₀ were measured on an infinite M200Pro plate reader (Tecan). After deduction of the background, luminescence units were normalized to cell density. DMSO treated control samples were normalized to 100% activity and the residual activity of inhibitor treated samples was determined. The average values of technical triplicates were calculated and then the standard deviation of the means was calculated over three independent experiments. Residual activities for the respective compound concentration were fitted to $Y = 100 / (1 + 10^{((\log_{10} C_{50} - X) * HillSlope)})$ (Y: residual activity in%; X: \log_{10} (concentration)) and then IC₅₀ was calculated in GraphPad Prism 6.0.

V – BIBLIOGRAPHY

V – BIBLIOGRAPHY

1. Nealson, K. H.; Platt, T.; Hastings, J. W. *J. Bacteriol.* **1970**, *104*, 313.
2. Kempner, E. S.; Hanson, F. E. *J. Bacteriol.* **1968**, *95*, 975.
3. Eberhard, A.; Burlingame, A. L.; Eberhard, C.; Kenyon, G. L.; Nealson, K. H.; Oppenheimer, N. J. *Biochemistry* **1981**, *20*, 2444.
4. Bainton, N. J.; Bycroft, B. W.; Chhabra, S. R.; Stead, P.; Gledhill, L.; Hill, P. J.; Rees, C. E.; Winson, M. K.; Salmond, G. P.; Stewart, G. S.; et al. *Gene* **1992**, *116*, 87.
5. Fuqua, W. C.; Winans, S. C.; Greenberg, E. P. *J. Bacteriol.* **1994**, *176*, 269.
6. Rutherford, S. T.; Bassler, B. L. *Cold Spring Harb. Perspect. Med.* **2012**, *2*, a012427.
7. Guo, M.; Gamby, S.; Zheng, Y.; Sintim, H. O. *Int. J. Mol. Sci.* **2013**, *14*, 17694.
8. Kelly, R. C.; Bolitho, M. E.; Higgins, D. A.; Lu, W.; Ng, W. L.; Jeffrey, P. D.; Rabinowitz, J. D.; Semmelhack, M. F.; Hughson, F. M.; Bassler, B. L. *Nat. Chem. Biol.* **2009**, *5*, 891.
9. Ng, W. L.; Perez, L. J.; Wei, Y.; Kraml, C.; Semmelhack, M. F.; Bassler, B. L. *Mol. Microbiol.* **2011**, *79*, 1407.
10. Lee, J.; Wu, J.; Deng, Y.; Wang, J.; Wang, C.; Wang, J.; Chang, C.; Dong, Y.; Williams, P.; Zhang, L. H. *Nat. Chem. Biol.* **2013**, *9*, 339.
11. Galloway, W. R.; Hodgkinson, J. T.; Bowden, S. D.; Welch, M.; Spring, D. R. *Chem. Rev.* **2011**, *111*, 28.
12. Jung, K. *Nat. Chem. Biol.* **2011**, *7*, 502.
13. Popat, R.; Cornforth, D. M.; McNally, L.; Brown, S. P. *J. R. Soc. Interface* **2015**, *12*, 20140882.
14. Ng, W. L.; Bassler, B. L. *Annu. Rev. Genet.* **2009**, *43*, 197.
15. Wang, B.; Muir, T. W. *Cell. Chem. Biol.* **2016**, *23*, 214.
16. Abraham, W. R. *Antibiotics (Basel)* **2016**, *5*, 3.
17. Welsh, M. A.; Eibergen, N. R.; Moore, J. D.; Blackwell, H. E. *J. Am. Chem. Soc.* **2015**, *137*, 1510.
18. Lee, J.; Zhang, L. *Protein Cell* **2015**, *6*, 26.
19. Goo, E.; An, J. H.; Kang, Y.; Hwang, I. *Trends Microbiol.* **2015**, *23*, 567.
20. Castillo-Juarez, I.; Maeda, T.; Mandujano-Tinoco, E. A.; Tomas, M.; Perez-Eretza, B.; Garcia-Contreras, S. J.; Wood, T. K.; Garcia-Contreras, R. *World J. Clin. Cases* **2015**, *3*, 575.
21. Brackman, G.; Coenye, T. *Curr. Pharm. Des.* **2015**, *21*, 5.
22. Scutera, S.; Zucca, M.; Savoia, D. *Expert Opin. Drug Discov.* **2014**, *9*, 353.
23. Flemming, H. C.; Wingender, J.; Szewzyk, U., *Biofilm Highlights*, Springer-Verlag Berlin Heidelberg, **2011**.
24. Bjarnsholt, T.; Moser, C.; Jensen, P. O; Høiby, N.; *Biofilm Infections*; Springer Science+Business Media,, 2011.
25. Olsen, I. *Eur. J. Clin. Microbiol. Infect. Dis.* **2015**, *34*, 877.
26. Davies, D. G.; Parsek, M. R.; Pearson, J. P.; Iglewski, B. H.; Costerton, J. W.; Greenberg, E. P. *Science* **1998**, *280*, 295.
27. Kirisits, M. J.; Parsek, M. R. *Cell Microbiol.* **2006**, *8*, 1841.
28. Fischer, J.; Lee, J. C.; Peters, G.; Kahl, B. C. *Clin. Microbiol. Infect.* **2014**, *20*, O414.
29. Traber, K. E.; Lee, E.; Benson, S.; Corrigan, R.; Cantera, M.; Shopsin, B.; Novick, R. P. *Microbiology* **2008**, *154*, 2265.

30. Bjarnsholt, T.; Jensen, P. O.; Jakobsen, T. H.; Phipps, R.; Nielsen, A. K.; Rybtke, M. T.; Tolker-Nielsen, T.; Givskov, M.; Hoiby, N.; Ciofu, O.; Scandinavian Cystic Fibrosis Study, C. *PLoS One* **2010**, *5*, e10115.
31. Joo, H. S.; Otto, M. *Chem. Biol.* **2012**, *19*, 1503.
32. Wang, Y.; Ma, S. *Curr. Med. Chem.* **2014**, *21*, 296.
33. Antunes, L. C.; Ferreira, R. B. *Crit. Rev. Microbiol.* **2009**, *35*, 69.
34. George, E. A.; Muir, T. W. *Chembiochem* **2007**, *8*, 847.
35. Queck, S. Y.; Jameson-Lee, M.; Villaruz, A. E.; Bach, T. H.; Khan, B. A.; Sturdevant, D. E.; Ricklefs, S. M.; Li, M.; Otto, M. *Mol. Cell.* **2008**, *32*, 150.
36. Kendall, M. M.; Sperandio, V. *MBio* **2016**, *7*, e01748-15.
37. Helman, Y.; Chernin, L. *Mol. Plant Pathol.* **2015**, *16*, 316.
38. Pacheco, A. R.; Sperandio, V. *Curr. Opin. Microbiol.* **2009**, *12*, 192.
39. Hughes, D. T.; Sperandio, V. *Nat. Rev. Microbiol.* **2008**, *6*, 111.
40. Ritchie, A. J.; Yam, A. O.; Tanabe, K. M.; Rice, S. A.; Cooley, M. A. *Infect. Immun.* **2003**, *71*, 4421.
41. Kravchenko, V. V.; Kaufmann, G. F.; Mathison, J. C.; Scott, D. A.; Katz, A. Z.; Grauer, D. C.; Lehmann, M.; Meijler, M. M.; Janda, K. D.; Ulevitch, R. J. *Science* **2008**, *321*, 259.
42. Smith, R. S.; Kelly, R.; Iglewski, B. H.; Phipps, R. P. *J. Immunol.* **2002**, *169*, 2636.
43. Draganov, D. I.; Teiber, J. F.; Speelman, A.; Osawa, Y.; Sunahara, R.; La Du, B. N. *J. Lipid. Res.* **2005**, *46*, 1239.
44. Zaborina, O.; Lepine, F.; Xiao, G.; Valuckaite, V.; Chen, Y.; Li, T.; Ciancio, M.; Zaborin, A.; Petrof, E. O.; Turner, J. R.; Rahme, L. G.; Chang, E.; Alverdy, J. C. *PLoS Pathog.* **2007**, *3*, e35.
45. Beury-Cirou, A.; Tannieres, M.; Minard, C.; Soulere, L.; Rasamiravaka, T.; Dodd, R. H.; Queneau, Y.; Dessaux, Y.; Guillou, C.; Vandeputte, O. M.; Faure, D. *PLoS One* **2013**, *8*, e83564.
46. Peterson, M. M.; Mack, J. L.; Hall, P. R.; Alsup, A. A.; Alexander, S. M.; Sully, E. K.; Sawires, Y. S.; Cheung, A. L.; Otto, M.; Gresham, H. D. *Cell Host Microbe* **2008**, *4*, 555.
47. Rothfork, J. M.; Timmins, G. S.; Harris, M. N.; Chen, X.; Lusic, A. J.; Otto, M.; Cheung, A. L.; Gresham, H. D. *Proc. Natl. Acad. Sci. U. S. A.* **2004**, *101*, 13867.
48. Koh, C. L.; Sam, C. K.; Yin, W. F.; Tan, L. Y.; Krishnan, T.; Chong, Y. M.; Chan, K. G. *Sensors (Basel)* **2013**, *13*, 6217.
49. Hopkins, A. L. *Nat. Chem. Biol.* **2008**, *4*, 682.
50. Cravatt, B. F.; Wright, A. T.; Kozarich, J. W. *Annu. Rev. Biochem.* **2008**, *77*, 383.
51. Evans, M. J.; Cravatt, B. F. *Chem. Rev.* **2006**, *106*, 3279.
52. Speers, A. E.; Cravatt, B. F. *Chembiochem* **2004**, *5*, 41.
53. Speers, A. E.; Adam, G. C.; Cravatt, B. F. *J. Am. Chem. Soc.* **2003**, *125*, 4686.
54. Paulick, M. G.; Bogoy, M. *Curr. Opin. Genet. Dev.* **2008**, *18*, 97.
55. Fonovic, M.; Bogoy, M. *Expert Rev. Proteomics* **2008**, *5*, 721.
56. Sadaghiani, A. M.; Verhelst, S. H.; Bogoy, M. *Curr. Opin. Chem. Biol.* **2007**, *11*, 20.
57. Sui, P.; Watanabe, H.; Ossipov, M. H.; Porreca, F.; Bakalkin, G.; Bergquist, J.; Artemenko, K. J. *Proteome Res.* **2013**, *12*, 2245.

58. Aye, T. T.; Low, T. Y.; Bjorlykke, Y.; Barsnes, H.; Heck, A. J.; Berven, F. S. *Anal. Chem.* **2012**, *84*, 4999.
59. Wright, M. H.; Sieber, S. A. *Nat. Prod. Rep.* **2016**, *33*, 681.
60. Wang, J.; Zhang, C. J.; Zhang, J.; He, Y.; Lee, Y. M.; Chen, S.; Lim, T. K.; Ng, S.; Shen, H. M.; Lin, Q. *Sci. Rep.* **2015**, *5*, 7896.
61. Shahiduzzaman, M.; Coombs, K. M. *Front. Microbiol.* **2012**, *3*, 308.
62. Nahnsen, S.; Bielow, C.; Reinert, K.; Kohlbacher, O. *Mol. Cell Proteomics* **2013**, *12*, 549.
63. Bottcher, T.; Sieber, S. A. *J. Am. Chem. Soc.* **2010**, *132*, 6964.
64. Eirich, J.; Orth, R.; Sieber, S. A. *J. Am. Chem. Soc.* **2011**, *133*, 12144.
65. Yang, P. Y.; Liu, K.; Ngai, M. H.; Lear, M. J.; Wenk, M. R.; Yao, S. Q. *J. Am. Chem. Soc.* **2010**, *132*, 656.
66. Nishino, M.; Choy, J. W.; Gushwa, N. N.; Oses-Prieto, J. A.; Koupparis, K.; Burlingame, A. L.; Renslo, A. R.; McKerrow, J. H.; Taunton, J. *Elife* **2013**, *2*, e00712.
67. Wirth, T.; Pestel, G. F.; Ganal, V.; Kirmeier, T.; Schuberth, I.; Rein, T.; Tietze, L. F.; Sieber, S. A. *Angew. Chem. Int. Ed.* **2013**, *52*, 6921.
68. Zhao, W.; Lorenz, N.; Jung, K.; Sieber, S. A. *Angew. Chem. Int. Ed.* **2016**, *55*, 1187.
69. Pichler, C. M.; Krysiak, J.; Breinbauer, R. *Bioorg. Med. Chem.* **2016**.
70. Yang, P.; Liu, K. *Chembiochem* **2015**, *16*, 712.
71. Geurink, P. P.; Prely, L. M.; van der Marel, G. A.; Bischoff, R.; Overkleeft, H. S. *Top. Curr. Chem.* **2012**, *324*, 85.
72. Lanning, B. R.; Whitby, L. R.; Dix, M. M.; Douhan, J.; Gilbert, A. M.; Hett, E. C.; Johnson, T. O.; Joslyn, C.; Kath, J. C.; Niessen, S.; Roberts, L. R.; Schnute, M. E.; Wang, C.; Hulce, J. J.; Wei, B.; Whiteley, L. O.; Hayward, M. M.; Cravatt, B. F. *Nat. Chem. Biol.* **2014**, *10*, 760.
73. Weerapana, E.; Speers, A. E.; Cravatt, B. F. *Nat. Protoc.* **2007**, *2*, 1414.
74. Weerapana, E.; Wang, C.; Simon, G. M.; Richter, F.; Khare, S.; Dillon, M. B.; Bachovchin, D. A.; Mowen, K.; Baker, D.; Cravatt, B. F. *Nature* **2010**, *468*, 790.
75. Kazlauskas, R.; Murphy, P. T.; Quinn, R. J.; Wells, R. J. *Tetrahedron Lett.* **1977**, *18*, 37.
76. de Nys, R.; Wright, A. D.; König, G. M.; Sticher, O. *Tetrahedron* **1993**, *49*, 11213.
77. Kuttly, S. K.; Barraud, N.; Pham, A.; Iskander, G.; Rice, S. A.; Black, D. S.; Kumar, N. J. *Med. Chem.* **2013**, *56*, 9517.
78. Gram, L.; de Nys, R.; Maximilien, R.; Givskov, M.; Steinberg, P.; Kjelleberg, S. *Appl. Environ. Microbiol.* **1996**, *62*, 4284.
79. Garcia-Contreras, R.; Perez-Eretza, B.; Lira-Silva, E.; Jasso-Chavez, R.; Coria-Jimenez, R.; Rangel-Vega, A.; Maeda, T.; Wood, T. K. *Pathog. Dis.* **2014**, *70*, 95.
80. Pan, J.; Ren, D. *Bioorg. Med. Chem. Lett.* **2013**, *23*, 6559.
81. Pan, J.; Xie, X.; Tian, W.; Bahar, A. A.; Lin, N.; Song, F.; An, J.; Ren, D. *Appl. Microbiol. Biotechnol.* **2013**, *97*, 9145.
82. Pan, J.; Song, F.; Ren, D. *Bioorg. Med. Chem. Lett.* **2013**, *23*, 4648.
83. Pan, J.; Bahar, A. A.; Syed, H.; Ren, D. *PLoS One* **2012**, *7*, e45778.
84. Garcia-Contreras, R.; Martinez-Vazquez, M.; Velazquez Guadarrama, N.; Villegas Paneda, A. G.; Hashimoto, T.; Maeda, T.; Quezada, H.; Wood, T. K. *Pathog. Dis.* **2013**, *68*, 8.

V – BIBLIOGRAPHY

85. Defoirdt, T.; Benneche, T.; Brackman, G.; Coenye, T.; Sorgeloos, P.; Scheie, A. A. *PLoS One* **2012**, *7*, e41788.
86. Defoirdt, T.; Crab, R.; Wood, T. K.; Sorgeloos, P.; Verstraete, W.; Bossier, P. *Appl. Environ. Microbiol.* **2006**, *72*, 6419.
87. Ren, D.; Sims, J. J.; Wood, T. K. *Environ. Microbiol.* **2001**, *3*, 731.
88. Hentzer, M.; Riedel, K.; Rasmussen, T. B.; Heydorn, A.; Andersen, J. B.; Parsek, M. R.; Rice, S. A.; Eberl, L.; Molin, S.; Hoiby, N.; Kjelleberg, S.; Givskov, M. *Microbiology* **2002**, *148*, 87.
89. Ren, D.; Sims, J. J.; Wood, T. K. *Lett. Appl. Microbiol.* **2002**, *34*, 293.
90. Morohoshi, T.; Shiono, T.; Takidouchi, K.; Kato, M.; Kato, N.; Kato, J.; Ikeda, T. *Appl. Environ. Microbiol.* **2007**, *73*, 6339.
91. Janssens, J. C.; Steenackers, H.; Robijns, S.; Gellens, E.; Levin, J.; Zhao, H.; Hermans, K.; De Coster, D.; Verhoeven, T. L.; Marchal, K.; Vanderleyden, J.; De Vos, D. E.; De Keersmaecker, S. C. *Appl. Environ. Microbiol.* **2008**, *74*, 6639.
92. Han, Y.; Hou, S.; Simon, K. A.; Ren, D.; Luk, Y. Y. *Bioorg. Med. Chem. Lett.* **2008**, *18*, 1006.
93. Vestby, L. K.; Lonn-Stensrud, J.; Moretro, T.; Langsrud, S.; Aamdal-Scheie, A.; Benneche, T.; Nesse, L. L. *J. Appl. Microbiol.* **2010**, *108*, 771.
94. Manefield, M.; Welch, M.; Givskov, M.; Salmond, G. P.; Kjelleberg, S. *FEMS Microbiol. Lett.* **2001**, *205*, 131.
95. Jones, M. B.; Peterson, S. N.; Benn, R.; Braisted, J. C.; Jarrahi, B.; Shatzkes, K.; Ren, D.; Wood, T. K.; Blaser, M. J. *Virulence* **2010**, *1*, 72.
96. Kaur, G.; Rajesh, S.; Princy, S. A. *Indian J. Microbiol.* **2015**, *55*, 349.
97. Wang, W.; Morohoshi, T.; Ikeda, T.; Chen, L. *Acta Biochim. Biophys. Sin.* **2008**, *40*, 1023.
98. Lowery, C. A.; Abe, T.; Park, J.; Eubanks, L. M.; Sawada, D.; Kaufmann, G. F.; Janda, K. *D. J. Am. Chem. Soc.* **2009**, *131*, 15584.
99. Wu, H.; Song, Z.; Hentzer, M.; Andersen, J. B.; Molin, S.; Givskov, M.; Hoiby, N. *J. Antimicrob. Chemother.* **2004**, *53*, 1054.
100. Cheng, Y.; Gao, B.; Liu, X.; Zhao, X.; Sun, W.; Ren, H.; Wu, J. *Int. J. Nanomedicine* **2016**, *11*, 1337.
101. Cheng, Y.; Zhao, X.; Liu, X.; Sun, W.; Ren, H.; Gao, B.; Wu, J. *Int. J. Nanomedicine* **2015**, *10*, 727.
102. Cheng, Y.; Wu, J.; Gao, B.; Zhao, X.; Yao, J.; Mei, S.; Zhang, L.; Ren, H. *Int. J. Nanomedicine* **2012**, *7*, 5641.
103. Ye, L.; Xu, G.; Huang, Y.; Zhou, Y.; Zhao, G.; Lei, Y. *Zhongguo Xiu Fu Chong Jian Wai Ke Za Zhi* **2010**, *24*, 871.
104. Lianhua, Y.; Yunchao, H.; Geng, X.; Youquang, Z.; Guangqiang, Z.; Yujie, L. *Cell Biochem. Biophys.* **2013**, *67*, 893.
105. Yujie, L.; Geng, X.; Huang, Y. C.; Li, Y.; Yang, K.; Ye, L.; Chen, X.; Zhao, G.; Yin, C. *Cell Biochem. Biophys.* **2013**, *67*, 1501.
106. Zhu, H.; Kumar, A.; Ozkan, J.; Bandara, R.; Ding, A.; Perera, I.; Steinberg, P.; Kumar, N.; Lao, W.; Griesser, S. S.; Britcher, L.; Griesser, H. J.; Willcox, M. D. *Optom. Vis. Sci.* **2008**, *85*, 292.
107. Jang, Y. J.; Sim, J.; Jun, H. K.; Choi, B. K. *Arch. Oral Biol.* **2013**, *58*, 1594.

108. Trizna, E. Y.; Khakimullina, E. N.; Latypova, L. Z.; Kurbangalieva, A. R.; Sharafutdinov, I. S.; Evtugin, V. G.; Babynin, E. V.; Bogachev, M. I.; Kayumov, A. R. *Acta Naturae* **2015**, *7*, 102.
109. Kayumov, A. R.; Khakimullina, E. N.; Sharafutdinov, I. S.; Trizna, E. Y.; Latypova, L. Z.; Thi Lien, H.; Margulis, A. B.; Bogachev, M. I.; Kurbangalieva, A. R. *J. Antibiot. (Tokyo)* **2015**, *68*, 297.
110. Yang, S.; Abdel-Razek, O. A.; Cheng, F.; Bandyopadhyay, D.; Shetye, G. S.; Wang, G.; Luk, Y. Y. *Bioorg. Med. Chem.* **2014**, *22*, 1313.
111. Pearce, A. N.; Chia, E. W.; Berridge, M. V.; Maas, E. W.; Page, M. J.; Webb, V. L.; Harper, J. L.; Copp, B. R. *J. Nat. Prod.* **2007**, *70*, 111.
112. Pereira, U. A.; Barbosa, L. C.; Maltha, C. R.; Demuner, A. J.; Masood, M. A.; Pimenta, A. L. *Bioorg. Med. Chem. Lett.* **2014**, *24*, 1052.
113. Won, T. H.; Jeon, J. E.; Kim, S. H.; Lee, S. H.; Rho, B. J.; Oh, D. C.; Oh, K. B.; Shin, J. J. *Nat. Prod.* **2012**, *75*, 2055.
114. Manefield, M.; de Nys, R.; Kumar, N.; Read, R.; Givskov, M.; Steinberg, P.; Kjelleberg, S. *Microbiology* **1999**, *145 (Pt 2)*, 283.
115. Manefield, M.; Rasmussen, T. B.; Henzter, M.; Andersen, J. B.; Steinberg, P.; Kjelleberg, S.; Givskov, M. *Microbiology* **2002**, *148*, 1119.
116. Koch, B.; Liljefors, T.; Persson, T.; Nielsen, J.; Kjelleberg, S.; Givskov, M. *Microbiology* **2005**, *151*, 3589.
117. Lin, B.; Wang, Z.; Malanoski, A. P.; O'Grady, E. A.; Wimpee, C. F.; Vuddhakul, V.; Alves Jr, N.; Thompson, F. L.; Gomez-Gil, B.; Vora, G. J. *Environ. Microbiol. Rep.* **2010**, *2*, 81.
118. Zang, T.; Lee, B. W.; Cannon, L. M.; Ritter, K. A.; Dai, S.; Ren, D.; Wood, T. K.; Zhou, Z. *S. Bioorg. Med. Chem. Lett.* **2009**, *19*, 6200.
119. Beechan, C. M.; Sims, J. J. *Tetrahedron Lett.* **1979**, *20*, 1649.
120. Manny, A. J.; Kjelleberg, S.; Kumar, N.; de Nys, R.; Read, R. W.; Steinberg, P. *Tetrahedron* **1997**, *53*, 15813.
121. Steenackers, H. P.; Levin, J.; Janssens, J. C.; De Weerd, A.; Balzarini, J.; Vanderleyden, J.; De Vos, D. E.; De Keersmaecker, S. C. *Bioorg. Med. Chem.* **2010**, *18*, 5224.
122. Rodríguez, S.; Camps, F.; Fabriàs, G. *J. Org. Chem.* **2001**, *66*, 8052.
123. Iglesias-Sanchez, J. C.; Santa Maria, D.; Claramunt, R. M.; Elguero, J. *Molecules* **2010**, *15*, 1213.
124. Wube, A. A.; Hufner, A.; Thomaschitz, C.; Blunder, M.; Kollroser, M.; Bauer, R.; Bucar, F. *Bioorg. Med. Chem.* **2011**, *19*, 567.
125. Lemaire, C.; Luxen, A.; Christiaens, L.; Guillaume, M. *J. Heterocycl. Chem.* **1983**, *20*, 811.
126. Gilleron, P.; Millet, R.; Domarkas, J.; Farce, A.; Houssin, R.; Henichart, J. P. *J. Pept. Sci.* **2006**, *12*, 140.
127. Baskar, B.; Dakas, P. Y.; Kumar, K. *Org. Lett.* **2011**, *13*, 1988.
128. Kim, D. W.; Song, C. E.; Chi, D. Y. *J. Org. Chem.* **2003**, *68*, 4281.
129. Visscher, I.; Stuart, M. C.; Engberts, J. B. *Org. Biomol. Chem.* **2006**, *4*, 707.
130. Zunszain, P. A.; Varela, O. *Tetrahedron: Asymmetry* **2000**, *11*, 765.
131. Makabe, H.; Tanaka, A.; Oritani, T. *Tetrahedron* **1998**, *54*, 6329.

132. Onyango, E. O.; Jacobi, P. A. *J. Org. Chem.* **2012**, *77*, 7411.
133. Nicolai, S.; Sedigh-Zadeh, R.; Waser, J. *J. Org. Chem.* **2013**, *78*, 3783.
134. Anetzberger, C.; Reiger, M.; Fekete, A.; Schell, U.; Stambrau, N.; Plener, L.; Kopka, J.; Schmitt-Kopplin, P.; Hilbi, H.; Jung, K. *PLoS One* **2012**, *7*, e48310.
135. Defoirdt, T.; Miyamoto, C. M.; Wood, T. K.; Meighen, E. A.; Sorgeloos, P.; Verstraete, W.; Bossier, P. *Environ. Microbiol.* **2007**, *9*, 2486.
136. Lerat, E.; Moran, N. A. *Mol. Biol. Evol.* **2004**, *21*, 903.
137. Schauder, S.; Shokat, K.; Surette, M. G.; Bassler, B. L. *Mol. Microbiol.* **2001**, *41*, 463.
138. Rajan, R.; Zhu, J.; Hu, X.; Pei, D.; Bell, C. E. *Biochemistry* **2005**, *44*, 3745.
139. Hilgers, M. T.; Ludwig, M. L. *Proc. Natl. Acad. Sci. U. S. A.* **2001**, *98*, 11169.
140. Ruzheinikov, S. N.; Das, S. K.; Sedelnikova, S. E.; Hartley, A.; Foster, S. J.; Horsburgh, M. J.; Cox, A. G.; McCleod, C. W.; Mekhalfia, A.; Blackburn, G. M.; Rice, D. W.; Baker, P. J. *J. Mol. Biol.* **2001**, *313*, 111.
141. Lewis, H. A.; Furlong, E. B.; Laubert, B.; Eroshkina, G. A.; Batiyenko, Y.; Adams, J. M.; Bergseid, M. G.; Marsh, C. D.; Peat, T. S.; Sanderson, W. E.; Sauder, J. M.; Buchanan, S. G. *Structure* **2001**, *9*, 527.
142. Gopishetty, B.; Zhu, J.; Rajan, R.; Sobczak, A. J.; Wnuk, S. F.; Bell, C. E.; Pei, D. *J. Am. Chem. Soc.* **2009**, *131*, 1243.
143. Shen, G.; Rajan, R.; Zhu, J.; Bell, C. E.; Pei, D. *J. Med. Chem.* **2006**, *49*, 3003.
144. Zhu, J.; Dizin, E.; Hu, X.; Wavreille, A. S.; Park, J.; Pei, D. *Biochemistry* **2003**, *42*, 4717.
145. Soly, R. R.; Meighen, E. A. *J. Mol. Biol.* **1991**, *219*, 69.
146. Miyamoto, C. M.; Sun, W.; Meighen, E. A. *Biochim. Biophys. Acta.* **1998**, *1384*, 356.
147. Sun, W.; Cao, J. G.; Teng, K.; Meighen, E. A. *J. Biol. Chem.* **1994**, *269*, 20785.
148. Matsumoto, K.; Tanaka, Y.; Watanabe, T.; Motohashi, R.; Ikeda, K.; Tobitani, K.; Yao, M.; Tanaka, I.; Taguchi, S. *Appl. Environ. Microbiol.* **2013**, *79*, 6134.
149. Chohan, S. N.; Copeland, L. *Appl. Environ. Microbiol.* **1998**, *64*, 2859.
150. Oba, Y.; Schultz, D. T. *Adv. Biochem. Eng. Biotechnol.* **2014**, *144*, 3.
151. Mansfield, J. R. *Curr. Pharm. Biotechnol.* **2010**, *11*, 628.
152. Thouand, G.; Marks, R.; *Advances in Biochemical Engineering/Biotechnology-Volume 3*, Springer International Publishing Switzerland, **2016**.
153. Thouand, G.; Marks, R.; *Advances in Biochemical Engineering/Biotechnology-Volume 1*, Springer-Verlag Berlin Heidelberg, **2014**.
154. Thouand, G.; Marks, R.; *Advances in Biochemical Engineering/Biotechnology-Volume 2*, Springer-Verlag Berlin Heidelberg: **2014**.
155. Haddock, S. H.; Moline, M. A.; Case, J. F. *Ann. Rev. Mar. Sci.* **2010**, *2*, 443.
156. Herring, P. J. *J. Biolumin. Chemilumin.* **1987**, *1*, 147.
157. Zarubin, M.; Belkin, S.; Ionescu, M.; Genin, A. *Proc. Natl. Acad. Sci. U. S. A.* **2012**, *109*, 853.
158. Meighen, E. A.; Dunlap, P. V. *Adv. Microb. Physiol.* **1993**, *34*, 1.
159. Dunlap, P. V.; Ast, J. C.; Kimura, S.; Fukui, A.; Yoshino, T.; Endo, H. *Cladistics* **2007**, *23*, 507.
160. Sperelakis, N. *Cell Physiology Sourcebook*; 4 ed.; Elsevier, **2012**.

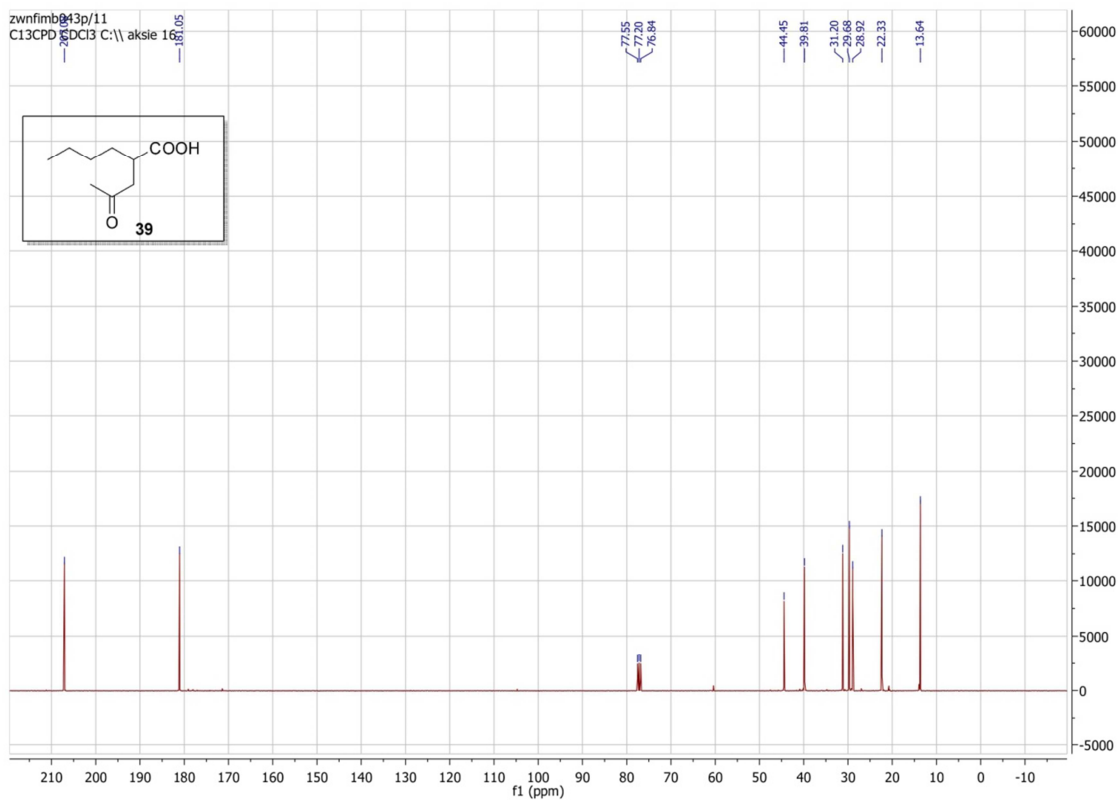
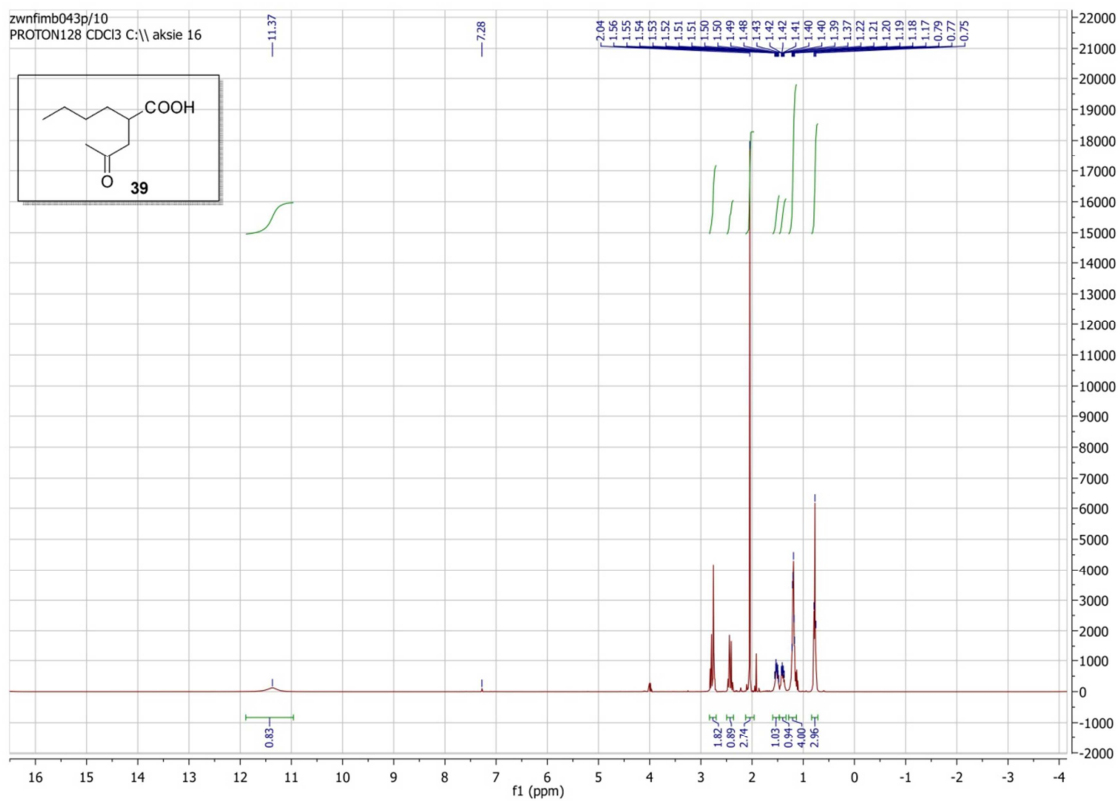
161. Wilson, T.; Hastings, J. W. *Annu. Rev. Cell. Dev. Biol.* **1998**, *14*, 197.
162. Meighen, E. A. *Microbiol. Rev.* **1991**, *55*, 123.
163. Hastings, J. W.; Potrikus, C. J.; Gupta, S. C.; Kurfurst, M.; Makemson, J. C. *Adv. Microb. Physiol.* **1985**, *26*, 235.
164. Zenno, S.; Saigo, K. *J. Bacteriol.* **1994**, *176*, 3544.
165. Zenno, S.; Saigo, K.; Kanoh, H.; Inouye, S. *J. Bacteriol.* **1994**, *176*, 3536.
166. Inouye, S. *FEBS Lett.* **1994**, *347*, 163.
167. Tinikul, R.; Pitsawong, W.; Sucharitakul, J.; Nijvipakul, S.; Ballou, D. P.; Chaiyen, P. *Biochemistry* **2013**, *52*, 6834.
168. Li, L.; Liu, X.; Yang, W.; Xu, F.; Wang, W.; Feng, L.; Bartlam, M.; Wang, L.; Rao, Z. *J. Mol. Biol.* **2008**, *376*, 453.
169. Hastings, J. W.; Balny, C. *J. Biol. Chem.* **1975**, *250*, 7288.
170. Kurfuerst, M.; Macheroux, P.; Ghisla, S.; Hastings, W. J. *Biochim. Biophys. Acta, Gen. Subj.* **1987**, *924*, 104.
171. Kurfurst, M.; Ghisla, S.; Hastings, J. W. *Proc. Natl. Acad. Sci. U. S. A.* **1984**, *81*, 2990.
172. Kalia, V. C. *Biotechnol. Adv.* **2013**, *31*, 224.
173. Jiang, T.; Li, M. *Expert Opin. Ther. Pat.* **2013**, *23*, 867.
174. Weinandy, F.; Lorenz-Baath, K.; Korotkov, V. S.; Bottcher, T.; Sethi, S.; Chakraborty, T.; Sieber, S. A. *ChemMedChem* **2014**, *9*, 710.
175. Zeiler, E.; Korotkov, V. S.; Lorenz-Baath, K.; Bottcher, T.; Sieber, S. A. *Bioorg. Med. Chem.* **2012**, *20*, 583.
176. Bottcher, T.; Sieber, S. A. *Angew. Chem. Int. Ed.* **2008**, *47*, 4600.
177. Gersch, M.; Gut, F.; Korotkov, V. S.; Lehmann, J.; Bottcher, T.; Rusch, M.; Hedberg, C.; Waldmann, H.; Klebe, G.; Sieber, S. A. *Angew. Chem. Int. Ed.* **2013**, *52*, 3009.
178. Thompson, S.; Mayerl, F.; Peoples, O. P.; Masamune, S.; Sinskey, A. J.; Walsh, C. T. *Biochemistry* **1989**, *28*, 5735.
179. Perez-Mendoza, D.; Sanjuan, J. *Curr. Opin. Microbiol.* **2016**, *30*, 36.
180. Chou, S. H.; Galperin, M. Y. *J. Bacteriol.* **2016**, *198*, 32.
181. Hengge, R.; Grundling, A.; Jenal, U.; Ryan, R.; Yildiz, F. *J. Bacteriol.* **2016**, *198*, 15.
182. Bush, M. J.; Tschowri, N.; Schlimpert, S.; Flardh, K.; Buttner, M. J. *Nat. Rev. Microbiol.* **2015**, *13*, 749.
183. Ha, D. G.; O'Toole, G. A. *Microbiol. Spectr.* **2015**, *3*, MB-0003-2014.
184. Liang, Z. X. *Nat. Prod. Rep.* **2015**, *32*, 663.
185. Whiteley, C. G.; Lee, D. J. *Biotechnol. Adv.* **2015**, *33*, 124.
186. Romling, U.; Galperin, M. Y.; Gomelsky, M. *Microbiol. Mol. Biol. Rev.* **2013**, *77*, 1.
187. McKee, R. W.; Kariisa, A.; Mudrak, B.; Whitaker, C.; Tamayo, R. *BMC Microbiol.* **2014**, *14*, 272.
188. Trimble, M. J.; McCarter, L. L. *Proc. Natl. Acad. Sci. U. S. A.* **2011**, *108*, 18079.
189. Waters, C. M.; Lu, W.; Rabinowitz, J. D.; Bassler, B. L. *J. Bacteriol.* **2008**, *190*, 2527.
190. Sharma, I. M.; Petchiappan, A.; Chatterji, D. *IUBMB Life* **2014**, *66*, 823.
191. Suppiger, A.; Schmid, N.; Aguilar, C.; Pessi, G.; Eberl, L. *Virulence* **2013**, *4*, 400.
192. Srivastava, D.; Waters, C. M. *J. Bacteriol.* **2012**, *194*, 4485.
193. Hengge, R. *Nat. Rev. Microbiol.* **2009**, *7*, 263.
194. Kazakov, A. E.; Rodionov, D. A.; Alm, E.; Arkin, A. P.; Dubchak, I.; Gelfand, M. S. *J. Bacteriol.* **2009**, *191*, 52.

V – BIBLIOGRAPHY

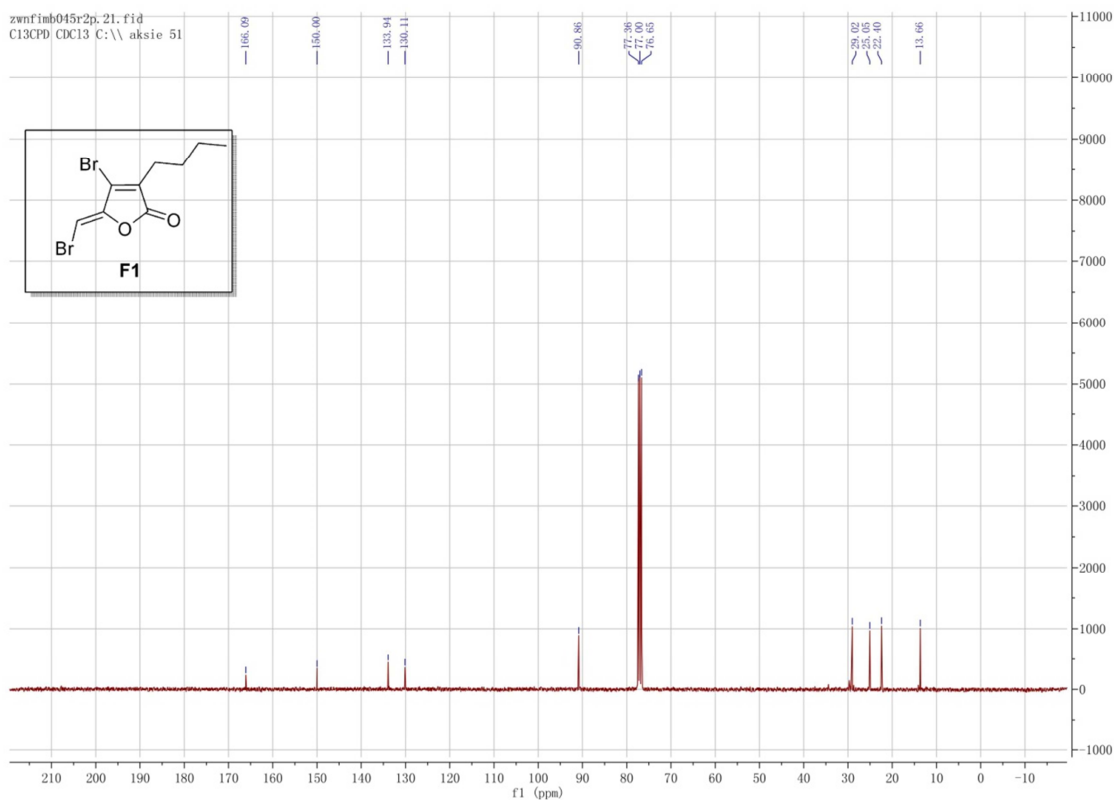
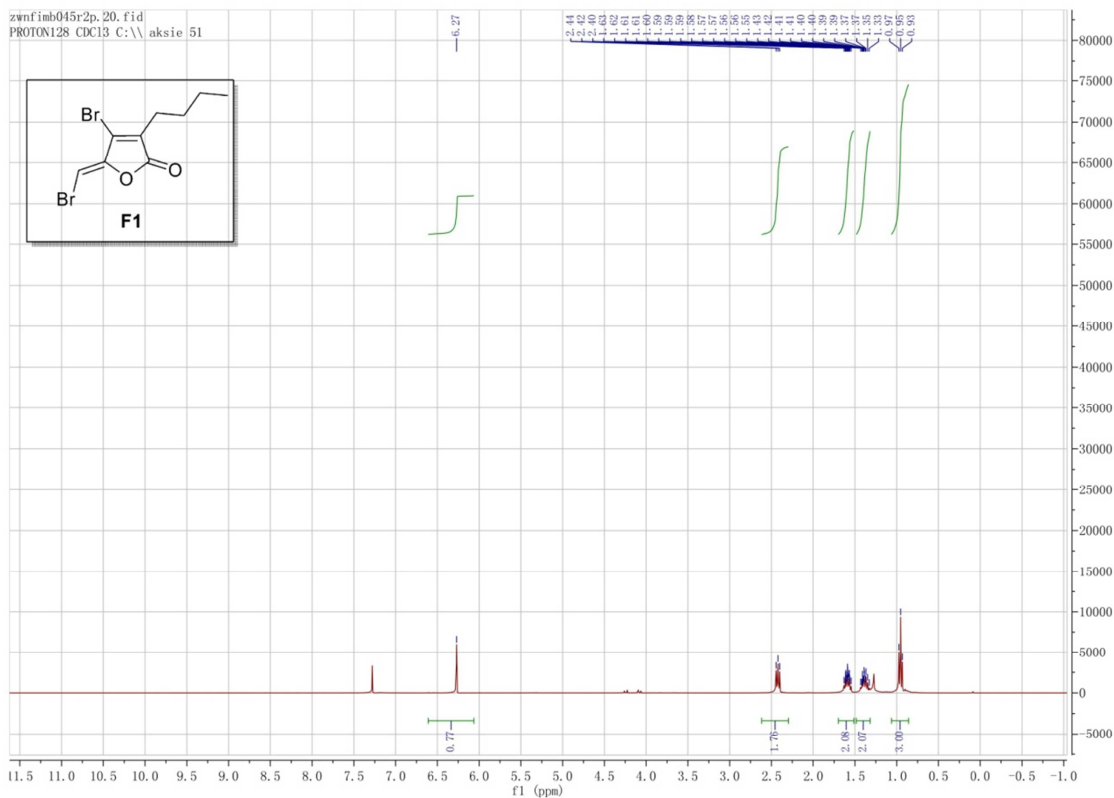
195. Fujita, Y.; Matsuoka, H.; Hirooka, K. *Mol. Microbiol.* **2007**, *66*, 829.
196. Greenberg, E. P.; Hastings, J. W.; Ulitzur, S. *Arch. Microbiol.* **1979**, *120*, 87.
197. Rui, H.; Liu, Q.; Ma, Y.; Wang, Q.; Zhang, Y. *FEMS microbiol. Lett.* **2008**, *285*, 155.
198. Timmen, M.; Bassler, B. L.; Jung, K. *J. Biol. Chem.* **2006**, *281*, 24398.
199. Brackman, G.; Defoirdt, T.; Miyamoto, C.; Bossier, P.; Van Calenbergh, S.; Nelis, H.; Coenye, T. *BMC Microbiol.* **2008**, *8*, 149.

VI – APPENDICES

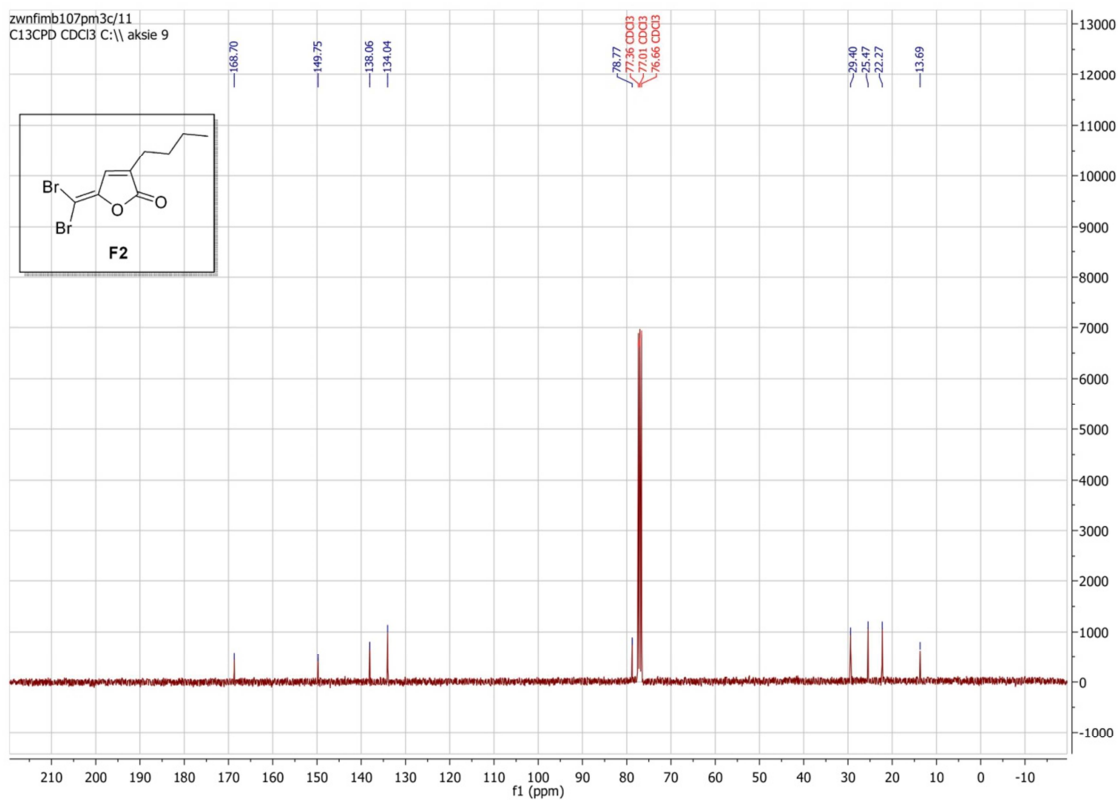
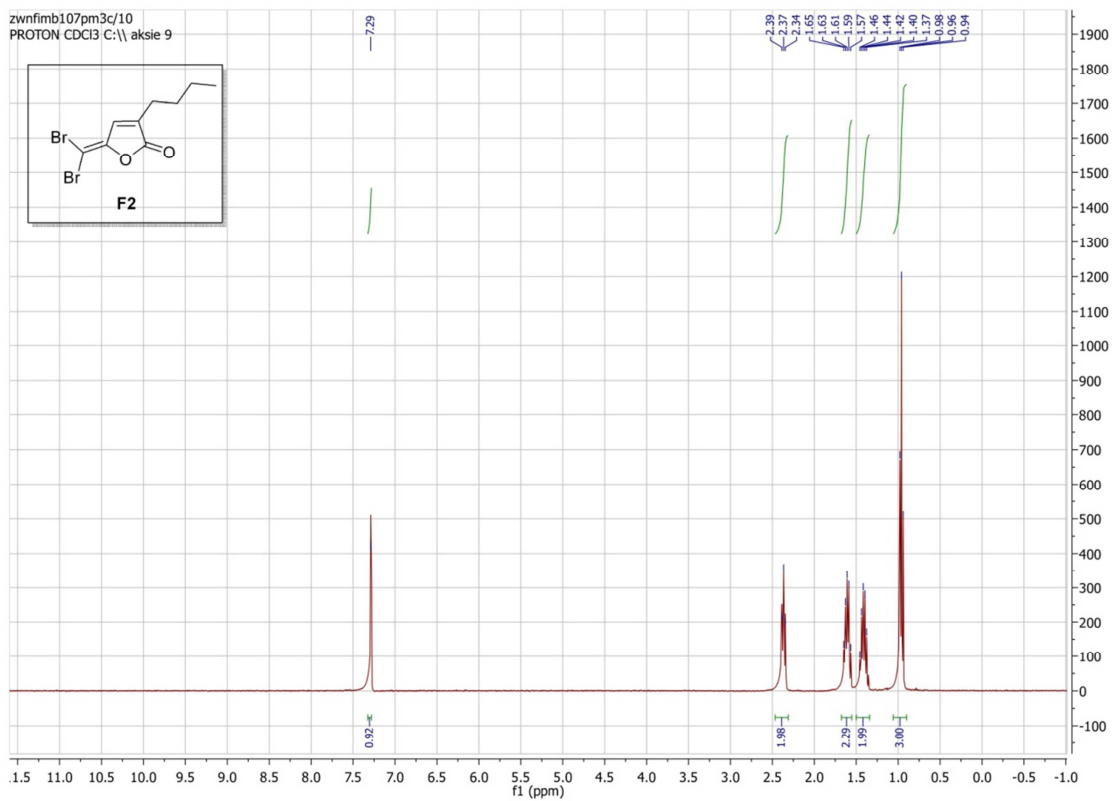
VI – APPENDICES



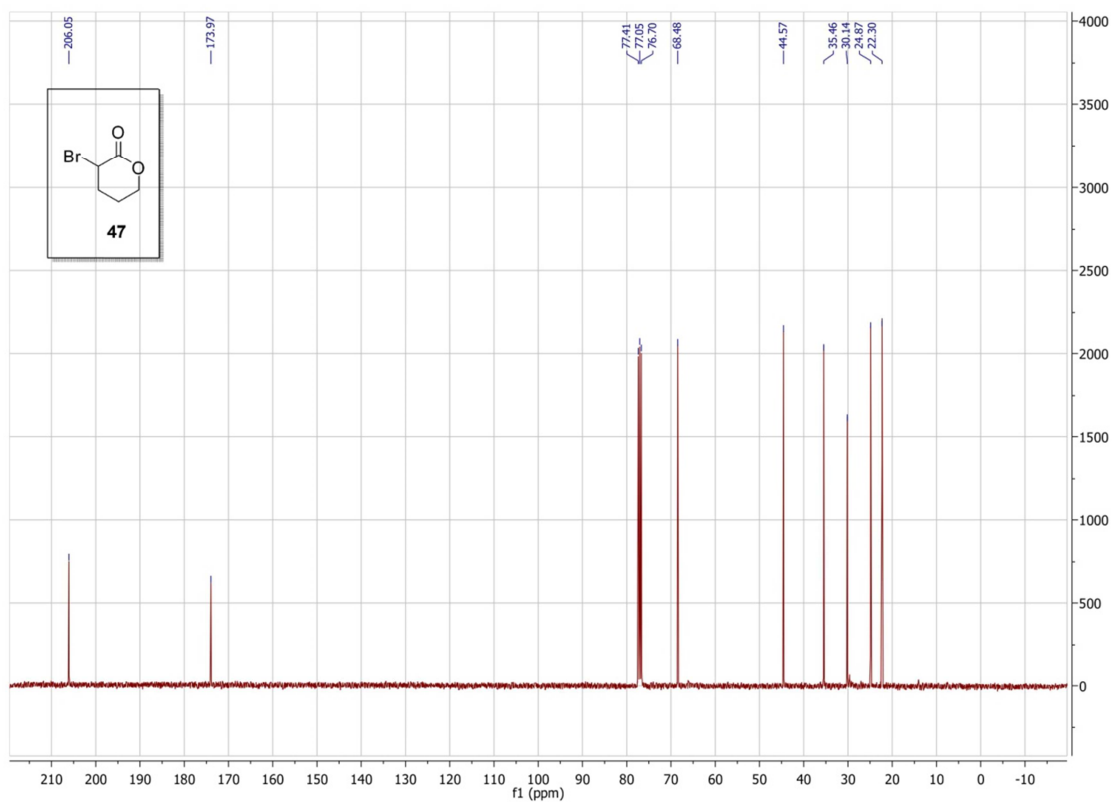
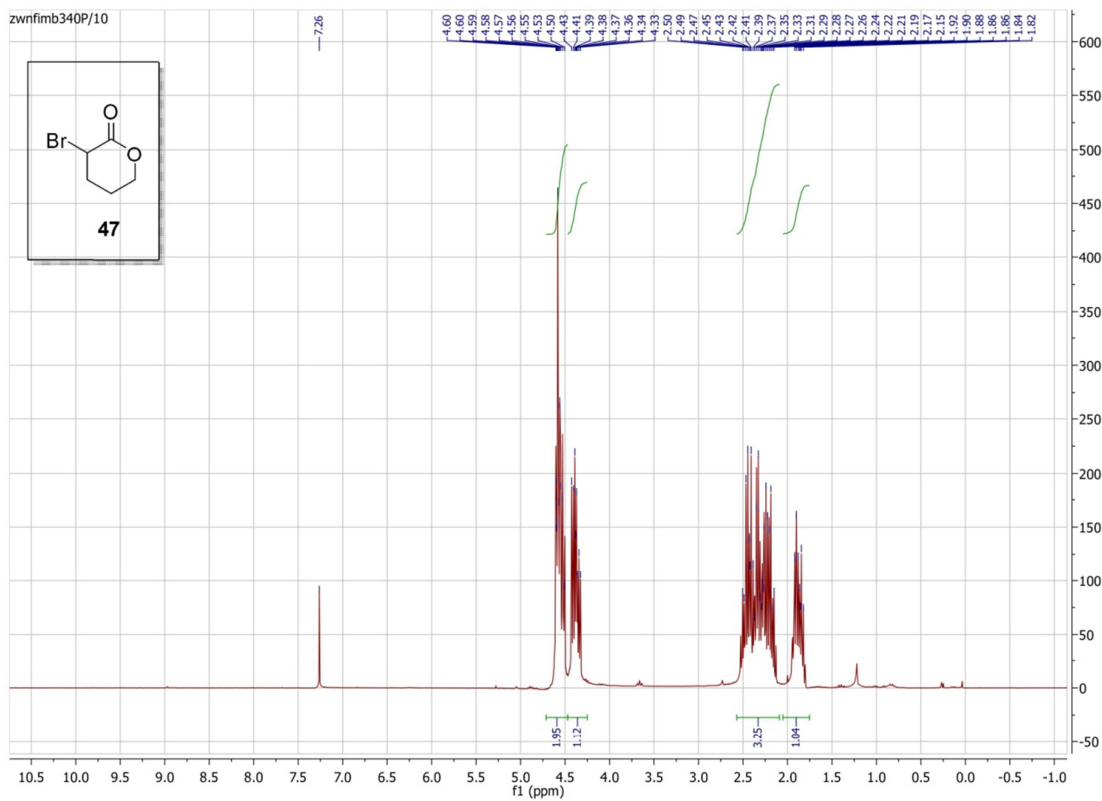
VI – APPENDICES



VI – APPENDICES

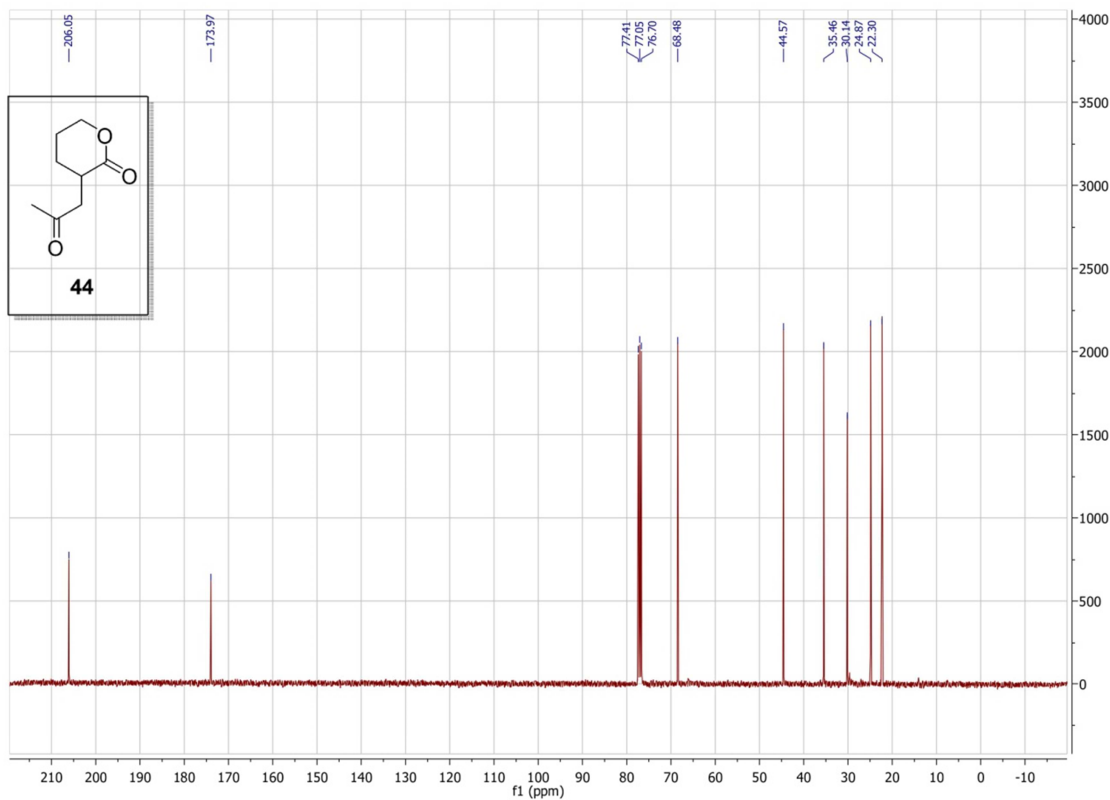
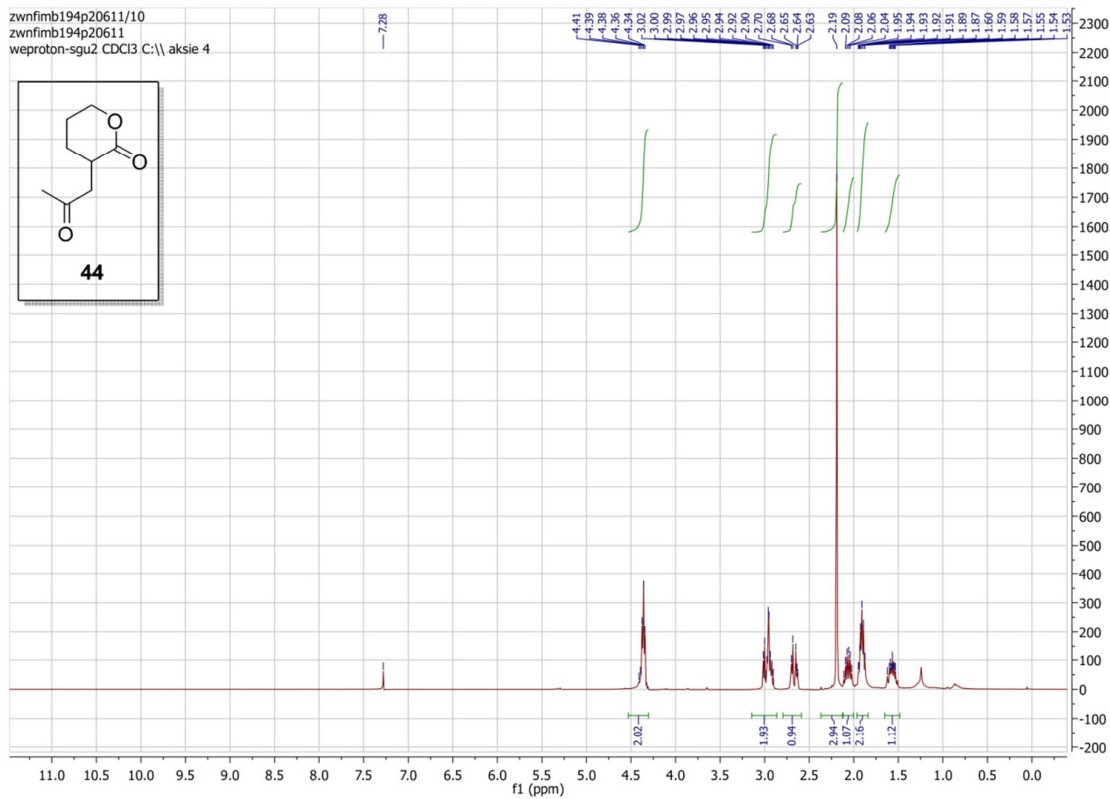
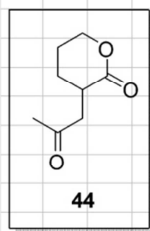


VI – APPENDICES

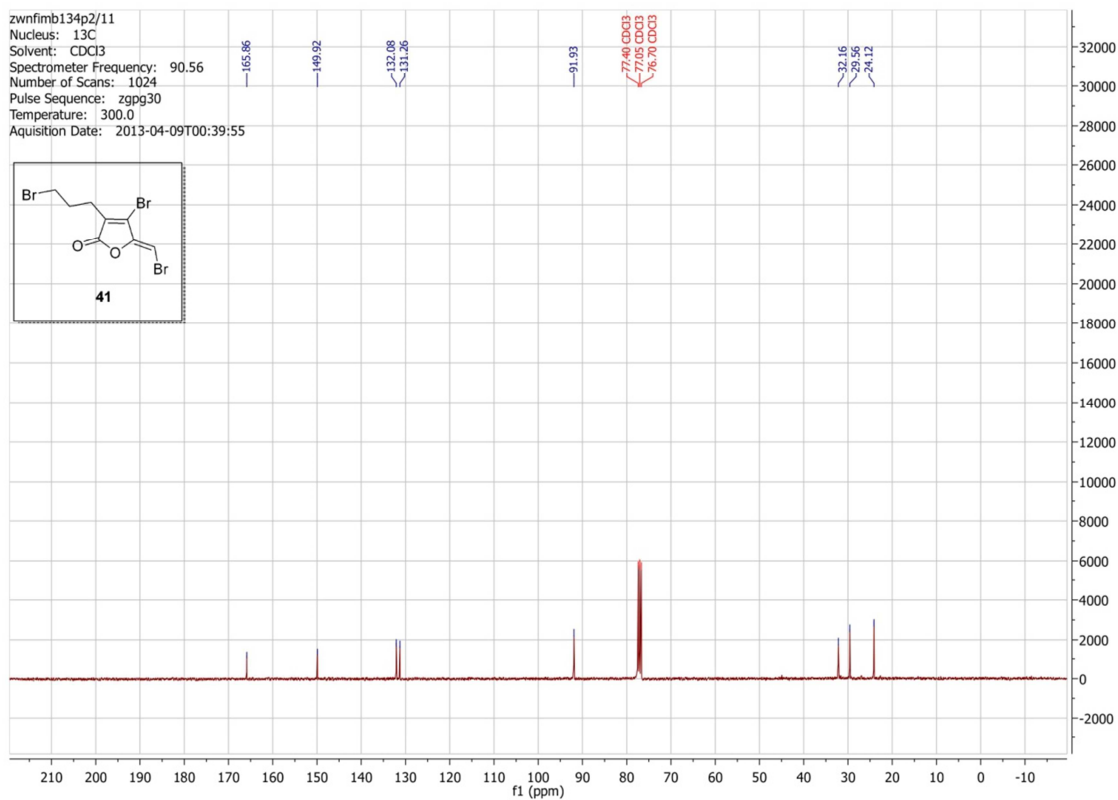
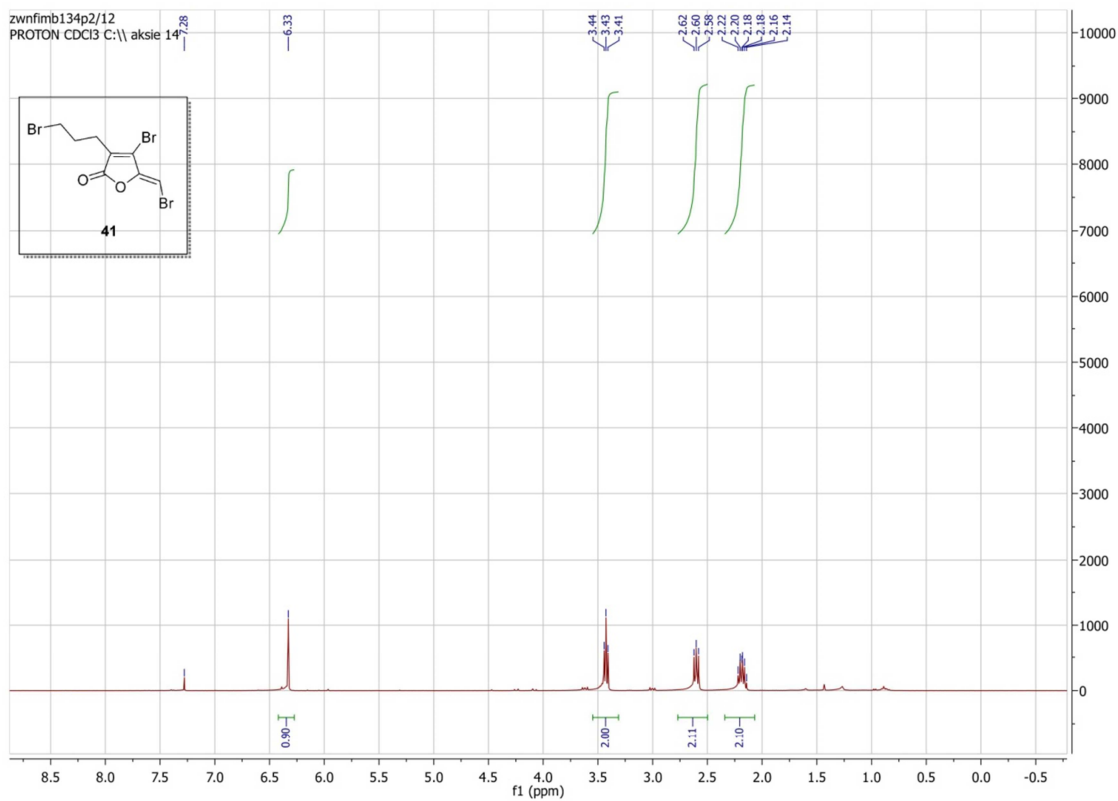


VI – APPENDICES

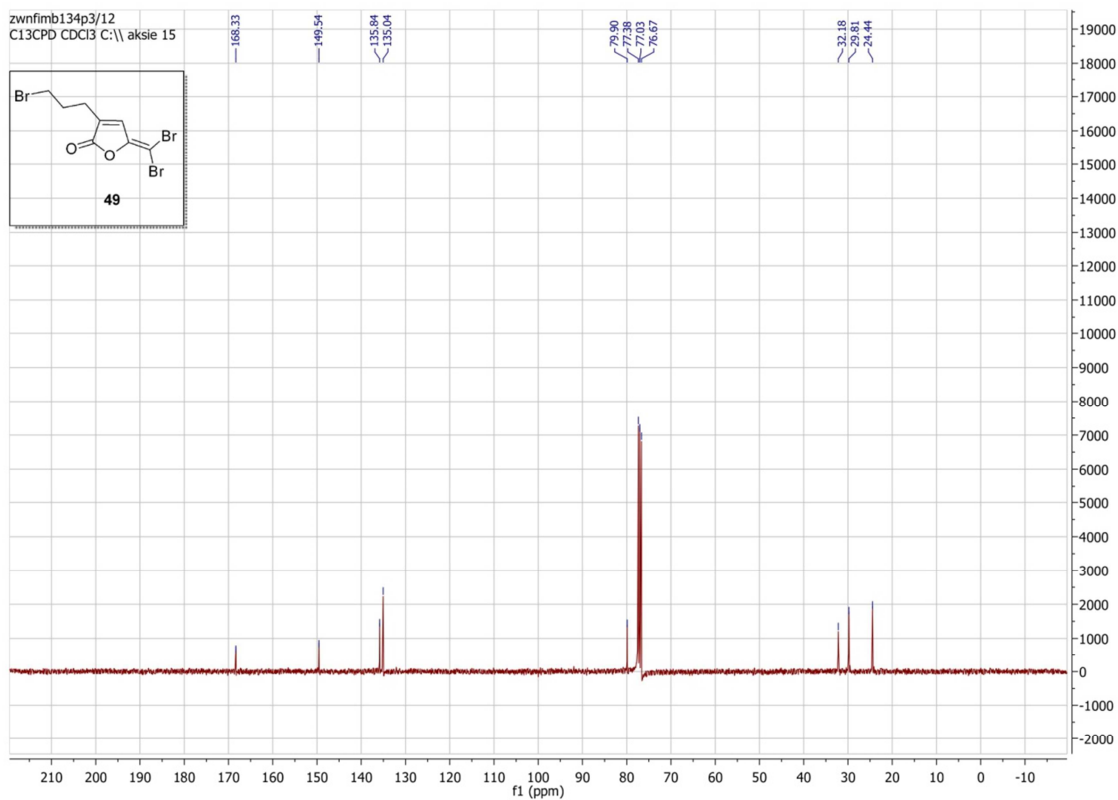
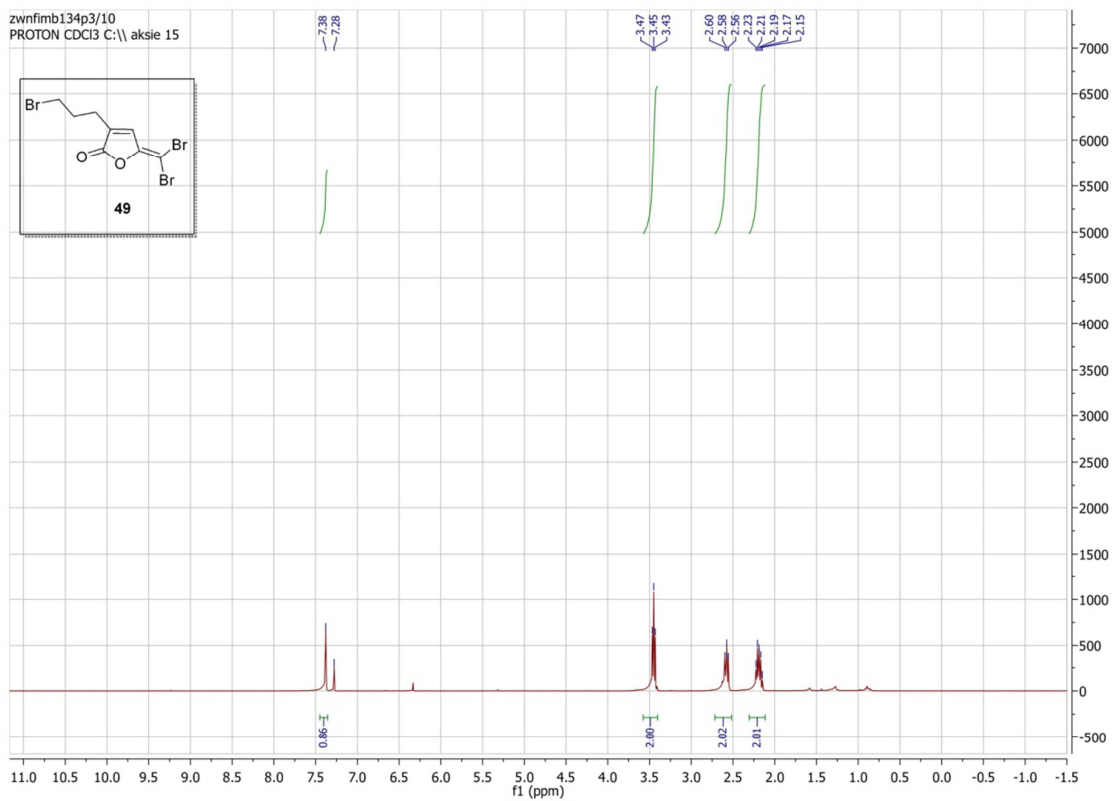
zwnfimb194p20611/10
zwnfimb194p20611
wepton-sgu2 CDCl3 C:\ aksie 4



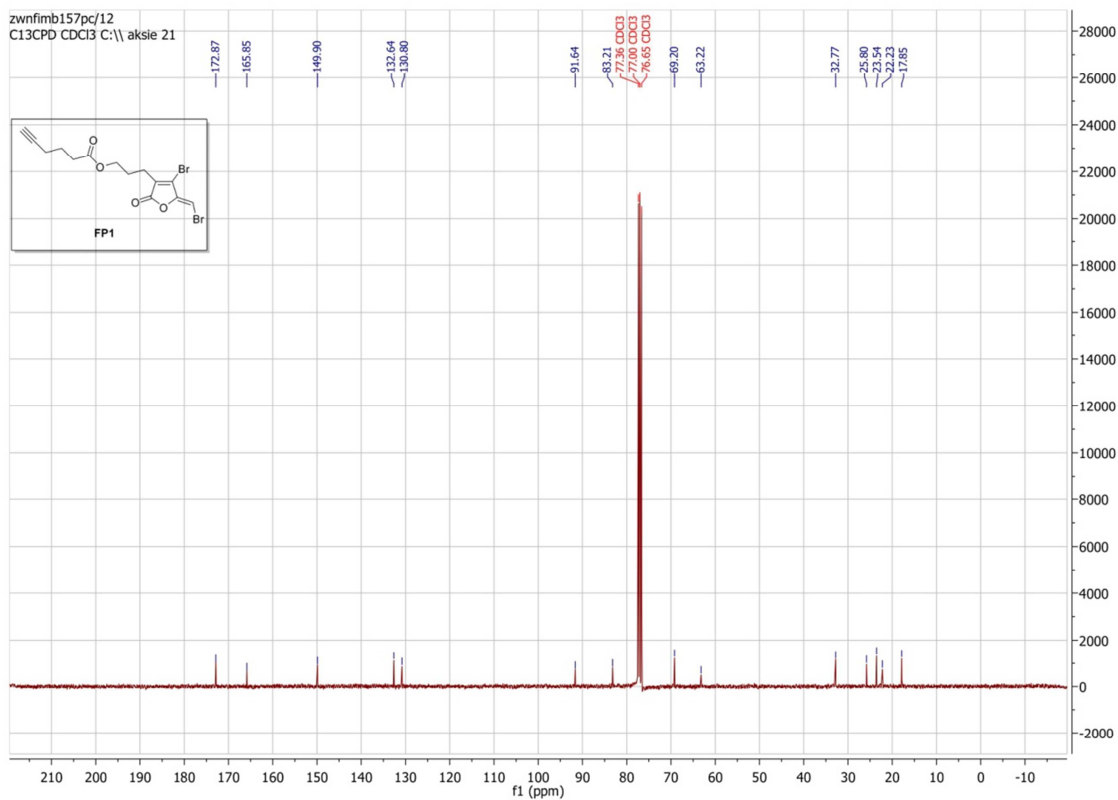
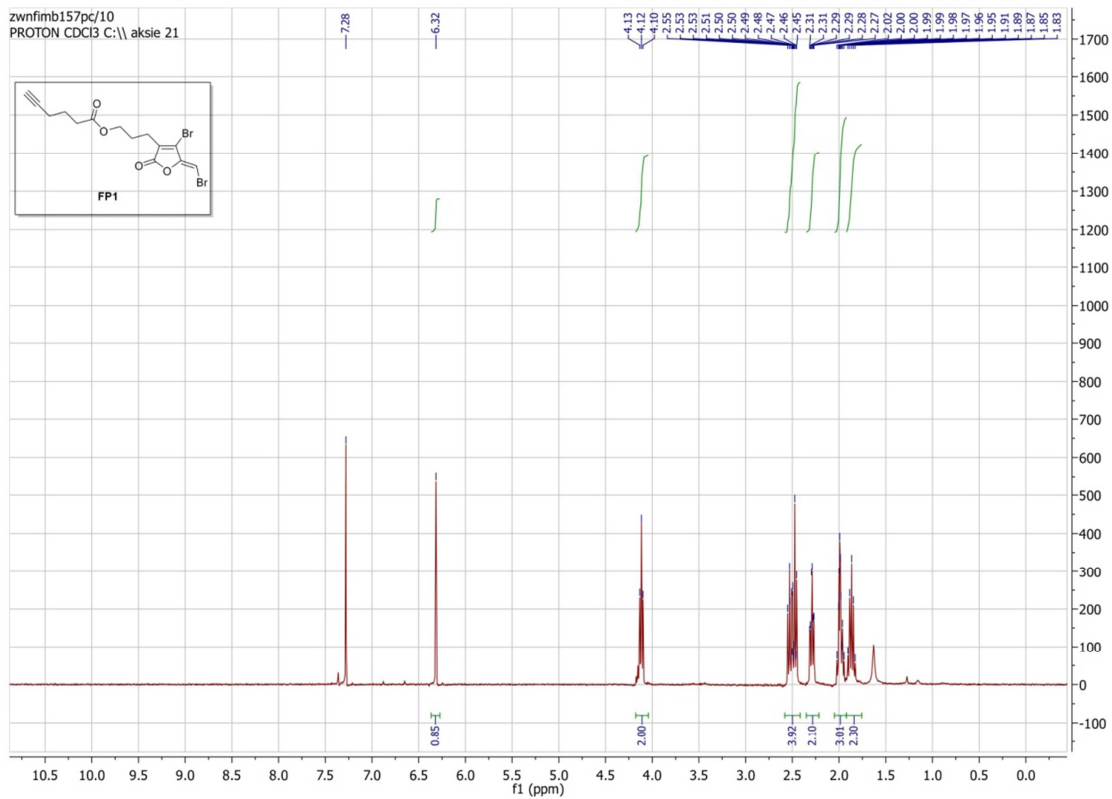
VI – APPENDICES



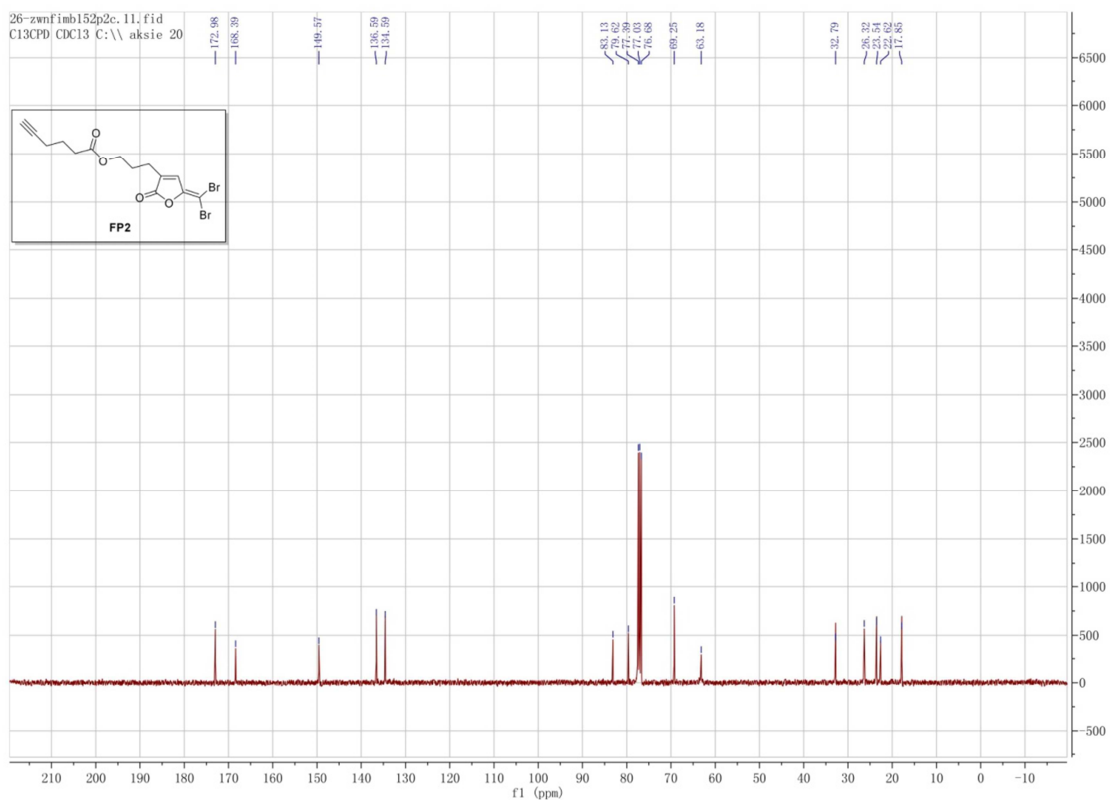
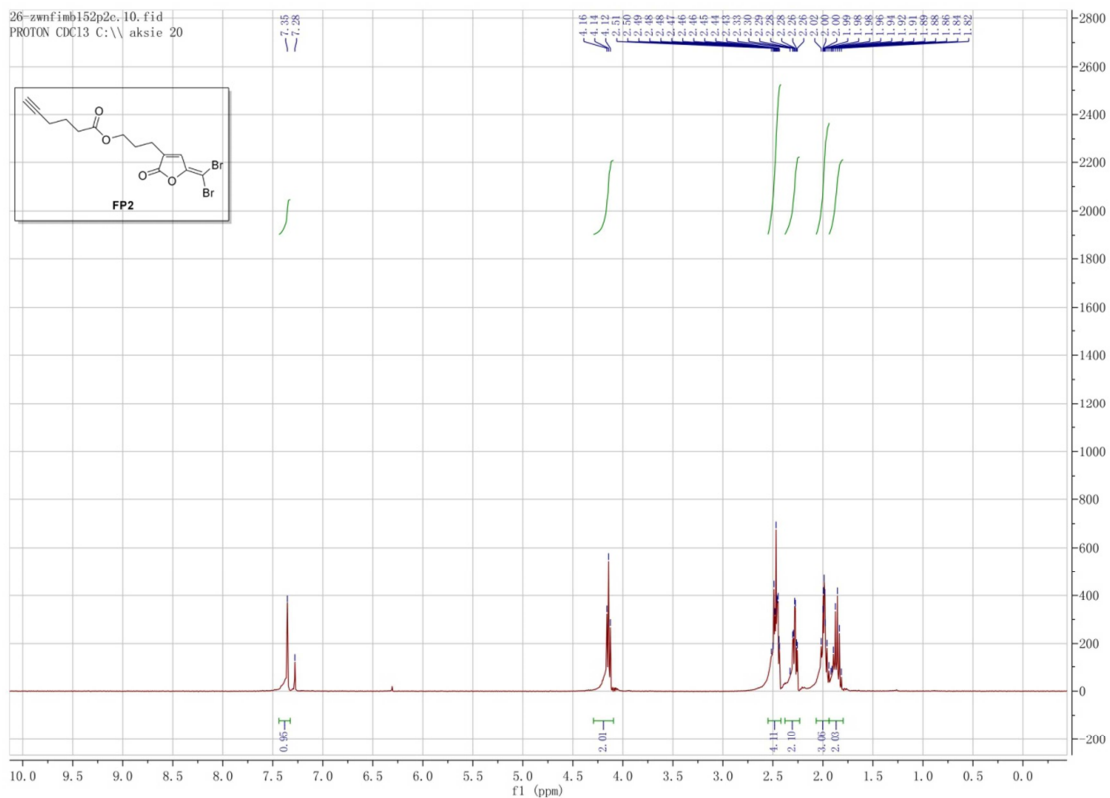
VI – APPENDICES



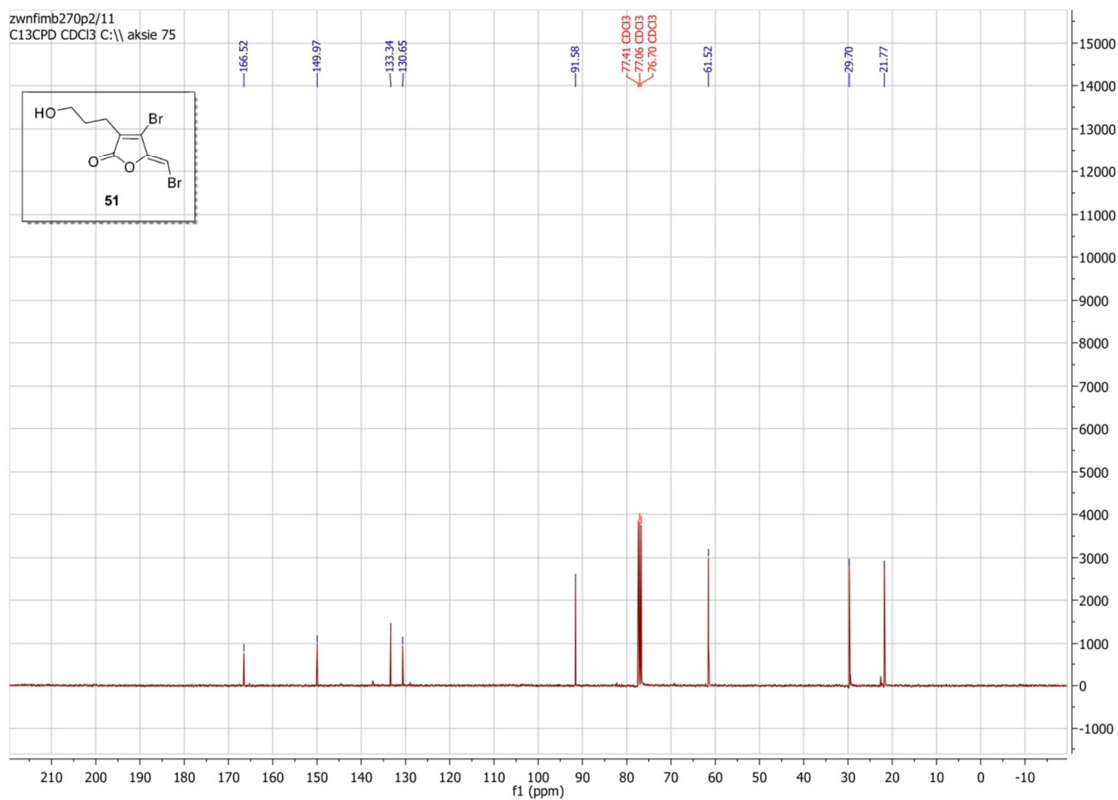
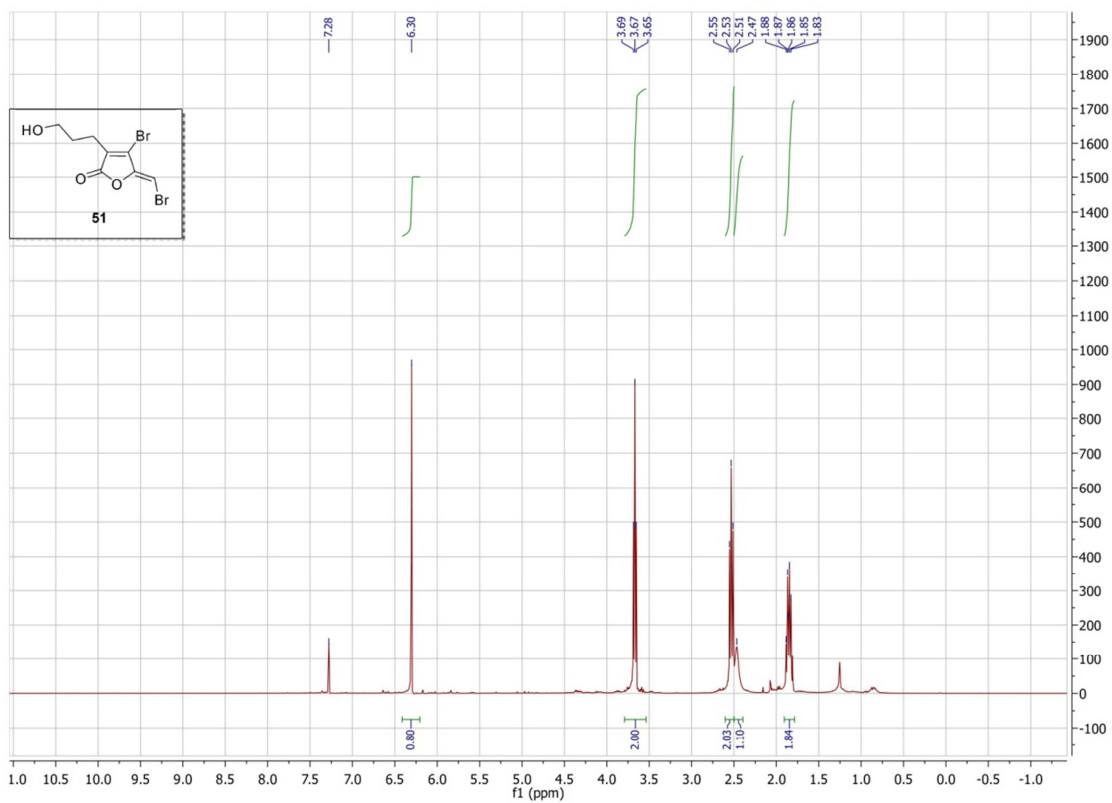
VI – APPENDICES



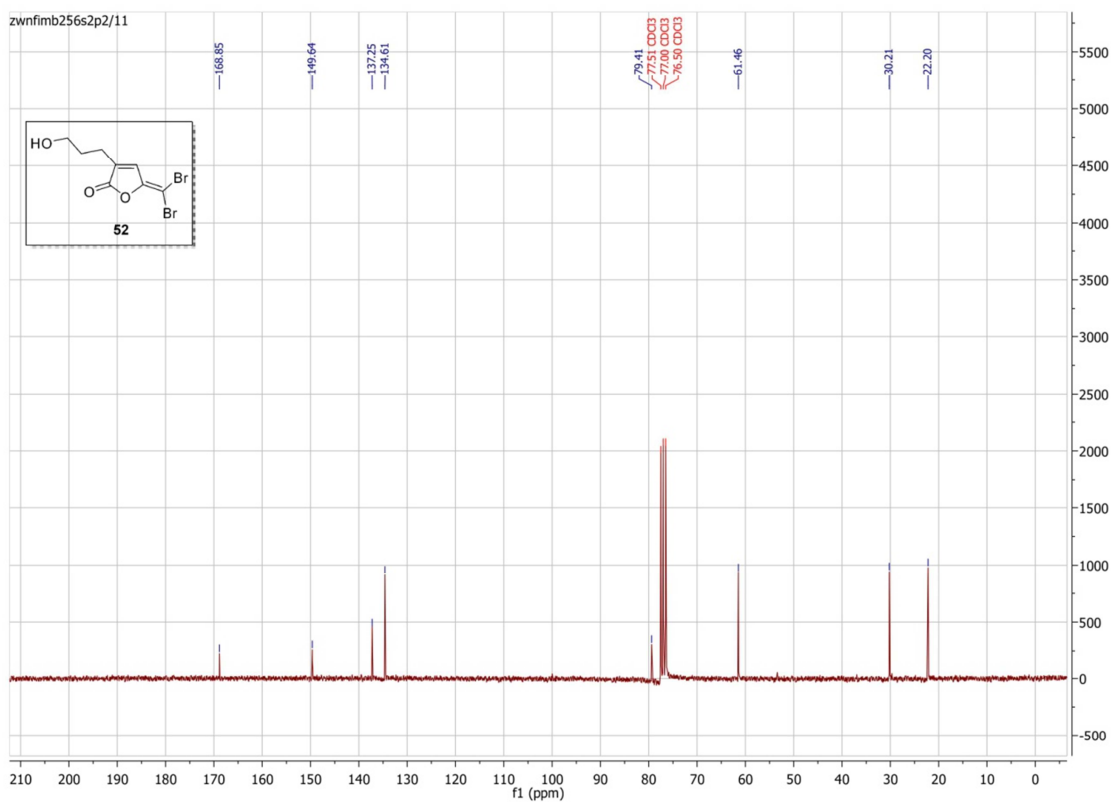
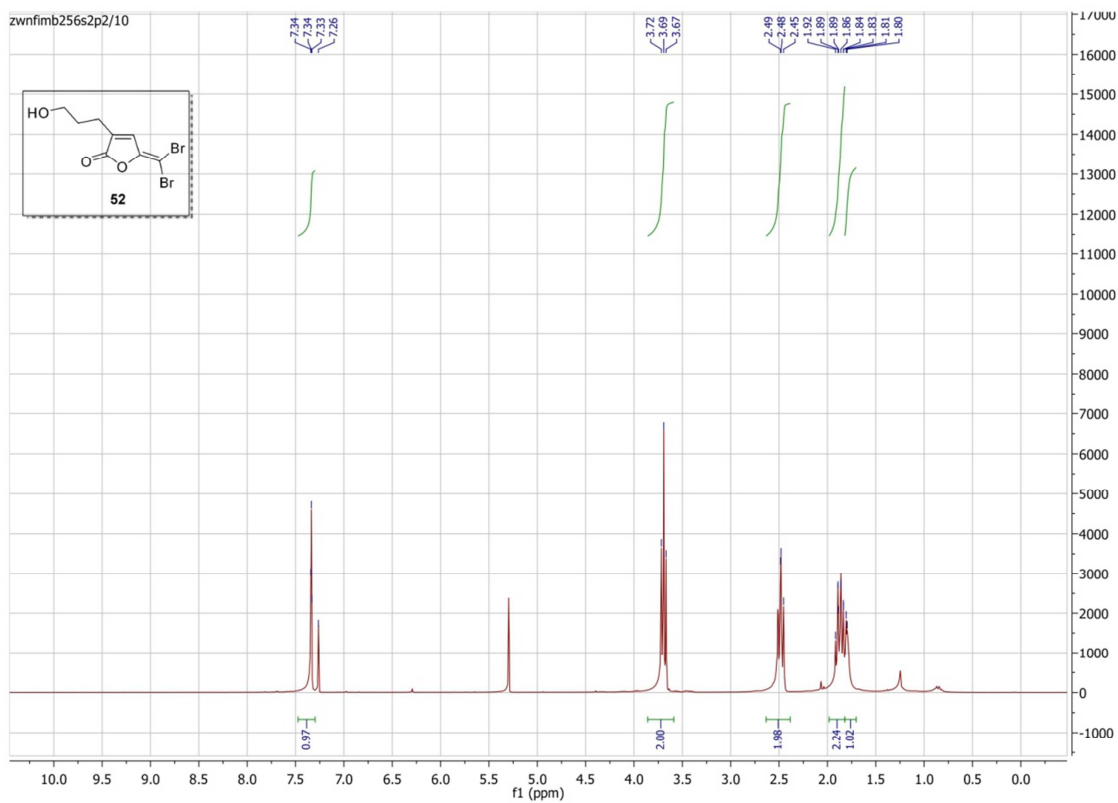
VI – APPENDICES



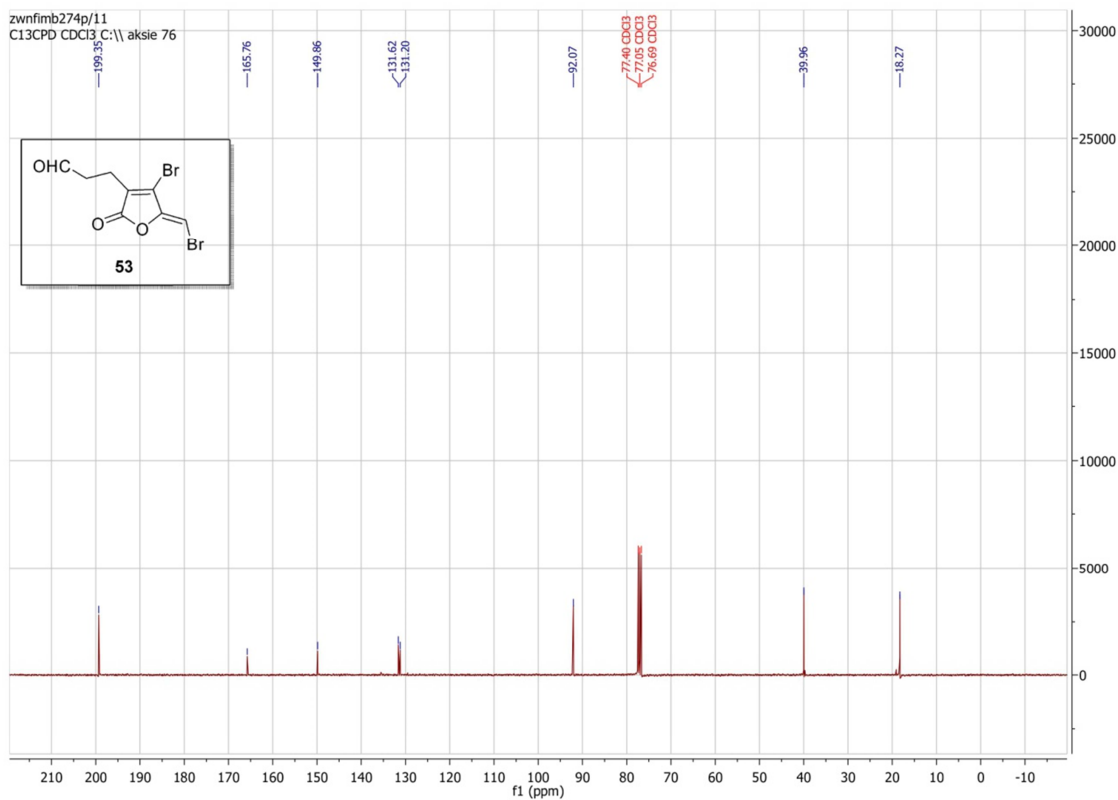
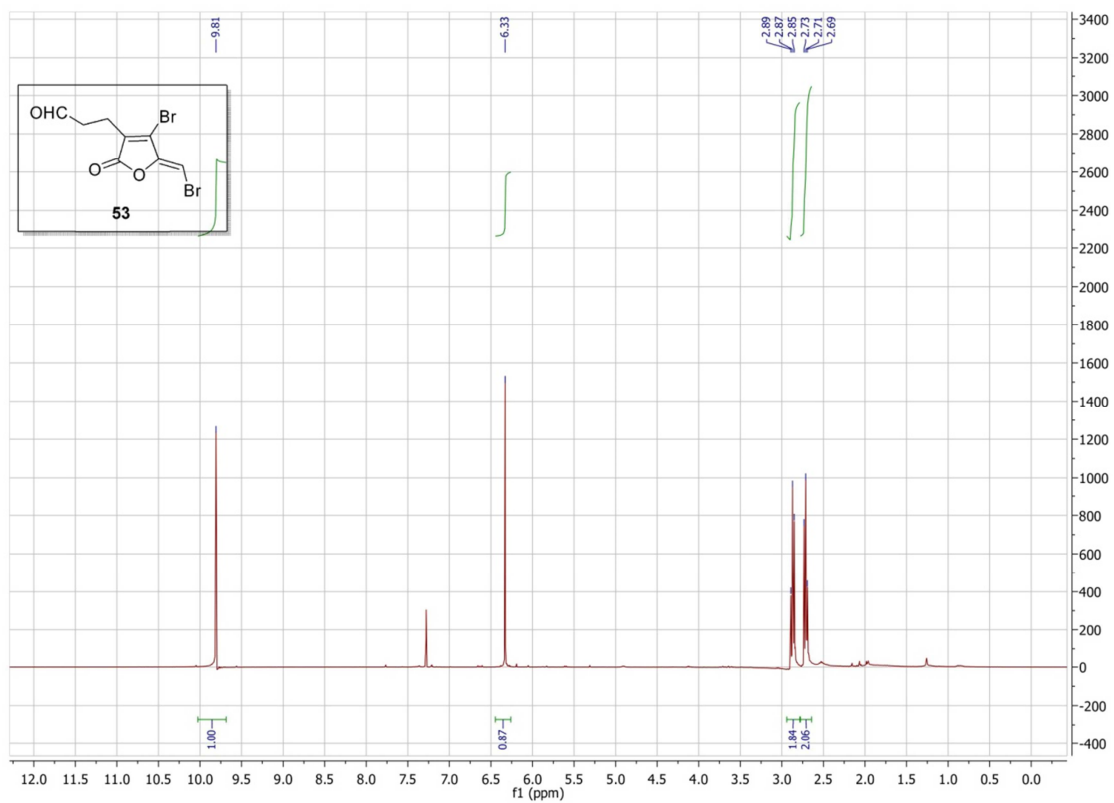
VI – APPENDICES



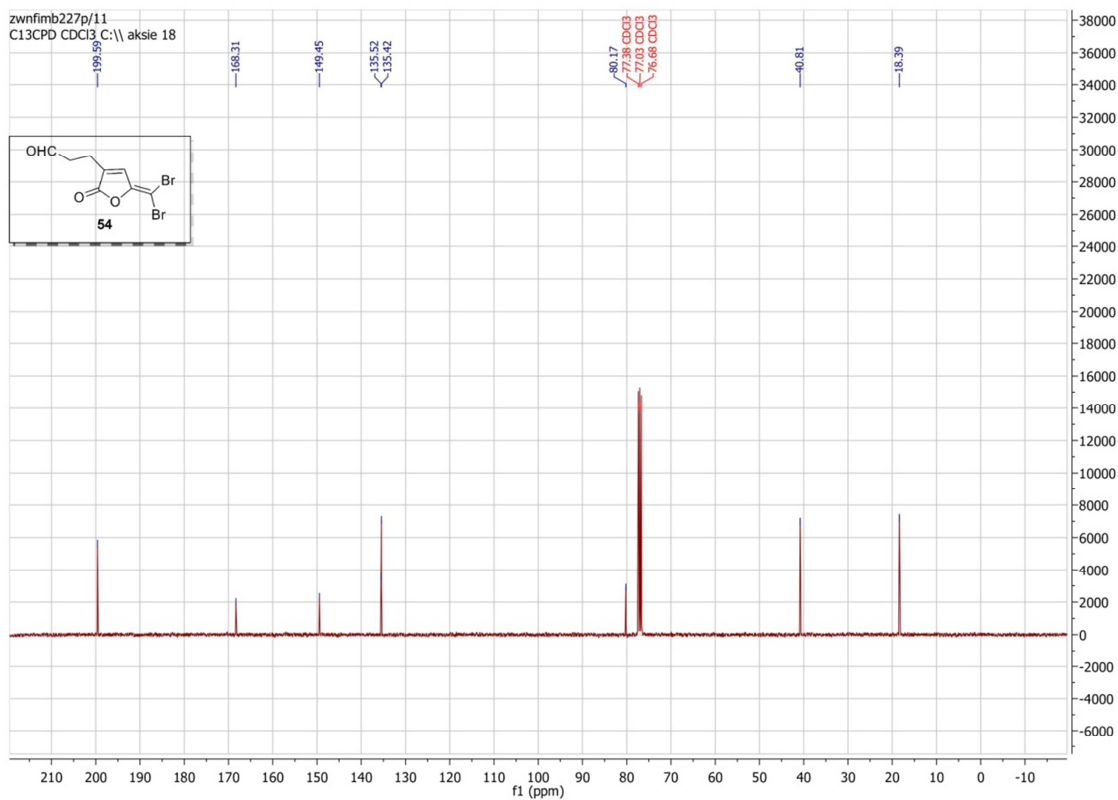
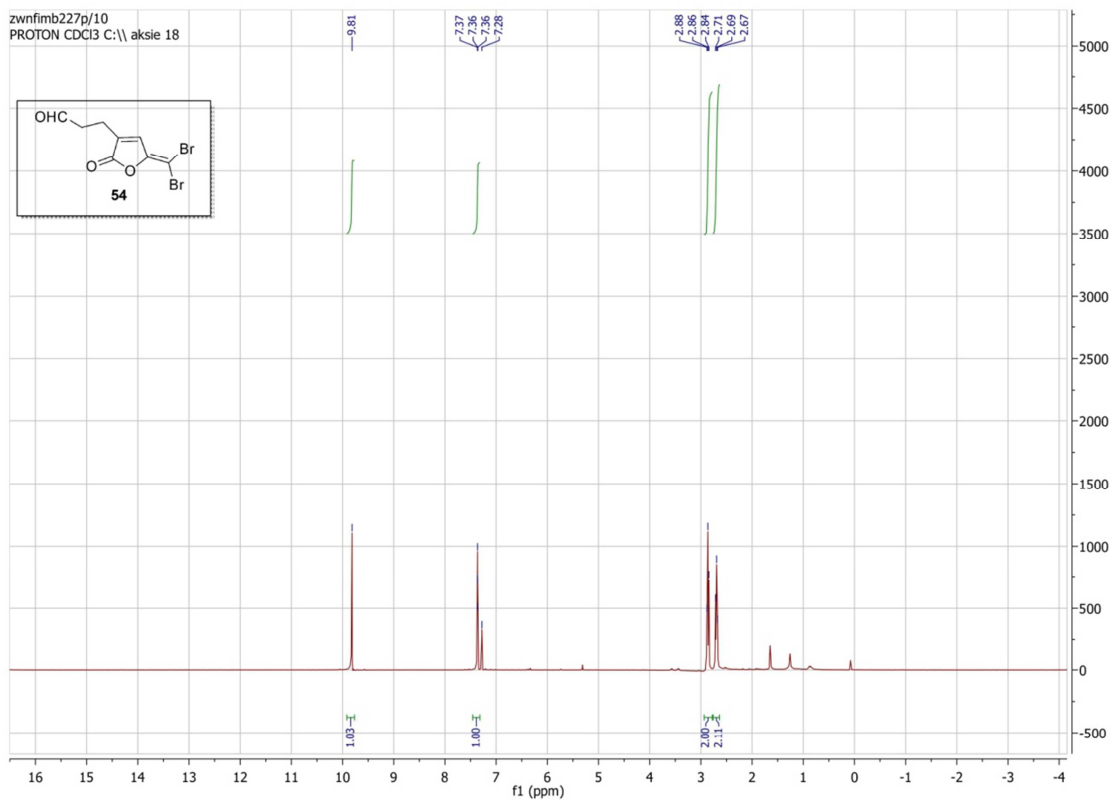
VI – APPENDICES



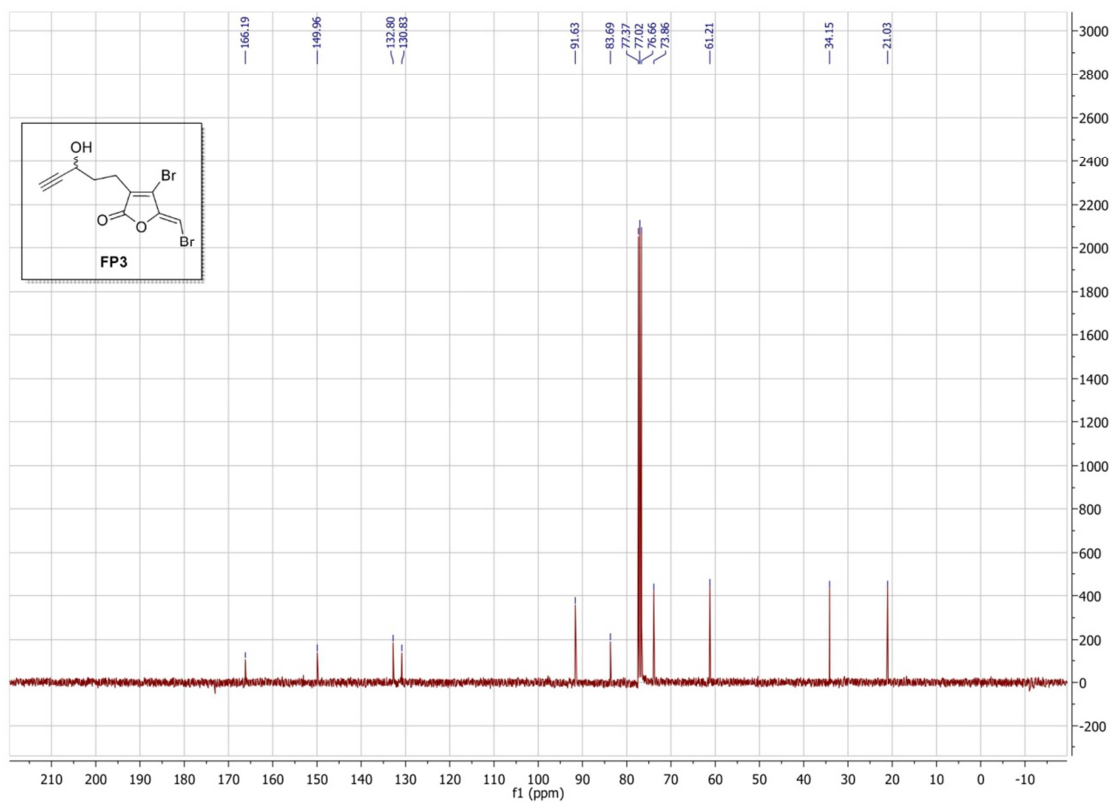
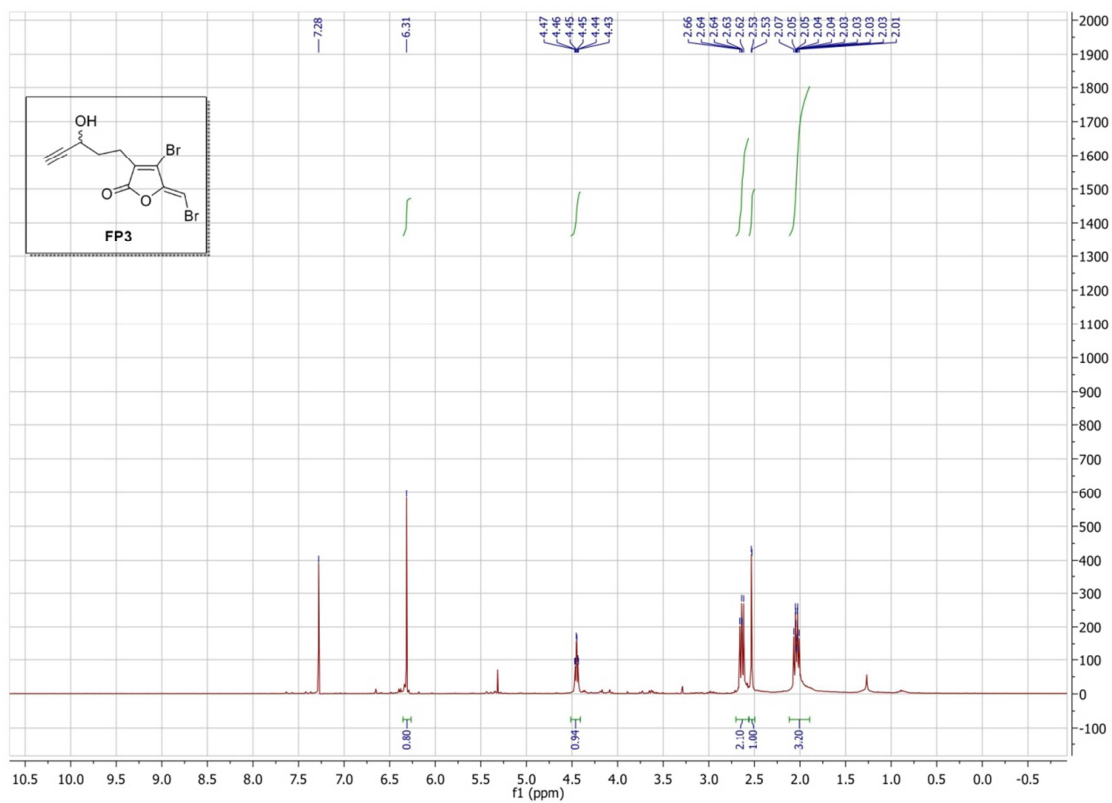
VI – APPENDICES



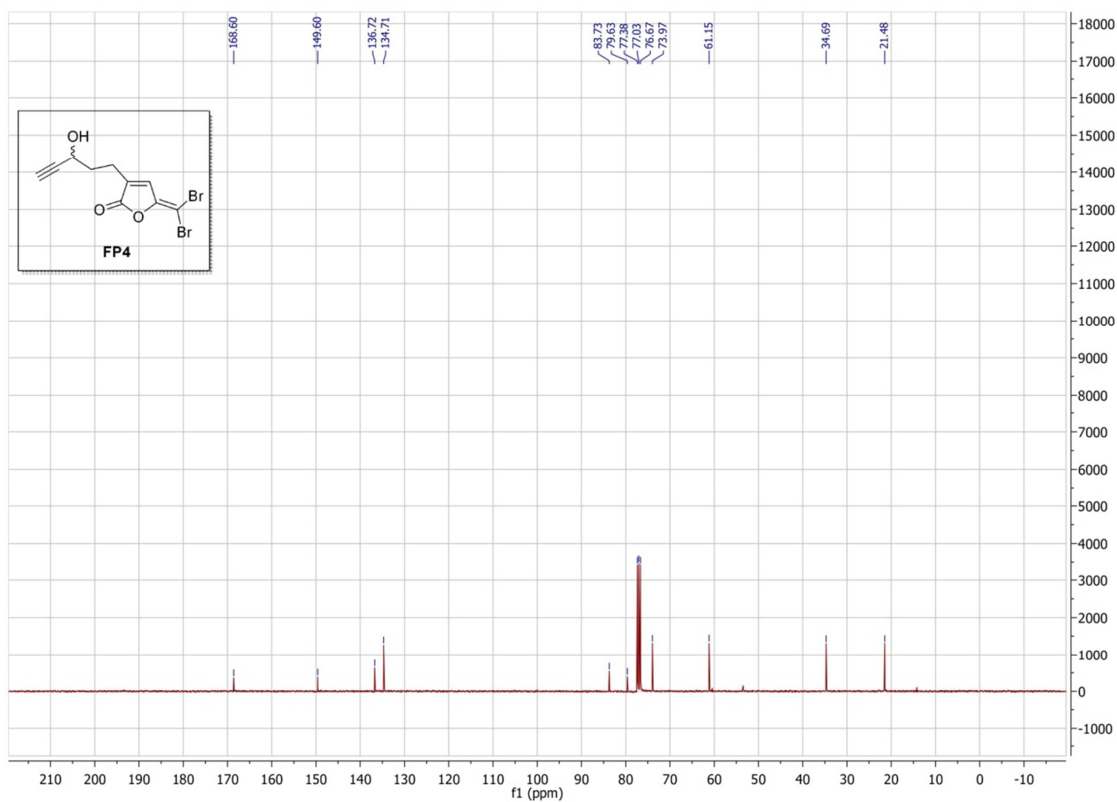
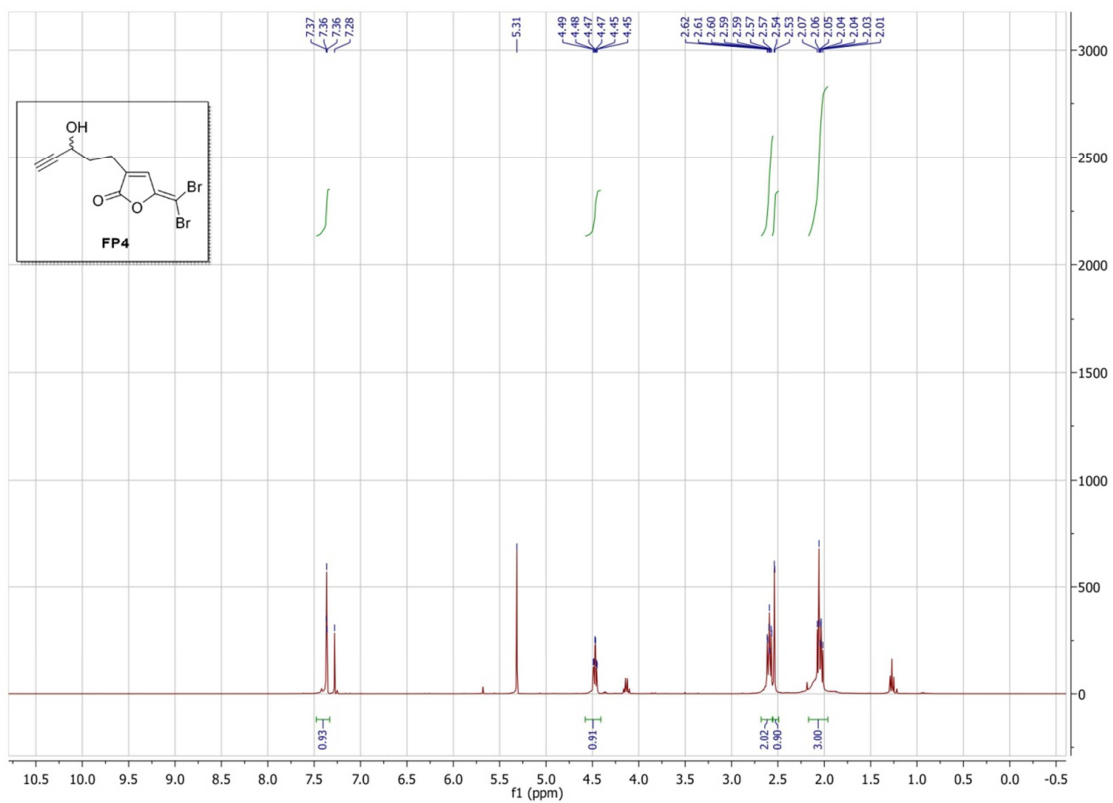
VI – APPENDICES



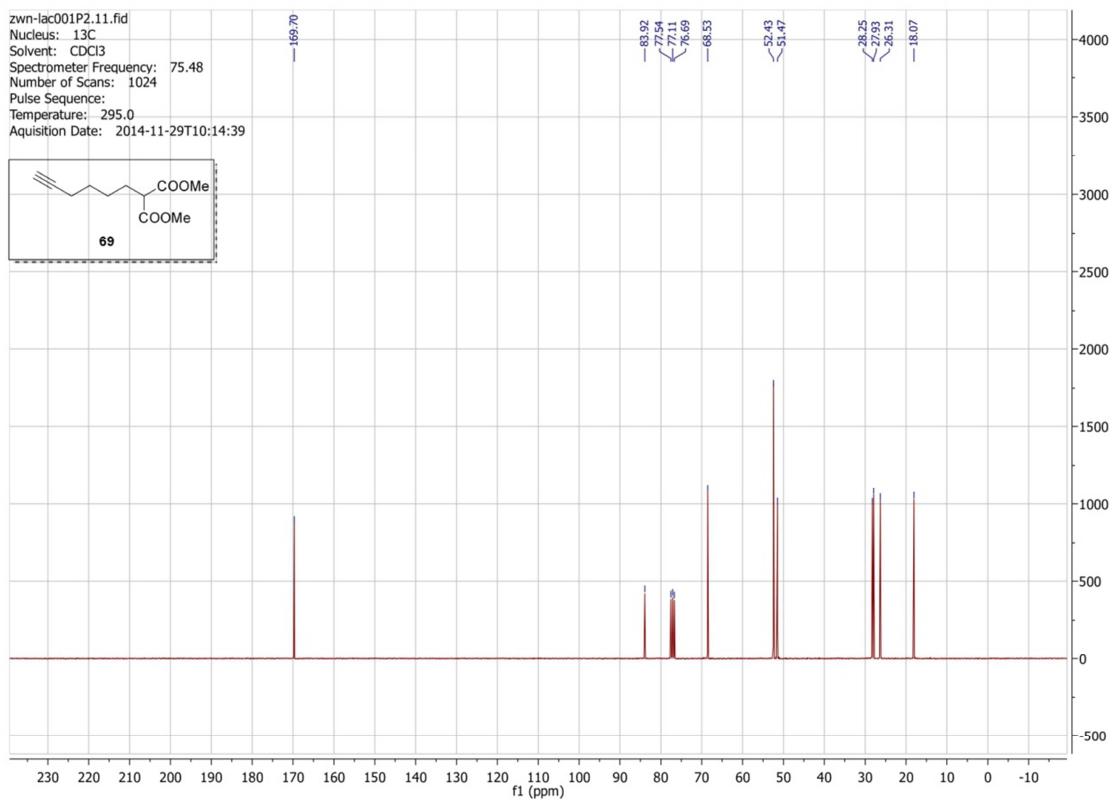
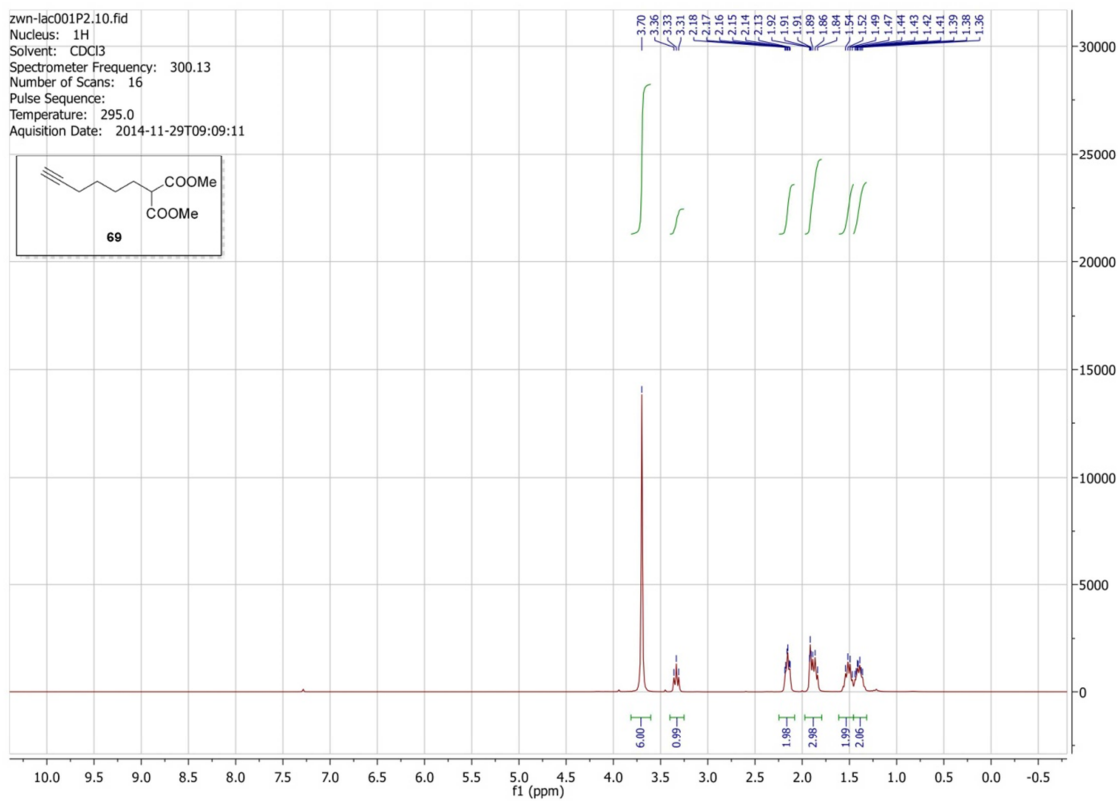
VI – APPENDICES



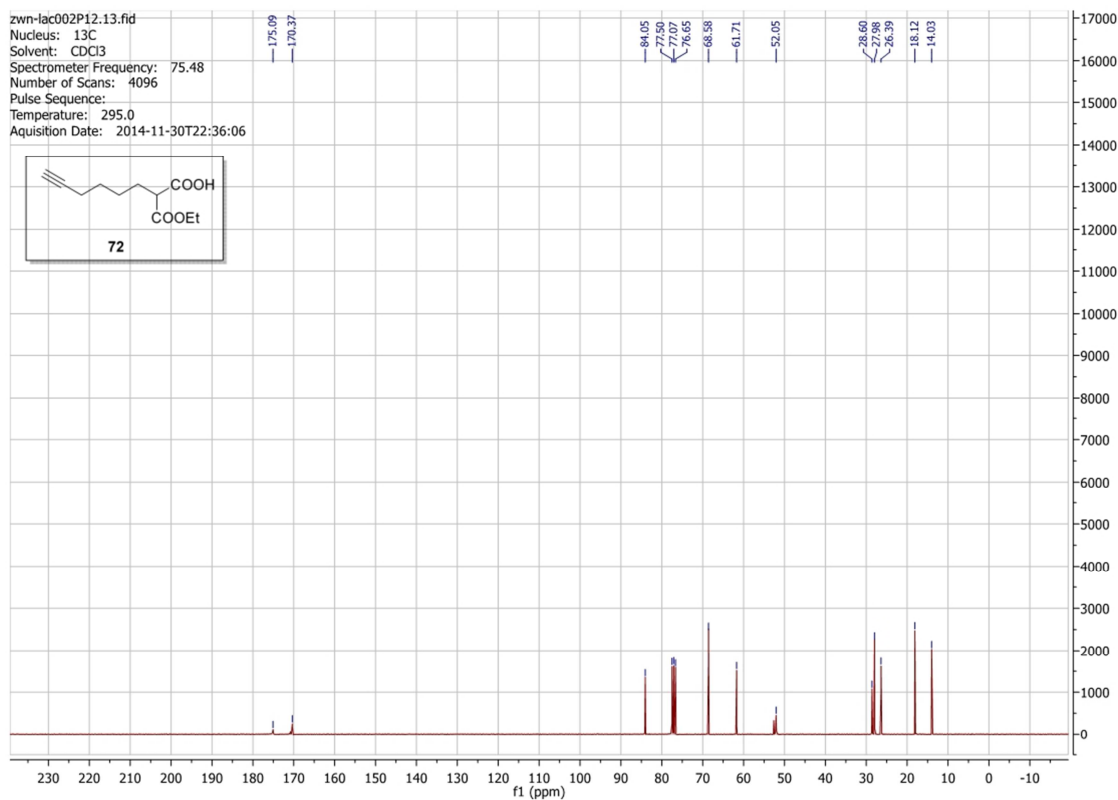
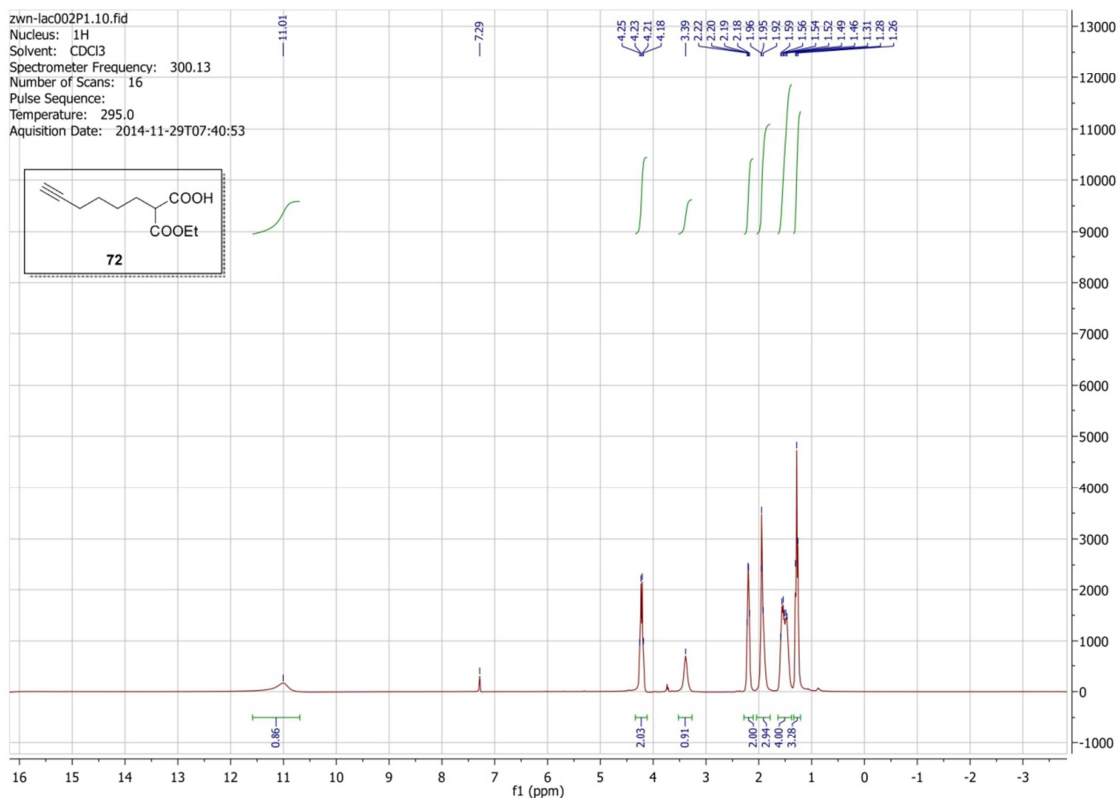
VI – APPENDICES



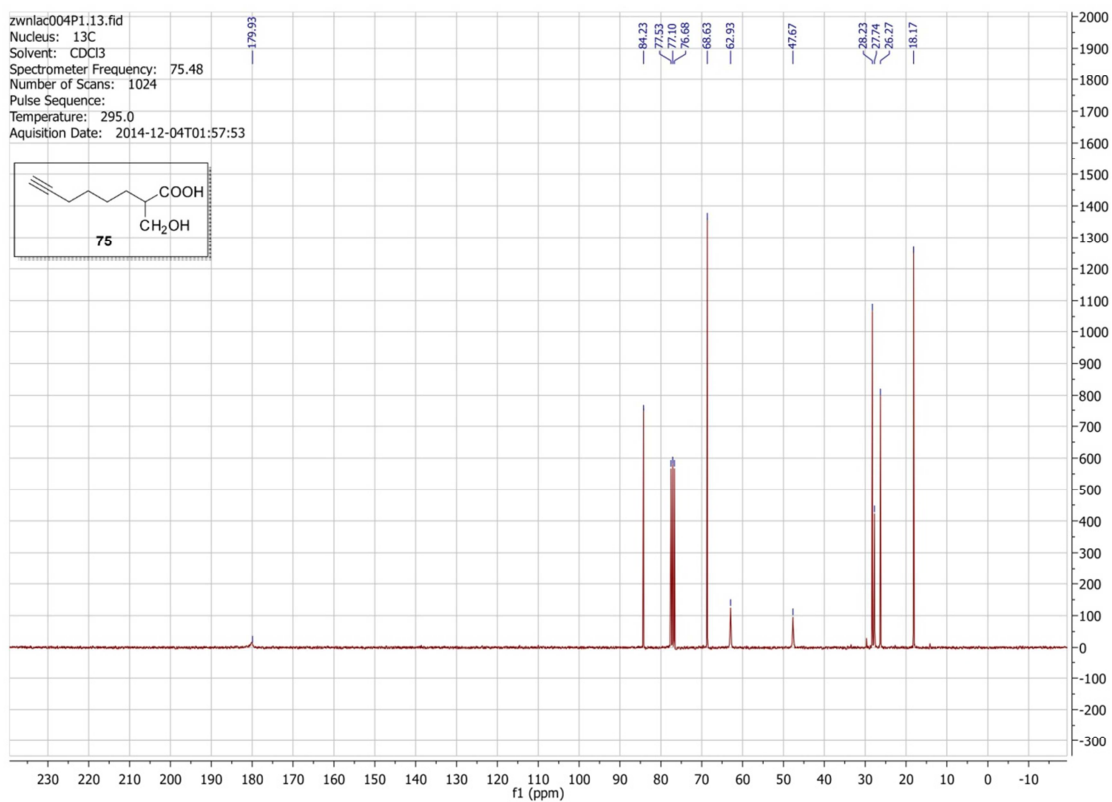
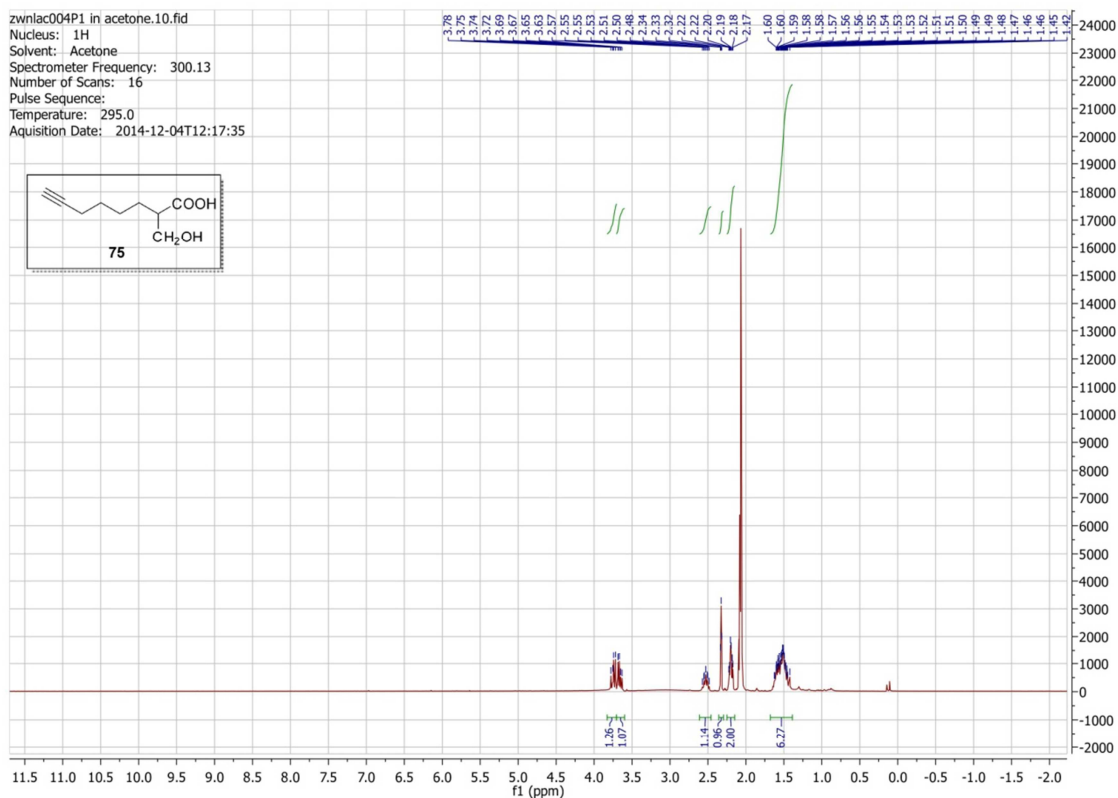
VI – APPENDICES



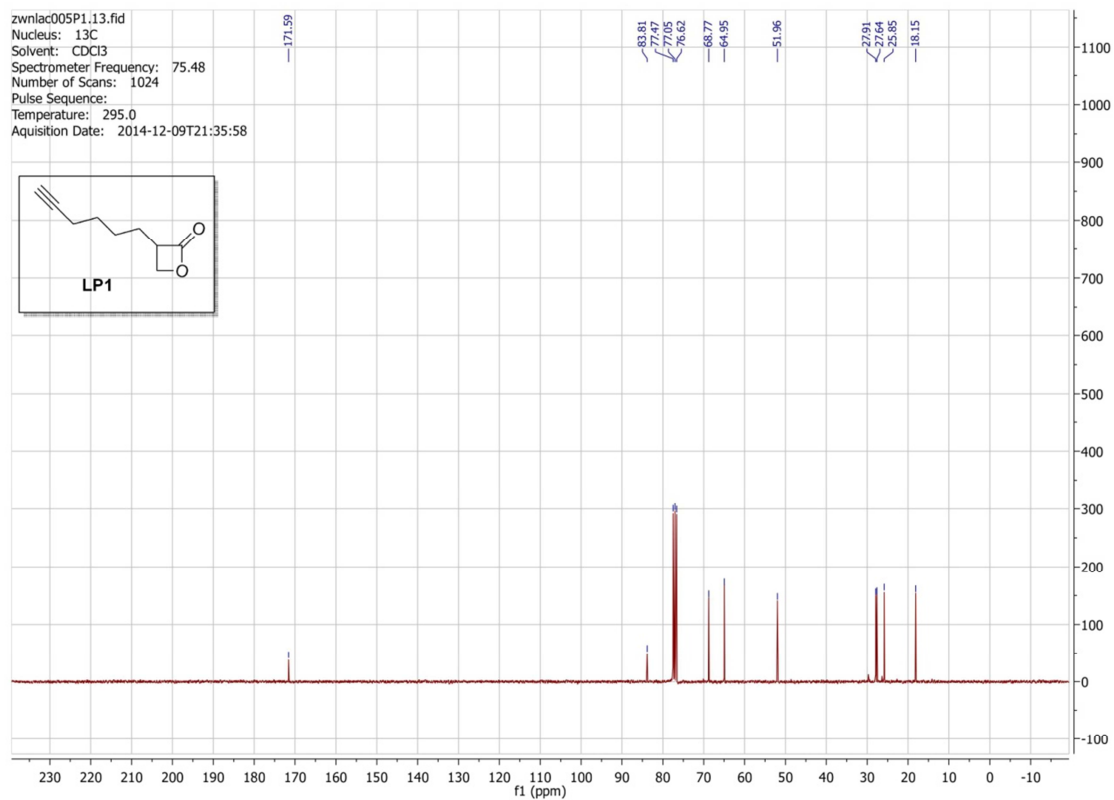
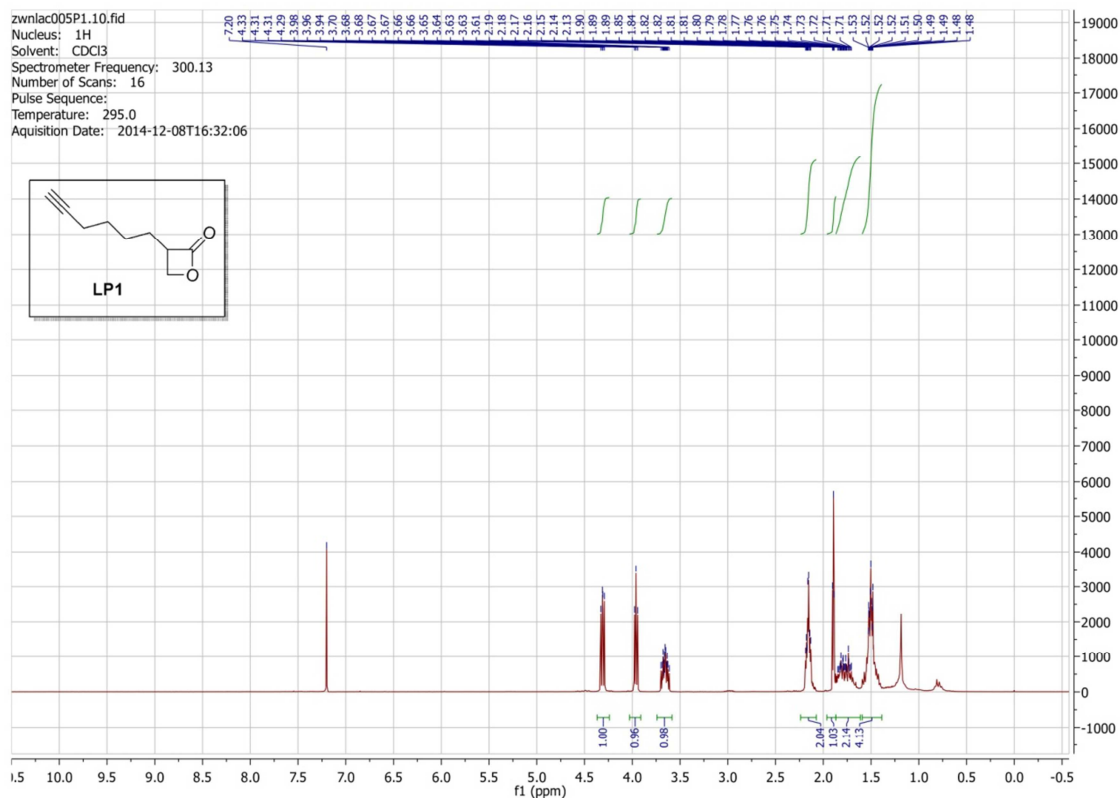
VI – APPENDICES



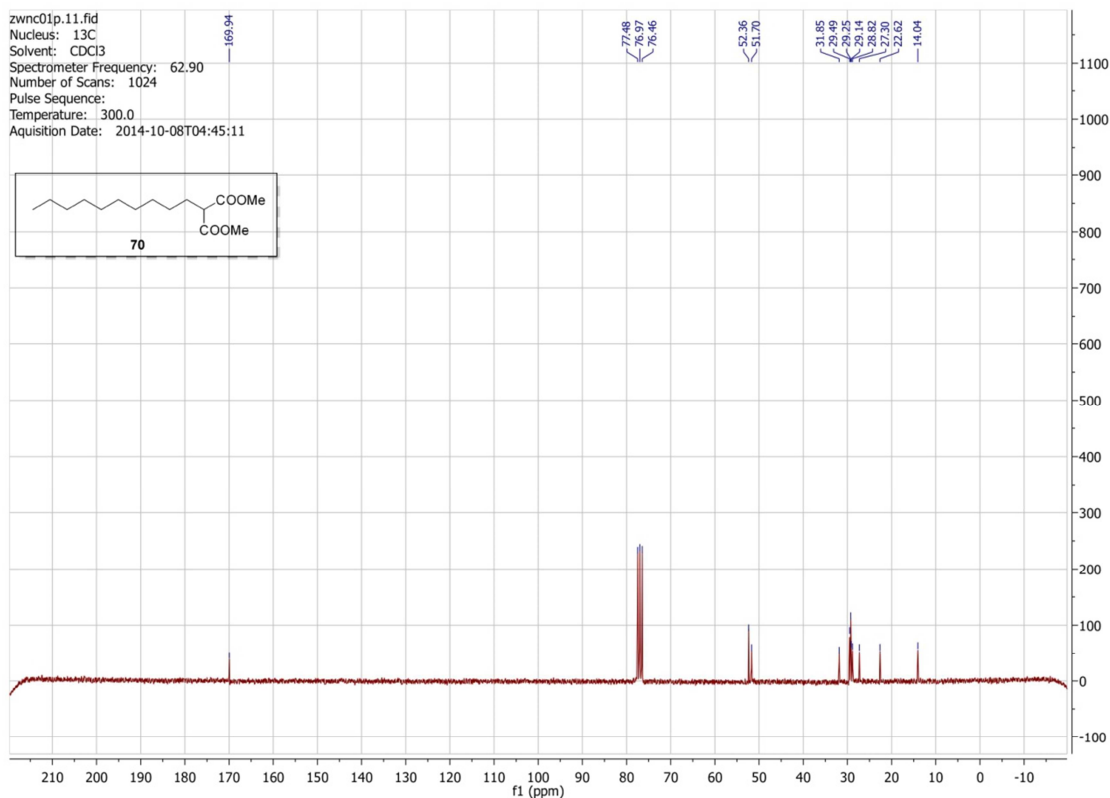
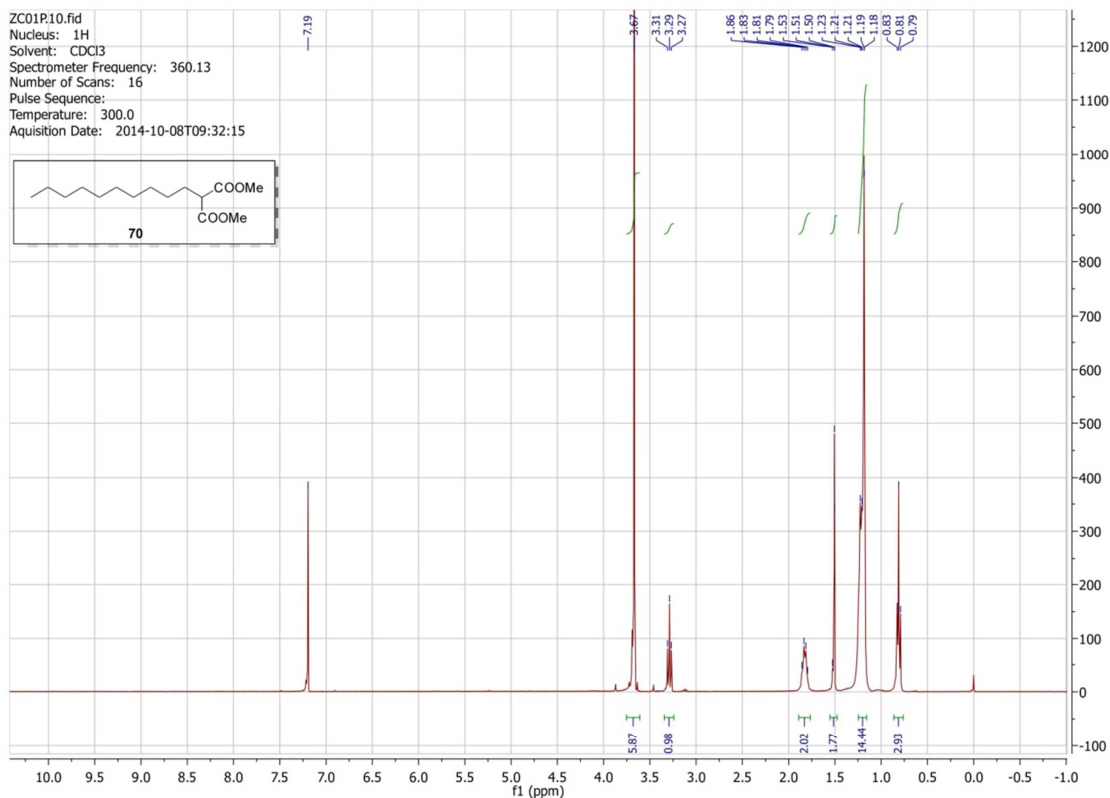
VI – APPENDICES



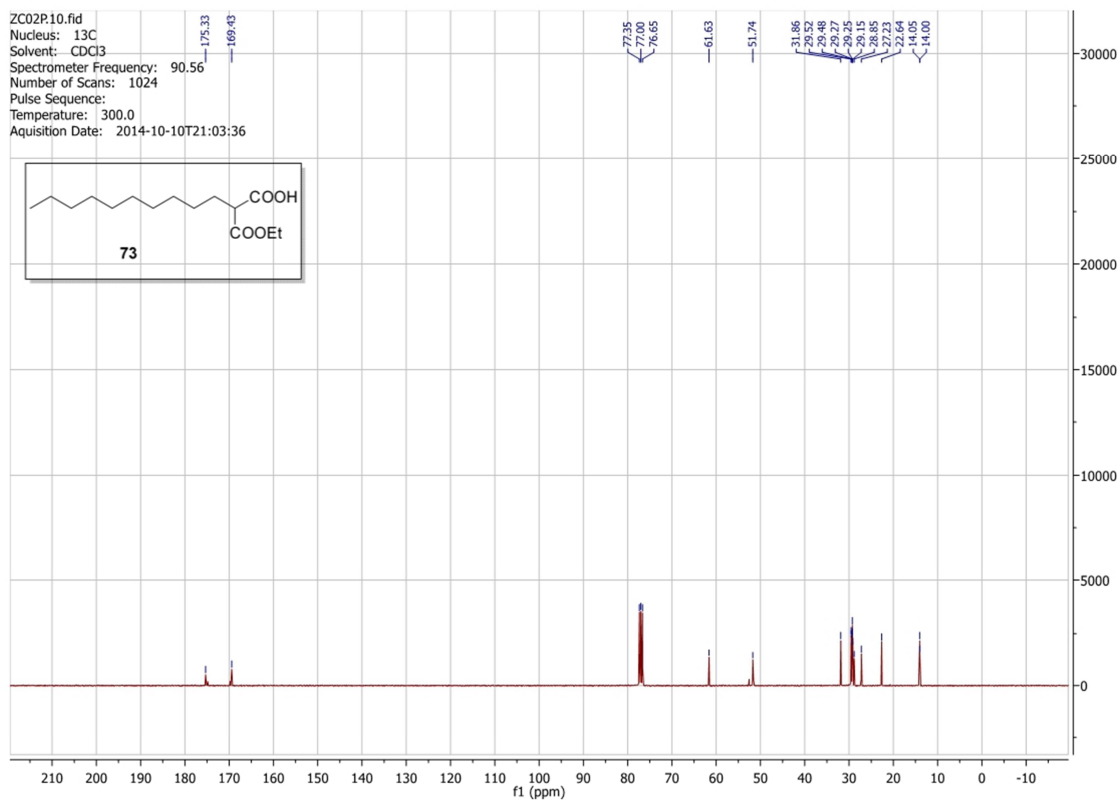
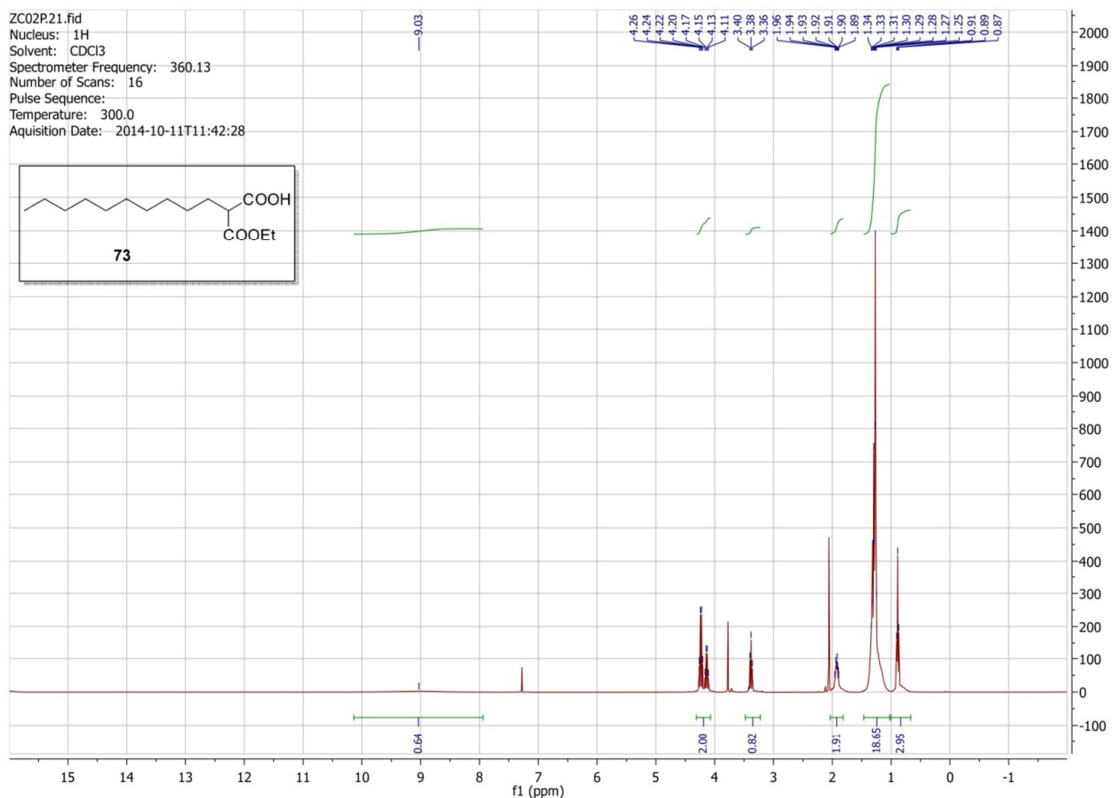
VI – APPENDICES



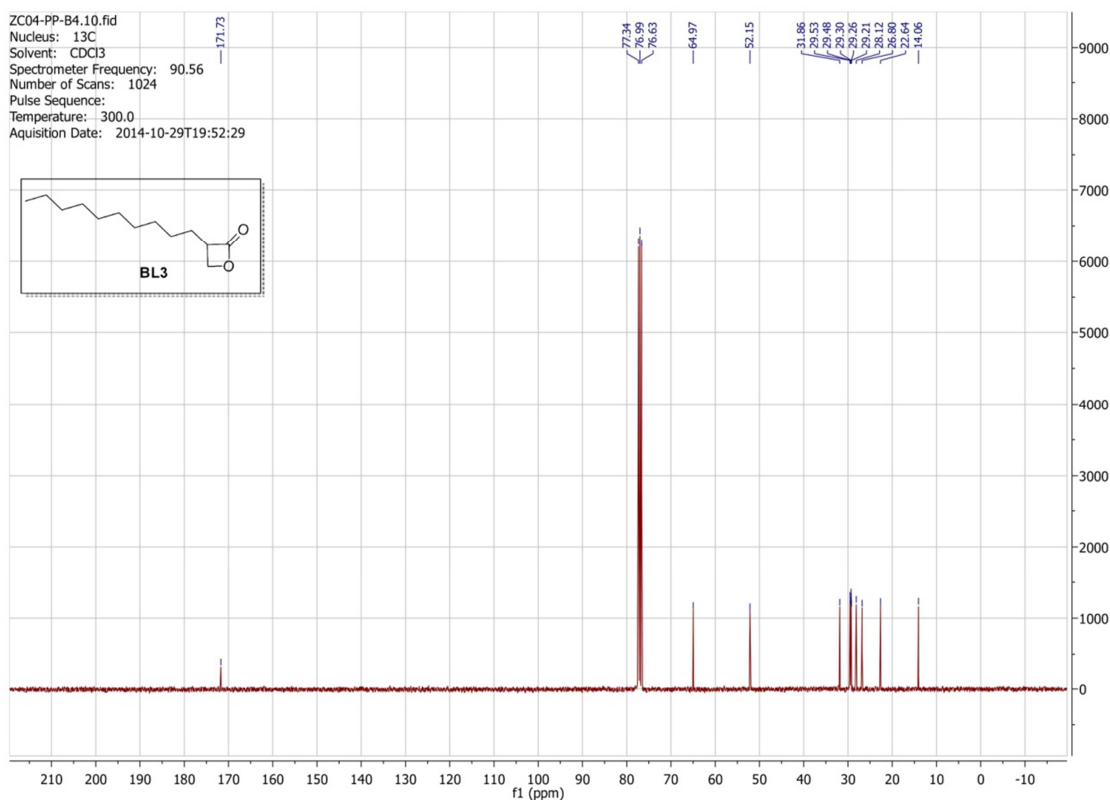
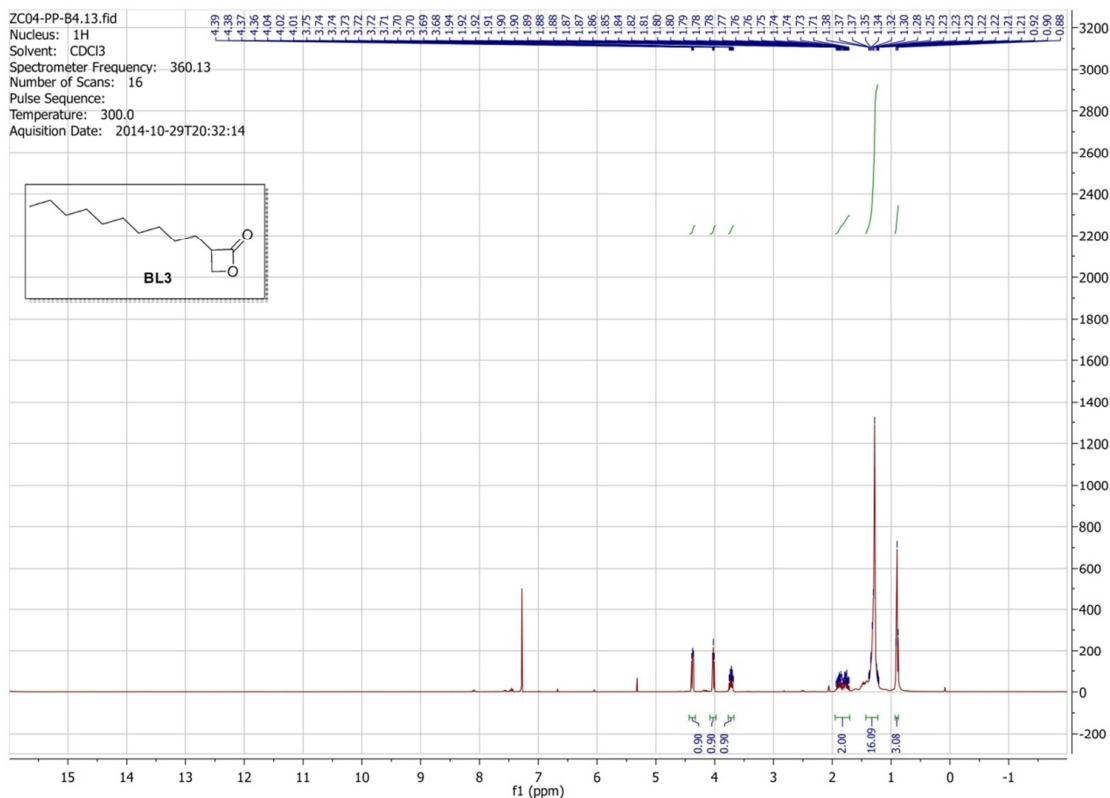
VI – APPENDICES



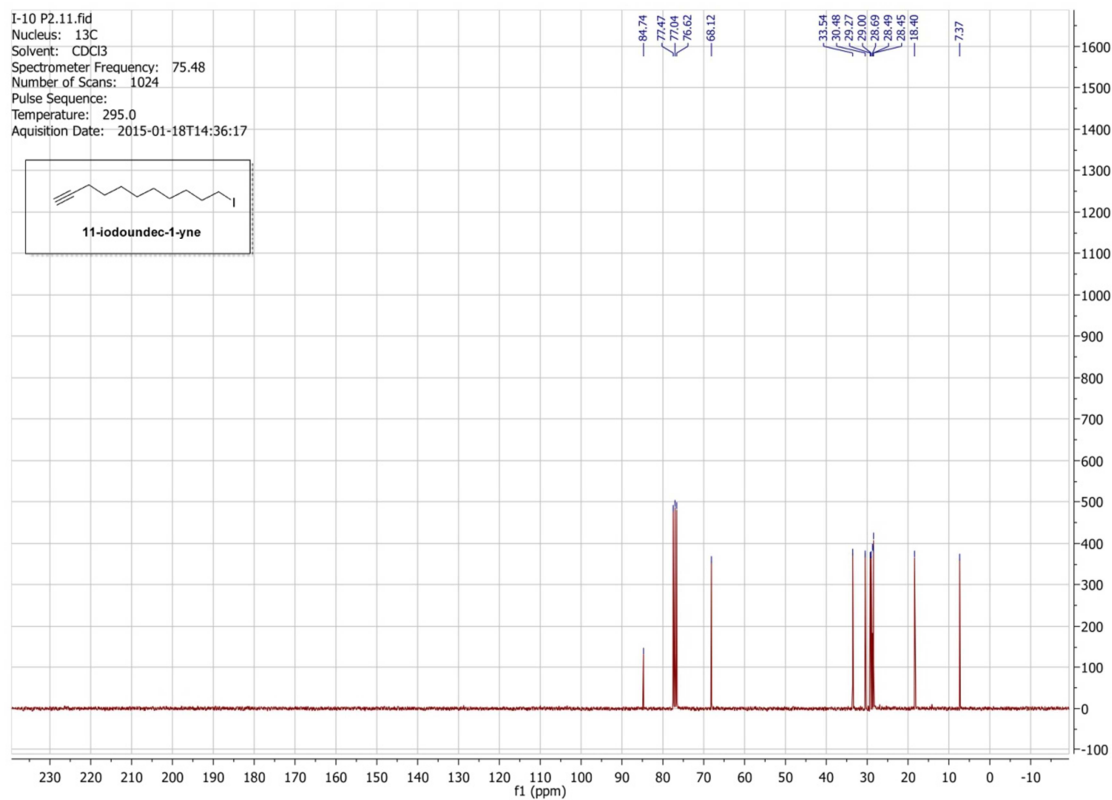
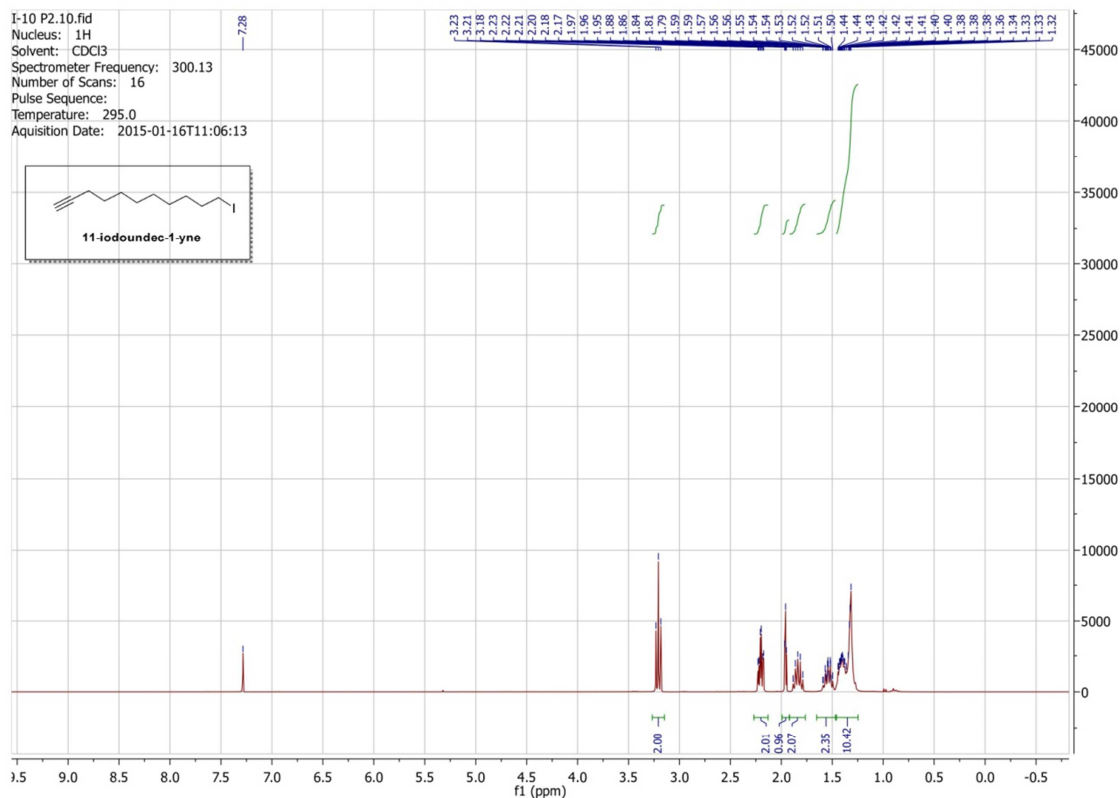
VI – APPENDICES



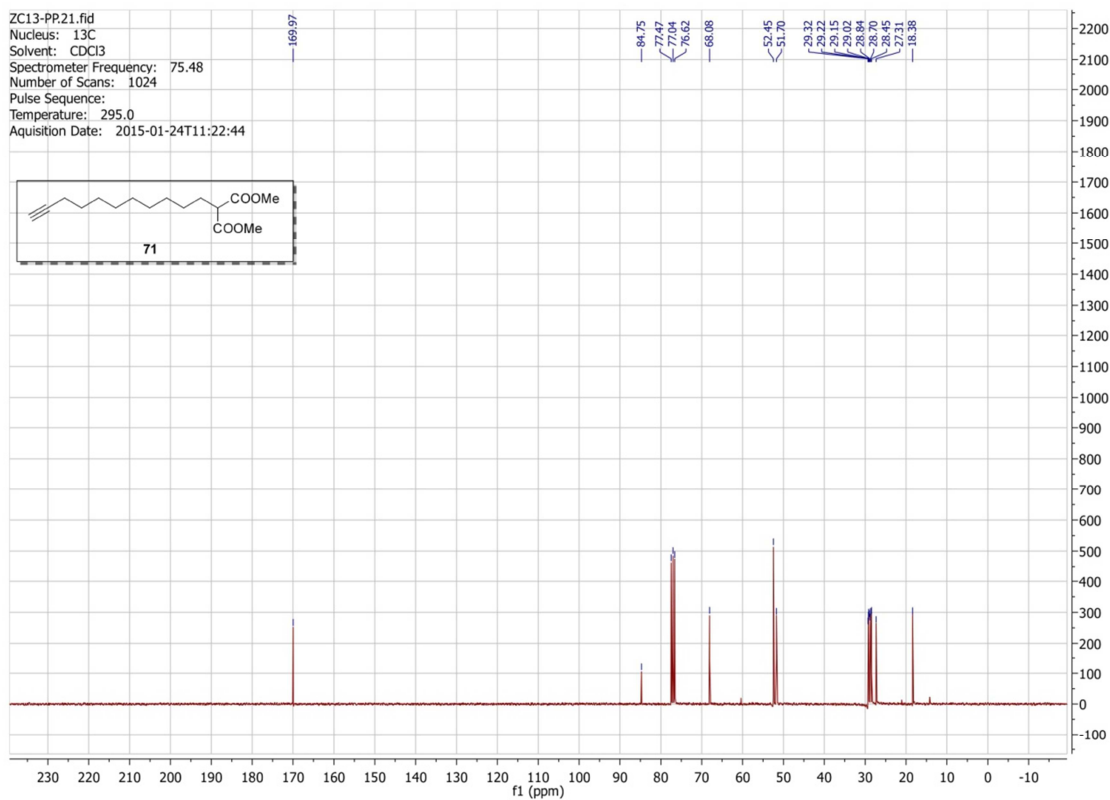
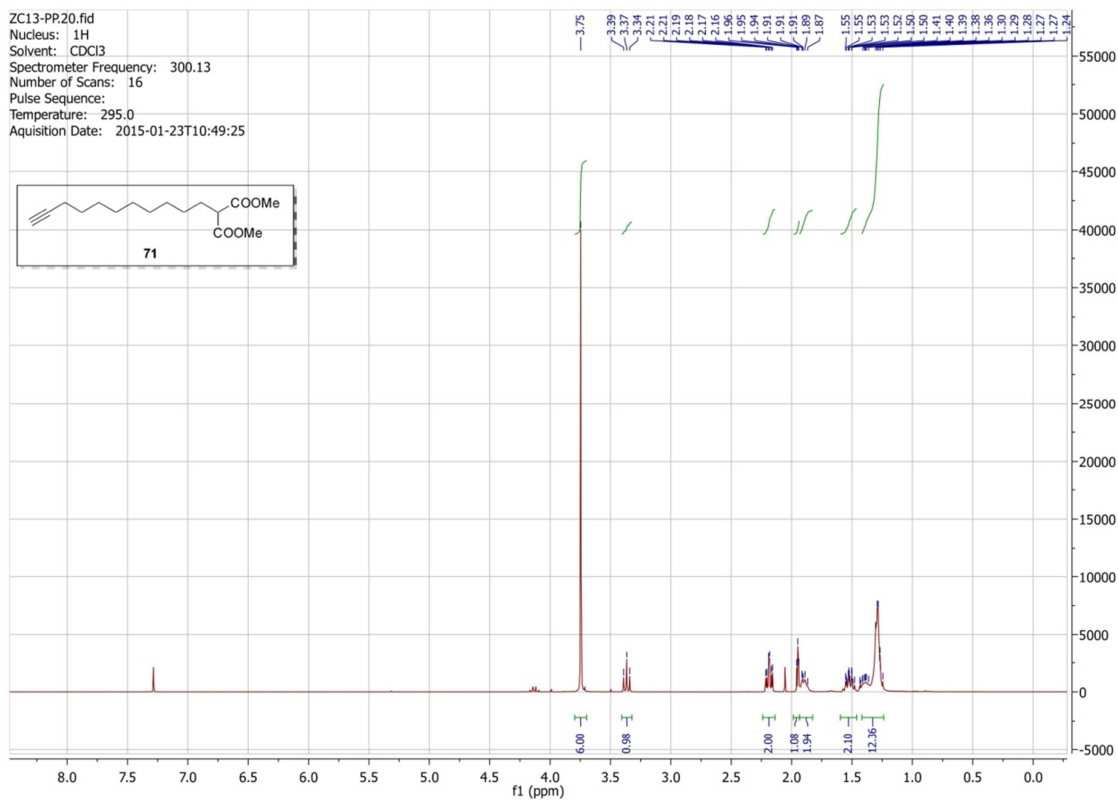
VI – APPENDICES



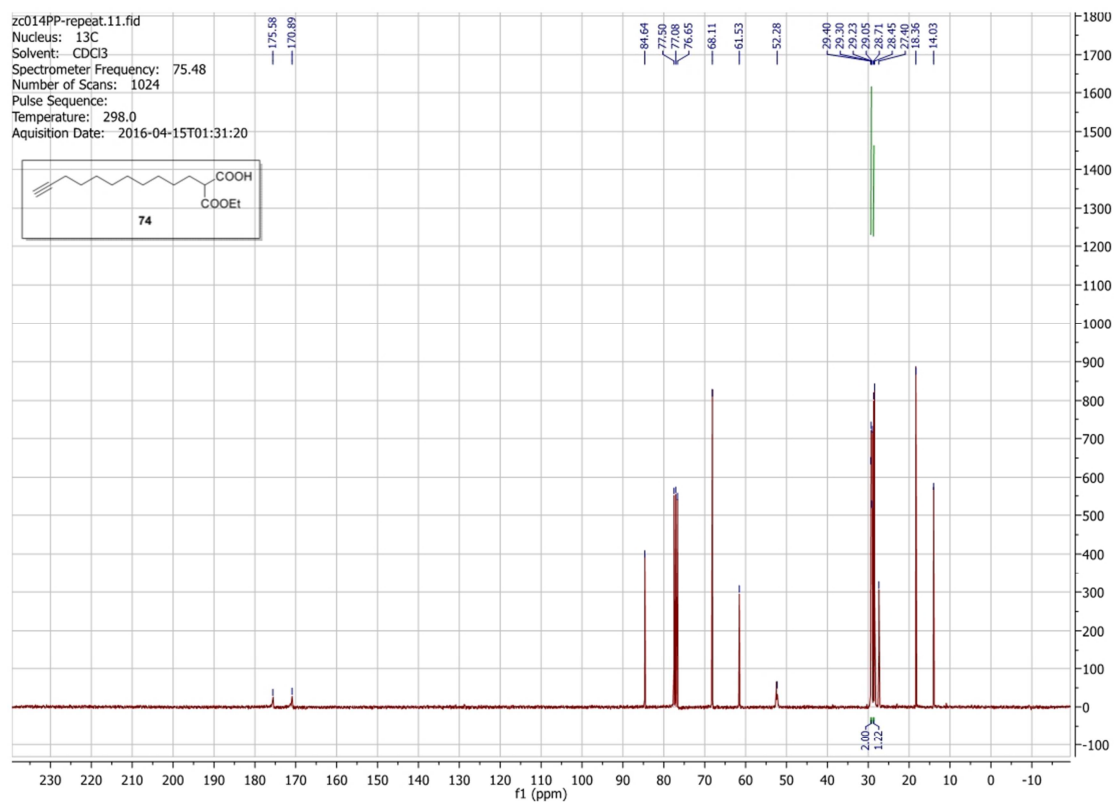
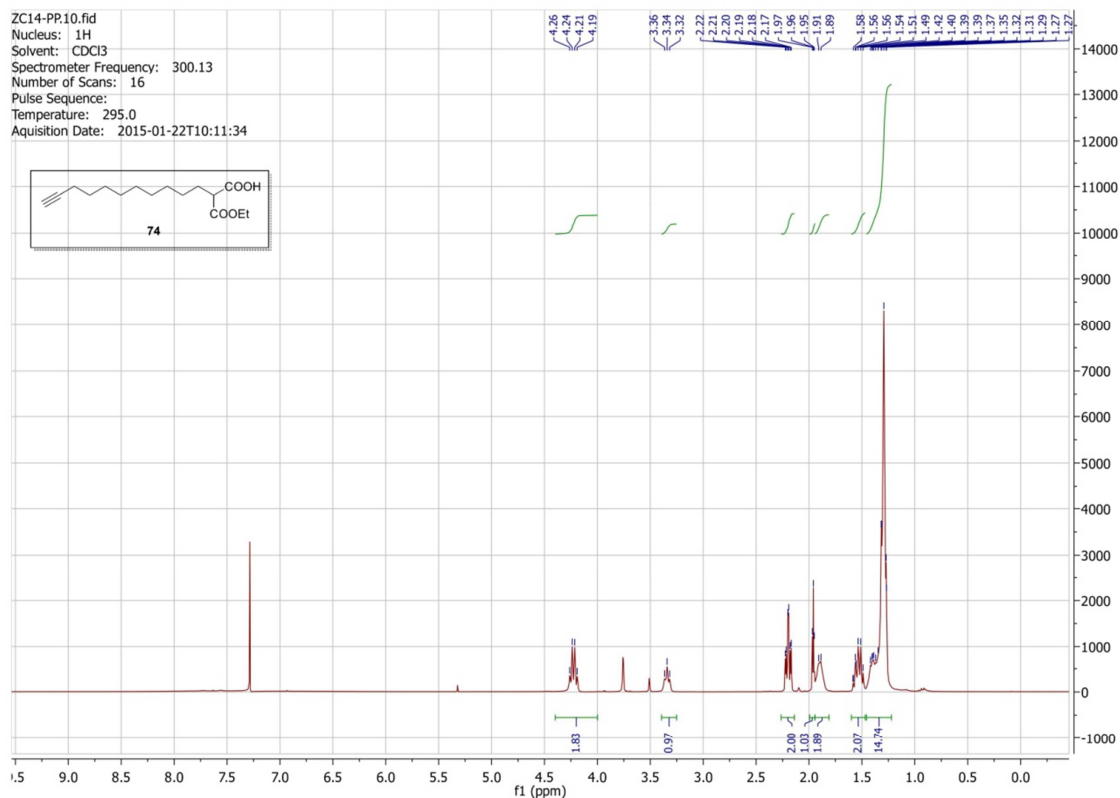
VI – APPENDICES



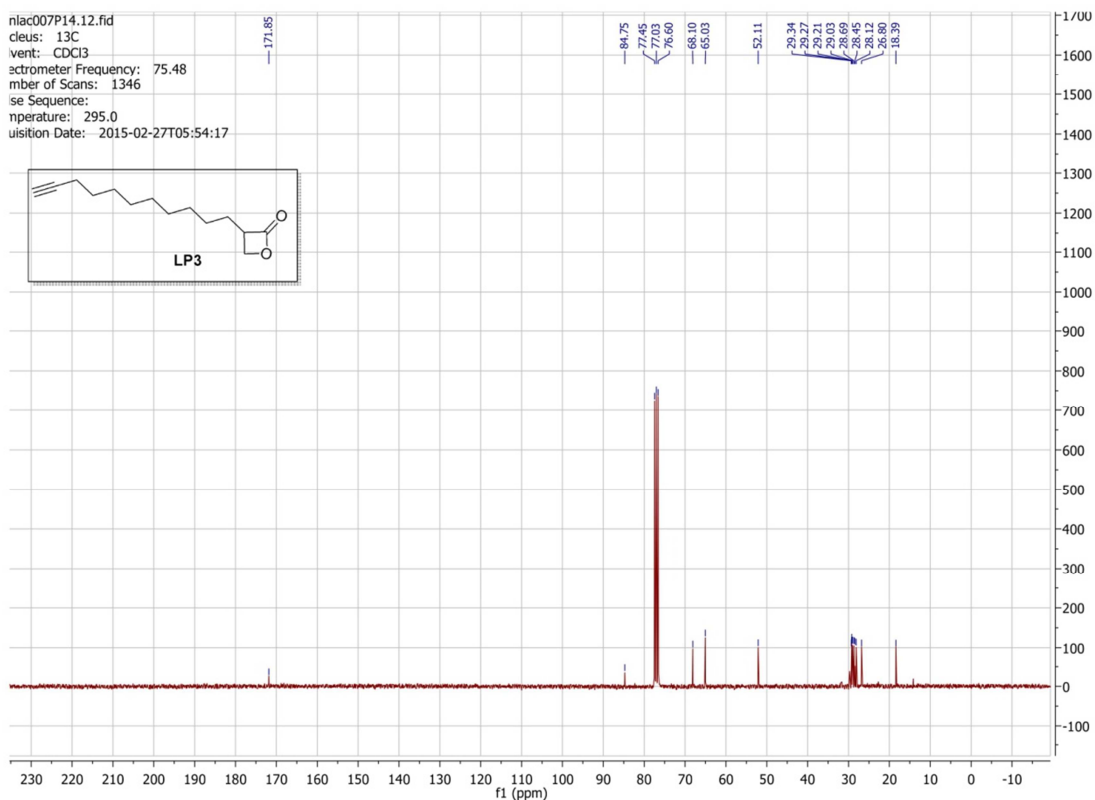
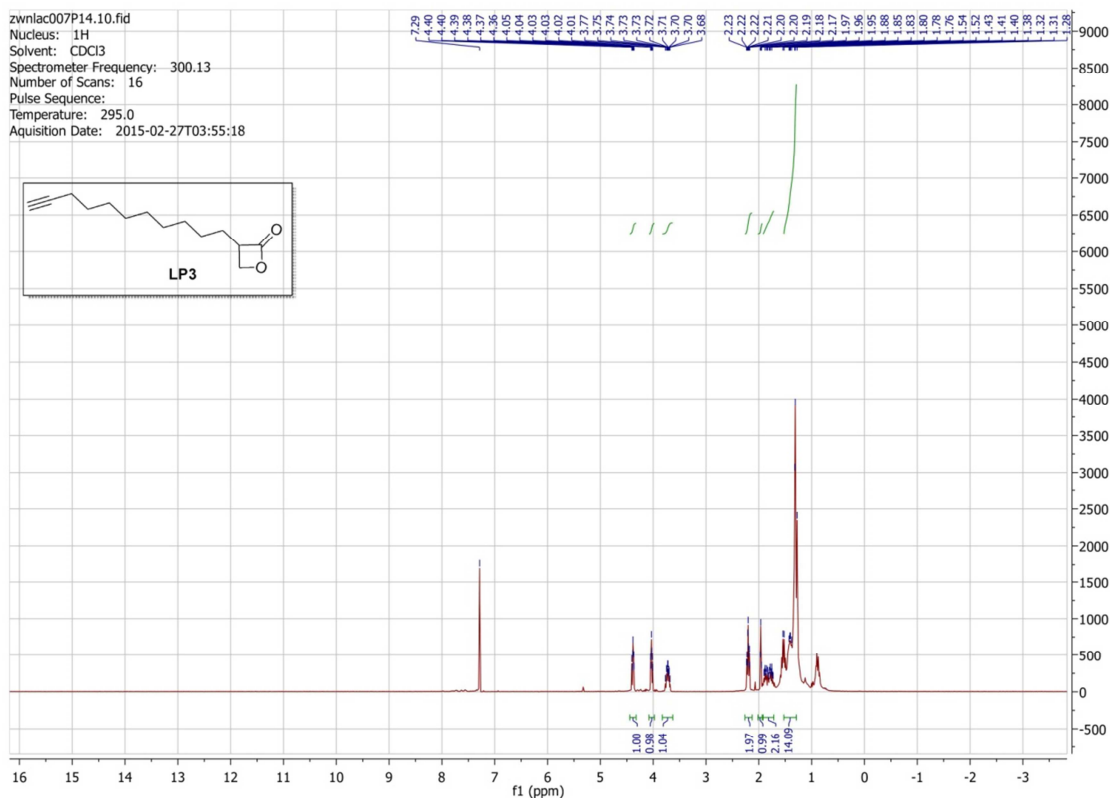
VI – APPENDICES



VI – APPENDICES



VI – APPENDICES



JOHN WILEY AND SONS LICENSE TERMS AND CONDITIONS

Jul 21, 2016

This Agreement between Weining Zhao ("You") and John Wiley and Sons ("John Wiley and Sons") consists of your license details and the terms and conditions provided by John Wiley and Sons and Copyright Clearance Center.

License Number	3911950633062
License date	Jul 18, 2016
Licensed Content Publisher	John Wiley and Sons
Licensed Content Publication	Angewandte Chemie International Edition
Licensed Content Title	Fimbrrolide Natural Products Disrupt Bioluminescence of Vibrio By Targeting Autoinducer Biosynthesis and Luciferase Activity
Licensed Content Author	Weining Zhao, Nicola Lorenz, Kirsten Jung, Stephan A. Sieber
Licensed Content Date	Nov 26, 2015
Licensed Content Pages	5
Type of Use	Dissertation/Thesis
Requestor type	Author of this Wiley article
Format	Print and electronic
Portion	Full article
Will you be translating?	No
Title of your thesis / dissertation	INVESTIGATION OF FIMBROLIDE AND BETA-LACTONE TARGETS RELATED TO THE INHIBITION OF QUORUM SENSING-REGULATED BIOLUMINESCENCE IN VIBRIOS
Expected completion date	Jul 2016
Expected size (number of pages)	180
Requestor Location	Weining Zhao Lichtenbergstraße 4 Chair of Organic Chemistry 2 Garching bei München, Bayern 85748 Germany Attn: Weining Zhao
Publisher Tax ID	EU826007151
Billing Type	Invoice
Billing Address	Weining Zhao Lichtenbergstraße 4 Chair of Organic Chemistry 2 Garching bei München, Germany 85748 Attn: Weining Zhao

Permission for reproduction by Angewandte Chemie International Edition, 18.07.2016, for DOI:
10.1002/anie.201508052.

VII – CURRICULUM VITAE

Weining Zhao

Born on 25th, September, 1986 in Jiyuan, Henan, China

October 2012 – July 2016, Doctoral study

Supervisor: Prof. Dr. Stephan A. Sieber, Chair of Organic Chemistry II, Technische Universität München.

Projects:

(1) Fimbricide natural products disrupt bioluminescence of *Vibrio* by targeting autoinducer biosynthesis and luciferase activity

(2) Mechanistic analysis of aliphatic beta-lactones in *Vibrio harveyi* reveals a QS independent mode of action

September 2009 - July, 2012, Master study

Supervisor: Prof. Dr. Francois Mathey and Prof. Dr. Zheng Duan,

Major: Organic Chemistry,

College of Chemistry and Molecular Engineering (formerly Department of Chemistry), Zhengzhou University.

September 2005 - July, 2009, Bachelor study

Major: Chemistry

College of Chemistry and Molecular Engineering (formerly Department of Chemistry), Zhengzhou University.